Cranfield University

Richard Marie ODIC

Raman Optical Time Domain Reflectometry for Aircraft Fire-Overheat Detection and Monitoring

School of Engineering

A dissertation submitted for the Degree of Doctor of Philosophy at Cranfield University

Cranfield University

School of Engineering
Optical Sensors Group

PhD
2004

Richard Marie ODIC

Raman Optical Time Domain Reflectometry

for

Aircraft Fire-Overheat Detection and Monitoring

Professor Ralph P. TATAM

July 2004

To Karine

Preface and Acknowledgements

This dissertation is submitted for the degree of Doctor of Philosophy at Cranfield University. The dissertation is the result of my own work and includes nothing, which is the outcome of the work done by others. Some of this work was previously reported in the dissertation "Technological Review" submitted to the University of Cranfield for the Certificate of Postgraduate Study in 2000.

It is a pleasure to express my gratitude to many who helped in the preparation of this dissertation. Firstly, I am extremely grateful for the opportunity that, Professor Tatam, my supervisor, and Dr Jones, gave me to do a PhD and for their supports, guidances and helpful discussions over the last 4 years. I am especially grateful for Professor Tatam continual support after I took over my position at Airbus Deutschland. Special thanks also go to my Siemens Cerberus industrial sponsor, Mr. Mangon, for imparting his knowledge and experience, in particular in the area of fire detection.

I would like to express also my sincere gratitude to those who have found the time to discuss my experimental work, and who have drawn my attention to background available in the literature. In particular I have benefited from useful discussions with Dr Chehura (Cranfield University), Dr Hartog (Sensa), Dr Heller (Heller Elektronic KG), Mr Grabow (Airbus Deutschland) and Mr Kallergis (Airbus Deutschland).

I would like to thanks Dr Staines, the group technical manager, who had provided an excellent service for the maintenance and improvement of apparatus as necessary. In addition, I am indebted to York Sensors Ltd. for the efficient design and manufacture of calibration components.

Many thanks also go to my dedicated proof-reader Dr Chabanis.

Finally, I would particularly like to bless my wife, Karine, for her love, support and continuous encouragement, and for our two boys who joined us during our PhDs.

Richard M Odic

July 2004

Abstract

The analysis of the development context for a distributed temperature detection system in an aircraft cargo compartment and the review of candidate technologies stressed the advantages of using the spontaneous Raman scattering principle with a signal processing in the time domain. Simultaneously, the wished detection performance defines the hardware specifications of the system.

For the "Cargo Compartment Fire Detection and Extinguishing" application, several design parameters were identified; namely: the spatial and sampling resolution, the temperature accuracy and its resolution, the possible sensing element length for a given peak optical power per pulse, the refreshment time to get a temperature profile over the sensing element length, the operating/survival temperature ranges and the mechanical constraints at the sensing element in operation or during installation and the possibility to discriminate an optical fibre break from an increase in temperature.

To reject the noise generated and amplified by the Avalanche Photo-Diodes (APD) and by the cascaded amplification modules, the numerical signals were processed using digital filters.

The detection system has also to early detect a fire while rejecting fire-like events. Its detection performances are, namely: a temperature profile refreshment time of 3s, a temperature resolution of ± 1°C around the alarm signal, a spatial resolution of 1.3m for a sensing element length of 500m. The detection of a temperature increase is a spatial analysis organized through specific algorithms. These algorithms involve processing the temperature time derivative, the spatial gradient, the variation of danger surfaces, an analysis of the temperature spatial frequencies and the calculation of the power spectral density and of the temperature covariance matrix.

Fire tests were performed and the optical fibre within a protective stainless steel tube was connected to a control unit to monitor the danger situation over an aircraft cargo compartment.

Table of Contents

1. Introduction

1.1 Background....1

1.2 Objective and Structure of the Thesis....3

2. Context of Development for a Distributed Temperature Detection System

2.1 Review of flight accidents involving fire....6

2.2 The question of false warnings....9

2.3 Improvement of the detection performances....13

2.4 The influence of international regulations....17

2.5 New technologies for new aircraft programs....21

2.6 Detection systems for retrofit or new applications....25

2.7 General requirements to equipment design and industrialisation....28

2.8 Conclusion....30

3. Technology Review and Principles of Selection

3.1 Review of potential applications for a DTS....41

3.1.1 Non-pressurized environment....43

3.1.1.1 Bleed leak detection [BLD]....43

3.1.1.2 Engine fire detection [EFD]....43

3.1.1.3 De-icing system control [DSC]....44

3.1.1.4 Landing gear overheat detection [LGD]....45

3.1.2 Pressurized environment....46

3.1.2.1 Thermal cargo monitoring [TCM]....47

3.1.2.2 Wire fire/overheat detection system [WFD]....47

3.1.2.3 Cabin temperature control [CTC]....48

3.1.2.4 Hidden area fire detection [HAD]....49

3.2 Review of potential detection technologies....50

3.2.1 Ultrasonic waveguide....51

3.2.2 Electrical time domain reflectometry....52

3.2.3 Distributed temperature system using discrete temperature sensors....53

3.2.4 Optical distributed temperature system....53

3.2.4.1 Raman OTDR....54

3.2.4.2 Raman OFDR....55

3.2.4.3 Brillouin scattering....56

3.2.4.4 Bragg gratings....57

3.2.4.5 Polarisation OTDR....58

3.2.4.6 OTDR using liquid core fibre....59

3.2.4.7 Other optical distributed temperature sensing systems....59

3.2.5 Other non optical technologies....61

3.2.6 Temperature / overheat detection system overview of aircraft suppliers..... 62
3.2.7 Summary of current measurement characteristics..... 62
3.2.7.1 Measurement selection criteria..... 63
3.2.7.2 Pre-selected technologies..... 64
3.3 Methodology for technology selection..... 65
3.3.1 The detection performances compared to the measurement criteria..... 65
3.3.2 The application requirements compared to the measurement criteria..... 66
3.3.3 Final technology selection..... 67
3.4 Raman OTDR versus Raman OFDR..... 70
3.5 Raman OTDR versus photon counting..... 73
3.6 Single pulse versus correlation OTDR..... 75
3.7 Conclusion..... 77

4. Raman OTDR Thermometry and Application Constraints

4.1 Raman effect in optical fibres..... 84
4.1.1 Raman backscattering process..... 84
4.1.2 OTDR principle..... 88
4.1.3 Operating wavelength and fiber dependancy..... 89
4.2 Raman backscattering related to detection performances..... 95
4.2.1 Spatial resolution..... 95
4.2.2 Temperature resolution..... 96
4.2.3 System detection range..... 98
4.2.4 Temperature profile and refreshment time..... 98
4.3 Raman backscattering sensitivity to environmental conditions..... 99
4.3.1 Sensing element and operating / survival temperature ranges..... 99
4.3.2 Mechanical and specific constraints..... 100
4.3.3 Optical fibre break considerations..... 102
4.3.4 Optical power balance for efficient sensing line interrogation..... 104
4.4 Conclusion..... 106

5. Metrological Requirements and Signal Processing

5.1 Description of the detection system modules..... 112
5.1.1 The pulsed laser diode..... 115
5.1.2 The laser diode driver..... 116
5.1.3 The optical demultiplexer..... 129
5.1.4 The detector and amplification chain..... 141
5.1.5 The digitalisation..... 145
5.2 Architecture of the tested system..... 146
5.2.1 The stakes of the new design..... 146
5.2.2 System temperature control..... 146
5.2.3 Vibration/shock-proof design..... 150
5.3 Detection performances analysis..... 151

5.3.1 Noise characteristics ... 152
5.3.2 Temperature resolution ... 155
5.3.3 Spatial resolution ... 156
5.3.4 Measurement time ... 157
5.3.5 Hot spot detection ... 159
5.3.6 Optical fibre length ... 160
5.3.7 Hardware control and monitoring ... 161
5.4 Digital signal processing opportunities ... 165
5.4.1 Averaging of the acquired signal data sets ... 165
5.4.2 Fourier transform and band-pass filter ... 167
5.4.3 Wiener filter ... 170
5.4.4 Soft thresholding using wavelet decomposition ... 175
5.4.5 Conclusion on post-signal processing ... 184
5.5 Compatibility to on-board system requirements ... 187
5.6 Conclusion ... 188

6. DTS Applied to Aircraft Cargo / Baggage Compartment

6.1 Early and multicriteria detection ... 192
6.2 Description of the water mist detection – activation concept ... 193
6.2.1 Total flood or zoning protection ... 193
6.2.2 The objectives of the MPS test procedures ... 193
6.2.3 The DTS as a tool for the evaluation of extinguishing agents ... 194
6.3 Installation of an optical fibre-based sensing element in aircraft ... 195
6.3.1 A specific cable design ... 195
6.3.2 The fibre blowing technique ... 195
6.4 Test programs ... 197
6.5 Detection-activation algorithms ... 198
6.5.1 Algorithms for initial fire detection ... 199
6.5.2 Algorithms for fire monitoring ... 204
6.5.3 Algorithms for fire suppression ... 205
6.5.4 Fire signature identification ... 207
6.6 Conclusion ... 210

7. Conclusions and Future Work

7.1 Overall Conclusions ... 213
7.2 Recommendation and Future Research ... 217

Glossary ... 219

Introduction

This thesis is concerned with understanding the needs of fire and overheat detection improvements on-board large aircraft using online temperature detection systems to propose a suitable technology. Today, aircraft suppliers are proposing the use of a loop of temperature sensors with a level of monitoring performance, which is not fully responding to the complexity of a fire or overheat situation. However, there is an increasing need to be able to better characterise the danger level, so as to inform the aircraft crew with regular, reliable and adequately detailed information. In order to achieve this, a detection technology shall provide evidence of robustness and shall demonstrate its capability to return faithfully the evolving criticality of a fire or overheat situation. On the selected, improved and tested technology, the overall objective was to question the feasibility of a demonstration in an "operational" environment.

1.1 BACKGROUND

In recent years fire sensors have evolved from threshold devices that sense a single fire signature to multi-mode, multi-criteria sensors that can employ algorithms for decision making. Airplane flight manuals contain the approved procedures to follow for a variety of situations. In the case of a cargo compartment fire detector alarm, the typical flight manual procedure is to shut off any applicable ventilation, discharge fire suppression agent if equipped, and divert and land at the nearest suitable airport. In addition to the direct costs associated with a diversion, there could also be an increased safety risk due to a variety of factors such as unfamiliar airports, less effective navigation aids, inadequate maintenance facilities, shorter runways, inferior airport rescue and fire fighting capabilities.

The review of flight accidents involving overheat or fire cases indicates the necessity

of an improvement of detection performance. New international regulations, new aeronautic applications for fire/overheat detection system, or new aircraft programs are also presented as opportunities to launch the development of a system in accordance with the system specification requirements.

Sensor systems which permit monitoring of the magnitude of temperature, and also its variation along the length of a continuous uninterrupted sensing element, offer a powerful and economical means of covering a large number of locations within a large area and are particularly attractive for obtaining a graphical or pictorial presentation of information.

A technology review was conducted to identify the most suitable distributed temperature detection system to cover a wide range of aeronautic applications. Regardless of the application, both for the control unit and the sensing element, the Distributed Temperature Sensor (DTS) system shall be designed to eliminate false warnings, to reduce the number of components to a minimum, to provide fast positive checks and troubleshooting procedures, to allow easy installation and substitution, to present small size, low weight and high reliability figures. These constraints impact directly on the design of the Raman DTS.

Cargo compartment fire detection is particularly interested in detection systems able to reduce drastically the false alarm rate and capable of ensuring a higher safety level. Halon gas, the cargo extinguishing agent, is to be replaced by an efficient ecological agent and therefore the cargo compartment application would require a system which ideally could monitor the fire-situation after the discharge of the extinguishing agent during the specified time period (nine hours). A candidate for the substitution of the extinguishing agent is a mixed system using a cooling water mist component in combination with nitrogen, an inert gas.

1.2 OBJECTIVE AND STRUCTURE OF THE THESIS

The objective of this thesis was to demonstrate the integration feasibility of a Distributed Temperature Detection System on large aircraft. To achieve this objective, a systematic analysis of the detection failures on aircraft and of the DTS technologies having already a "proof-of-concept" available allowed the selection of a unique technology and the launch of the research for a technological improvement.

Many interconnections exist between the chapters; for example the constitutive equations and model parameters from chapter 4 are used for the construction of the detection system described in chapter 5 and 6. The knowledge determined in chapters 2 and 3, on fire detection and distributed temperature-sensing technology respectively help to understand the fire test procedures and results from chapter 6. The content of each chapter is summarized below in more details.

Chapter 2 gives a status of the aviation incidents and accidents related to fire or overheat over 22 years up to 2002 and presents in detail the repercussions and possible improvements. Background on international regulations and trends for the new aircraft programs are also provided.

Chapter 3 explains how the technology selection was operated and describes, per identified application, the various detection requirements and environmental conditions that should be considered. Based on an accurate knowledge of potential fire scenarios, the development of the DTS targeted the following set of detection performances: a temperature profile refreshment time of 3s, a temperature resolution of ±3°C around the alarm signal, ±5°C outside the alarm range, a sampling interval of 0.5m, a temperature detection range between -55°C and +300°C (long term), a maximum sensing element length of not less than 500m. Detection and monitoring algorithms are available and are refined using the full size of an A340 cargo compartment. Finally, the Raman Optical Time Domain Reflectometry is decided as the technology to be developed for the application "Thermal Cargo Monitoring". In measurements undertaken using fibre-optic DTS, an optical fibre is positioned along the object of interest and laser pulses are passed through the optical fibre. The laser

beam is scattered in the fibre, and Raman scattered light (which has two components, Stokes light and anti-Stokes light) is generated and measured on its return to its point of origination. The intensity of the Raman scattering depends on the temperature of the optical medium.

In chapter 4, the Raman effect in optical fibres is detailed and the level of the optical signals reaching the photodetectors are calculated. It allows the specification of the amplification characteristics.

Chapter 5 examines the different system modules and its global architecture. A relationship is then established between the set of the module characteristics and the detection performance. The amplification model of the received optical signal is also fully developed in this chapter. To reduce the criticality dependent on the hardware development of the pre-amplification stage, which has to be generating a low level of noise, the study in this chapter aims to show that signal processing techniques can improve significantly the temperature accuracy of the fire monitoring system. Besides, an evaluation of the system compatibility to on-board system requirements is carried out.

The detection algorithms, the test program and results are explained in the chapter 6 and illustrate the maturity of the detection system concept

Finally, in chapter 7, the overall conclusions of the work are presented and the directions for future research are given.

• Odic, R.M.; Tatam, R.P., "Distributed Temperature Sensor for Aeronautic Applications". The International Conference on Optical Fibre Sensors, Portland (USA), May 2002.

• Odic, R.M.; Tatam, R.P., "Distributed Temperature Detection for Large Aircraft Systems". Conference on Sensors for Aircraft Systems, Institute of Physics, London (UK), May 2003.

• Odic, R.M.; Tatam, R.P., "Detection, Control and Monitoring of Fire in Aircraft Cargo Compartment". SPIE Photonics East 2003, Optical Technologies for Industrial and Environmental Sensing, Rhode Island (USA), October 2003.

Context of Development for a Distributed Temperature Detection System

2.1 Review of flight accidents involving fire 6
2.2 The question of false warnings 9
2.3 Improvement of the detection performances 13
2.4 The influence of international regulations 17
2.5 New technologies for new aircraft programs 21
2.6 Detection systems for retrofit or new applications 25
2.7 General requirements to equipment design and industrialisation 28
2.8 Conclusion 30

A significant aspect of aeronautic fire/overheat (F/O) protection is to identify a developing emergency situation in a timely manner, and to alert the occupants of the aircraft (A/C). The other common functions are the transmission of an alarm notification, the shut down of electrical, air handling equipment or special process operations and the initiation of automatic suppression systems.

The development of a new aeronautic fire detection system is here described as a process necessitating the consideration of key parameters. The review of flight accidents involving overheat or fire cases, balanced with the "unwanted alarm" rates from the detection systems involved indicates the necessity of an improvement of detection performance. New international regulations, new aeronautic applications for (F/O) detection system, or new A/C programs are also presented as opportunities to launch the development of a system in accordance with the system specification requirements.

2.1 REVIEW OF FLIGHT ACCIDENTS INVOLVING FIRE

The objectives of this study are to assess the potential benefits, in terms of reduction of fatalities, by statistically identifying which parts of the A/C are the most affected by F/O events leading to an accident. The term accident refers here to such an event associated with the operation of an aircraft in which there were one or more fatalities.

Although the number of fatalities per 100 000 flight hours decreased significantly within the last 20 years [U.S. Department of Transportation, 2003], the projected increase in the demand for air travel in the 21st century is such that unless the current accident rate can be improved, the public will find the number of accidents together with the associated loss of life, unacceptable.

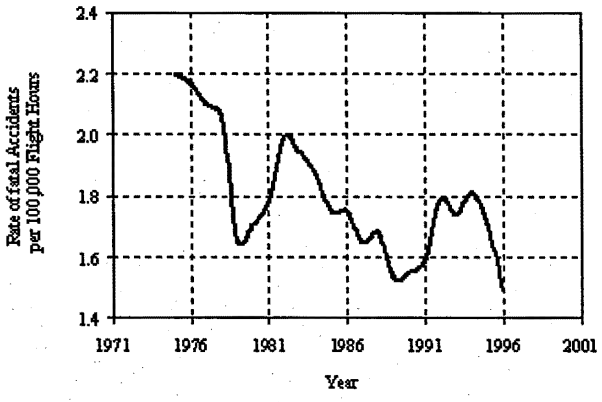

Figure 2.1-1 Rate of fatal accidents per 100,000 Flight Hours 1975 through 1996

Fire is involved in approximately 60% of aircraft accidents [Muir, 2003]. Historically, improvements in standards for initial type certification have frequently been based on lessons learned from the continued airworthiness process [The Federal Aviation Administration, 2003b]. Consequently, making the continued airworthiness process more effective is one axis to improving safety in the near term and to providing a foundation for improvements in the long term.

Reports have been collected from the crashDATABASE.com server [Rupp, 2003] to

draw an analysis on Large Aircraft Accidents with fatalities related to fire or overheat situations.

Accidents, where the starting location of the fire or overheat situation was unknown, were not taken into account, neither were events where it was not possible to say if the danger was or was not detected. The small percentage of unwanted alarm cases given by Detection Systems and leading to an aircraft accident, or accidents resulting from wars, terrorist actions, hijacking, lightening…were also not included in this analysis.

The 22 accident cases, happening on Airbus, Boeing, McDonnell Douglas and extracted from 1980 to 2002, were arranged into 9 categories corresponding to aircraft areas where the F/O event started, namely: Engine, Cabin, Auxiliary Power Unit (APU), Cockpit, Landing Gear, Wing, Cargo Hold, Hidden Area or Electronic Bays. The Hidden Areas are zones in the aircraft with a low level of maintenance operations, for example in the lower centre fuselage section of large aircraft.

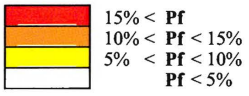

	Warning	No Warning
Engine		
Cabin		
APU		
Cockpit		
Landing Gear		
Wing		
Cargo Hold		
Hidden Area		
Electronic Bays		

Figure 2.1-2 Distribution of accident with fatalities as a function of the selected A/C Area "Pf" stands for the probability that an accident with fatalities has been initiated in the considered zone of the aircraft and where a warning (first column) or no warning (second column) was given.

Out of the total number of accident with fatalities, we notice that about 60% were having a danger detected, and that the Engine, the Cabin, the Wing and the Cargo Hold areas had the highest probabilities.

One significant reason for the lack of progress could well be that with the very low accident rate that the industry has achieved over the past few decades, no single safety feature is likely to be cost effective [Taylor, 1996]. The suggestion is then to aim at having a collection of safety features waiting on the shelf until their need is agreed by all concerned. To achieve this we must concentrate R&D on minimizing, to an acceptable level, the disbenefits of any feature.

The previous analysis aims to identify zones in large aircrafts, which are more likely to be the start of a F/O. Pinpointing the difference of occurrences per zone may indeed reduce the development costs. In fact, the identification of these zones enables the requirement to be separated in terms of detection, and to evaluate wether a detection or an extinction system development would bring the most benefit to the overall security of the aircraft.

While improving the accuracy and early warning capabilities of the detection systems or the efficiency of extinguishing agents [Sarkos, 2003]; the aircraft manufacturers, the airlines, the regulations are aiming at improving survivability during post-crash fires and preventing uncontrollable in-flight fires. Survivable accident is one in which the fuselage remains relatively intact, the crash forces do not exceed the limits of human tolerance, [Murray, 1995] there are adequate occupant restraints, and there are sufficient escape provisions.

Over the past ten years, the Federal Aviation Administration (FAA) and most other aviation authorities worldwide have implemented modifications, which have vastly improved fire safety in transport aviation, and increased the survivability rate [Hill *et al.*, 1998]. The greatest improvements in fire safety have been gained in the area of materials flammability upgrading. Further reduction in fatalities [Warren *et al.*, 1998] is now expected, along that development axis, through enhanced aircraft fire penetration resistance.

2.2 THE QUESTION OF FALSE WARNINGS

An unwanted alarm occurs when any signal activated by an automatic protection device, when any alarm or any kind of direct or indirect signal given to the aircraft crew, is not the result of a fire/overheat event.

Unwanted alarms not only put at risk the airplane occupant's life, but also endanger people's life on the ground. A fire alarm system that repeatedly gives unwanted alarms produces mistrust in the detection system and compromises the fire safety objectives. In case of a genuine fire, the crew will for example have a slower response to the danger and might cause delays in evacuation. A high "unwanted alarm" rate is linked to high airline maintenance costs and direct costs due to a possible diversion of the aircraft. The "no go" situations and their associated delays degrade also the opinion the passengers have of their "favourite" airline.

The first type of potential failure is when a system that has been designed and installed to meet detection performance objectives fails to meet those objectives. The failure may be the result of an operational failure or fault, or it may result from changes in the environment or hazards that affect the system ability to meet its objectives. The second failure mechanism is when the objectives of the fire/overheat alarm system have not been properly matched and integrated with the overall fire safety mission. A third type of failure is when a system "fails positive" due to false or nuisance alarms.

The unwanted alarms consist of false alarms and nuisance alarms [Conforti, 1998a]. The false alarms are a result of stimuli (which are not targeted by the original design of the detection system), including among others system malfunction, electrical problems, electromagnetic interferences, lightning strikes and aging of components. Nuisance alarms are those caused by non-threatening events but "detection criteria-like" stimuli. For optical smoke detection system, it can be for example non-fire aerosols like cooking fumes, steam, dust, insecticide, cigarette smoke…

These situations can also be the result of a poor product design or production, wrong selection of the model of detector and of its location, poor quality in installation, commissioning and maintenance.

The status of the unwanted alarm rate in Cargo Compartments of Large Aircraft has been largely analysed [Blake, 2000]. The number of reported unwanted alarms shows an increasing trend. Without improvements in the technology used for fire detection, it would be expected to accelerate due to the addition of 3000 aircraft with class D compartments, with fire detection and suppression systems that should have been installed by March 2001. The ratio of unwanted cargo compartment fire detector alarms to actual fire or smoke events is increasing and is at 200 to 1 between 1995 and 1999.

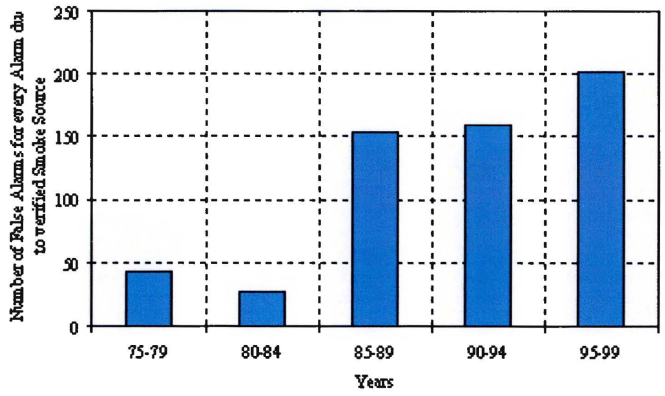

Figure 2.2-1 Number of unwanted alarms for every alarm due to verified Smoke Source

After years of successful development and of lessons learnt, the detection system suppliers still face the complexity of a continuously evolving environment. This situation is potentially occurring in the A/C wherever the detection system is inputting an alarm equipment.

The unwanted alarm cases were searched by the Accident/Incident Database System [The Federal Aviation Administration, 2003a] using the keywords Fire or Overheat or Flame or Smoke, and Aircraft, and "Boeing" or "Airbus". The cases considered

took place between 1980 and 2002. The objective is to isolate zones in the aircraft, where the unwanted alarm occurrence is significant in comparison with the other protected sectors. The database contains 205 unwanted alarm records where the all nine selected A/C zones are considered.

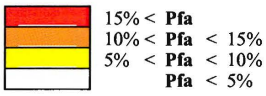

	Unwanted Alarms
Engine	
Cabin	
APU	
Cockpit	
Landing Gear	
Wing	
Cargo Hold	
Hidden Area	
Electronic Bays	

Figure 2.2-2 Distribution of the number of unwanted alarms as a function of the selected A/C Area "Pfa" stands for the probability that an unwanted alarm may occur in a considered area. It is calculated within the ensemble of the selected A/C regions.

One may simply notice that among the identified zones in the aircraft the "Engine" detection system is the most significant contributor to the generation of unwanted alarms, followed by the "APU" and the "Cargo Hold" detection systems. The high levels of EMI, mechanical and acoustic stress mostly explain the observed false alarm rates in the Engine and APU detection applications, whereas the multiplicity of the aerosol types in the Cargo Hold makes uneasy the discrimination between the "Fire" and the "non-Fire" situations. It is therefore necessary to identify the potential remedies to an overall situation of false alarm and of nuisance alarm on A/C.

A deeper exploitation of the detected signals may be one axis of improvement. A better understanding of the detection environment may indeed allow the tuning of the detection system sensibility to better match the targeted spectrum of fire cases. A de-correlation towards the variability of the background may also help to move away from the environmental conditions related to the traditional nuisance alarm situations [Ugarte *et al.*, 2001]. Increasing the number of sensors will also provide a higher fire

detection probability for a fixed nuisance alarm probability. Whereas the use of the difference of sensor outputs with highly correlated background zone will reduce the nuisance alarm probability for a given threshold. In any case, one may only advise to build a systemic analysis to identify the chain of events leading to a false warning. Among the various aircraft zones for which fire protection is required, the cargo compartments are specific in this sense that their characteristics are very variable in terms of dimensions and topologies as well as environmental conditions and fire threats [Mangon, 2001]. However, the description of the potential fire sources, the analysis of the fire ignition process and the study of the fire propagation conditions will inevitably help to understand and to minimize the gap between the detection system performances and the fire diversities. As an example, theoretical analysis and test results showed that a released energy model and an associated algorithm of prediction were suitable to fire detection study [Yan *et al.*, 2001]. In a closed space, genuine and deceptive fires are theoretically considered as a thermodynamic system. These systems cause the increments of entropy, which demonstrate the release of kinds of energy such as heat, light radiation and material losses (smoke, gasses etc.).

One may also assume that a combination of several criteria to trigger a fire alarm would bring a significant benefit in terms of discrimination capabilities, provided that the nuisance alarm spectra associated to these additional detection criteria do not degrade the global system performances [Gottuk *et al.*, 1999]. The main goal is here to provide faster response to real fire threats while providing better nuisance alarm immunity compared to conventional single-criteria type detectors.

The false alarms can be avoided by simple and rigorous design rules, methodical test phases and clear installation and maintenance procedures [Fitzgerald, 1989]. Following the crash of a Boeing 737 in January 1974, 78 new instances of mis-wiring on 74 aircrafts were found in the systems designed to flag and extinguish fires in engines and cargo compartment.

The terms "false alarms" will here after cover proper false and nuisance alarms.

2.3 IMPROVEMENT OF THE DETECTION PERFORMANCES

The analysis of the A/C accident scenarios and the status of the unwanted alarms generated by on-board detection systems call for an improvement of the definition of the detection objectives and of the associated chain of alert. The last point suggests an opportunity axis to reduce the unwanted alarm rate. The following discussion will explore some potential ways to better exploit the detector output signals, to better follow the evolution of danger and provide earlier an alarm with more confidence.

For much of their history F/O detectors have been threshold devices, alarm decisions are made when the signal exceeds some fixed threshold level. In the language of modern digital electronics this means that the detector is operating on a singe bit of information [Bukowski *et al.*, 1999]. As an example, some thermal detectors operate on the rate-of-rise principle (alarm when the rate of temperature rise exceeds a fixed value). Even where the thermal detector has dual elements (fixed temperature and rate-of-rise) they indicate an alarm when either element exceeds its threshold. As opposed to a single bit criterion, a two-bit criterion device is for instance one thermal detector, which operates such that a rapid increase in temperature causes it to decrease the fixed temperature value at which it activates. One light scattering type smoke detector from the 1970's incorporated a circuit that increased the sensitivity (decreased the alarm threshold) if the rate of rise of the smoke signal exceeded a threshold value.

Multi-criteria detection and additional signal processing might contribute to lower the nuisance alarm rate but might also help to narrow the gap between what is the reality of the danger and what is returned by the sensing system. In theory, if one could determine a unique pattern in the signal from real fire sources, it would be possible to differentiate these from nuisance sources. The first successes in increased intelligence required the combination of different sensors sometimes called multi-mode sensors. The more bits available on which to base an alarm decision, the better

that decision can be made and the lower is the rate of both false positives (nuisance alarms) and false negatives (unwanted fires not detected).

Fuzzy logic allows multi sensors to utilize multiple criteria to signal an unwanted fire, but as the sensor inputs increased it became very difficult to think through the logic of their interaction.

Neural networks were the next advance where the system is "trained" in how to categorize various patterns of signals. As an example, in conjunction with a Fourier Transform (using Infra-Red spectroscopy), neural networks have already demonstrated their efficiency as an advantageous signal processing method [Chen *et al.*, 1999]. The underlying problem with signal cross correlation, fuzzy logic, and neural networks is that they represent an empirical fit to data. The correlations, logic tables, or training process are developed by exposing the sensors to fires and nuisance sources and determining the coefficients or settings that alarm to all fires and ignore most nuisance sources. Though neural networks can learn on the field, from past situations, since it is impossible to include in the tests all fires and nuisance sources, the applicability of this approach is somewhat limited to highly controlled applications. What is needed is therefore a system that knows enough about fire itself to decide on signal patterns that it has never encountered before.

Similarly to the unwanted alarm study, using the same keywords, the incidents were searched by the Accident/Incident Database System [The Federal Aviation Administration, 2003a] where the fire or the overheat situation was or was not detected. When there was a "warning" and it was justified by the observation of a fire, of an overheat or of a technical problem susceptible to lead to a danger, the probability "Pi" that such an event occurs for a given A/C zone shows that the engine and the cabin are the most exposed. When there was "no warning" but a fire, an overheat or a technical problem had happened, the probability "Pi" values are more equally distributed among the zones of the A/C.

Respectively from 1980 to 2002, on large Airbus and Boeing aircrafts, 343 "justified detection" and 260 "no detection" cases were found. While more than 75% of the incidents with "Warning" are noticed from the "Engine" environment (52%) and within the "Cabin" (24%), it is more contrasted for the "No Warning" incidents where two contrasted groups are clearly noticeable: group A, 5 zones each above 14%, gathering more than 85% of the incident cases and group B the 4 other areas.

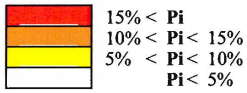

	Warning No Fatalities	No Warning No Fatalities
Engine		
Cabin		
APU		
Cockpit		
Landing Gear		
Wing		
Cargo Hold		
Hidden Area		
Electronic Bays		

Figure 2.3-1 Distribution of the number of incidents with "Warning" and of incidents with "No Warning" as a function of the selected A/C Area

Group A joins together detection applications where one may find harsh environmental conditions, or where there was no operative detection system in place or where the detection performances were not compatible with the suddenness of the event. Group B is a set of areas where there is basically only a few cases of undetected F/O but unwanted alarms (cargo hold), fatalities (wing), well-controlled environment (electronic bays), or known conditions (hidden area).

One key to success could come from the clear definition of the non-fire state. Significant information can be gained from detectors when the environment is in a non-fire state [Grosshandler, 1998b]. Other information that would be useful in discriminating the two states could come from air pressure and velocity sensing; temperature fluctuations dimensioning; unburned fuel concentration measurements; O_2, H_2O, and CO_2 levels; CO, NO_x, HCl, HCHO, or other trace species levels; the size and make-up of particulates.

One may also draw attention to the Computational Fluid Dynamic (CFD) codes, for

which computer speeds have advanced to the point that meaningful numerical predictions now can be made for relatively complex and realistic fire/overheat scenarios. Computer simulation can be here an optimisation means for the detection system performances.

Another route for improvements is to bring intelligence into the detection system using the benefits of the statistical tools. The multivariate statistical approach, called principal component analysis [McAvoy *et al.*, 1996], is used to compress the sensor information down to a small number of variables that can be interpreted more easily than the raw sensor signals themselves. Besides, a detection algorithm based on the comparison of the short and long-term power spectral densities of monitored input signal sequences from "fire sensors" was presented by Duisburg University [Klose *et al.*, 1991]. The algorithm is as well suited for single and multiple input detection, but one risk of such a method might well be the variation in time of the danger signal compared to the temporal window taken as a reference.

New sensing technologies may either sometimes bring significant performances to replace existing systems or can complement still operational but more traditional techniques. As such, the video smoke detection system [Wieser *et al.*, 2001] and the infra-red video detection system seem to have large application opportunities as long as they can take advantage of a large enough observation window to operate their necessary image processing.

As performed by the National Institute of Standards and Technology [Cleary *et al.*, 1999], which is about to produce fire signatures and nuisance signatures characteristic of cargo compartment environment, a rigorous analysis of the detection application requirements may help also to isolate more rapidly the most applicable technologies for the designated environment and reduce therefore the development efforts.

2.4 THE INFLUENCE OF INTERNATIONAL REGULATIONS

The international regulations for aircraft fire safety have an immediate impact on the development of F/O detection systems. Indeed, aircrafts will be authorized to land in countries around the world with systems in compliance with the certification rules established by the local authorities. In principle, the local authorities are following the international regulations.

Over the past fifteen years, the Federal Aviation Administration (USA), and most other aviation authorities worldwide have implemented modifications to aircraft fire safety standards [Hill *et al.*, 1998], [Sarkos, 2003]. Those modifications have vastly improved fire safety in transport aviation. The main modifications are explained here.

- The "Seat Cushion Fire Blocking" rule requires that all cabin seat cushions in transport aircraft meet a large oil burner test.
- The "Floor Level Lighting" rule is a requirement for emergency lighting near the floor in an aircraft.
- The "Low Heat/Smoke Release Panel" rule established for the large surface material in an aircraft cabin (ceiling, sidewall, stowage bins, partitions, etc.).
- The "Radiant Heat Resistant Evacuation Slide" rule is a requirement for the slide to resist the heat from a large fuel fire nearby.
- The "Flight Recorder Thermal Protection" rule. The intense fuel fire test exposure duration was doubled. A low temperature, long duration test requirement was also added.
- The "Cabin Fire Extinguisher" rule requires for the transport aircraft to carry at least two Halon 1211 extinguishers.
- The "Lavatory Smoke Detection/Extinguishment" rule requires smoke detectors in all transport aircraft lavatories as well as a fixed extinguisher in lavatory trash receptacles.
- The "Burnthrough Resistant Cargo Liners" rule requires a severe burnthrough test for ceiling and sidewall cargo liners in inaccessible cargo compartments.
- The "Blanket Flammability" rule, this new flammability test method measures the ignition resistance of airline blankets subjected to a small source.

- The "Cargo Compartment Fire Protection" rule. A major consideration in the issuance of this rule was the potential explosive hazards of aerosol cans carried in passenger luggage and the demonstrated effectiveness of halon fire suppression in controlling cargo fires involving aerosol cans.
- The "Combi Aircraft Fire Protection" rule. This airworthiness directive (AD) ensures adequate fire protection in "combi" aircraft, or aircraft containing both passenger and cargo compartments on the main deck.

The description of these rules brings to the front the importance of the changes of the selected aircraft materials, of the modification in the aircraft interior and also stresses the necessity to follow closely the evolution of the certification tests. The detection system designer will have therefore to adjust the equipment performances to the new environment.

Other influences can also produce big changes. After the 1996 Value Jet accident, the Air Line Pilots Association was pleased to see the FAA requiring both detection and suppression systems in almost all cargo compartments. Specifically, FAA required that airlines convert their Class D compartments that depend on fire containment by limiting the available oxygen via a tight compartment liner into Class C compartments that have both detection systems and extinguishment systems [Blake *et al.*, 1998]. Nevertheless, the association settled that pilots need better and more reliable information about the cargo compartment status [Phillips *et al.*, 1998]. Since it is the heat that presents the greatest threat to the pilot and the continued safety of the flight, the pilots must have this information. This may lead to a very significant market of new detectors for fire monitoring applications.

Still in the cargo compartment, to overcome the unwanted alarm rate, the industry is willing to use multiple sensors. As we have seen previously, this option brings intelligence into the detection system to face the multitude of fire scenarios. However, the certification guidelines for using these types of fire detectors on aircraft do not currently exist [Blake, 2001] but testing is being conducted to define the types of fires that should be detected and the production of smoke, heat and gases from these fires. Here again the designer must anticipate the changes on the fire

detection technology to be induced by outspread certification guidelines.

In 1987, an international treaty, the Montreal Protocol, was established to control the release of materials that cause stratospheric ozone depletion. Under the Protocol, the production of halon fire and explosion protection agents was phased out in all industrialized countries at the end of 1993 [Tapscott *et al.*, 1998]. On aircraft, halon gasses (the term halon is used here to denote Halons 1211, 1301 and 2402) are used for several fire extinction applications. Its ban leads therefore to a profound re-thinking of the co-operation between the detection and extinction systems. There are four general types of fire and explosion protection applications for Halons.

Table 2.4-1 Modes of Fire Extinguishing on large A/C with Halon Gas as Extinguishing Agent

Type of application	Applicability to A/C Fire Protection	Extinction means
Total-flooding	- Cargo Compartments - Engine Nacelles, APU	Halon is discharged into a space to achieve a gas or vapour concentration sufficient to extinguish or suppress an existing fire
Streaming	- Handheld extinguishers - Lavatory Protection	The agent is applied directly onto a fire or into the region of a fire. This is usually accomplished using manually operated portable units
Explosion suppression	- Cargo Compartments	Halon is discharged into a space to suppress an explosion that has already been initiated
Inertion		Halon is discharged into a space to prevent an explosion or a fire from occurring

This illustrates the difficulty to come with a full ban of Halon gases used in extinction application, when moving for example in cargo compartment from a total-flooding protection to a streaming application. At the moment there is indeed no alternative agent to Halon able to reach the requirements while operating in total-flooding mode. Alternatives like Water Misting [Notarianni, 1993], Particulate Aerosols, Inert Gases, Gas Generators or some of their combinations are currently under investigation [Grosshandler, 1995]. One may also notice that a streaming protection system might require putting in place a checking system (a detection system) to monitor the effect of the extinction agent on fire.

The future of Fire Safety is also through Research and Development. We can

partition it in terms of three major areas: Materials, Fire Management and Systems. R&D on Materials consists of the development of improved or new fire test methods and criteria for aircraft materials. Fire Management refers to rapid and reliable detection of aircraft fires and effective fire extinguishment or suppression. Systems addresses the need for the protection of vital aircraft systems from the effects of fire or preventing malfunction of these systems from causing or accelerating the spread of a fire. The three topics may induce the need of new regulations and in turn the need of a redefinition of the detection system requirements.

The types of in-flight fire that can become a problem are those that originate in hidden or inaccessible areas [Sarkos, 2003]. Hidden fires involve materials such as thermal acoustical insulation, and wiring and cable, installed behind the cabin sidewall, above the ceiling and beneath the floor. Investigation of these fires has revealed extensive contamination in hidden areas, for example, thick grease dust on cable, stained insulation battery, etc. Work is clearly needed to address the contamination problem in hidden areas.

Apart from the Cargo Hold Compartments situation, most aircraft in-flight fires are electrical in nature and are usually controlled before having any effect on flight safety. Arc tracking failures have occurred in civilian and military aircraft. Electrical faults from frayed wires have also occurred in service because of failed or improper securing of wiring and cable. Therefore, more comprehensive test methods may be required for electrical wiring as well as improved methods for securing and protecting cable and wiring. Another aspect of the problem that needs to be investigated is the effect of aging or time in service.

2.5 NEW TECHNOLOGIES FOR NEW AIRCRAFT PROGRAMS

The lessons learnt from accidents are drivers for the design of future aircrafts. Additional considerations include emerging technology, fire safety improvements and the quality of the functionalities proposed to the airlines and passengers. Also, past regulatory activities/interior design changes alter the perception of the need for R&D and impact on cost/benefit computations. The goal is however to make aircraft as fire-safe as is technologically possible.

The need for faster and more intelligent decision making regarding the presence or absence of a fire threat has become more acute in a number of critical applications [Grosshandler, 1998a]. The following questions might help to refine the strategy in terms of new development for a F/O detection system:

- What fire detection systems are currently being used in the commercial aircraft industries?
- What are the industries' definitions of a "false" or "nuisance" alarm, and what are the primary sources?
- Are new, low-unwanted-alarm technologies emerging that are practical for use aboard aircraft?
- What physical environmental conditions (e.g. temperature, pressure, moisture, particulate levels, air flows, gas concentrations...) are most likely to be confused with the early stages of a fire on board an airplane?
- What activities or events are most likely to generate these conditions (e.g. maintenance, cleaning, normal heating and cooling, rain, human presence, operation of adjacent equipment...)?

Conducted in reference to the environment the detection system has to scrutinize and in reference with the specific requirements of the aircraft program, the analysis aims to define the "environment of detection" combined to the "most-suitable-technology".

One may think therefore to new approaches, to new kinds of fire detection [Freiling,

2001]. Currently, advanced fire detection technologies are targeting the recognition of fire or overheat signatures. In the Cargo Hold or in inaccessible areas of the aircraft; the new technologies under consideration include gas sensing with semi-conducting metal oxide sensors in thick- or thin-film technology or/and electrochemical cells; the optical smoke sensing with light attenuation or back-scattering devices; near infra-red and visible light sensing with CCD and/or CMOS. However, the gas sensors are, for instance, particularly sensitive to the nuisance alarm spectrum of the cargo hold environment.

Although the majority of early warning fire detection applications can be covered by photoelectric and ion detectors, these technologies are too sensitive for very dirty, dusty or wet areas [Conforti, 1998b]. Use of these standard types of fire detectors in harsh environments would result in a high occurrence of nuisance alarms. A "harsh environment detector" needs to provide early detection while eliminating nuisance alarms and the need for frequent maintenance. To do this, in areas at low level of maintenance, or "hidden areas", these detectors need to be provided with protection from airborne particles such as dust, Water Mist (WM), insects, aerosols, fuel and hydraulic vapours.

With regard to the engine dry bays and engine compartments, the harsh environment makes accurate fire detection and response a difficult task. Fires on-board aircraft may be caused by impacts of projectiles, electrical sparks, etc. The combination of heat, fumes, and oil from the hydraulics, fuel lines, etc., inside an aircraft dry bay can account for most false alarms or failures of conventional smoke/heat sensors [Foo, 1996]. A CCD camera is reported as offering real-time detection in these environments. Using a set of heuristics derived from a combination of histogram and image subtraction analyses, it is possible to detect and categorize life-threatening fires from non-fire events.

In the same movement of extending the demand for smarter detection systems, the extinguishing systems seem to require more control so as to provide in real-time the

efficiency of response to the fire threat and so provide to the aircraft crew information to react accordingly. Besides, some fire extinguishing agents are performing enough to question the necessity of a detection system and are therefore narrowing the perimeter of investigation for a given fire protection application.

The vulnerability of the upper deck to post-crash fire in future double-decked aircraft carrying more than 600 passengers such as the Very Large Civil Transport (VLCT) A/C is a major concern of aircraft manufacturers and regulatory authorities. The anticipated difficulty of exercising an emergency evacuation from high elevations would become even more life threatening if a chimney-like effect created an unusually hazardous fire on the upper deck. Enhanced fire protection of the VLCT upper deck would tentatively encompass three R&D activities. First is the development of fire-stops and barriers to prevent upward spreading of the fire from the lower deck. Second, is the protection of the upper deck floor from the effects of a fire from below. Finally, an enhanced fire protection of the upper cabin interior based on the effectiveness of improved fire resistant materials has to be analysed against on-board cabin water spray system [Sarkos, 2003].

Another objective is to minimize or to eliminate fire hazards associated with aircraft systems. Past accidents and full-scale tests indicate that improvements in oxygen and hydraulic systems could improve both post-crash and in-flight fire safety. Near term R&D is required to determine what improvements are feasible to prevent or minimize hydraulic fluid fires, while methods of reducing the quantity of oxygen accidentally released should be explored (e.g., flow restrictors, fuses or solid oxygen generators). The ultimate answer may be an oxygen generation system utilizing gas separation membrane technology, which would probably require a long term R&D program. These efficient and compact membrane devices can separate an incoming air stream into two existing streams with the composition of one of them being a nitrogen enriched air mixture that is approximately 95 percent nitrogen and 5 percent oxygen. The aircraft nomenclature for these systems includes On-Board Inert Gas

Generating Systems (OBIGGS) and On-Board Oxygen Generating System (OBOGS). An OBIGGS installation would have two potential inerting applications. The first is fuel tank inerting in the High Speed Civil Transport (HSCT) as well as in current A/C if deemed appropriate (elevated skin temperatures on the fuselage and wings is a major concern, particularly as it relates to fuel volatility). An OBOGS installation, if it had the capacity for continuous on-demand supply for aircraft passengers, would eliminate fire hazards posed by current systems employing bottle oxygen or solid oxygen generating canisters.

Challenges of new aircraft programs are also to limit the risk of unnecessary passenger evacuations and undue emergency landings. This category of requirement requires more intelligence in the detection system to reduce the nuisance alarm rate and in taking stringent precautions in the integration of the on-board detectors or in identifying specificities of the detection technology itself to decrease the false alarm rate.

The question is also now for potential suppliers to be able to activate a development project as soon as a new A/C program has been activated. A spiral development process, which was successfully utilized on the Boeing 777 avionics controller, emphasizes modelling and prototyping, and promotes early definition and validation of design decisions [Black, 1998]. The rapid prototyping spiral development process includes three major loops: Virtual Development, Rapid Prototyping, and Flight Development.

The number of on-board sensors interfacing with the cockpit avionics shows that there is an advantage to push ahead the integration of equipment on busses for data transfer. The flow rate of data to be transferred is growing from aircraft to new aircraft. The Boeing 777 aircraft is the first commercial aircraft to implement an optical fibre On-board Local Area Network (OLAN), the ARINC 636 [Anderson, 1997]. It is localized in the flight deck, in the electronic bay, and as a Cabin LAN overhead of the passenger cabin.

2.6 DETECTION SYSTEMS FOR RETROFIT OR NEW APPLICATIONS

The retrofit of on-board F/O detection system intends to realise a virtual elimination of false warnings, an increased operational readiness through reliability, decreased operational costs, a re-established crew confidence in flight safety.

As an example, the retrofit on A/C has addressed the replacement of the originally used electronic type sensing elements for the engine F/O warning system. These systems are known to provide a high frequency of false warning incidents and require extensive maintenance to remain serviceable. A modification program to remove the electronic F/O warning systems was launched to replace them with a pneumatic type safety system. Electronic and pneumatic F/O detectors differ in the fact that they are operationally opposite. The current electronic systems have an operational logic for the true alarm signal to the pilot. This logic operates the same whether there is a true alarm or false alarm. Both alarms are the result of resistance decreases in the sensing wire. Damage or simple in-service deterioration of the sensor, such as kinks, nicks, severe bends, or moisture can result in falsely signaled alarms. The wide use of the pneumatic detector is for aircraft and crew protection and is solely based on the improved reliability over electronic systems, while minimizing parts consumption and maintenance man-hours.

As we can see, the previous modification is targeting mainly a decrease of the number of false warnings. As a second example, a wireless smoke detection and fire suppression system has the prime objectives of reducing installation time, of lowering overall costs and weight. The complex problem of having to install a smoke detection and fire suppression system during a heavy maintenance cycle is over. The wireless system can be installed during short inspection interval. Airlines and other installers have calculated anywhere from 40 to 60 percent fewer installation man-hours for the wireless system versus a wired system. However, with each added functionality (here the functionality of wireless-transmitting the signals) coupled

with the fact of having an embedded battery per detector will likely bring additional failure modes and may reinforce the number of false warnings. Targeting a retrofit market, we will therefore keep in mind that the performance improvement has to be reached using a mastered and simple technological principle, which will avoid operational unexpected failure conditions leading to unwanted alarms.

A third example will lead to examine the case of a new detection technology. This new detection technology associated to the measurement and the associated signal processing is also suggested to be part of a confirmation system in the Cargo Hold [Boucourt, 2001]. The detection system, a camera working in the near infrared, aims to detect all the characteristics of a fire: hot spots, flames, smoke, and radiations. However, the camera needs to be in a position where the all cargo compartment can be examined. The small gap between the ceiling of the cargo compartment and the top of the containers will here be a major disadvantage for this technology. Besides, maintenance operations will here be necessary so as to guarantee a clean camera window, and not generate non-fire events or not degrade the detection performances of the system. Here, as a lever to access retrofit applications, the improvement direction is clearly to focus on the widening of the detection spectrum compared to current systems, unfortunately at the cost of neglecting the stringency of the environmental conditions like for instance the diversity of the loading procedures and the diversity of aerosols potentially present in cargo compartments.

It is possible to draw a status of the current potentialities for F/O detection improvement per operational zone on aircraft.

On Figure 2.6□1, a "Very Early Detection" is considered as a detection taking place strictly less than a minute after a F/O event occurs. The necessity to have a "Danger Localization" is coming from the fact that this additional functionality could permit isolating zones in the A/C where F/O has to be fought and/or could shorten the checking/repair operation durations with a preliminary in-flight diagnostic. "Post-Monitoring of F/O" is more than a "nice to have" but will help the pilot to take the

best decision at the right time. The field "[DS+] or [DS1 <+> DS2]" is about all possible improvements of the current detection systems, which would not be "Very Early Detection", "Danger Localization" or "Post-Monitoring of F/O". Feasible ameliorations from the current detectors or improvements will be done by the adjunction of a complementary detection system to potentially reduce the number of nuisance alarms.

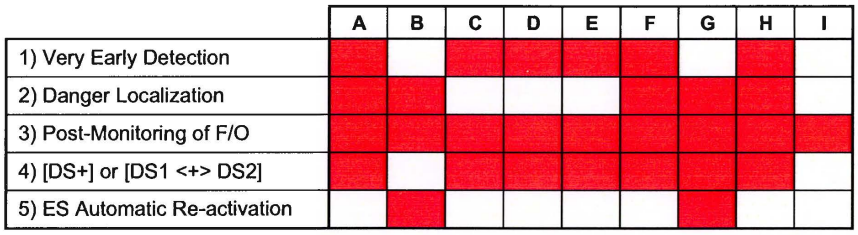

Figure 2.6-1 Fire safety and retrofit requirements
A: Engine — B: Cabin — C: APU — D: Cockpit — E: Landing Gear
F: Wing — G: Cargo Hold — H: Hidden Area — I: Electronic Bays
Spreading of the "nice to have" or of the required improvements as a function of the A/C Area

"ES Automatic Re-activation" highlights the possibility that the pilot could not be the prime decider in a re-activation of the Extinguishing System and addresses also the question of a change from a total flooding extinction to a zoning suppression.

In the frame of this work, we will therefore focus on the definition of a system, to improve simultaneously the key parameters of a good retrofit operation. This means to reduce the maintenance burden and the unwanted alarm rate while bringing additional interesting detection functionalities and keeping the technology simple as much as possible.

2.7 GENERAL REQUIREMENTS TO EQUIPMENT DESIGN AND INDUSTRIALISATION

The critical path to present to aircraft manufacturers an outstanding F/O detection system involves gaining a complete understanding of the international standards and a good knowledge of the internal system description process from the concerned aircraft manufacturer.

Although the joint aviation requirements JAR-25 [Joint Aviation Authorities, 1994], dedicated to large airplanes, aims to minimize certification problems, and also to facilitate the export and import of aviation products, it should be borne in mind that an importing country may require equipment additional to those in the JAR-25 for operational purposes. In other words, this means that a supplier, while designing and manufacturing has to take into account all additional requirements from the civil aviation authorities of the different countries ordering the aircraft. The compliance to the international directives is obviously more easily reached when a close development partnership exists.

Having the Airbus process as an example, on one hand, we see the clear definition of requirements and guidelines for the system design by the airframe manufacturer or his delegated system designer. These requirements and guidelines address product, process and documentation issues and are joined together in a reference document named ABD0200 Airbus directives and procedures [Airbus S.A.S., 1997].

On the other hand, another reference document called ABD0100, Equipment – Design – General Requirements for Suppliers [Airbus S.A.S., 1998] aims to define the general requirements to be addressed by the suppliers of the equipment for use in Airbus aircrafts. These requirements are applicable to equipment design and industrialisation in parallel with the purchaser technical specification, PTS, from the aircraft manufacturer and are specific to that equipment.

The PTS writing is part of the procurement process, which targets to involve closely

the supplier in all design decisions and changes. The suppliers are approached by Airbus with a Request for Technical Information, RFTI, which informs about the basic functionalities the system has to fulfill, which asks to sign a non-disclosure agreement document, to release some preliminary technical concepts and to provide a Rough Order of Magnitude (ROM) for cost figures. A Request For Information, RFI, addressed to the same potential suppliers, will bring the complementary information on the technical proposals, on the budgetary cost estimates and on the key business terms. These two phases last usually not more than 6 months and end with the creation of a vendor short list. Then comes the Request For Proposal, RFP, which will intensify the relationships between Airbus and the pre-selected suppliers along more than 4 months of "Plateau Phase", which sees Airbus and supplier specialists co-located and working together. The general conditions of purchase, the detailed technical proposal, the checking of the compliance to the General Requirements for Equipment and System Suppliers, GRESS process, a price agreement between the two parties and the contractual terms agreed on specifications, qualification and certification tests are also part of this procurement phase. This phase ends with the signature of the contract and starts the development and industrialization phase, where costs, weight, and safety and reliability becomes the prioritized concerns. The qualification and certification test procedures will be also supported by documents like for the Environmental Conditions and Test Procedures for Airborne Equipment, the DO-160D [EUROCAE, 1997], and for the Software Considerations in Airborne Systems and Equipment Certification, the DO-178B [EUROCAE, 1992].

These details stress the fact that the tighter and tighter aircraft program development timeframe means for the suppliers to have constantly a product development strategy available in phase with the improvement wishes of the customer. This compulsory reactivity needs a very good understanding of the aeronautic design and industrialization processes and more and more a self-funding capability to support the non-recurrent cost involved inherent to the development process.

2.8 CONCLUSION

The review of the consequences of a F/O detection system malfunction and of the complexity to discriminate a F/O situation, from operational conditions interfering with the detection system alarm process show that for some A/C areas there is a clear need to improve the F/O detection performances or for other areas to introduce F/O detection capabilities.

A status of the probability of accidents / incidents as a function of the detection area is taken to guide the technology selection assuming logically that the stringency of the environment defines in part the technology to consider. For a given detection system, in a given aircraft environment, we define separately different families of F/O events, where the number of events per family is taken as:

A: false warnings (unwanted alarms).
B: F/O situations detected correctly and not leading to an A/C accident.
C: F/O situations detected correctly and leading to an A/C accident.
D: F/O situations without alarm and leading to an A/C accident.
E: F/O situations without alarm but not leading to an A/C accident.

$$\eta_D = \left[\frac{B+C}{B+C+D+E}\right]$$

Equation 2.8-1 Detection system efficiency
Number of cases where the detector has correctly detected, out of the full number of real fire/overheat situations.

$$P_{fa} = \left[\frac{A}{A+B+C}\right]$$

Equation 2.8-2 False alarm probability
Number of cases where the detection system has detected a fire/overheat when no danger was ever confirmed, out of the full number of warnings carried out by the detection system.

$$P_{nd} = \left[\frac{D+E}{B+C+D+E}\right]$$

Equation 2.8-3 Non-detection probability
Number of cases where the detector has not detected a real fire/overheat, out of the full number of real fire/overheat situations.

The accidents following a false alarm event (no fire or overheat situation) were not considered here.

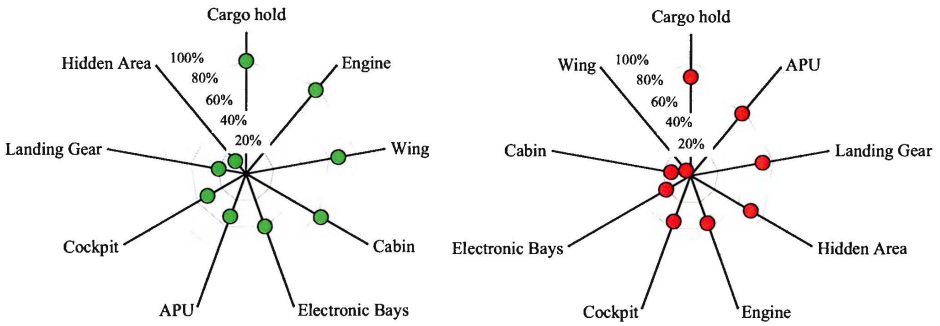

(a) detection system efficiency **(b)** false alarm probability

Figure 2.8-1 Detection system performances per given A/C environment.

As an example the detection system of the cargo hold presents a detection efficiency of 80% (Figure 2.8-1, (a)) were on Airbus A/C a real fire never remained undetected within the delay of one minute (Figure 2.8-1, (b)) imposed by the JAR/FAR 25.85 [Schmoetzer, 2001]. The false alarm rate calculated here is particularly low in comparison with analysis coming from other databases less focused on false alarms leading to dangerous incidents. It is the case, for instance, of the analysis carried out by Mr. David Blake from the NIST, who reported about 200 false alarms for every alarm due to verified smoke source [Blake, 2000] in US registered aircraft.

The unwanted alarm rate is the first parameter to be analyzed to measure the success of the integration of a detection system for a specific application. The key characteristics from each aircraft zone and the relevant regulations will drive therefore the technology selection.

Hence, the next step is to isolate a technology that offers a low unwanted alarm rate using a more reliable spectrum of detection (either a larger detection spectrum, potentially using a multi-criteria algorithm, or a detection spectrum that is more de-correlated from the operational environment). This technology will be able to be brought to maturity in phase with the development timeframe of new large aeroplanes or with the retrofit operations supported by the civil aviation authorities.

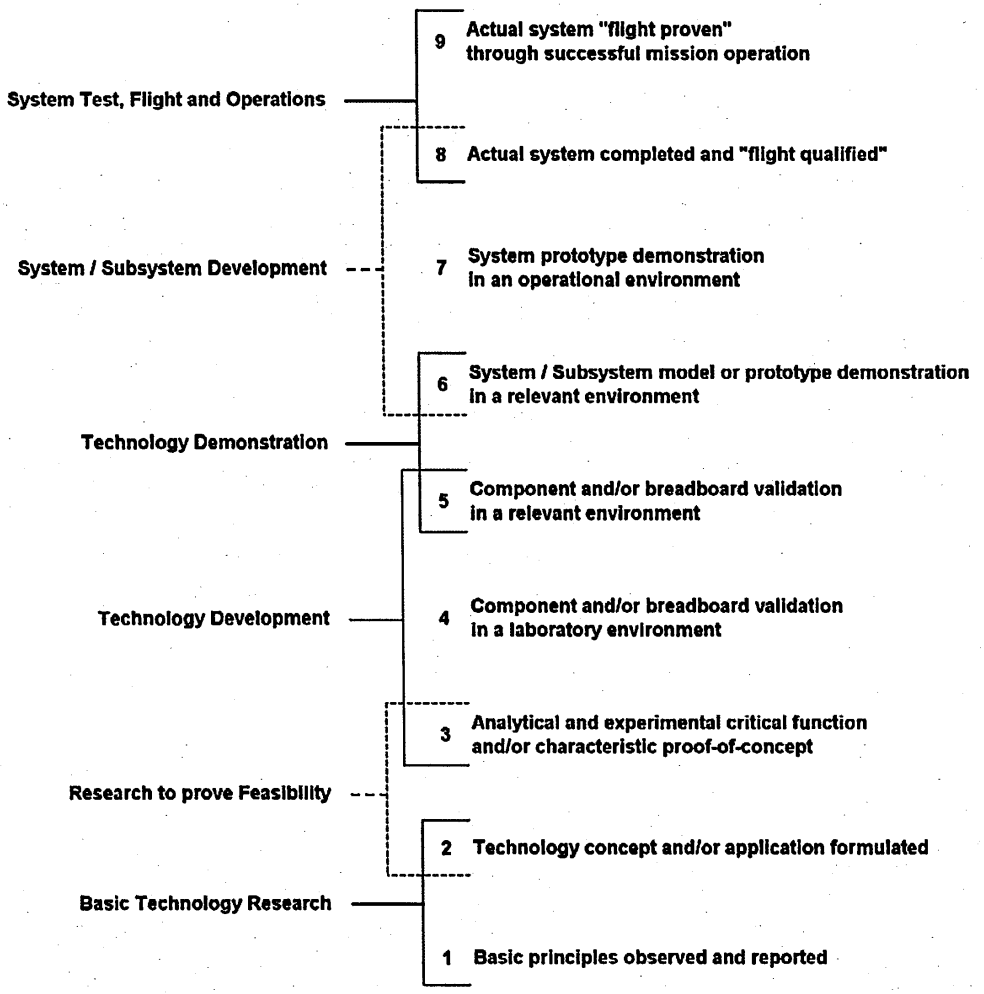

Figure 2.8-2 Technology readiness levels

The technology readiness levels have been defined by British Aerospace Defence Military Aircraft Division and are considered as being applicable to a technology evaluation for commercial aircraft.

So as to reach stage 8 as quickly as possible(Figure 2.8-2), "System/Subsystem Development – Actual system completed and flight qualified", we will evaluate further the technologies having a "technology readiness level" equal or bigger than 2, "Basic Technology Research – Technology concept and/or application formulated".

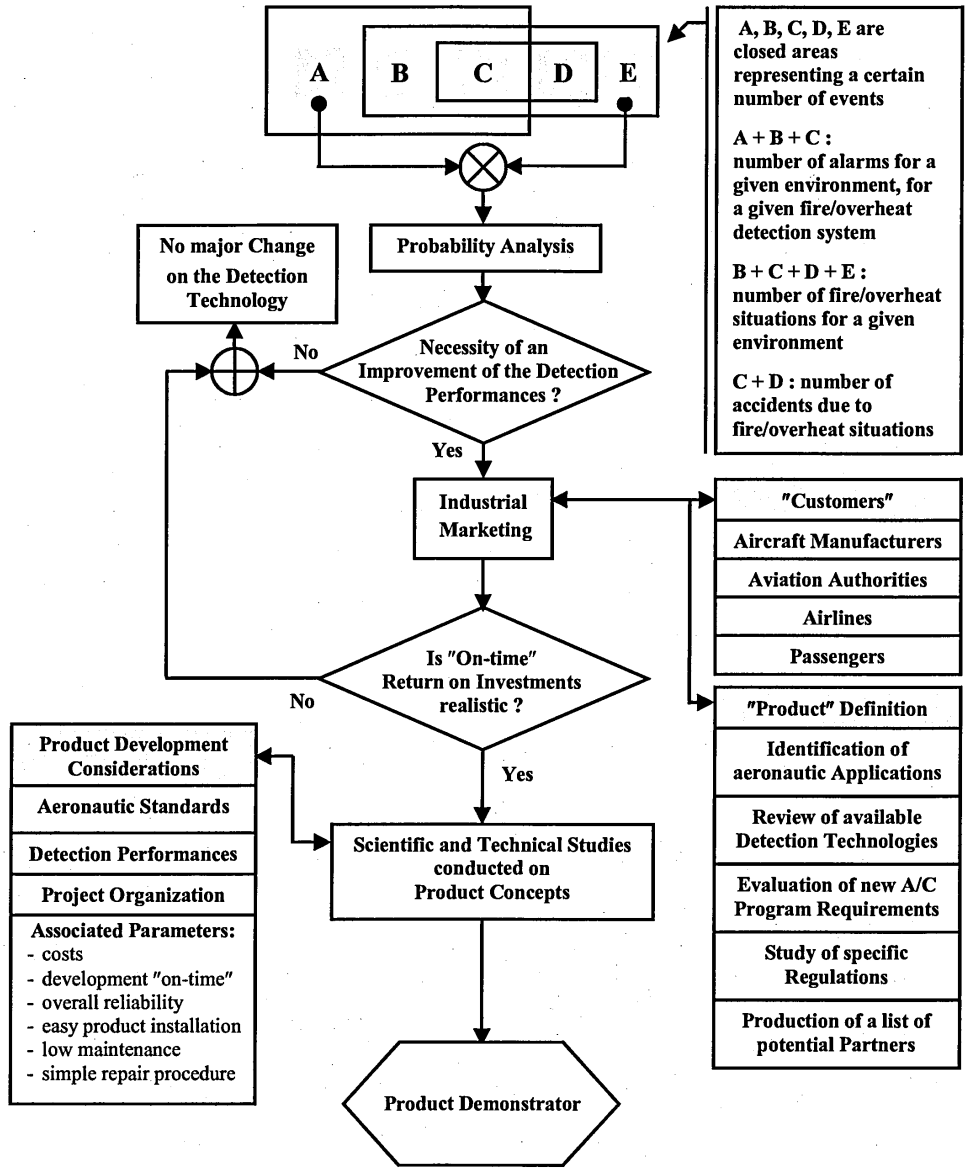

Figure 2.8-3 Analysis Process for the Development of a Fire/Overheat Detection System

Assuming than the "On-time Return on Investments" will be realistic (Figure 2.8-3), the following work will demonstrate the setting of a "Product Demonstrator".

REFERENCES

Airbus S.A.S. ABD0200. Requirements and Guidelines for the System Designer. Issue B. 1997.

Airbus S.A.S. ABD0100. Equipment - Design - General Requirements for Suppliers. X.ABD, issue D. 1998.

Anderson, D. E. "777 Optical Local Area Network". 0-7803-4150-3/97 1997 IEEE. 1997.

Black, R. H. "Rapid Development of Avionics Systems". 0-7803-5086-3/98 1998 IEEE. 1998.

Blake, D. "Aircraft Cargo Compartment Smoke Detector Alarm Incidents on U.S.-Registered Aircraft, 1974-1999". DOT/FAA/AR-TN00/29. Ed. U.S. Department of Transportation, Federal Aviation Administration. 2000.

---. "Initial Development of improved Aircraft Cargo Compartment Fire Detection Certification Criteria". AUBE'01. 12th International Conference on automatic Fire Detection. Edited by: National Institute of Standards and Technology. 2001.

Blake, D.; O'Sullivan, J.; Hammann, S.; Kolleck, M., and Cleary, T. "Aircraft Cargo Area Fire Detection". Nuisance Alarms in Aircraft Cargo Areas and Critical Telecommunications Systems: Proceedings of The Third NIST Fire Detector Workshop. Edited by: National Institute of Standards and Technology. 1998.

Boucourt, G. "Two dimensional multi detection fire sensor, system architecture & performances". AUBE'01. 12th International Conference on Automatic Fire Detection . Edited by: National Institute of Standards and Technology. 2001.

Bukowski, R. W. and Reneke, P. A. "New Approaches to the Interpretation of Signals from Fire Sensors". Sensors Expo. Proceedings. Edited by: National Institute of Standards and Technology. 1999.

Chen, Y.; Serio, M. A., and Sathyamoorthy, S. "Development of a Fire Detection System using FT-IR Spectroscopy and artificial neural Networks". Sixth International Symposium. Edited by: International Association for Fire Safety Science. 1999.

Cleary, T. and Grosshandler, W. Evaluation of Fire Detection Technology for Suitability in Aircraft Cargo Compartments . Ed. National Institute of Standards and Technology. 1999.

Conforti, F. "Fewer unwanted Alarms: Technology and Education are helping to reduce the Occurence of unwanted Fire Alarms". Annual Conference on Fire Research. 1998a. Vol. NISTIR 6242.

---. "Detection in difficult Environments". Annual Conference on Fire Research. Edited by: National Institute of Standards and Technology. 1998b. Vol. NISTIR 6242.

EUROCAE. EUROCAE ED-12B / RTCA DO-178B. Software Considerations in Airborne Systems and Equipment Certification. 1992.

EUROCAE. EUROCAE ED-14D / RTCA DO-160D. Environmental Conditions and Test Procedures for Airborne Equipment. 1997.

Fitzgerald, K. "Probing Boeing's crossed connections". IEEE Spectrum. 1989. pp.30-35.

Foo, S. Y. "A rule-based Machine Vision System for Fire Detection in Aircraft dry Bays and Engine Compartments". Knowledge-Based Systems. 1996. Vol. 9. pp.531-540.

Freiling, A. "New Approaches to Aircraft Fire Protection". AUBE '01. 12th International Conference on Automatic Fire Detection. 2001.

Gottuk, D. T.; Peatross, M. J.; Roby, R. J., and Beyler, C. L. "Advanced Fire Detection using Multi-Signature Alarm Algorithms". AUBE '01. 12th International Conference on Automatic Fire Detection. 1999.

Grosshandler, W. L. "In Search of alternative Fire Suppressants". Symposium on thermal Science and Engineering in Honor of Chancelor Chang-Lin Tien. Edited by: National Institute of Standards and Technology. 1995. pp.275-282.

---. "Nuisance Alarms in Aircraft Cargo Areas and Critical Telecommunication Systems". Nuisance Alarms in Aircraft Cargo Areas and Critical Telecommunication Systems: Proceedings of The Third NIST Fire Detector Workshop. 1998a. Vol. NISTIR 6146.

---. "Evaluating Fire Detection System Response to Nuisance Sources". Nuisance Alarms in Aircraft Cargo Areas and Critical Telecommunications Systems: Proceedings of the Third NIST Fire Detector Workshop. Edited by: National Institute of Standards and Technology. 1998b.

Hill, R. G. and Blake, D. R. "A Review of Recent Civil Air Transport Accidents/Incidents and their Fire Safety Implications". Edited by: Federal Aviation Administration. 1998.

Joint Aviation Authorities. JAR-25. Large Aeroplanes. Ed. CAA. 1994.

Klose, J. and Siebel, R. "A Fire Detection Algorithm using Second Order Statistics". Fire Safety Science: Proceedings of the third International Symposium. Edited by: Fire Safety Science. 1991. pp.943-953.

Mangon, P. "Fire Detection for Aircraft Cargo Compartments, Reduction of False Alarms". AUBE '01. 12th International Conference on Automatic Fire Detection. 2001.

McAvoy, T. J., Milke, J., and Kunt, T. A. "Using Multivariate Statistical Methods to detect Fires". Fire Technology. 1996. Vol. 32. 1. pp.6-24.

Muir, H. "Airplane of the 21st Century: Challenges in Safety and Survivability". Cranfield University. Http://www.gwu.edu/~cms/aviation/track_i/muir.htm. Access Date: 2003.

Murray T. M. "Airplane Accidents and Fires". Chapter: "Improved Fire- and Smoke-Resistant Materials for Commercial Aircraft Interiors: A Proceedings". Edited by "National Academy Press". pp.7-24. 1995.

Notarianni, K. A. "Water Mist Fire Suppression Workshop Summary". Fire Research Today, SFPE Bulletin. 1993. pp.8-9.

Phillips, T. and Huggins, P. "A Perspective From the Cockpit". Cabin & Fire Safety. Edited by: Accident Survival Committee. Air Line Pilots Association. 1998.

Rupp, D. "crashDATABASE.com, Commercial Aviation Accident Database". Http://www.crashdatabase.com. Access Date: 2003.

Sarkos, C. P. "Future Trends in Aircraft Fire Safety R&D". FAA, Federal Aviation Administration, Fire Safety Section. Http://www.gwu.edu/~cms/aviation/track_i/sarkos.htm. Access Date: 2003.

Schmoetzer, K. "Aircraft Fire Detection: Requirements, Qualification and Certification Aspects". AUBE '01. 12th International Conference on Automatic Fire Detection. 2001.

Tapscott, R. E. and Speitel, L. C. "Halon Replacement Options for Aircraft". International Aircraft Fire and Cabin Safety Research Conference. Edited by: DOT/FAA/William J. Hughes Technical Center, USA. 1998.

Taylor, A. F. "A Review of Fire Related Accidents, 1985-1995". AGARD Symposium on Aircraft Fire Safety. 1996.

The Federal Aviation Administration. "Accident/Incident Database System". Https://www.nasdac.faa.gov. Access Date: 2003a.

The Federal Aviation Administration. "Recommended Safety Management Process". Improving the Continued Airworthiness of Civil Aircraft. Http://bob.nap.edu/html/airworthiness/ch4.html. Access Date: 2003b.

U.S. Department of Transportation. "APPENDIX IX. Accidents, Fatalities, and Rates, 1975-1996". U.S. General Aviation. National Transportation Library. Http://www1.faa.gov/docs/J-AP9.doc. Access Date: 2003.

Ugarte, M. F., Zequeira, R. I., and Lopez, F. "An approach for the compensation of the background

variability in fire detection systems". Infrared Physics & Technology. 2001. Vol. 42. pp.23-30.

Warren, K. and Cherry, R., "Fuselage Hardening for Fire Suppression: Safety Benefit Analysis based on Past Accidents". R. G.W. Cherry & Associates Limited. Hertford, England. 1998.

Wieser, D. and Brupbacher, T. "Smoke Detection in Tunnels using Video Images". AUBE'01. 12th International Conference on Automatic Fire Detection. Edited by: National Institute of Standards and Technology. 2001.

Yan, S.; Wang, S., and Dou, Z. "An Energy Model in Fire Detection and Integrated Analysis on False Alarms". AUBE '01. 12th International Conference on Automatic Fire Detection. 2001.

Technology Review and Principles of Selection

3.1 Review of potential applications for a DTS 41
3.1.1 Non-pressurized environment 43
3.1.1.1 Bleed leak detection [BLD] 43
3.1.1.2 Engine fire detection [EFD] 43
3.1.1.3 De-icing system control [DSC] 44
3.1.1.4 Landing gear overheat detection [LGD] 45
3.1.2 Pressurized environment 46
3.1.2.1 Thermal cargo monitoring [TCM] 47
3.1.2.2 Wire fire/overheat detection system [WFD] 47
3.1.2.3 Cabin temperature control [CTC] 48
3.1.2.4 Hidden area fire detection [HAD] 49

3.2 Review of potential detection technologies 50
3.2.1 Ultrasonic waveguide 51
3.2.2 Electrical time domain reflectometry 52
3.2.3 Distributed temperature system using discrete temperature sensors 53
3.2.4 Optical distributed temperature system 53
3.2.4.1 Raman OTDR 54
3.2.4.2 Raman OFDR 55
3.2.4.3 Brillouin scattering 56
3.2.4.4 Bragg gratings 57
3.2.4.5 Polarisation OTDR 58
3.2.4.6 OTDR using liquid core fibre 59
3.2.4.7 Other optical distributed temperature sensing systems 59
3.2.5 Other non optical technologies 61
3.2.6 Temperature / overheat detection system overview of aircraft suppliers 62
3.2.7 Summary of current measurement characteristics 62
3.2.7.1 Measurement selection criteria 63
3.2.7.2 Pre-selected technologies 64

3.3 Methodology for technology selection 65
3.3.1 The detection performances compared to the measurement criteria 65
3.3.2 The application requirements compared to the measurement criteria 66
3.3.3 Final technology selection 67

3.4 Raman OTDR versus Raman OFDR 70

3.5 Raman OTDR versus photon counting 73

3.6 Single pulse versus correlation OTDR 75

3.7 Conclusion 77

In this chapter, a number of technologies are presented in detail as potential DTS systems for aeronautic applications. The use of measurement selection criteria as minimum requirements for a technology to be further analysed put the number of available industrial technologies to five. Describing now the foreseen aeronautic applications for DTS systems, three distinct groups of applications are created. The characteristics of the remaining technologies are then compared with the application constraints. Finally other technological selection criteria are shown and the most appropriate DTS technology is drawn for a group of applications having similar characteristics.

3.1 REVIEW OF POTENTIAL APPLICATIONS FOR A DTS

This section is intended to provide the basic technical requirements in terms of performance and installation in view of a potential aeronautic application of the Distributed Temperature Sensing (DTS) technology. Strictly based on its functioning principle, the DTS technology could be considered for numerous aerospace uses. The following applications will be considered in the frame of the evaluation:

1) Bleed Leak Detection [**BLD**]

2) Engine Fire Detection [**EFD**]

3) Thermal Cargo Monitoring [**TCM**]

4) Wire Fire Detection [**WFD**]

5) Cabin Temperature Control [**CTC**]

6) Hidden Area fire Detection [**HAD**]

7) Landing Gear overheat Detection [**LGD**]

8) De-icing System Control [**DSC**]

There are no well-established requirements for such systems to date. The performance and installation requirements as defined below, are based on those currently known for applications 2 and 3 and anticipate possible additional requirements that can be expected for applications 4 through 8. In general, the DTS system shall be designed to eliminate false warnings; reduce the number of components to a minimum; provide fast positive checks and troubleshooting procedures; allow easy installation. It is possible to isolate several characteristics that the DTS system should have regardless of the application, both for the control unit and the sensing element.

When the Product is considered as a stand-alone system including its controller and the sensing element (SE), the DTS Control Unit (DTS_CU) shall have a size below 3 MCU, a weight below five kilograms and use for example typical aerospace connectors such as ARINC 600. The DTS system operation shall not be affected by

mechanical damages to the Sensing Element (SE) such as twists, flattening, dents, kinks, crushing or flexion. The standard "EUROCAE ED-14D/RTCA DO-160D Environmental Conditions and Test Procedures for Airborne Equipment" will be taken as a reference for the definition of the system environmental conditions.

The sensing element are those ruggedized cables or wires utilized to sense the overheat condition or monitor ambient temperature changes. The maximum individual SE length shall range, depending on the application, from 0.3m to 300 meters and the total maximum SE length shall range, depending on the application, from 20 meters to 300 meters. The number of connectors necessary should be typically comprised between 1 and 30. The SE cross-section diameter shall range between 2mm and 10mm. For existing applications 2 and 3, the SE shall withstand, with no degradation in performance or reliability, a minimum bending-radius of 25mm. The SE shall be designed to that any point along the element may undergo a minimum of 10 cycles of 0 to 90 angular degree bends without deterioration. In the case of a threshold DTS application, the "sampling interval" might indicate the minimum length of sensing element when heated at a test temperature (test performed to check the time necessary for the system to show an alarm in compliance with the temperature accuracy) and/or the maximum length of sensing element to be heated at a detection threshold for the system to show an alarm. The aeronautic applications are evaluated using the following parameters:

1•	System response time (s)	[to be less than 10s]
2•	Temperature accuracy (°C)	[to read typically 1°C steps]
3•	Temperature resolution (± °C)	[not more than ±3°C is the target]
4•	Temperature detection range (°C)	[-55°C to +300°C is expected]
5•	Sampling interval (m)	[from 0.2m to 0.5m is expected]
6•	Temperature points per loop	[100 to 1500 is expected]
7•	Number of sensing loop	[1 to 4 might be required]
8•	SE length per loop (m)	[20m to 300m might be required]
9•	SE bending radius (mm)	[down to 25mm might be required]
10•	Number of connectors per loop	[to be minimized]

3.1.1 NON-PRESSURIZED ENVIRONMENT

The non-pressurized areas for F/O detection are under the responsibility of Airbus France. In the frame of the study we will review the wing and the landing gear F/O protection.

3.1.1.1 BLEED LEAK DETECTION [BLD]

Leakages occur in ducts located all along aircraft wings. A detection system is in used to detect overheat situations within the wings. This application is currently covered in civil and military aerospace vehicles. The detection methods however are based on conventional technology such as pneumatic or eutectic salt cables, which present different characteristics at different temperatures. For these applications the requirements as defined below are based on current aircraft manufacturer requirements. A SE fault (e.g. cable break for example) shall be detected and localized. The failure localization performance shall be in accordance with the alarm localization performance [Jones *et al.*, 1996]. The construction and operation of the wing/body overheat elements are similar to the LanDing Gear (LDG) system. The alarm temperature set points are different for the wing and body overheat detection sense elements. Elements actuate at a first threshold, approximately 124°C for these areas. The SE will have to function over the temperature range -55°C to +250°C, and not be adversely affected by exposure to the ambient temperature range -65°C to +250°C.

3.1.1.2 ENGINE FIRE DETECTION [EFD]

In commercial aircraft, the electronics are positioned to be air-cooled. Because of the high temperatures in jet engines, many sensors are located remotely from the real measurement points, for example hydraulic fluid pressure sensors at the ends of isolation tubes. High-temperature sensors and signal processing electronics could increase aircraft reliability and performance by providing better response in turbine controls, and by eliminating the weight of cooling systems and high-performance

cabling [Berkcan, 1992]. The harsh environment of an engine compartment makes accurate fire detection and response a difficult task. Fires on-board aircraft may be caused by impacts of projectiles, electrical sparks. The combination of heat fumes and oil from the hydraulics, fuel lines, inside an aircraft engine compartment can be accounted for most false alarms or failures of conventional smoke / heat sensors [Lei *et al.*, 1998]. Monitoring accurately the engine temperature profile could lead to both an improvement of the pilot's response speed to a fire (to activate extinguishing nozzles for example) and to facilitate ground maintenance/repair operations by a location pre-analysis of a default. In accordance with the Technical Standard Order TSOC11d, the SE installed in the engine bay detects an integrated average temperature of 260°C and shall detect the crossing of a set temperature threshold of 550°C. The SE shall function over the temperature range -30°C to +150°C and not be adversely affected by exposures to the ambient temperature range -65°C to +150°C.

3.1.1.3 DE-ICING SYSTEM CONTROL [DSC]

Icing of an aircraft occurs when it flies through a cloud of small super cooled water droplets. A portion of the water droplets impinges on the aircraft components and results in ice formation. The growth of ice on an aircraft wing results in a sharp increase in drag and a reduction in lift. This causes deterioration in the aerodynamic performance of the aircraft.

Because ice can be difficult to see, airlines do not always know when de-icing is necessary. Despite all the advances that have made air travel safer than ever, the accumulation of ice on airplane wings continues to be one of aviation's most insidious problems [Sarter *et al.*, 2001]. In the past 25 years, 35 air-carrier incidents worldwide have been attributed to inadequate ground de-icing. Icing was blamed for the 1992 crash of USAir Flight 405, which killed 27 people after a failed take-off in a snowstorm. Still more accidents take place when ice accumulates while a plane is in flight. Some airplanes cannot use engine heat to melt ice, so any ice that accumulates in-flight is removed by pneumatically inflating rubber bladders installed along the

wings. For planes on the ground, maintenance crews use various chemicals to melt ice and prevent it from reforming. Traditionally, crews visually determine whether either de-icing method is needed. However, visual inspection is sometimes unreliable, because ice can be difficult to see. As a result, airlines are increasingly relying on various devices including magneto-strictive, electromagnetic, and ultrasonic sensors to alert them to the presence of ice and the need to implement de-icing measures [Cober *et al.*, 2001]. Ice affects a plane's performance by hampering the wing's lift capability. Even a relatively small amount of ice can have a serious impact on performance; planes can face the threat of chunks of ice breaking off, flying into the engines, and causing extensive damage. Even in cases where accumulation isn't severe enough to jeopardize safety, it still forces the aircraft to burn more fuel to compensate. Though detection of ice is difficult, in-flight icing isn't a significant problem for large, fast commercial aircraft, which use turbine-engine bleed air to melt any ice that might start to form on the wings. Furthermore, the cruising altitudes of these aircraft are generally well above any precipitation, so ice would only be a potential concern during take-off and landings. Ice formation when a plane is on the ground is much more common, affecting aircraft of all sizes and speeds. Airlines normally remove ice from wings by coating them with various de-icing and anti-icing solutions. A distributed temperature detection system able to detect the presence of ice on wing edges shall be analysed [Jackson *et al.*, 2001].

3.1.1.4 LANDING GEAR OVERHEAT DETECTION [LGD]

Landing gear brakes are currently controlled in temperature with thermocouples. The brake temperature indicating system provides the Captain and the flight Engineer / Second Officer brake temperature information [Lockheed-California Company, 1970]. The flight Engineer / Second Officers brake temperature panel displays brake temperature selectable by wheel pair. An amber indicator light comes on when any one brake reaches a temperature of 275°C. A red indicator light comes on when any one brake reaches a temperature of 400°C. When the overheat indicator light comes

on, the brake temperature indicator light on the pilots annunciator panel comes on. Another landing gear temperature detection system is under consideration by tyre manufacturers. Having embedded temperature detection system within tyres would bring substantial improvements to aircraft safety. The possibility would be indeed to monitor the tyre temperature profile so as to be warned as soon as possible and be able to land when a fire/overheat has started. Tyre temperature rise over long taxi rolls have been measured for various operational conditions and may reach up to 200°C after a Rejected Take-off [Bobo, 1985].

The power density and interface temperatures generated at the wear surfaces of carbon-carbon composite aircraft brakes during landing operations have been estimated to be $1MW.m^2$ and 950°C respectively. The power density generated during rejected take-off is $2MW.m^2$ and interface temperatures have been estimated to lie in the range 1300-1500°C; even higher temperatures, exceeding 2000°C, have been cited. This temperature range, combined with the temperature levels described above for warning signals, shows the robustness required for a landing gear temperature detection system. Heat generation in tyres is governed by inelastic energy. This energy is highly dependent on the stress and strain evolution during the tyre deformation process [Kerner, 1986]. These in turn depend on the material properties of the tyre. Therefore, to monitor tyre heat generation, it is necessary to acquire accurate knowledge about the heat transfer rates from tyres to sensors during take-off and landing stages. The installation of a DTS system and the specific LDG environmental conditions are here the major concerns.

3.1.2 PRESSURIZED ENVIRONMENT

The pressurized areas for fire/overheat detection are allocated to Airbus Germany. The areas included in the study are related to the cabin, the cargo compartments, and the zones with low frequency of maintenance operations or the F/O protection for cable bundles.

3.1.2.1 THERMAL CARGO MONITORING [TCM]

As presented earlier [FAA, 1991], a DTS can be a very complementary fire detection system (to smoke detectors) and employed as a secondary detection system in cargo holds and also used to monitor the efficiency of the extinguishing agent against a fire threat [Tanaka *et al.*, 1997].

Since the signing of the Montreal Protocol, extensive efforts have been devoted to the search for Halon alternative(s) to replace Halon 1301 (CF Br), an ozone depleting substance, as a fire suppressant. A comprehensive agent screening and performance evaluation program were conducted in order to identify potential Halon replacements for in-flight aircraft engine nacelle, dry bay and cargo holds fire protection. A DTS system can provide here again [Brite Euram Project, 1995, Brite Euram Project, 1999] the possibility to detect and control a fire in a A340 cargo hold and to activate the Water Mist nozzles selectively where the fire threat is detected in the compartment. All IHRWG works can be cited as references for this application.

3.1.2.2 WIRE FIRE/OVERHEAT DETECTION SYSTEM [WFD]

The parameters leading to an accelerated deterioration of aircraft wire insulation were recognized empirically as moisture, mechanical strain and temperature. The wire tested, identified as MIL-W-81381, uses an aromatic polyimide insulation, which is widely used in electrical wiring systems for aerospace applications due to its high dielectric strength, low weight, non-flammability and high temperature capability. During the aircraft's service life the wire is installed to bend diameters of 1.25mm, relative humidity up to 100% and temperatures to at least 100°C.

The environmental conditions lead to ageing of the wire insulation. Deteriorated cable bundles may produce electrical hazards. The need of a new fire detection system is therefore verified: a Wire F/O Detection system.

Alarm thresholds for heat rates of rise and static temperatures, response time and sampling resolution have to be specifically defined.

A MIL-W-81381 wire was using a tested 400Hz power source to determine the AC corona inception and extinction voltages. The voltages are between $975V^{rms}$ and $1025V^{rms}$. The "time-/-current-to-smoke" test is used to determine the current and duration required to produce smoke from a wire specimen. Smoke shall not come sooner than 45s after a specimen is powered at 40 amps; 10s at 50 amps. Tests to evaluate the heat generation of faulty wires would have to be evaluated in comparison with the wire certification tests, so as to define the alarm temperature (or temperature time derivative) thresholds.

3.1.2.3 CABIN TEMPERATURE CONTROL [CTC]

A well-controlled ventilation system in cabins is determinant for passenger's comfort during a flight. The accuracy of the temperature measurements taken in cabins allows the ventilation system to adjust the temperature regulation [Lehle, 1994]. Thus, the system shall be able to control the cabin ambient temperature [Penrod *et al.*, 1998].

Fatal accidents originating from in-flight cabin fires comprise only about 1% of all fatal accidents in the civil jet transport fleet. Nevertheless, the impossibility of escape during flight accentuates the hazards resulting from low visibility and toxic gases. It is therefore important to use a temperature detection system that measures accurately temperatures and, detects at an early stage the beginning of a fire. A DTS system would be able to fulfil these two needs provided it can be competitive with regard to the existing system cost.

To some extent, this application can be compared to the Thermal Cargo Monitoring [TCM] application but with the system requiring a higher temperature accuracy. The aircraft fuselage is pressurized in flight and has an air distribution system, which provides ventilation jets from the ceiling level air inlets running along the cabin length. A fixed quantity of ventilation air is metered into the cabin and air discharge is handled primarily by pressure controlling outflow valves in the rear lower part of the fuselage. In a Boeing 757, the current maximum fresh air cabin ventilation flow

is $78m^3/min$.

In-flight fires pose three major immediate threats, (i) incapacitation or death of the occupants from toxic gases, (ii) catastrophic damage to the aircraft structure or systems leading to loss of control, (iii) disabling the flight crew's performance of critical functions necessary for flight, landing and evacuation. All three threats have been the cause of significant fatalities in accidents involving in-flight fire. A DTS system would also allow both to control more accurately the ventilation system and to reduce the time necessary for the crew to react in case of a cabin fire.

3.1.2.4 HIDDEN AREA FIRE DETECTION [HAD]

Many aircraft components and structures are manufactured from aluminium alloys. Thermal damage to aircraft can occur due to fire, lightning strikes or through leaking hot air ducting. Some areas in an aircraft can be visited only occasionally for periodical maintenance operations and thus have no easy means of access. Such places will have nevertheless to be controlled in the next aircraft generation. Because corrosion, fatigue increase over time the probability of safety issues in these areas and that a temperature increase is a common outward sign of equipment degradation. DTS system can be particularly adapted for protecting "hidden areas".

The DTS system shall be able to provide an indication in the form of an electrical signal when the temperature rises at a certain rate or overruns temperature thresholds. Alarm thresholds for heat rates of rise and static temperatures, the response time and sampling resolution need particularly to be defined [Dyson *et al.*, 1996]. Some system characteristics especially in measurement performances can be very comparable to those defined for a **[WFD]** DTS system.

3.2 REVIEW OF POTENTIAL DETECTION TECHNOLOGIES

Probes that are useful for monitoring temperature along a line may be divided into four classes according to the type of information that they provide.

Point monitor:

♦ **Class I** provides a measurement of temperature at a specific single position. A single couple of "temperature-location" is supplied (location is defined by the installation). A single alarm signal for temperature threshold crossing might be supplied.

Distributed monitor:

♦ **Class II** provides the magnitude of a maximum/average temperature along a line. This type of sensing system may not be able to provide an evolving maximum/average temperature value but only information such as a temperature threshold crossing.

Location distributed monitor:

♦ **Class III** provides the magnitude and position at which a certain temperature occurs along a line. This type of sensing system may not be able to provide an evolving maximum temperature value but only information such as a temperature threshold crossing at one or several locations.

Location-temperature distributed monitor:

♦ **Class IV** measures the temperature at a plurality of positions, thus providing a temperature profile along a line. Distributed temperature systems being a member of Class IV can be classified either as a quasi distributed system if the sensing element is made up of discrete sensing units, or as a fully distributed system.

3.2.1 ULTRASONIC WAVEGUIDE

Ultrasonic waves are vibrations at a frequency above human hearing, with respect to sensing and measurements. High frequency avoids interference from many audible low-frequency noises due to wind, machinery, pumps and vibration of large bodies. Attenuation often imposes the upper limit on the maximum usable frequency. An active ultrasonic detection system for sensing lines comprises a transmitter to interrogate the medium or the measurand in question. Pulsed transmissions are usually characterized in terms of spectral content, which expresses the intensity, the centre frequency, the pulse duration and the repetition frequency. Modulations include AM, FM and PM. The ratio of amplitude received over for example two different distances allows calculation of the attenuation coefficient. Attenuation includes absorptive, scattering and beam spread losses. The receiver transducer is often the same as the transmitting transducer as in non-destructive testing pulse-echo interrogation.

In dispersive materials or structures, the wave velocities also depend on their respective frequencies much as the speed of light in a glass prism depends on the wavelength of light. The loss in intensity as a function of distance or time depends on beam spread, scattering losses and absorption losses. The sound velocity slightly decreases with temperature increase and attenuation coefficient increase. The sound velocity slightly increases also with pressure increase while the attenuation coefficient is little influenced [Lynnworth L.C. *et al.*, 1970]. The transmission, reflection and mode conversion of ultrasonic waves at a boundary depends on the boundary conditions such as bonded versus lubricated, and on the incident conditions by which is meant wave type, geometry or angle of incidence and, if applicable, the polarization. At the interface of two adjacent media, the sound pressure transmission and reflection coefficients are given in terms of the characteristic acoustic impedance. The spatial resolution of the detection system is function of the interrogating wavelength of an ultrasonic pulse. Resonators generally yield higher precision than time-of-flight systems, but they require transducers responsive over

the full range of resonant frequencies to be sensed, but now, with 1-ns time resolution readily achieved in the MHz region, time of flight is the method of choice.

Schlumberger Ind. Ltd. presents a distributed temperature sensor comprising an elongate ultrasonic wave-guide having a number of zones along its length, each zone having a grating formed on it. This is typically achieved by incorporating uniformly spaced notches or bands (or collars) throughout the zone [Kulczyk, 1990]. The grating spacing in each zone is different, so that each grating reflects a characteristic frequency. This frequency varies as the temperature of the zone varies, so if wide-band ultrasonic pulses are launched into the wave-guide, the temperature of each zone can be determined from the reflected frequencies. This technology is considered as a class IV quasi-distributed temperature detection system.

3.2.2 ELECTRICAL TIME DOMAIN REFLECTOMETRY

The electrical time domain reflectometry may provide an electrical method for monitoring the temperature distribution along a line. The electrical characteristics of the line will fluctuate with temperature [Pal *et al.*, 1989].

The usual representation for an electrical transmission line model consists of incrementally small inductances, resistances, conductances and capacitances. Time domain reflectometry has been used extensively for detection of faults in transmission line, wave-guide and optical fibre systems. In fact radar may be regarded as TDR instrument that uses free space as the propagation medium. A TDR instrument basically consists of a circuit that launches a pulse of energy into a medium and then monitors the launching point for reflected energy. The magnitude of the reflected pulse of energy indicates the size discontinuity in the medium and the time delay of the returned pulse indicates the distance to the discontinuity.

A travelling wave voltage pulse is launched on the transmission line by applying a voltage pulse to the input. From the above analysis, we have found the behaviour of the transmission line in the frequency domain. We can use Fourier analysis to merge

the input voltage waveform in the time domain. The pulse is transformed into the frequency domain and then the transmission line reflection transfer function multiplies the input voltage spectrum. The resulting voltage spectrum is transferred back to the time domain with an inverse Fourier transform. Provided that a temperature sensitive cable is manufacturable to be compliant with the ETDR technology principle, this system can be categorized as a fully distributed class IV DTS.

3.2.3 DISTRIBUTED TEMPERATURE SYSTEM USING DISCRETE TEMPERATURE SENSORS

This sensing technology is using discrete temperature sensors (for example thermocouples) to collect, on an extended area, a number of temperature data and their associated locations. Two main possibilities for signal processing maybe envisaged. Some systems use a bus line or a network of individual temperature sensors, each having an individual link cable so as to collect each point sensor data and/or to communicate with associated transmission units; others use wireless temperature systems. It has to be noticed that optical fibres can also provide discrete measurements along a line. Among others the Bragg grating temperature detection systems that are located along an optical fibre, which can be assimilated to a bus line for discrete temperature sensors. This technology will be described in "3.2.4 Optical distributed temperature system".

The principle will be recognized as delivering the detection performances of a quasi-distributed class IV system.

3.2.4 OPTICAL DISTRIBUTED TEMPERATURE SYSTEM

Sensor systems, which permit monitoring the magnitude of a physical parameter, and also its variation along the length of a continuous uninterrupted optical fibre, offer a powerful and economical means of covering a large number of locations within a significant area.

In the last few years, the advent of digital circuits has caused great progress to be made in measurement and control equipment. Such digital circuits require an increased number of more accurate and versatile sensors for physical quantities of all types. The development of digital systems coincides with the introduction of optical fibres and the opto-electronic transmitting and receiving elements associated therewith. The advantages of such systems are well known: they include a wide bandwidth, electrical isolation, relative insensitivity to electric noise, the ability to withstand extreme temperature changes and explosive or corrosive environments, low weight and small space requirements.

The Raman effect has been employed, due to its temperature dependence. It is an effect where light propagating in the medium is modulated by the material vibrations and rotations at a molecular level. Unfortunately, silica does not have a large Raman scattering coefficient, but its convenience as a fibre optic material does to make overcoming this important difficulty.

3.2.4.1 RAMAN OTDR

The earliest form of distributed sensor was the well-known optical time domain reflectometry (OTDR). In 1980, Rogers suggested for the first time a method for the measurement of the spatial distribution of magnetic and electric fields, pressure, and temperature, using OTDR concepts in conjunction with polarised light sources.

A pulsed semiconductor laser is coupled into a section of fibre via a directional coupler, which serves also to couple the backscattered light fraction, captured and returned via the fibre under test, to the avalanche photodiode detector. For uniform fibres, the detected component of the scattered light varies as the product of the launched energy and the bi-directional attenuation between the source and detector, because the scattering coefficient does not vary significantly along the length. As a result, the method has proved extremely useful for measuring the spatial variation of fibre attenuation. The scattering occurring in both glass- or liquid-cored fibre is

primarily of the Rayleigh type. The Stokes and anti-Stokes signals are filtered and processed separately to reduce the acquisition noise then combined to determine the temperature along the line [Tozaki *et al.*, 1990]. The spatial interval seen is dependent upon the Digital-to-Analog-Convector (DAC) processor clock. Some experiments have been carried out at various wavelength, it is then possible to deduct the Raman backscattered power as a function of the fibre length [Paton *et al.*, 1990]. The analysis of Raman shifted backscattered in a U.V. grade silica fibre using a pump laser at 337nm shows a maximum fibre length to power extinction of about 250m while using a 900nm laser source would potentially achieve few kilometres.

The technology offers several potential for a fully distributed class IV DTS.

3.2.4.2 RAMAN OFDR

This method is essentially similar to the FMCW (Frequency Modulated Continuous Wave) technique used in radar systems. If an FMCW system is operated in backscattering mode in a continuous monomode fibre, the beat signal produced at the detector increases in frequency in direct proportion to the distance from which the light is backscattered. If the detected beat signal is displayed on a conventional electronic spectrum analyser, the power in each frequency increment represents the level of scattered light received from a short section of fibre situated at a distance corresponding to the frequency offset observed [Glombitza *et al.*, 1993].

The probe laser power of frequency f_0 is coupled into the fibre at the position z=0. The light of this laser is sinusoidally intensity-modulated by an electro-optic modulator or by the current of a laser diode. Equidistant modulation frequencies f_{mod} can be used, whereas the probe light is modulated not simultaneously with these different frequencies but one after another. The modulator is driven by a signal generator [Gogolla *et al.*, 1999].

As the frequency-slew rate of current-ramp-driven semiconductor laser diodes may be very high (100 GHz/s is easily achievable) and the frequency resolution of

commercial electronic spectrum analysers is a few Hz or less, the technique has a far superior distance resolution capability than OTDR methods. Resolution predictions are of the order of 1mm, taking into account the reduced velocity of light in the fibre. However, a major potential problem with OFDR is the coherence function of the source, which will modulate the received spectrum and therefore distort any spatial variation of scattering that it is desired to observe. Another approach to the problem uses a variation of the FMCW method, where a frequency-modulated sub-carrier is arranged to amplitude-modulate the source. This removes the problems of source coherence and is applicable to multimode systems, but presents a reduced resolution due to the lower frequency-slew rate possible with electronic sub-carrier systems.

The system is quoted as a fully distributed class IV DTS.

3.2.4.3 BRILLOUIN SCATTERING

Stimulated Brillouin scattering has been proposed initially as a means of enhancing the performance of OTDR field tests, but more recently, the frequency shift of the Brillouin gain spectrum has been demonstrated to be sensitive to temperature and strain, leading to series of elegant experiments on the determination of axial strain, for example in installed cables. In this case, the fibre was interrogated from one end by a continuous wave (CW) source and from the other by a pulsed source, the difference in wavelength between these sources being carefully controlled to be equal to the Brillouin frequency shift (of order 10-20GHz depending on the operating wavelength). The lower frequency wave (which can be CW or pulsed) is then amplified, the gain being dependent on the match between the frequency difference of the two sources and the local frequency shift. From the time variation of the amplified signal, the local gain can thus be determined. Independent calibration of the gain spectrum versus strain or temperature thus allows these measurands to be mapped along the fibre from measured values of the gain along the fibre. One of the keys to this measurement has been the development of the diode-pumped, single frequency, tuneable Nd: YAG ring laser, capable of delivering of the order of 1mW

into single mode fibres with remarkably narrow (5kHz) linewidth.

The fully distributed measurement of strain/temperature is possible [Horiguchi *et al.*, 1995]. Here, a fraction of the optical power launched down a fibre is scattered at some point in the fibre, causing it to change optical wavelength and return towards the optical source. Critically, the wavelength of the returning light depends upon the strain/temperature of the fibre at the point at which the light was scattered.

One solution to de-convolve the strain from temperature is to pass a single fibre twice over the same region in such a way that one section is isolated from the strain and only affected by temperature. This approach makes the installation of the sensing optical fibre cable complicated.

If it is desired to measure strain and temperature simultaneously along the same length of a single optical fibre, then both the amplitude and frequency shift of the Brillouin backscattered light has to be detected. In order to measure the temperature, the ratio of the amplitude of the Brillouin peaks against the Rayleigh peaks is measured and the frequency shift is a measure of the strain at the position from where the light is backscattered [Naruse *et al.*, 1999]. The Brillouin frequency shift is the frequency difference between the pump and the Stokes waves.

The system is quoted fully distributed class IV DTS.

3.2.4.4 BRAGG GRATINGS

A class of the interferometric optical fibre sensor is that of the in-fibre Bragg grating. This system is usually addressed with broadband sources especially when multiplexed systems are considered. The Bragg Grating device consists of a periodic refractive index modulation produced within a length of the fibre core and acts as a multiple reflecting structure. For a structure periodicity of Λ and a core refractive index of n, the condition for which the back reflections from the grating elements are in phase is given by:

$$\lambda_B = 2.n.\Lambda$$

Equation 3.2-1 Bragg wavelength of reflection from a Bragg grating
Λ: grating spacing. n: fibre core refractive index (usually Ge-doped fibre core). λ_B is the associated Bragg wavelength of reflection. Grating reflectivity up to and in excess of 95% is possible with typical line widths of 0,1nm (20GHz).

The grating transmission is complementary to that observed in reflection [Le Gall *et al.*, 1997]. The grating is a band-pass filter in reflection and a notch filter in transmission. The shift in the central wavelength $\Delta\lambda_B$ for a temperature change of ΔT is dominated by refractive index changes in the fibre core [Cavaleiro *et al.*, 1999, Du *et al.*, 1999]. The gratings written by photo-refractive technique are reported to be permanent in nature and are unaffected by temperature changes up to about 300°C. Multiplexing of the Bragg gratings can be provided by tuning each grating element i in a serial quasi distributed array to a slightly different central $\lambda_{B,i}$ and with a $\Delta\lambda = \lambda_{B,i+1} - \Delta\lambda_{B,i}$ for separation large enough to prevent wavelength overlap.

The technology is quoted as quasi-distributed class IV DTS.

3.2.4.5 POLARISATION OTDR

The practical "single mode" fibre must be regarded as a two-mode fibre, with the fundamental mode split into two orthogonally polarised states aligned in directions determined by the symmetry conditions of the fibre. These polarisations travel at slightly differing speeds β_X and β_Y, and the linear birefringence, is given by $\Delta\beta = \beta_X - \beta_Y$. There are many sources of linear birefringence, which depends on the environment of the fibre (lateral pressure, V-groove clamp, free bending, bending under tension, bending over rough surface under tension, external electric field, optical electric field, polarised ultraviolet light) [Wuilpart *et al.*, 2002].

Circular birefringence tends to rotate the state of polarisation within a fibre (twist stress, magnetic field along the axis without linear birefringence). This birefringence is often defined by the beat length L_B, namely the length at the end of which the polarisations along the two neutral and orthogonal axes of the fibre have become

phase-shifted by 2π rad [Fougeres, 2002]. This length can be less than 1mm for specific fibres. The origin of this stress is, therefore, the cooling of the non-homogenous structure and depends on the temperature. This dependence is of the order of 10^{-3}/°C. It is the object of polarisation sensing system to depict physical parameter fluctuations by an analysis of birefringence variations.

The system is quoted as a fully distributed class IV DTS.

3.2.4.6 OTDR USING LIQUID CORE FIBRE

In liquids, the scattering arises from real-time thermodynamic fluctuations in the refractive index and therefore the scattering shows a significant temperature coefficient [Altkorn *et al.*, 1997]. The OTDR signals from the liquid-filled fibre can return the temperature profile along the fibre. The measurements can be done here with a somewhat greater signal-to-noise ratio than for conventional OTDR measurements on solid-cored fibre [Hartog, 1983]. This remote temperature sensing system uses an optical fibre in which the sensor is optical and passive, with no electrical power required at the sensor. The temperature-sensing section of the fibre optic makes use of a transparent liquid as core or cladding and in which the transparent liquid has a temperature-dependent index of refraction [He *et al.*, 1995].

The system is quoted as a fully distributed class IV DTS.

3.2.4.7 OTHER OPTICAL DISTRIBUTED TEMPERATURE SENSING SYSTEMS

The alternative optical technologies identified are necessitating the design of a specific sensing element. One may consider for example erbium doped optical fibres where the gain is temperature dependent. It is verified that the Amplified Spontaneous Emission (ASE) is much smaller than that the Rayleigh backscattering. However, combined with standard OTDR system features, using Erbium-doped optical fibre remains a simple method to enhance temperature detection sensitivity.

Similarly, fibres with a high fluorescence capability might also be attractive to

optimise the performance of a Raman DTS. The re-emission spectrum of most fluorescent materials generally exhibits a significant temperature variation. Thus, if an optical arrangement similar to that used for Raman OTDR is constructed, with a laser exciting source as before and with the detector filters now selected to examine regions of the fluorescent decay spectrum having the maximum possible differential temperature variation, a distributed temperature sensor should be possible. Although fluorescent doping necessarily increases the loss in the optical fibres, it is found that this is, for short-distance (less than 100m) operation, more than offset by the much higher fluorescent light levels theoretically attainable. If suitable fibres can be produced, it is likely to be an attractive method for distributed thermometry in the future.

Some investigations on the design of specific optical fibres to extend the available temperature range have also been carried out [Bryant *et al.*, 1991]. Polyimide and gold-coated fibres have been shown to be suitable for use in high temperature optical fibre thermometry. The coatings provide mechanical stability for the fibre and the Raman ratio technique has been demonstrated to be valid for these fibres to temperatures of at least 330°C for polyimide and 600°C for gold-coated fibres (long term → more than 4 hours).

It is possible to improve the detection performance of a system using specific signal processing methodology. The influence of detector noise on temperature-measurement accuracy with IR systems has been studied [Chrzanowski *et al.*, 1998]. The results show that the influence of detector noise depends strongly on the number of spectral bands employed in the system. Errors in temperature measurement with multi-band systems caused by detector noise decrease when the difference between the number of system spectral bands n and the number of measured unknowns m rises. Thus for a system to be robust to noise the difference n-m should be as great as possible.

From the analysis of these different improvement solutions, the technology selection

process also aims to identify the best compromise between a performing Sensing Element and a simple Control Unit.

3.2.5 OTHER NON OPTICAL TECHNOLOGIES

Two main sensing families of non-optical DTS technologies present attractive detection performances. The first system is an over-temperature sensor and locator utilising a temperature sensitive cable comprising an electrical conductor, a dielectric, and a conductive polymeric composition (CPC) such that the dielectric separates the electrical conductor from the CPC. An over-temperature condition at any point along the cable is detected by a drop in the capacitance of the cable, as measured from one end of the cable [Lutz, M. A., 1982]. The location of the over-temperature point on the cable is determined by comparing the reduced capacitance from the control end to the over-temperature point with the capacitance of the full cable length. This cable possesses flexibility, ruggedness and durability. A massive resistance increase at this over-temperature location which when combined with a capacitance measuring technique, makes it possible to locate the over-temperature position. When the critical sensing temperature is exceeded in the solid conductive polymeric composition, the resistance increase can be four or more orders of magnitude over a small temperature range (e.g. 5°C to 10°C). The large resistance change is necessary to electrically isolate the portion of the cable beyond the hot spot so that it does not contribute to the capacitance of the cable between the control end and the hot spot, thus making precise location of the hot spot possible.

The second system relies on a longitudinal resistance temperature sensor, which sees its resistance decreasing at the "hot-spot" between two conductors separated by a dielectric [McQueen, M. M., 1990]. Melt-able plastic devices utilise a twisted pair of wires, each wire encased in melt-able plastic material. When the temperature exceeds the material's melting point, the wires touch. To reuse the sensor, the shorted section must be cut out and replaced. A continuous thermistor cable comprises two conductors separated by continuous negative temperature coefficient of resistivity

material. As the temperature of such cable rises, the resistance between the two conductors fails. Once the temperature falls, the resistance returns to its original high value. Eutectic salt type devices utilise a salt compound between two conductors. At the eutectic temperature, the compound melts and its resistance falls, connecting the conductors. When the temperature falls, the compound solidifies and the resistance returns to its original high value.

These two options achieve the performance of a Class III DTS.

3.2.6 TEMPERATURE / OVERHEAT DETECTION SYSTEM OVERVIEW OF AIRCRAFT SUPPLIERS

The major competitors have entered the aeronautic market proposing distributed temperature detection mainly for the engine fire detection application. Barber Colman, Fenwall, Systron Donner, Walter Kidde, Whittaker, Thermocoax, Siemens Cerberus Division are the companies that are most active in the field. Resistive cable made of eutectic salts, networks of discrete temperature sensors (thermocouples or temperature sensitive diodes separated by a delay line), pneumatic or hydraulic systems (hollow tube filled with gas or compressible fluids) have been the technologies selected by these aircraft suppliers. Their systems are ranging from class II to quasi-distributed class IV DTS.

3.2.7 SUMMARY OF CURRENT MEASUREMENT CHARACTERISTICS

Characteristics are presented in Table 3.2□1 for each physical principle. Performances describe the current optimum detection capabilities of the associated technologies.

Table 3.2-1 Compliance table for DTS main aeronautic qualification tests
IV': does mean "System Class IV - ['] for quasi-distributed system. NA does mean "Not applicable".

Technology / Physical Principle	System Class	Spatial Resolution [m]	Temperature Resolution [°C]	Measurement Time [s]	Maximum Length [m]
Ultrasonic Waveguide	IV'	> 0.15	±1	< 1	< 20
Electrical Time Domain Reflectometry	IV	> 0.01	±1	< 1	a few 10
Discrete Temperature Sensors	IV'	> 0.3	±1	< 1	a few 10
Raman OTDR	IV	> 0.5	±1	< 3	a few 1000
Raman OFDR	IV	> 0.5	±1	< 3	a few 1000
Stimulated Brillouin Scattering	IV	> 0.1	±1	about 60	a few 1000
Bragg Gratings	IV'	> 0.1	±1	< 3	a few 10
Polarisation OTDR	IV'	> 0.2	±1	< 3	a few 10
OTDR using Liquid Core Fibre	IV	> 0.5	±1	< 3	a few 100
Capacitance Cable	III	NA	±5	< 1	a few 10
Resistance Cable	III	NA	±1	< 1	a few 10

3.2.7.1 MEASUREMENT SELECTION CRITERIA

The selection of the technology to be developed for aeronautic applications will be done on the basis of the following required measurement performances, called here Measurement Selection Criteria (MSC):

- Measurement time: $\leq 3s$
- Temperature resolution: $\leq \pm 1°C$
- Sampling interval: $\leq 0.5m$
- Maximum sensing element length: $\geq 300m$
- Temperature detection range: -55°C; +300°C
- Minimum number of temperature points: 50
- The system will be a class IV DTS

These values are selected on the ground of former experiments performed in the framework of the "**FIRE** Detection **A**nd Suppression Simulation" project, an EU funded BRITE/EuRam research project concerned with the development of fine water mist systems as a possible replacement for halon fire suppression system currently used in aircraft cargo holds [Brite Euram Project, 1995]. These values have

to be considered as application requirements and as detection performances for the candidate technologies. The selection is rejecting technologies taking into account the fact that no industry related to the technology analysed is supplying equipment in conformity (or near) with the MSC. Moreover, a certain technology is rejected if a lack of dynamism is perceptible in the concerned field, which might mean that no outstanding progress is to be expected for related applications in the near future. The maximum sensing element length has to be considered with respect to the possibility that the sensing loops have to be multiplexed. Note : the "**E**lectrical **T**ime **D**omain **R**eflectometry: **ETDR**" is rejected because of the important effort of development to design a sensing element covering the full required "Temperature detection range".

3.2.7.2 PRE-SELECTED TECHNOLOGIES

The pre-selected technologies are investigated further with respect to the application requirements. These technologies are namely: the ultrasonic waveguide, the discrete temperature sensors, the Raman OTDR and OFDR, the fibre Bragg gratings and the polarization OTDR.

3.3 METHODOLOGY FOR TECHNOLOGY SELECTION

The pre-selected detection technologies and the application requirements are compared using the same Measurement Selection Criteria. What is the maturity status of a technology compared to the selected set of detection requirements? What is the application demand in terms of detection performances?

3.3.1 THE DETECTION PERFORMANCES COMPARED TO THE MEASUREMENT CRITERIA

From the previous description, it is possible to categorize the 8 applications into 3 groups with their own characteristics. The BLD and DSC applications call for a technology to be installed on aircraft wings. The first application is the detection of overheats along bleed air ducts, the second is the detection of ice accretion on the leading edge of an airfoil. For this group, the common characteristics in decreasing order of importance are the spatial resolution, the temperature accuracy and the detection range.

The EFD and the LDG are two detection applications strongly calling for system robustness and reliability and deal with cylindrical symmetry, which can be an advantage for systems not having the capability of a very accurate spatial resolution. For these two applications, the temperature detection range, the system response time and the temperature accuracy are the priorities as far as the detection performances are concerned.

The TCM, WFD, HAD and CTC applications appeal to systems dedicated to the protection of large areas. The specificity of TCM is that a 2D rectangular spreading of the SE is necessary contrary to the others where the SE is installed lengthways. This field is in relation with the expertise field of Siemens Cerberus Division, the fire detection in aircraft cargo holds. For this group of applications, the common detection performances preferred are the temperature detection range, the temperature accuracy and the spatial resolution and sensing element length per loop

The relationship between the technologies and the measurement parameters is the description of how a technology is fulfilling various measurement requirements. To give to these requirements a notation between 1 and 10 is establishing a ranking (1 is very important, 10 is the less important parameter out of the 10).

The ranking factors RF_k^i ($\in$ [1; 10]) are evaluated against the measurement parameters MP_i, ($i \in [1; 10]$) for each application k ($k \in [1; 8]$). The requirements for a given potential aeronautic applications are given a notation between –5 and +5 (0 is excluded) to evaluate the degree of needs towards the same measurement parameters. These notations are called enhancement values $EV_j^i \in \{[-5; -1] \cup [+1; +5]\}$ dedicated to a measurement parameter for a technology j, ($j \in [1; 6]$). It shall be noted that enhanced values are invariant against the applications (+5 is qualitatively the best result).

Therefore the quality factors describe the relation "Technology-Application". They describe the level of appropriateness a technology has towards the considered aeronautic applications.

$$QF_k^i = \sum_{i=1}^{10} RF_k^i . EV_j^i$$

Equation 3.3-1 Quality factors for technology selection process

This evaluation method is an evaluation tool to determine the most appropriate technology covering the most interesting aeronautic applications for Siemens Cerberus SA.

3.3.2 THE APPLICATION REQUIREMENTS COMPARED TO THE MEASUREMENT CRITERIA

For the "Thermal Cargo Monitoring" application, we obtain the following relationship.

Table 3.3-1 Technology performances against measurement parameters and definition of quality factors for the thermal cargo monitoring application

	Measurement Parameters	RF	Technologies					
			Acoustic	Discrete	Raman OFDR	Raman OTDR	FBG	Polarisation
[1]	• System response time (s)	7	5	4	-4	2	3	-1
[2]	• Temperature resolution (°C)	6	-1	2	1	-2	5	-4
[3]	• Temperature accuracy (± °C)	8	1	-1	-1	-1	4	-5
[4]	• Temperature detection range (°C)	10	2	1	3	3	-5	-3
[5]	• Sampling interval (m)	5	4	3	2	1	-3	2
[6]	• Number of temperature points per loop	9	-2	-4	4	4	-4	3
[7]	• Number of sensing loop	1	3	5	-2	-4	2	5
[8]	• Sensing element length per loop (m)	4	-5	-3	5	5	1	4
[9]	• Sensing Element bend radius (cm)	2	-4	-2	-3	-3	-2	-2
[10]	• Number of connectors per loop	3	-3	-5	-5	-5	-1	1
	Quality Factor, QF	[TCM]	25	-5	43	60	-19	-44

The same analysis is made for the remaining applications.

3.3.3 FINAL TECHNOLOGY SELECTION

The quality factors range between –56 and +76.

Table 3.3-2 Quality factors between the applications and the pre-selected technologies

Applications	Technologies					
	Acoustic	Discrete	Raman OFDR	Raman OTDR	FBG	Polarisation
BLD	48	19	-44	-28	-5	-12
EFD	76	73	-6	7	-8	-24
TCM	25	-5	43	60	-19	-44
WFD	13	-9	62	71	-28	21
CTC	42	18	29	43	6	-56
HAD	24	13	50	57	-22	26
LGD	35	36	-13	7	40	-51
DSC	45	43	44	16	17	-19

Table 3.3-2 is normalized using 12 spreading intervals. The selection process result is shown

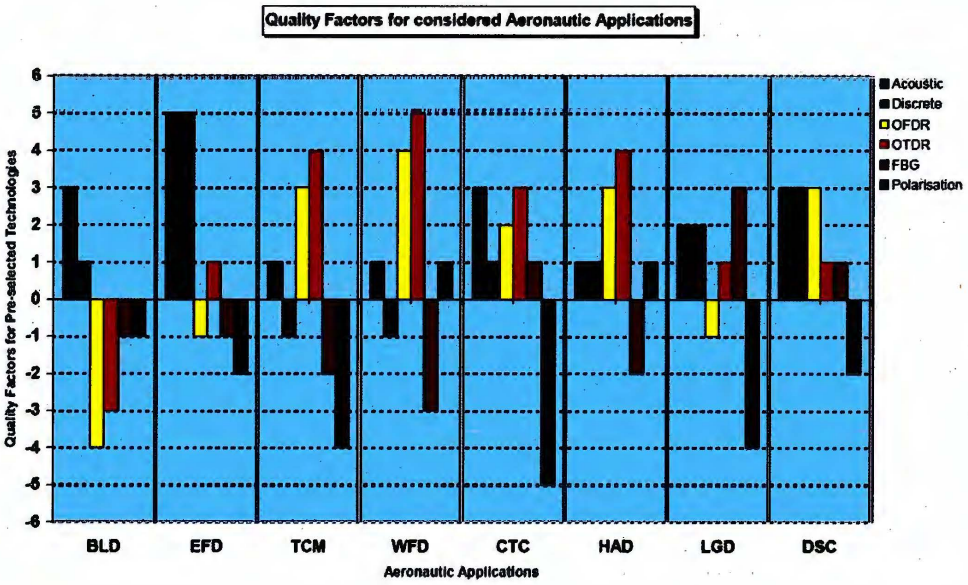

Figure 3.3-1 Normalised representation of the quality factors between the applications and the pre-selected technologies

One may draw a short conclusion on the capability of a technology to fulfill the requirements associated to the considered technologies.

The ultrasonic waveguide technology seems to be particularly well appropriate for applications necessitating only relatively short SE lengths. It can be noticed an outstanding notation for EFD application. Discrete sensors (mainly thermocouples) are well represented on aircraft. The drawback of this technology is the overall number of deported electronic units required to settle a temperature sensor network. For some applications, this presents major non-conformities to their specific environmental constraints. The OFDR/OTDR Raman technology is particularly well dedicated to the group of applications for large area protection. The bad result obtained against BLD can be explained by the number of connectors required. The temperature detection range and sampling interval performances prevent this technology from being really adaptable to aeronautic applications.

The "temperature accuracy" and "temperature detection range" of the POTDR technology presents a lack of accurate detection performances and rules out any possibility the technology would have to be used in the cited applications when compared to other available technologies. Because the expertise field of Cerberus is part of this group of applications, and because this group contains an interesting number of applications, the study will focus on the large area protection. The applications belonging to this group are being all new aeronautic applications except for TCM. Performances required for these applications are close enough to be able to develop a unique product. Therefore analysing their associated normalised Quality Factors, it is possible to identify 3 qualified technologies when we considered Quality Factors superior to 1. Then, only Raman Optical Time or Frequency Domain Reflectometry technologies OTDR / OFDR are common to all these applications, whereas the Acoustic technology (ultrasonic wave-guide from Schlumberger) might be used in cabins.

3.4 RAMAN OTDR VERSUS RAMAN OFDR

Alternatives to OTDR interrogation are direct intensity monitoring and a variety of optical frequency domain reflectometry techniques. OFDR can be applied to physical measurement parameters, for example, strain, pressure, force, temperature, etc., where the measurand can be coupled mechanically to a periodic deformation of an optical fibre [Pierce *et al.*, 2000]. In coherent OFDR, the operating frequency of a narrow-linewidth source is modulated, and the associated beats arising from reflections (discrete or continuous) within the optical fibre system under inspection are monitored on a spectrum analyser whose frequency axis corresponds to a position along the fibre axis. Use of a CW laser diode source allows for easy modulation of the optical frequency by direct current modulation.

OFDR can also be used as a backscattering technique for fault diagnosis and fibre loss measurement [Ghafoori-Shiraz *et al.*, 1986]. The sinusoidally modulated laser beam, the frequency of which changes stepwise, is launched into the fibre and the backscattered light phase amplitude and frequency responses are measured at the same input end and processed, i.e., inverse-Fourier transformed, to obtain the temporal response of the fibre, the variations of the back-reflected signal along the fibre length.

When we consider a single reflection at the far end of a test fibre with a length of z_0, the reflection position z_0 is related to the beat frequency f_b by using a frequency-sweep rate γ as follows:

$$z_0 = \frac{v_g}{2.\gamma}.f_b$$

Equation 3.4-1 Relation between the fibre length z_0 and the system beat frequency

where v_g is the group velocity of the lightwave, and the frequency-sweep rate γ is defined using a sweep time T_{swp} and a frequency sweep span ΔF as follows:

$$\gamma = \frac{\Delta F}{T_{swp}}$$

Equation 3.4-2 Frequency-sweep rate

The beat spectrum has a sharp line at the frequency f_b, and the spatial resolution Δz_B is determined by the frequency-resolution bandwidth ΔB of the spectrum analyser as follows:

$$\Delta z_B = \frac{v_g}{2.\gamma}.\Delta B$$

Equation 3.4-3 C-OFDR spatial resolution

where the frequency sweep is assumed to be entirely linear with respect to time [Tsuji *et al.*, 1997b]. Since the beat signal is generated within the duration of the finite sweep time, the spatial resolution limitation is:

$$\Delta z_{min} = \frac{v_g}{2.\gamma}.\frac{1}{T_{swp}} = \frac{v_g}{2.\Delta F} \cong \frac{v_g}{\gamma}.\Delta \upsilon$$

Equation 3.4-4 C-OFDR spatial resolution

Therefore a wide frequency-sweep span ΔF is needed for high-spatial resolution (typically 100MHz for 1m). If the linewidth $\Delta \upsilon$ of the lightwaves is sufficiently narrow or γ is sufficiently fast, the achievable spatial resolution approaches Δz_{min}. The optical-frequency-sweep nonlinearity brings about a temporal change in the beat frequency f_b for a constant fibre length z_0. It causes additional beat-spectrum broadening and degrades the spatial resolution. The use of time-gated spectral analysis to reduce the spectral broadening caused by the sweep nonlinearity (when the beat frequency change is small and the sweep linearity is good) shows, as the time gate narrows, that the measurement efficiency in time is considerably decreased [Tsuji *et al.*, 1997a].

In R-OFDR sensor, low-power lasers of wavelengths around 1320 or 1550nm can be used. In this range, the attenuation and dispersion of standard telecommunication

fibres are very low. Because of the low noise in a frequency-domain measurement, a modulated laser diode of 100mW CW-power implies the same SNR as a pulsed laser of about 7W in a time-domain application [Gogolla *et al.*, 1999]. The signal processing to obtain a temperature profile can be demonstrated as presenting no major difficulties for current electronic components [Geng *et al.*, 2002].

Table 3.4-1 summarizes the discrepancies of various performances for an OFDR system in comparison with an OTDR system. A table cell is marked green when a system aspect (system architecture, emitter, ...) in front of an aeronautic pre-requisite (performance in A/C environment, reliability, ...) is seen as comparable for both technologies. The cell is yellow, when the OFDR has a slight disadvantage and red when the disadvantage is judged critical.

Table 3.4-1 Performance of an OFDR compared to an OTDR DTS

OFDR versus OTDR	Performance in A/C environment	Reliability	Integration	Cost	Power consumption
System Architecture					
Emitter					
Receiver					
CPU					
Power Supply					
Signal Processing					
A/C Interface					

In general, the review demonstrates no significant advantages of the OFDR technology over the OTDR within the context of the measurement selection criteria. Moreover, the system costs (RC, NRC), the remaining efforts to reach the equipment integration and the system electrical payload have been identified as risks for its acceptance as part of a development for short-term coming aircrafts. Therefore OTDR is the optimum choice.

3.5 RAMAN OTDR VERSUS PHOTON COUNTING

The common principle of all photodetectors is the photoelectric effect. A photon impinging on a sensitive layer is absorbed, while emitting a charged carrier pair. The current corresponding to one photon, or one carrier pair is too tiny to be directly measurable [Huttner *et al.*, 2000]. In avalanche photodiodes (APD), each free carrier emitted by the photons is accelerated by a high voltage and emits several new carriers during collisions with surrounding atoms. It is the same principle as in nuclear reaction, where each particle has enough energy to generate new particles, thus creating an avalanche process.

Using the APD in Geiger mode is when a single photon is like a trigger using up all the energy stored in the device. In this regime, the gain in the device can reach several thousands, thus generating a macroscopic current that is easily detectable. The problem is that the output current is no longer proportional to the input. One, two or three photons would give the same current.

To be able to measure the intensity of a pulse, it is necessary to attenuate the light beam to ensure that the average number of photons per pulse is much lower than one. Each time a pulse is sent, we may or may not obtain a count. But if many pulses are sent, the average number of counts will reflect the input intensity. Each detected photon generates the same current pulse. The only remaining task is to count the number of pulses. A digital measurement instrument based on photon counting can thus be simpler and more robust than analog instruments, based on standard detection. A full measurement takes several seconds.

In the short wavelength region (from 0.8 to 1μm) at room temperature the two methods are demonstrated as identical in terms of generated Noise Equivalent Power [Healey, 1984]. To obtain data from any photon correlation experiment demands serious attention to optimising both the measuring system and experimental conditions [Brown *et al.*, 1997]. The laser must have sufficient power, be stable

under all likely conditions, and usually be restricted to a single transverse mode. Surfaces surrounding the point of measurement must not introduce optical noise. Flare reduction in the receiver optics may be improved with spatial and spectral filtering, and careful choice of stops, baffle, and surface coatings. Performance may be compromised by thermal, mechanical or electrical instabilities caused by exposure to environmental excesses. Errors may even be introduced by preprocessing hardware and software before proper information is extracted.

The time-correlated single photon counting (TC-SPC) technique was used in a distributed anti-Stokes Raman thermometry (DART) sensor. A spatial resolution of 30cm over a range of 30m was demonstrated. The measurement time needed to achieve a temperature resolution of ±4°C was 3 minutes [Feced *et al.*, 1997b].

Present commercial systems suffer from the existence of dead-zones along the network due to intense Fresnel reflections generated by connectors or other optical components [Feced *et al.*, 1997a]. One may design a system using photon counting principle to overcome the dead-zone limitation by monitoring the spontaneous Stokes Raman emission to avoid the intense Fresnel reflections.

Despite these good operational and metrological performances, the photon counting technique is explained here as very demanding in terms of equipment specifications and mounting precautions. Besides, recently demonstrated detection performances show that the basic required detection performances are far from being fulfilled. The components used as part of the system are also sensitive to environmental condition changes. Analogue detection will be therefore preferred to the photon counting technique.

3.6 SINGLE PULSE VERSUS CORRELATION OTDR

The use of higher power lasers and the parallel averaging of all data points on a single probe shot have provided some improvements to the standard OTDR technique, they have been unable to remedy a limitation that is fundamental to all conventional OTDR designs: the trade/off between signal-to-noise ratio (which determines dynamic range and measurement time) and response resolution. Spread-spectrum techniques are proposed to increase the dynamic range of an OTDR [Thomas, 1997] and significantly reduce the required measurement time, without sacrificing resolution. The response resolution of a measurement is the minimum separation between two faults that allows these faults to be clearly distinguished. Increasing the SNR of an OTDR measurement results in increased dynamic range in a given measurement time, or alternatively, a reduction in the number of averages required to obtain a given result [Nazarathy *et al.*, 1989]. The spread-spectrum technique such as correlation offers the possibility of providing measurements with improved SNR. The method consists in correlating the detected signal with the probe signal. In this case, it is the duration of the autocorrelation of the probe signal that determines the response resolution rather than the duration of the probe signal itself, which may be long and energetic.

Correlation OTDR has been presented where the transmitted pulse in the optical fibre is correlated to the backscattered signal. In the simulation, 100bits have been correlated and 10^5 averages have been made. Both transmitted traffic and incoming traffic have been simulated with a binary random data source [Biain *et al.*, 1994]. The correlation and averaging processes achieve a $34.8dB_{OPT}$ improvement in the SNR. When the phase at the receiver shifts by one "bit", the reference code for that backscatter signal must also change by one "bit". If the reference signal is simply the original probe signal delayed by an appropriate number of bits, the bit rate of the modulating code determines the spatial resolution of the instrument. It also means that the bandwidths of the spread spectrum and pulsed probe signals are identical, for

the same spatial resolution [Thomas, 1997]. Once encoded, a matched receiver is necessary in order to retrieve the information from a spread spectrum signal. This comprises a correlator that multiplies the received spread spectrum signal with a local reference code. These two signals are correlated when the local reference matches that of the input signal. When they are correlated, the broadband input signal collapses down to restore the original information. Otherwise, any uncorrelated input is spread by the local reference signal. A filter at the output of the correlator rejects all but the wanted signal.

The novelty of the spread spectrum technique lies solely in the nature of the stimulus. The correlation process then takes this long and energetic probe signal and compresses it into an equivalent form of a narrow, high-energy pulse. Ideally, the code should possess an orthogonal autocorrelation function, i.e. it should have zero amplitude side-lobes. The code would then offer perfect discrimination.

Despite the clear evidence of detection performance advantages of the spread spectrum techniques, which improve the average launched power and thereby make more efficient the use of the time available for signal averaging, the preferred solution stays the standard analog OTDR detection. Its hardware simplicity indeed makes it particularly attractive as opposed to the need of a certain modulation process, at laser diode driver level, for the correlation OTDR.

3.7 CONCLUSION

This chapter has endeavoured to show that sensor systems which permit monitoring the magnitude of temperature, and also its variation along the length of a continuous uninterrupted sensing element, offer a powerful and economical means of covering a large number of locations within a significant area and are particularly attractive for obtaining a graphical or pictorial presentation of information. The technological selection process is rather simple in terms of measurement performances, since the technologies available have specificities, which are or are not compliant with aeronautic application constraints. It was necessary to compare SE and CU pre-selected system costs, as well as their respective commercial positions on the DTS industrial market. Raman Optical Reflectometry systems came out dedicated to a group of four aeronautic applications. It is recognised that, eventually, optical fibre sensors will have to be at least roughly price competitive with electrical sensors in order to gain widespread acceptance. Whereas Raman Reflectometry is the most adequate for the selected applications: Thermal Cargo Monitoring (complementary fire detection to smoke detectors and/or detection system for "zoning extinguishing system"), Wire Fire Detection (electrical cables protection), Cabin Temperature Control (cabin temperature regulation for passenger comfort and possibly cabin fire detection system), Hidden Area Fire Detection (protection of areas not easy to access and then where maintenance operation are not frequent), Ultrasonic Wave-guide technology might be further analysed for the Engine Fire Detection application. The Raman technology development work has consisted firstly of deciding the signal processing type to be used to collect Raman back-scattered signals. Several possibilities have been investigated: the time domain, the frequency domain analysis, the photon counting and the correlation OTDR options. The analog Raman OTDR has been selected. The following steps are then to study theoretically and experimentally all aspects of an operational Raman DTS system: the behaviour of stimulation signals in optical fibres as well as the architecture of the control unit and the transformations required to make it match aeronautic application needs.

REFERENCES

Altkorn, R., Koev, I., Van Duyne, R. P., and Litorja, M. "Low-loss Liquid-Core Optical Fiber for Low-Refractive-Index Liquids: Fabrication, Characterization, and Application in Raman Spectroscopy". Applied Optics. (1997) Vol. 36. Iss. 34. pp.8992-8998.

Berkcan, E. "Optical Sensors and Multiplexing for Aircraft Engine Control". Proceedings of the SPIE. The International Society for Optical Engineering. (1992) Vol. 1799. pp.176-186.

Biain, G., Dawson, J. F., and Tozer, T. C. "New Technique for Nonintrusive OTDR based on Traffic Data Correlation". Electronics Letters. (1994) Vol. 30. Iss. 17. pp.1443-1444.

Bobo, S. N. "Long Taxi Rolls Can Lead to Catastrophic Blow-outs". ICAO Bulletin. (1985) pp.34-37.

Brite Euram Project. "Fire Detection and Suppression Simulation Project". Project Nb. BE95-1977. (1995)

Brite Euram Project. "FIREDETEX. New Fire Smoke Detection and Fire Extinguishing System for Aircraft Applications". Project Nb. GRD1-1999-10342. (1999)

Brown, R. G. and Smart, A. E. "Pratical Considerations in Photon Correlation Experiments". Applied Optics. (1997) Vol. 36. Iss. 30. pp.7480-7492.

Bryant, G. W., Paton, A. T., Scott, J. C., and Stuart, A. D. "Assessment of Special Fibres for Distributed anti-Stokes Raman Ratio Thermometry". International Journal of Optoelectronics. (1991) Vol. 6. Iss. 1-2. pp.91-100.

Cavaleiro, P. M., Araujo, F. M., Ferreira, L. A. , Santos, J. L., and Fahari, F. "Simultaneous Measurement of Strain and Temperature Using Bragg Gratings Written in Germanosilicate and Boron-Codoped Germanosilicate Fibers". IEEE Photonics Technology Letters. (1999) Vol. 11. Iss. 12. pp.1635-1637.

Chrzanowski, K. and Szulim, M. "Measure of the Influence of Detector Noise on Temperature-Measurement Accuracy for Multiband Infrared Systems". Applied Optics. (1998) Vol. 37. Iss. 22. pp.5051-5057.

Cober, G. S., Korolev, A. V., and Isaac, G. A. "Assessing Characteristics of the Rosemount Icing Detector under Natural Icing Conditions". AIAA 2001-0397. (2001)

Du, W.-C., Tao, X.-M., and Tam, H.-Y. "Fiber Bragg Grating Cavity Sensor for Simultaneous Measurement of Strain and Temperature". IEEE Photonics Technology Letters. (1999) Vol. 11. Iss. 1. pp.105-107.

Dyson, E., Hashemi, A., and Wong, H. "High-Power Electronics Heat Rejection From Aircraft Skin". Journal of Enhanced Heat Transfer. (1996) Vol. 3. Iss. 3. pp.165-176.

FAA. "Aircraft Command in Emergency Situations (ACES); Phase I: Concept Development - Concept B". DOT/FAA/CT-90/21. (1991)

Feced, R., Farhadiroushan, M., and Handerek, V. A. "Zero Dead-Zone OTDR with High-Spatial Resolution for Short Haul Applications". IEEE Photonics Technology Letters. (1997a) Vol. 9. Iss. 8. pp.1140-1142.

Feced, R., Farhadiroushan, M., Handerek, V. A., and Rogers, A. J. "Advances in High Resolution Distributed Temperature Sensing Using the Time-Correlated Single Photon Counting Technique". IEE Proceedings Optoelectronics. (1997b) Vol. 144. Iss. 3. pp.183-188.

Fougeres, A. "Polarization OTDR: Locating High-PMD Fibers". EXFO Application Note 087. (2002)

Geng, J., Xu, J., Li, Y., Wei, G., and Guo, C. "The Development of the Model and Arithmetic for the Fully Distributed Fiber Optic Sensor Based on Raman Optical-Fiber Frequency-Domain Reflectometry (ROFDR)". Sensors and Actuators A. (2002) Vol. 101. pp.132-136.

Ghafoori-Shiraz, H. and Okoshi, T. "Fault Location in Optical Fibers Using Optical Frequency Domain Reflectometry". Journal of Lightwave Technology. (1986) Vol. LT-4. Iss. 3. pp.316-322.

Glombitza, U. and Brinkmeyer, E. "Coherent Frequency-Domain Reflectometry for Characterization of Single-Mode Integrated-Optical Waveguides". Journal of Lightwave Technology. (1993) Vol. 11. Iss. 8. pp.1377-1384.

Gogolla, T. and Farahani, M. A. "Spontaneous Raman Scattering in Optical Fibers with Modulated Probe Light for Distributed Temperature Raman Remote Sensing". Journal of Lightwave Technology. (1999) Vol. 17. Iss. 8. pp.1379-1391.

Hartog, A. H. "A Distributed Temperature Sensor Based on Liquid-Core Optical Fibers". Journal of Lightwave Technology. (1983) Vol. LT-1. Iss. 3. pp.498-509.

He, G. S., Casstevens, M., Burzynski, R., and Li, X. "Broadband, Multiwavelength Stimulated-Emission Source Based on Stimulated Kerr and Raman Scattering in a Liquid-Core Fiber System". Applied Optics. (1995) Vol. 34. Iss. 3. pp.444-454.

Healey, P. "Optical Time Domain Reflectometry - A Performance Comparison of the Analogue and Photon Counting Techniques". Optical and Quantum Electronics. (1984) Vol. 16. pp.267-276.

Horiguchi, T., Shimizu, K., Kurashima, T., Tateda, M., and Koyamada, Y. "Development of a Distributed Sensing Technique Using Brillouin Scattering". Journal of Lightwave Technology. (1995) Vol. 13. Iss. 7. pp.1296-1302.

Huttner, B. and Brendel, J. "Photon-Counting Techniques for Fiber Measurements". Lightwave Special Reports. (2000) pp.112-120.

Jackson, D. G., Owens, D. G., Cronin, D. J., and Severson, J. A. "Certification and Integration Aspects of a Primary Ice Detection System". AIAA 2001-0398. (2001)

Jones, M. E., Duncan, P. G., Crotts, R., Shinpaugh, K., Greene, J. A., Murphy, K. A., Gunther, M. F., and Claus, R. O. "Multiplexing Optical Fiber-based Pressure Sensors for Smart Wings". Proceedings of the SPIE. The International Society for Optical Engineering. (1996) Vol. 2718. pp.338-344.

Kerner, H. "Investigation of Main Landing Gear Tire Temperatures During Taxy-Out at Heavy Take-off Masses.". American Institute of Aeronautiics and Astronautics, Inc. (1986)

Kulczyk, W. K. "Ultrasonic Distributed Temperature Sensor". Sensors and Actuators. (1990) Vol. A21-A23. pp.663-669.

Le Gall, F., Loaec, F., Devoldere, N., Loisel, B., Mehadji, K., and Moisan, M. "Modal Characterisation Using Bragg Gratings in Photosensitive SiO2-Si Strip Waveguides". IEEE Photonics Technology Letters. (1997) Vol. 9. Iss. 6. pp.788-790.

Lehle, W. "Airbus A330/340 Environmental Control System". Liebherr-Aero-Technik Gmbh. (1994) Vol. 941519. pp.1442-1450.

Lei, J.-F. and Will, H. A. "Thin-Film Thermocouples and Strain-Gauge Technologies for Engine Applications". Sensors and Actuators A. (1998) Vol. 65. pp.187-193.

Lockheed-California Company. "L-1011 Tristar, Manual Wiring Manual". (1970) Vol. 10.

Lutz M. A. [Inventor], "Continuous Sense and Locate Device", Nb: US004487057 (1982).

Lynnworth L.C. and Patch, D. R. "New Sensors for Ultrasound: Measuring Temperature Profiles". Materials Research and Standards. (1970) pp.6-11.

McQueen M. M. [Inventor] , "Distributed RTD", Nb: US005117216 (1990).

Naruse, H. and Tateda, M. "Trade-off between the Spatial and the Frequency Resolutions in Measuring the Power Spectrum of the Brillouin Backscattered Light in an Optical Fiber". Applied Optics. (1999) Vol. 38. Iss. 31. pp.6516-6521.

Nazarathy, M., Newton, S. A., Giffard, R. P., Moberly, D. S., Sischka, F., Trutna, W. R., Foster, and Foster, S. "Real-Time Long Range Complementary Correlation Optical Time Domain Reflectometer". Journal of Lightwave Technology. (1989) Vol. 7. Iss. 1. pp.24-38.

Pal, Z. M. and Johnston, R. H. "Simulation of Pipeline Holiday Detection by Time Domain

Reflectometry". Copyright Material IEEE. Paper No. PCIC-89-41. (1989) pp.103-108.

Paton, A. T. and Scott, J. C. "U.V. Optical Fiber Distributed Temperature Sensor". SPIE Fiber Optic and Laser Sensors VIII. (1990) Vol. 1367. pp.274-281.

Penrod, S. L., Unger, P. D., and Rohrbach, R. P. "Filtration of Aircraft Cabin Air Odors in 100% Relative Humidity, Low Temperature Conditions". Proceedings of the ASME. Heat Transfer Division. (1998) Vol. 361-3. pp.139-146.

Pierce, S. G., MacLean, A., and Culshaw, B. "Optical Frequency-Domain Reflectometry for Microbend Sensor Demodulation". Applied Optics. (2000) Vol. 39. Iss. 25. pp.4569-4581.

Sarter, N. B., Schroeder, B., and McGuirl, J. "Supporting Decision-Making and Action Selection Under Time Pressure and Uncertainty: The Case of Inflight Icing". AIAA 2001-0543. (2001)

Tanaka, A. and Xin, H. "Effects of Structural and Stacking Configuration of Containers for Transporting Chicks in their Microenvironment". American Society of Agricultural Engineers. Transactions of the ASAE. (1997) Vol. 40. Iss. 3. pp.777-782.

Thomas, R. "Spread Spectrum and Coherent Detection Techniques for Distributed Optical Fibre Sensing". Submitted for the Degree of Doctor of Philosophy from King's College London. (1997)

Tozaki, T., Kato, M., Inada, K., Shiota, T., Wada, F., Takahashi, K., and Sawaguri, T. "Raman Backscattering Characteristics of the Optical Fiber and Distributed Temperature Sensor". Fujikura-Technical-Review. (1990) Vol. 19. pp.25-30.

Tsuji, K., Shimizu, K., Horiguchi, T., and Koyamada, Y. "Spatial-Resolution Improvement in Long-Range Coherent Optical Frequency Domain Reflectometry by Frequency-Sweep Linearisation". Electronics Letters. (1997a) Vol. 33. Iss. 5. pp.408-410.

Tsuji, K., Shimizu, K., Horiguchi, T., and Koyamada, Y. "Coherent Optical Frequency Domain Reflectometry Using Phase-Decorrelated Reflected and Reference Lightwaves ". Journal of Lightwave Technology. (1997b) Vol. 15. Iss. 7. pp.1102-1109.

Wuilpart, M., Ravet, G., Megret, P., and Blondel, M. "Polarization Mode Dispersion Mapping in Optical Fibers With a Polarization-OTDR.". IEEE Photonics Technology Letters. (2002) Vol. 14. Iss. 12. pp.1716-1718.

Raman OTDR Thermometry and Application Constraints

4.1 Raman effect in optical fibres 84
4.1.1 Raman backscattering process 84
4.1.2 OTDR principle 88
4.1.3 Operating wavelength and fiber dependancy 89

4.2 Raman backscattering related to detection performances 95
4.2.1 Spatial resolution 95
4.2.2 Temperature resolution 96
4.2.3 System detection range 98
4.2.4 Temperature profile and refreshment time 98

4.3 Raman backscattering sensitivity to environmental conditions 99
4.3.1 Sensing element and operating / survival temperature ranges 99
4.3.2 Mechanical and specific constraints 100
4.3.3 Optical fibre break considerations 102
4.3.4 Optical power balance for efficient sensing line interrogation 104

4.4 Conclusion 106

Raman spectroscopy of optical fibres and optical time domain reflectometry are combined to create a distributed temperature sensing system. Commercial Raman DTS are today covering the needs of numerous ground applications. However, some of the detection performances required for the selected aeronautic applications are either not achieved by ground systems or available only when using a bulky or expensive technology, or at the cost of relaxing a dependant performance. The aeronautic industry is very cautious in the introduction of new technology, therefore the study will investigate a number of possible improvement, where shall be demonstrated the validity of hardware selection as much as the simplicity of signal processing algorithms.

In this chapter, the review of the Raman backscattering phenomenon in optical fibres aims to describe the optimisation path by an adequate component selection in view of the detection performances requested in chapter 3. Details on the implications of the key detection performances are provided and evaluated in front of essential operating environmental and failure conditions.

4.1 RAMAN EFFECT IN OPTICAL FIBRES

When light is transmitted through a medium, the electric and magnetic components of the light interact with the microstructure of that medium to produce the effects of scattering. It may have an elastic interaction with the inhomogeneous microscopic structure of the glass, which leads to Rayleigh scattering, or an inelastic interaction with the molecule vibration and lattice vibration of the glass, which leads to Raman and Brillouin scattering.

A description of the nature of the different possible losses is provided, as well as recommendations for the choice of the laser source characteristics and of the fibre to optimise the detection performances.

4.1.1 RAMAN BACKSCATTERING PROCESS

There are many optical loss factors for silica fibres [Yoshida *et al.*, 1981], as shown in Figure 4.1-1. Electron transition absorptions in the UV region and Si-O bond vibration absorption in the infrared region are intrinsic absorptions of silica glass.

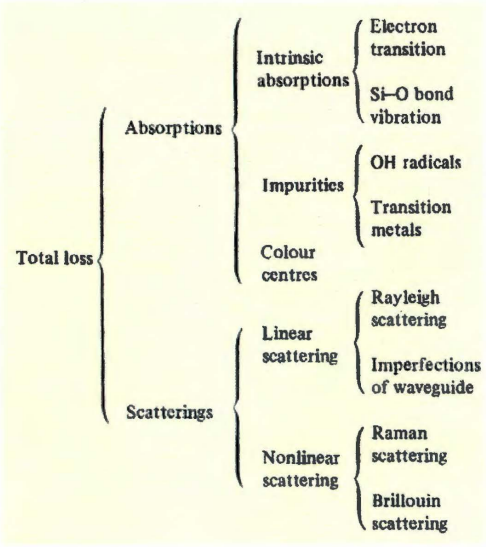

Figure 4.1-1: The schematic diagram of total loss in optical fibres

The low-loss wavelength band of the fibres exists in a region between these absorptions. Absorption due to OH radicals contained in core glass degrades the loss characteristics. The presence of 1ppm OH radicals in core glass almost corresponds to $1dB.km^{-1}$ losses at 945nm. Absorption due to contamination by transition metals causes almost no problem at all with the present manufacturing technology, which uses high-purity raw materials. The Rayleigh scattering phenomenon is caused by the refractive index fluctuation in glass, which is small compared with its wavelength. This refractive index fluctuation is caused by thermal fluctuation of glass frozen in a state of thermal equilibrium at a certain melting temperature T. The Rayleigh scattering α in the case of a single-component material can be obtained by the following expression:

$$\alpha = \frac{8\pi^3}{3\lambda^4} n^8 p^2 kT\beta$$

Equation 4.1-1 Rayleigh scattering in the case of a single-component material

where λ is the wavelength, n the refractive index, p the photo-elastic coefficient, k Boltzmann's constant, T absolute temperature and β the isothermal compressibility. In the case of multi-component glass, Equation 4.1-1 is modified by introducing a concentration fluctuation term. Concerning scattering losses due to the imperfection of waveguides, it is reported that the core-cladding imperfections were mainly caused by bubbles outside the core and that these imperfections can be avoided by appropriately selecting the drawing conditions and by their precise control.

Describing vibrational excitations in a crystal is usually done with the concept of phonons. Phonons are described with a wave-function. The equation of motion for this wave-function describes how temperature and sound propagates through the solid as vibrational excitations. If the atoms move in opposite directions to each other the propagation is associated with optical phonons, if on the other hand the atoms move in unison the propagation is associated with acoustic phonons. The crystal

lattice is three-dimensional, therefore there exist both longitudinal and transversal optical and acoustic phonons. From a crystal structure point of view, glasses are different from their crystal counterparts in that they lack long-range order, but of course still sound and heat are transferred. One can describe Raman scattering as due to optical phonons and Brillouin scattering as due to acoustic phonons. Despite the many differences between SRS and SBS, they can both be described by propagating vibrational excitations and therefore we can derive the governing equations for SRS and SBS simultaneously.

The effects of light scattering are classified by the relation between the frequencies of the incident and those of the scattered photons. When these frequencies are equal, one speaks of unshifted scattering, i.e., Rayleigh or elastic scattering. But if these frequencies differ, the term shifted or inelastic scattering is used. An example is Raman scattering. Here, the frequency shifts equal the characteristic vibrational frequencies of the molecules. For Raman shifts in the range 100-600cm^{-1}, the Raman cross-section is found to depend linearly on the Germania concentration [Davey *et al.*, 1989]. Photons scattered to lower frequencies are termed Stokes lines and those scattered to higher frequencies are the anti-Stokes lines [Gogolla *et al.*, 1999].

If one assumes the interaction of a molecular system with a harmonic electric field initiated by a laser of angular frequency ω_0, one can interpret the Raman scattering as an inelastic scattering of a photon of energy $h\omega_0/2\pi$ with a molecule of initial energy state E_1 and final state E_2.

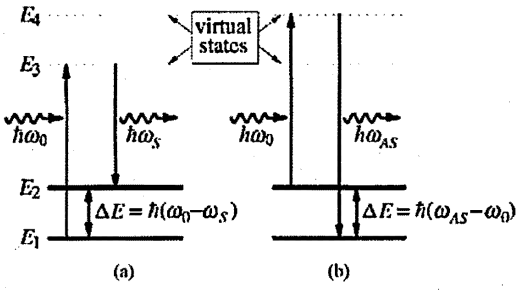

(a) Stokes scattering **(b)** anti-Stokes scattering

Figure 4.1-2: The schematic diagram of Rayleigh and Raman scattering.

Now we suppose the scattering system as one vibrating molecule with the fixed energy states E_1 and E_2. By elastic or inelastic collision of an incident photon with the molecule, the system initially in the state E_1 is excited to the virtual nature of the state E_3, no real absorption takes place, but only light scattering. In the case of Rayleigh scattering, the final state equals E_1. Thus this process is characterised by the transition $E_1 \rightarrow E_3 \rightarrow E_1$. The transition $E_1 \rightarrow E_3 \rightarrow E_2$ (see Figure 4.1-2 (a)) represents the Raman Stokes scattering. The transition $E_2 \rightarrow E_4 \rightarrow E_1$ (see Figure 4.1-2 (b)) represents the Raman anti-Stokes scattering. Here the initial state is E_2, it is excited by molecule vibration. By interacting with an incident photon, the molecule is excited to the virtual state E_4 and may drop spontaneously to the lowest energy level E_1. The vibration energy levels E_1 and E_2 are occupied according to the Bose-Einstein phonon distribution. Consequently, the anti-Stokes transitions are rare in comparison to the Stokes transitions and the intensity of the Stokes wave is higher than that of the anti-Stokes wave. With increasing temperature, the probability for an anti-Stokes transition increases.

By assuming phase matching and neglecting group velocity dispersion and higher-order Raman processes [Alfano *et al.*, 1988], a predicted ratio of the Stokes spectral width to the primary spectral width without dispersion is:

$$X = \frac{\Delta\omega_{Raman}}{\Delta\omega_{Laser}}$$

Equation 4.1-2 Ratio of the Raman spectral width to the laser source spectral width

In glass fibre the ratio X is equal to 2.

$$\Delta\lambda_{Stokes} \cong 2.\left[1+2.\frac{\Delta\lambda_{Stokes}^{shift}}{\lambda_{source}}\right].\Delta\lambda_{source}$$

$$\Delta\lambda_{anti-Stokes} \cong 2.\left[1-2.\frac{\Delta\lambda_{anti-Stokes}^{shift}}{\lambda_{source}}\right].\Delta\lambda_{source}$$

Equation 4.1-3 Rayleigh scattering in the case of a single-component material

The spectral broadening of the Raman lines is about two times that of the laser line. As an example at 905nm, a source having a spectral width of 4nm, the spectral Stokes or anti-Stokes shift is about 36nm [Liu *et al.*, 1991], therefore the Stokes spectral width is approximately 8.5nm and the anti-Stokes spectral width is 7.5nm without dispersion. However, the measured ratio of these spectral broadenings was reported from Alfano to be 2.9 ± 0.1.

4.1.2 OTDR PRINCIPLE

The principle of OTDR has been discussed by a number of authors [Dakin *et al.*, 1985], [Geiger *et al.*, 1995]. From these references, it follows that there is a close similarity between conventional, Rayleigh-backscatter OTDR and Raman-backscatter OTDR. Short pulses of light are launched into the fibre and the scattering at a given range determined from the return power after a time interval appropriate to that round-trip distance.

$$\left|\begin{array}{l} P_{AS}(z) = \frac{1}{2}.P_0.W.S.\alpha_{AS}(z).V_g.\exp\left[-\gamma_{AS}^{T}.z\right] \\ P_S(z) = \frac{1}{2}.P_0.W.S.\alpha_S(z).V_g.\exp\left[-\gamma_S^{T}.z\right] \end{array}\right.$$

Equation 4.1-4 Anti-Stokes and Stokes backscattered power at range z

The only additional equipment required for Raman OTDR is a spectrometer to reject the Rayleigh scattered light and pass the desired Raman spectral components [Kikuchi *et al.*, 1988]. The return power P(z) from scattering in the fibre at range z is given by Equation 4.1-4, where P_0 is the peak power launched (Watt), W is the pulse width (second), S is the backscatter capture fraction of the fibre, i.e. the proportion of

the scattered light collected by the fibre in the reverse direction. S depends on the numerical aperture of the fibre, the angular distribution of the scattered light and the distribution of scattering cross-section across the core [Whitbread *et al.*, 1989]. The Raman scattering loss coefficients $\alpha_{AS}(z)$ and $\alpha_S(z)$ are the attenuation coefficients at range z for the anti-Stokes, Stokes signals respectively [Healey, 1986]. The parameters γ^T_{AS} and γ^T_S are the total attenuation coefficients resulting from the respective average attenuations of the forward travelling (γ_R) and backscattered pulses (γ_{AS} or γ_S) and of the total optical losses on line. V_g is the average group velocity ($V_g = c/n_1$). It can be seen that any change of the fibre parameters [Eriksrud *et al.*, 1984, Mickelson *et al.*, 1982], its numerical aperture, local loss changes induced by an environmental constraint, will cause variations of backscattered power P_* and will be reflected in the OTDR profile [Kee *et al.*, 1999]. Both the amplitude and the location of these variations can be determined from that profile. OTDR can therefore be used as an interrogation technique to determine both the strength and the position of the external perturbations.

4.1.3 OPERATING WAVELENGTH AND FIBER DEPENDANCY

As a pulse of light proceeds through the fibre, it widens in the time domain. This spreading is caused by dispersion. It is important to consider dispersion effects because pulse spreadings will reduce spatial resolution. There are three primary sources of dispersion in fibres [Powers, 1993]: material dispersion (also called chromatic dispersion), waveguide dispersion and modal delay (or group delay). Material dispersion and waveguide dispersion are caused by the same physical effect: the dependence of the index of refraction of glass on wavelength.

Material dispersion is caused by the index of refraction being a function of wavelength. All sources of light have some degree of spectral width to their output, therefore the longer wavelengths with their faster velocities will arrive at the receiver before the shorter wavelengths, thereby stretching the pulse. In the following study,

n_1 is the axial optical fibre core index, n_2 is the cladding index and a is the core radius. The pulse spreading due to material dispersion is given by:

$$\Delta\tau_{mat} = -\frac{L}{c}.\frac{\Delta\lambda}{\lambda}.\lambda^2.\frac{d^2n_1}{d\lambda^2}$$

Equation 4.1-5 Pulse spreading due to material dispersion

where $\Delta\lambda$ is the spectral width of the source, λ is the source nominal wavelength and $d^2n_1/d\lambda^2$ is the second derivative of the core index of refraction with respect to wavelength. $\lambda^2.(d^2n_1/d\lambda^2)$ characterises the material dispersion of the fibre.

$$DS_{mat.} = -\frac{1}{c\lambda}.\left[\lambda^2.\frac{d^2n_1}{d\lambda^2}\right]$$

Equation 4.1-6 Normalised delay from material dispersion

$DS_{mat.}$ is the normalised delay. At 900nm, for a typical monomode silica glass $\lambda^2.(d^2n_1/d\lambda^2) = 0.018$ then $DS_{mat.} = -67ps.km^{-1}.nm^{-1}$. Therefore, an optical fibre length of 0.5km and a source spectral width of 4nm give a pulse spreading of 0.13ns.

Usually the waveguide dispersion is negligible in multimode fibres and in single-mode fibres operated at wavelength below 1000nm. This waveguide dispersion results from the propagation constant of a mode being a function of the ratio of the core diameter to the wavelength. The net delay due to the waveguide dispersion is:

$$\tau_{wg} = \frac{L}{c}.\left[\frac{d\beta}{dk}\right]$$

Equation 4.1-7 Net delay due to waveguide dispersion

β is the mode propagation coefficient and $k = 2.\pi/\lambda$. The normalized propagation constant b is defined by:

$$b = \frac{\left[\beta^2/k^2\right] - n_2^2}{n_1^2 - n_2^2} \quad \Rightarrow \beta \approx n_2.k.(b.\Delta + 1)$$

Equation 4.1-8 Normalised propagation constant

where $\Delta = (n_1^2 - n_2^2)/(2.n_1^2)$. It can be shown with $V = (2.\pi.a/\lambda).n_1.(2.\Delta)^{1/2}$ that:

$$\Delta\tau_{wg} = -\frac{V}{\lambda}.\Delta\lambda.\frac{d\tau_{wg}}{dV} \approx -\frac{n_2.L.\Delta}{c}.\frac{\Delta\lambda}{\lambda}.\left[V.\frac{d^2(Vb)}{dV^2}\right]$$

Equation 4.1-9 Net delay due to waveguide dispersion

Therefore, considering a 9/125 single-mode fibre with $n_1 = 1.48$ and $\Delta = 0.22\%$ operating at 1300nm, a 0.5km optical fibre length and a source spectral width of 4nm, the waveguide dispersion is 8ps.

Group delay is important in multimode fibres. It is caused by the different path lengths associated with each of the modes of a fibre, as well as the differing propagation coefficients associated with each of mode. Since modal dispersion is due to the existence of various modes, it is not present in single-mode fibres.

For a multimode step-index fibre, the time delay between the fastest and slowest pulse is the modal pulse delay distortion and is given by:

$$\Delta\tau_{modal} = \frac{L.(n_1 - n_2)}{c}.\left[1 - \frac{\pi}{V}\right]$$

Equation 4.1-10 Modal pulse delay distortion

This expression ignores the constant delay common to all modes and represents only the difference in propagation times. Therefore, considering a 50/125 multimode step-index fibre with $n_1 = 1.46$ and $\Delta = 1\%$ operating at 905nm, a 0.5km optical fibre length, the modal dispersion is about 24ns.

For a multimode graded-index fibre, we must account for the inhomogeneous

velocity of the light as well as the sinusoidal paths in the fibre. It has to be noted that the higher-order modes have longer path lengths because of their further excursion from the axis, their average velocity will be higher because of the increased velocity as the rays moves away from the centre axis. The higher velocity cancels the effect of the longer path, and modes that leave the axis at the same time will arrive at the next axis crossing at the same time. More exact analysis of the selected graded index fibre provides the optimum value for the profile index $\alpha_{opt.} \cong 2 - (12.\Delta/5)$. The modal dispersion for multimode graded-index optical fibre can then be described as:

$$\Delta\tau_{modal} \approx \begin{cases} \dfrac{n_1.\Delta.(\alpha-\alpha_{opt})}{(\alpha+2).c}.L & \alpha \neq \alpha_{opt} \\ \dfrac{n_1.\Delta^2}{2c}.L & \alpha = \alpha_{opt} \end{cases}$$

Equation 4.1-11 Modal pulse delay distortion

L is the length of the fibre. For negative $\Delta\tau_{modal}$, the higher-order modes are arriving before the lower-order modes. Therefore, considering a 50/125 multimode graded-index fibre with $n_1 = 1.46$, Δ=1%, a 0.5km optical fibre length, the modal dispersion is about 0.13ns if $\alpha = \alpha_{opt} = 2$ and 0.64ns if $\alpha \neq \alpha_{opt}$ [$\alpha = 0.95\ \alpha_{opt}$, $\alpha_{opt} = 2$].. We note that small differences between α_{opt} and the achieved α cause a major change in the value of this ratio. This high sensitivity to values of α leads to tight tolerances on its value.

The modal pulse delay distortion is therefore significantly larger for a step-index fibre compared to a gradient-index fibre. The graded-index multimode fibres provide a wider bandwidth than the alternative step-index design. However, it has been shown that the backscatter factor S, i.e. the proportion of the scattered light collected by the fibre in the reverse direction, for a step-index and graded-index multimode fibre are:

$$S = \frac{3}{8}.\left[\frac{NA}{n_1}\right]^2$$

Equation 4.1-12 Backscatter factor S for a step-index multimode fibre

$$S = \frac{1}{4}.\left[\frac{NA}{n_1}\right]^2$$

Equation 4.1-13 Backscatter factor S for a graded-index multimode fibre

where NA is the numerical aperture and n_1 is the refractive index at core centre.

This gives a backscatter factor of 8.51×10^{-3} for a step-index and of 5.68×10^{-3} for a graded-index multimode fibre [Hartog, 1981].

The selection of the wavelength of the source is mainly determined by the spectral attenuation of the fibre and the desired range of the system. The loss in general increases with decreasing wavelength for wavelengths shorter than about 1.6μm, owing to the predominance of the Rayleigh-scattering process, which increases with the inverse fourth power of the wavelength.

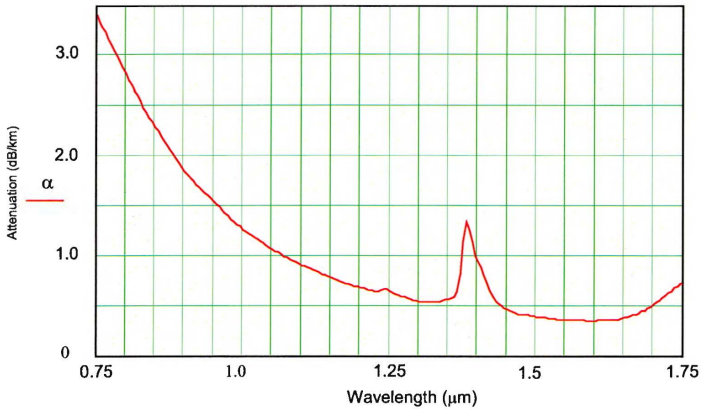

Figure 4.1-3 Typical spectral attenuation curve for a 50/125 multimode optical fibre

The 1dB/km peaks at 1.39μm and 1.24μm, on Figure 4.1-3, are absorption peaks, which result from the presence of OH^- ions (impurities) in the glass.

There is no doubt that a DTS for aeronautic applications will have to use multimode fibres [Hartog *et al.*, 1984]. A single-mode design is unsuitable: the low launching efficiency into this fibre, together with its low backscatter coefficient [Brinkmeyer, 1980], splicing difficulties and many other factors are indicating major non-conformities to the environmental conditions.

The use of a large core fibre increases the power that can be launched into the fibre, in rough proportion to the core diameter. The selection of the diameter affects its minimum bending radius: larger diameter fibres must, all other things being equal, generally be bent over wider radii than smaller diameter fibres, owing to the problem of stress fatigue, which can result in the growth of cracks in the fibre and, eventually, in fibre failure. On the other hand, a larger core diameter facilitates splicing and connecting fibres. However, the numerical aperture of larger core-diameter fibres tends to be smaller. A minimum numerical aperture of 0.22 is the design baseline. For all silica fibres, short distances favour high values of the numerical aperture, since this choice results in higher signal levels and the higher loss per unit length may not be highly significant over short distances.

Thus for shorter ranges, as for aeronautic applications, a short wavelength would be selected since the higher attenuation per unit length is not important in this case and the shorter wavelength results in a stronger initial backscatter signal, owing to the increasing scatter at the shorter wavelengths. For this reason, the DTS could be operated at a wavelength of 905nm, a wavelength for which high power semiconductor sources are available and which is optimum for lengths of order 1-2km. It can be noted also that good quality fibres have no significant impurity-related losses at wavelengths shorter than about 1μm.

4.2 RAMAN BACKSCATTERING RELATED TO DETECTION PERFORMANCES

In conventional optical time domain reflectometers an optical pulse is launched into an optical fibre and the backscattered light is detected in a sampling receiver. The output of this receiver is amplified, filtered and finally put through an electronic signal processor to improve the signal-to-noise-ratio. One may focus therefore in this paragraph on the determination of the optical pulse characteristics to ensure a performing distributed temperature detection. The system performances are therefore also relying on the sensing element specifications as well as on the system electronic core architecture.

4.2.1 SPATIAL RESOLUTION

The spatial resolution denotes the ability of the OTDR system to distinguish between defects or perturbations that occur in close proximity. The minimum distance [Geiger *et al.*, 1995] between two reflective points to avoid any overlap of the response is called the one-way two-point resolution $R_{S\text{-}OTDR}$:

$$R_{S-OTDR} = \frac{c}{2.n_1}.W_{FWHM}$$

Equation 4.2-1 One-way two-point resolution

where c/n_1 is the speed of light in the fibre and W_{FWHM} is the full-width at half maximum of the optical pulse. $R_{S\text{-}OTDR}$ is also termed the spatial resolution. A FWHM of 10ns would therefore give a spatial resolution of 1m. It has been shown in 4.1.3 that the optical fibre bandwidth is also of importance for targeted small spatial resolution.

Some instrumentation effects, such as post-detection bandwidth or digital sampling intervals, etc, may limit the resolution. A discrete reflection can be used therefore determine the spatial resolution. When detecting the Rayleigh or Raman backscattering components, such a reflection will be taken for example from a

broken optical fibre or from a sharp and localized temperature variation. To obtain a high resolution the launched pulse width should be narrow and considerable signal averaging will be required to obtain a good signal-to-noise ratio. To solve the problem, it has been proposed to launch a semiconductor laser beam modulated with a pseudorandom bit sequence [Everard *et al.*, 1989]. The received signal is then multiplied by a delayed version of the pseudorandom signal, which because of the autocorrelation function allows the spatial information to be obtained without ambiguity. The system described reported a $2^{15} - 1$ maximal length pseudorandom sequence, which repeats after 32767 bits. It should be noted that to obtain a dynamic range a very pure sequence has to be generated and therefore the pulses need to be accurate both in pulse amplitude and zero crossing position. However, the signal processing associated with this technique, the interface management between the laser diode driver and the signal post-processing software, as well as the additional costs from the modulation stage lead us, as shown also in Chapter 3, to the conclusion that for an aeronautic system the pulse width shortening to influence the spatial resolution will be preferred.

4.2.2 TEMPERATURE RESOLUTION

The temperature resolution ΔT of the system is defined to be that which causes a change of the signal level equal to the noise level of the system. Therefore, the signal-to-noise ratio of the system is related to the temperature resolution by:

$$SNR_{AS} = \frac{1}{R_{AS}.\Delta T_{AS}}$$

$$SNR_{S} = \frac{1}{R_{S}.\Delta T_{S}}$$

Equation 4.2-2 Signal-to-Noise Ratios as a function of the temperature resolutions

where R_{AS} and R_S are the rate of change of the signal intensity with temperature for the anti-Stokes and Stokes signals. R_{AS} and R_S can be derived as:

$$R_{AS} = \frac{dI_{AS}}{I_{AS}} = \frac{h.c.\Delta\nu}{k.T} \cdot \frac{\exp[h.c.\Delta\nu/k.T]}{\exp[h.c.\Delta\nu/k.T]-1} \cdot \frac{dT}{T}$$

$$R_S = \frac{dI_S}{I_S} = \frac{h.c.\Delta\nu}{k.T} \cdot \frac{1}{\exp[h.c.\Delta\nu/k.T]-1} \cdot \frac{dT}{T}$$

Equation 4.2-3 Signal intensity rate of change with temperature for anti-Stokes and Stokes signals

where h is Planck's constant, c is the free space velocity of light, k is Boltzmann's constant, T is the absolute temperature, $\Delta\nu$ is the frequency Raman shift in fused silica. The anti-Stokes signal is found to have a temperature sensitivity of about 0.7%/°C, while the Stokes signal sensitivity is reaching 0.1%/°C. To compensate against propagation losses along the fibre, we normalize the anti-Stokes scattered signal with the Stokes scattered signal. The ratio $\Re$ between the anti-Stokes I_{AS} and Stokes I_S intensities is given by:

$$\Re(T) = \frac{I_{AS}}{I_S} = \frac{R_S}{R_{AS}} \cdot \frac{dI_{AS}}{dI_S} = C_R \cdot \left[\frac{\lambda_S}{\lambda_{AS}}\right]^4 \exp\left[-\frac{hc.\Delta\nu}{kT}\right]$$

Equation 4.2-4 Raman anti-Stokes and Stokes intensity ratio function of the rates of change

C_R is a constant, λ_S is the Stokes wavelength and λ_{AS} is the anti-Stokes wavelength. Therefore, the temperature sensitivity of the intensity ratio can be found easily by differentiating Equation 4.2-4. The main advantage of the measurement of the intensity ratio of the Stokes and anti-Stokes Raman backscattered signal [Yang, 1995] in the fibre lies in providing an absolute indication of the temperature of the medium, irrespective of the light intensity, the launch conditions, the fibre geometry and even the composition. The main three system parameters, namely the pump optical power [Chang *et al.*, 1997, Landahl *et al.*, 1998], the photo-receiver gains and the amplification gains will therefore be adjusted so as to optimize the two acquisition channels in terms of their respective SNR.

4.2.3 SYSTEM DETECTION RANGE

To avoid sampling more than one point at the same time, the maximum repetition rate of the pulse transmitter must be limited to $c/(2.n_1.L)$ where c is the free space velocity of light, n_1 is the fibre axis index and L is the length of the fibre. This means that for a 500m long optical fibre ($n_1 = 1.46$), the pulse driver frequency can have a maximum pulse repetition frequency of about 200kHz.

A forecast on the necessity to carry out about 2000 averages to reach a temperature resolution of ±3°C within 3s is dimensioning the hardware of the driver for the pulsed laser diode. At first, without any considerations of signal attenuation, pulsing at 2kHz would allow monitoring a 50km long optical fibre [Ko *et al.*, 1996, Spirit *et al.*, 1989]. However, when interrogating the sensing element in a single-ended configuration, it is clear that to preserve the spatial resolution and to simply be in a position to read the information at the furthest ending of the fibre, one may take into consideration both its optical fibre bandwidth and its attenuation characteristics [Samson, 1990]. The first shall be as high as the application is requiring, the second shall be as small as the SNR should be at the furthest point of the fibre.

4.2.4 TEMPERATURE PROFILE AND REFRESHMENT TIME

The performance of an optical fibre sensor is ultimately determined by the time it takes to update a set of measurements. Unlike OTDR systems that measure the transmission properties of a fibre network, where long integration times are permissible, fibre sensors must respond quickly and so should have measurement times for F/O detection of a few seconds. What sets the instrument's response time is the signal-to-noise ratio after amplification (which might be improved with post signal processing like for example signal averaging), which in turn depends on: the required measurement accuracy and the instrument hardware performances [Thomas, 1998].

4.3 RAMAN BACKSCATTERING SENSITIVITY TO ENVIRONMENTAL CONDITIONS

The range of applications for fibre-optic distributed temperature sensors based on Raman scattering is developing in fields for which the variety of the environmental conditions is questioning the continuous quality of the targeted measurements. These environmental conditions might be to a certain extent found in the aeronautic applications described in chapter 3 (and detailed for example in the "DO-160D, the Environmental Conditions and Test Procedures for Airborne Equipment" document [EUROCAE, 1997]).

4.3.1 SENSING ELEMENT AND OPERATING / SURVIVAL TEMPERATURE RANGES

In most external environments and all-harsh environments some form of ruggedisation of fibre is necessary [Smith *et al.*, 1996]. The level of robustness to be provided on the sensing element is clearly a trade-off between the environment and what the applications dictates to be the response time of the sensor cable [Fitch *et al.*, 1992]. Thermal response in this sense is not a parameter available from the cable manufacturers so various experiments will have to be carried out for the DTS qualification tests to measure it experimentally. The aeronautic applications selected are covering an operating temperature range from -55°C to +300°C. The survival range from +300 to +500°C is the temperature range where the system can have degraded detection performances but when coming back to the operating temperature range will recover its essential performances. It has to be said that when such an event would occur on an aircraft (maximum duration is evaluated to 9 hours), the sensing element will be replaced.

Some studies have produced interesting results in terms of a temperature-resistant design of the sensing element [Iida *et al.*, 1994]. The increase of optical loss caused by hydrogen at high temperatures, quartz with very low levels of impurities and structural defects is used in the fibre material. A carbon-ceramic, which is resistant to decomposition at high-temperature is used in the sheath system. The optical fibre is

enclosed in a stainless steel tube to improve its mechanical features and a nitrogen atmosphere is used in the tubing to restrain deterioration of the ceramic materials at high temperature.

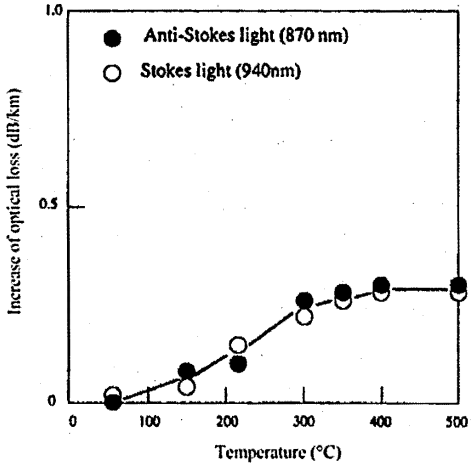

Figure 4.3-1: Characteristics of optical loss in high temperature environment

At 500°C, the increase in optical loss was 0.3dB/km, a value, which presents no problem for temperature measurement applications. The accuracy of measurements using this fibre was within 2°C in the range of 0 to 500°C.

It has been shown also that the fluctuations of these optical losses tend to disappear [Feced *et al.*, 1997] after several temperature cycles performed over the full survival range .

4.3.2 MECHANICAL AND SPECIFIC CONSTRAINTS

In the aerospace industry, the specified operating and survival temperature ranges (see 4.3.1) are coupled with a sometimes-stringent vibration operating range. A DTS design will have to make sure that no interaction from the vibration spectrum on the sensing line can be perturbing the data acquisition for a reliable and fully segregated temperature measurement [Hurtig *et al.*, 1996].

As the attenuation of the light level increases with an increase in the degree of micro-

bending along the fibre, the anti-Stokes and Stokes signal intensities might also be impacted and the temperature measurement might be corrupted. A separate characterization of the sensing line for its (micro-) bending and temperature responses has shown for example an attenuation of light of 1dB/km for a 200μm multimode optical fibre, when applying locally (along 50mm) a 12kPa pressure [Knowles *et al.*, 1998]. It has to be noted that a minimum of 20 pressure cycles through the full pressure range (7 to 25kPa) had to be carried out to see the hysteresis effect coming to a minimum.

The information about the stress levels for the cable along the line can be considered for the selection of the polymer coatings on optical fibres with regard to their impermeability to water. A multimode optical fibre (200μm core) is reported to see a 14% increase of its fused silica OH content in 200 hour, when immersed in water and undergoing a tensile stress of 1.56Gpa [Walrafen *et al.*, 1984]. The tensile stress will have to be compared to an installation realistic situation and the experiment re-conducted with the selected DTS optical fibre.

The backscattered power received by the detector is affected by both the forward loss of the probe pulse and the reverse attenuation of the scattered light. One loss source is resulting from a pure geometrical configuration of the fibre: the variation of its core diameter at different position along the propagation direction. The backscatter power level changes associated with these diameter variations fibre can be explained in terms of their effect on the reverse-travelling light [Conduit *et al.*, 1981]. The phenomenon is caused by attenuation of the backscattered light, which, since it contains high order modes, is sensitive to mode conversion and differential mode attenuation.

Although the transport of radioactive elements in aircraft is unusual, it is possible to briefly address the consequences of radiation on the sensing element [Jensen *et al.*, 1998, Takada *et al.*, 1998]. In presence of radiation, the temperature measured appears lower than the correct value. In order to apply the DTS system in a

radioactive environment as a reliable and stable temperature monitor, it is necessary to put in place special correction techniques. It is for example possible to discriminate the radioactive effect from the temperature event by comparing information from different points along the fibre.

4.3.3 OPTICAL FIBRE BREAK CONSIDERATIONS

An identified failure associated to the sensing element, which could lead to the decision of an emergency landing and therefore potentially to a classified catastrophic event, is a fibre break.

The loss along the fibre will be monitored to detect if the fibre has broken (or has developed a high loss). The system should then determine which zone if any, has been affected (a fibre break will lead to a warning signal to be defined with the certification/airworthiness authorities) and declare it to the A/C Central Maintenance Computer (CMC) and possibly to the Flight Warning Computer (FWC).

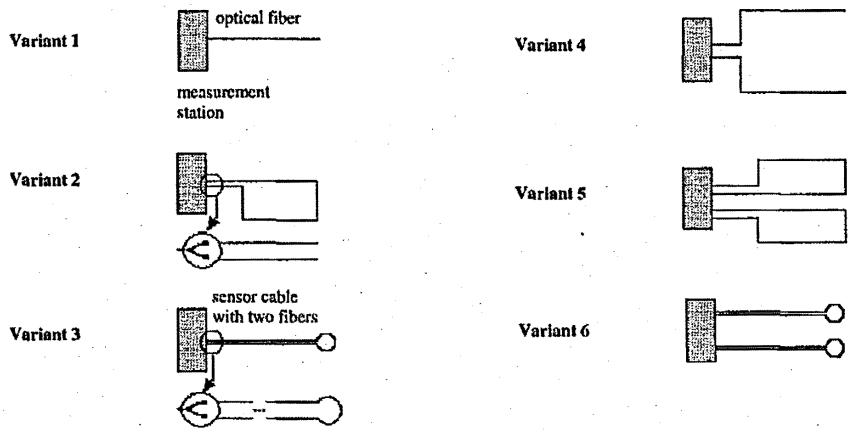

Figure 4.3-2: Basic topology and internal structure of sensor cables with optical fibres

The position of the break will also be identified to continue monitoring the temperature profile using the double-ended configuration (this configuration, after detailed reliability analysis, might be proven necessary only for diagnostic purposes). The double-ended measurement has two advantages. First the effects of fibre loss are

eliminated from the temperature measurement, making the system insensitive to micro-bends and connections. Both of these loss sources may vary and result in a change of signal intensity. Measuring from both ends and taking the geometric mean of the two eliminates this source of error, provided the fibre does not experience dynamic loss changes during the course of a measurement cycle (i.e. within about 1s). Secondly, the temperature profile measurement can be made along the total length of the fibre in the event of a break. Since the fibre is probed from each end, temperature information will continue to be available up to the break as measured from each end. Thus, assuming only one break, the integrity of the system is maintained. The loop configuration for break recovery, as seen on Figure 4.3-2, can be implemented in different ways as shown through the variants 2, 3, 5 and 6 [Nitz *et al.*, 1998]. The reflections that may be caused by the break will be suppressed in the immediate vicinity to prevent false alarms occurring. In the case of a single fibre, either the double-ended configuration is managed using an optical switch or both endings will be interrogated using two separated emitter-receiver channels. This also applies for the situation when there is more than one break in the fibre, in which case the suppression will cover the whole of the area between the breaks. If a break occurs in a zone when it is an alarm condition, the alarm condition will be clamped. And all the zones that are encompassed by a multiple break condition will also have the alarms clamped. These situations might indeed result of a fire damage.

Even though, a single-end measurement is very unlikely to be the favourite configuration, mainly because of a lack of redundancy evidence, the study will investigate the working principle details and improve the performances of variant 1. However, variant 2 with 2 independent emitting-receiving modules (solution without switch) is considered as the most realistic architecture for an on-board DTS.

4.3.4 OPTICAL POWER BALANCE FOR EFFICIENT SENSING LINE INTERROGATION

The Rayleigh scattering loss factor, using the BTL model [Hartog, 2001] as a function of the parameter $Dn(NA)=NA^2/2.N_1^2$ is calculated as being equal to 1.1, NA being equal to 0.2 and N_1 to 1.46. The scattering losses being proportional to λ^{-4}, the loss factors are then 1.64dB.km^{-1} for the Rayleigh signal (α_R at 905nm), 1.92dB.km^{-1} and 1.41dB.km^{-1} for the anti-Stokes and Stokes signals (α_* at 870 and 940nm respectively).

For a Rayleigh signal about 36dB below the pump signal, the normalized backscatter factor, which is independent of scattering loss and filtering losses, can be estimated. The anti-Stokes and Stokes signals are about 28dB and 18dB lower than the Rayleigh signal level respectively (α_{F*}).

The total optical loss amount (α_{opt}) reaches about 12dB, taking into account for the total light travel, namely: the loss through the wavelength demultiplexer, the total budget for splices and connectors, the reference coil, the laser to pigtail optical coupling. The photocurrent before multiplication is then:

$$I_*(z) = P_0.W.R_*.\eta_*.10^{-\left[(z.(\alpha_R+\alpha_R^{ex}+\alpha_*+\alpha_*^{ex})+\alpha_{opt})/10\right]}$$

$$\eta_* = \frac{1}{2}.S.V_g.\alpha_*.\alpha_{F*}$$

Equation 4.3-1 Anti-Stokes or Stokes photocurrent $I_*(z)$ before multiplication from distance z

The optical pulse peak power P_0 is 10W with a coupling efficiency of about 30%, the pulse width W is assumed to be 13ns and the APD responsivity R_* is 0.47 and 0.33A/W for the anti-Stokes and Stokes signals. The group velocity V_g is about $3.10^8/N_1$.

The excess losses α_R^{ex} and α_*^{ex} are assumed independent of the input wavelength at the wavelength range of interest ($\alpha_R^{ex} = \alpha_*^{ex} = 1$). The backscatter factor S is detailed in Equation 4.1-12 and Equation 4.1-13 and is considered here to be equal to 5.68 ×

10^{-3}. The distance z is expressed in kilometers.

One may therefore anticipate the following level of Raman signals before multiplication at the respective APDs:

	Anti-Stokes Signal	Stokes Signal	
z = 100m	1.26	6.46	**nA**
z = 500m	0.75	4.06	**nA**

Table 4.3-1 Photocurrent before multiplication from distance z

Further analysis could also demonstrate the limitations system architecture has towards the number of splicing and connectors. However, one of the main objective of the study is to offer the aircraft manufacturers the possibility of a permanently installed and easily removable sensing element (objective is a maximum of two connecting points to the control unit) as one part of a concept to improve the reliability figures of commonly used F/O detection systems.

4.4 CONCLUSION

The Rayleigh and Raman scattering processes were explained and the spectral broadening of the Raman spectral lines estimated to about 12 nano-seconds is taken as sizing criteria for the demultiplexer filters. The radar equations associated with the anti-Stokes and Stokes signals have highlighted the important parameters, for example the coupled optical energy into the fibre. The fibre attenuation and the optical pulse width play a major role in the system detection range and the spatial resolution respectively. Besides the material dispersion, the waveguide dispersion and the modal delay are widening the propagating pulse in the time domain. The cumulative effect of these dispersions limits the achievable spatial resolution. Although the backscatter factor for a multimode step-index fibre is 50% higher than for a graded-index fibre, one shall select the later to be in a position to reach a 1m spatial resolution for a 500m long sensing element. The choice of the operating wavelength is driven by the fibre spectral attenuation, the desired range of the system, but also by the low-cost, reliability, and the power figures of the laser diode and the spectral responsivity of the corresponding photodetectors. A NIR wavelength is selected. The relationships were established between the spatial, the temperature resolutions, the detection range, the refreshment time and the system configuration.

The analysis of the Raman signal behaviour over the full survival temperature range shows no major "non-conformities" to the selected applications. The application of a pressure on a fibre is increasing the local optical losses and will have to be the object of dedicated specifications for the sensing element installation. The analysis of the most probable system architectures to mitigate, in operation, a fibre break, has lead to the recommendation of a one-fibre, double-ended system using two emitting-receiving modules (one at each fibre ending). Finally, resulting from an optical signal at a distance z and considering a total budget of 12dB of total optical losses, the APD photocurrents before multiplication are evaluated to be about 1nA for the anti-Stokes signal and 5nA for the Stokes signal.

REFERENCES

Alfano, R. R. and Ho, P. P. "Self-, Cross-, and Induced-Phase Modulations of Ultrashort Laser Pulse Propagation". Journal of Quantum Electronics. (1988) Vol. 24. Iss. 2. pp.351-364.

Brinkmeyer, E. "Analysis of the Backscattering Method for Single-Mode Optical Fibers". Journal of the Optical Society of America . (1980) Vol. 70. Iss. 8. pp.1010-1012.

Chang, J., Baiocchi, D., Vas, J., and Thompson, J. R. "First Stokes Pulse Energy Statistics for Cascade Raman Generation in Optical Fiber". Optics Communications. (1997) Vol. 139. pp.227-231.

Conduit, A. J., Payne, D. N., Hartog, A. H., and Gold, M. P. "Optical Fibre Diameter Variations and their Effect on Backscatter Loss Measurements". Electronics Letters. (1981) Vol. 17. Iss. 8. pp.308-310.

Dakin, J. P., Pratt, D. J., Bibby, G. W., and Ross, J. N. "Temperature Distribution Measurement using Raman Ratio Thermometry". SPIE Fiber Optic and Laser Sensors III. (1985) Vol. 566. pp.249-256.

Davey, S. T., Williams, D. L., Ainslie, B. J., Rothwell, W. J. M., and Wakefield, B. "Optical Gain Spectrum of GeO2-SiO2 Raman Fibre Amplifiers". IEE Proceedings. (1989) Vol. 136, Pt. J. Iss. 6. pp.301-306.

Eriksrud, M., Mickelson, A. R., and Lauritzen, S. "Backscattering Signatures from Optical Fibers with Differential Mode Attenuation". Journal of Lightwave Technology. (1984) Vol. LT-2. Iss. 2. pp.139-145.

EUROCAE. EUROCAE ED-14D / RTCA DO-160D. Environmental Conditions and Test Procedures for Airborne Equipment. (1997).

Everard, J. K. A. and Thomas, R. "Distributed Optical Fibre Temperature Sensor Using Spread-Spectrum Techniques". Electronics Letters. (1989) Vol. 25. Iss. 2. pp.140-142.

Feced, R., Farhadiroushan, M., Handerek, V. A., and Rogers, A. J. "A High Spatial Resolution Distributed Optical Fiber Sensor for High-Temperature Measurements". Review of Scientific Instruments. (1997) Vol. 68. Iss. 10. pp.3772-3776.

Fitch, A., Basey, W., and Nicolis, A. W. "Distributed Temperature Measurement on a Power Cable Using Optical Fibres Incorporated in the Construction". Mains Cables Energy Division BICC Cables Ltd. Wrexham. (1992) pp.282-285.

Geiger, H. and Dakin, J. P. "Low-Cost High-Resolution Time-Domain Reflectometry for Monitoring the Range of Reflective Points". Journal of Lightwave Technology. (1995) Vol. 13. Iss. 7. pp.1282-1288.

Gogolla, T. and Farahani, M. A. "Spontaneous Raman Scattering in Optical Fibers with Modulated Probe Light for Distributed Temperature Raman Remote Sensing". Journal of Lightwave Technology. (1999) Vol. 17. Iss. 8. pp.1379-1391.

Hartog, A. H., "Wavelength-Dependent Effects in Optical-Fibre Waveguides". University of Southampton. Southampton. (1981).

Hartog, A. H. "Private Communications". Bell Telephone Laboratories Model of Scattering Loss. (2001)

Hartog, A. H. and Gold, M. P. "On the Theory of Backscattering in Single-Mode Optical Fibers". Journal of Lightwave Technology. (1984) Vol. LT-2. Iss. 2. pp.76-82.

Healey, P. "Instrumentation Principles for Optical Time Domain Reflectometry". Journal of Physics E: Scientific Instruments. (1986) Vol. 19. pp.334-341.

Hurtig, E., Grosswig, S., and Kuehn, K. "Fibre Optic Temperature Sensing: Application for Subsurface and Ground Temperature Measurements". Tectonophysics. (1996) Vol. 257. pp.101-109.

Iida, O., Onoda, D., and Kono, S. "Expansion of Measuring Range for a Fiber-Optic Distributed Temperature Sensor and Applications to Commercial Plants". IMTC'94. (1994) pp.265-268.

Jensen, F. B. H., Takada, E., Nakazawa, M., Kakuta, T., and Yamamoto, S. "Consequences of Radiation Effects on Pure-Silica-Core Optical Fibers Used for Raman-Scattering-Based Temperature Measurements". IEEE Transactions on Nuclear Science. (1998) Vol. 45. Iss. 1. pp.50-58.

Kee, H. H., Lees, G. P., and Newson, T. P. "1.65um Raman-Based Distributed Temperature Sensor". Electronics Letters. (1999) Vol. 35. Iss. 21. pp.1869-1871.

Kikuchi, K., Naito, T., and Okoshi, T. "Measurement of Raman Scattering in Single-Mode Optical Fiber by Optical Time-Domain Reflectometry". IEEE Journal of Quantum Electronics. (1988) Vol. 24. Iss. 10. pp.1973-1975.

Knowles, S. F., Jones, B. E., Purdy, S., and France, C. M. "Multiple Microbending Optical-Fibre Sensors for Measurement of Fuel Quantity in Aircraft Fuel Tanks". Sensors and Actuators A. (1998) Vol. 68. pp.320-323.

Ko, P. K. Y., Demokan, M. S., and Tam, H. "Distributed Temperature Sensing with Erbium-Doped Fiber Amplifiers". Journal of Lightwave Technology. (1996) Vol. 14. Iss. 10. pp.2236-2245.

Landahl, E., Baiocchi, D., and Thompson, J. R. "A Simple Analytic Model for Noise Shaping by an Optical Fiber Raman Generator". Optics Communications. (1998) Vol. 150. pp.339-347.

Liu, K. X. and Garmire, E. "Undertanding the Formation of the SRS Stokes Spectrum in Fused Silica Fibers". IEEE Journal of Quantum Electronics. (1991) Vol. 27. Iss. 4. pp.1022-1030.

Mickelson, A. R. and Eriksrud, M. "Theory of the Backscattering Process in Multimode Optical Fibers". Applied Optics. (1982) Vol. 21. Iss. 11. pp.1898-1909.

Nitz, S. and Iwainsky, A. "Design and Utilization of Fiber Networks for Temperature Monitoring along Cable Lines". Proceedings of IECON'98. Proceedings of the 24th Anual Conference IEEE Industrial Electronics Society. (1998) pp.1824-1828.

Powers J. P. "An introduction to Fiber Optic Systems". Edited by "2nd". *Richard D. Irwin.* (1993).

Samson, P. J. "Analysis of the Wavelength Dependence of Raman Backscatter in Optical Fibre Thermometry". Electronics Letters. (1990) Vol. 26. Iss. 3. pp.163-165.

Smith, P. and Shepherd, W. "Optical Fibre Continuous Temperature Sensing of Trace Heating Systems". BICC Thermoheat. (1996)

Spirit, D. M. and Blank, L. C. "Raman-Assisted Long-Distance Optical Time Domain Reflectometry". Electronics Letters. (1989) Vol. 25. Iss. 25. pp.1687-1689.

Takada, E., Kimura, A., Jensen, B. H., and Nakazawa, M. "Correction Techniques of Radiation Induced Errors for Raman Distributed Temperature Sensor and Experiment at the Experimental Fast Reactor: JOYO". Journal of Nuclear Science and Technology . (1998) Vol. 35. pp.547-553.

Thomas, R., "Spread spectrum and coherent detection techniques for distributed optical fibre sensing". King's College. London. (1998).

Walrafen, G. E., Krishnan, P. N., and Hardison, D. R. "Raman Investigation of the Rate of OH Uptake in Stressed and Unstressed Optical Fibers". Journal of Lightwave Technology. (1984) Vol. LT-2. Iss. 5. pp.646-649.

Whitbread, T. W., Wassef, W. S., Allen, P. M., and Chu, P. L. "Profile Dependence and Measurement of Absolute Raman Scattering Cross-Section in Optical Fibres". Electronics Letters. (1989) Vol. 25. Iss. 22. pp.1502-1503.

Yang, S., "Design and Construction of a Raman OTDR System for Distributed Optical Fibre Sensing". UMIST. Manchester. (1995).

Yoshida, K., Furui, Y., Sentsui, S., and Kuroha, T. "Loss Factors in Optical Fibres". Optical and Quantum Electronics. (1981) Vol. 13. Iss. 1. pp.85-89.

5.1 DESCRIPTION OF THE DETECTION SYSTEM MODULES

The laboratory test bench was modular so as to be able to improve progressively the detection performances and the capabilities of the F/O distributed detection system to withstand the specific aeronautic operating conditions. A block diagram of the system is shown in Figure 5.1-2. The modules, which are held at locations A, B, C and also shown in Figure 5.1-1 and Figure 5.1-3, are described in the following sections, namely: A, the laser diode driver; B, the optical demultiplexer; C, the amplification chain.

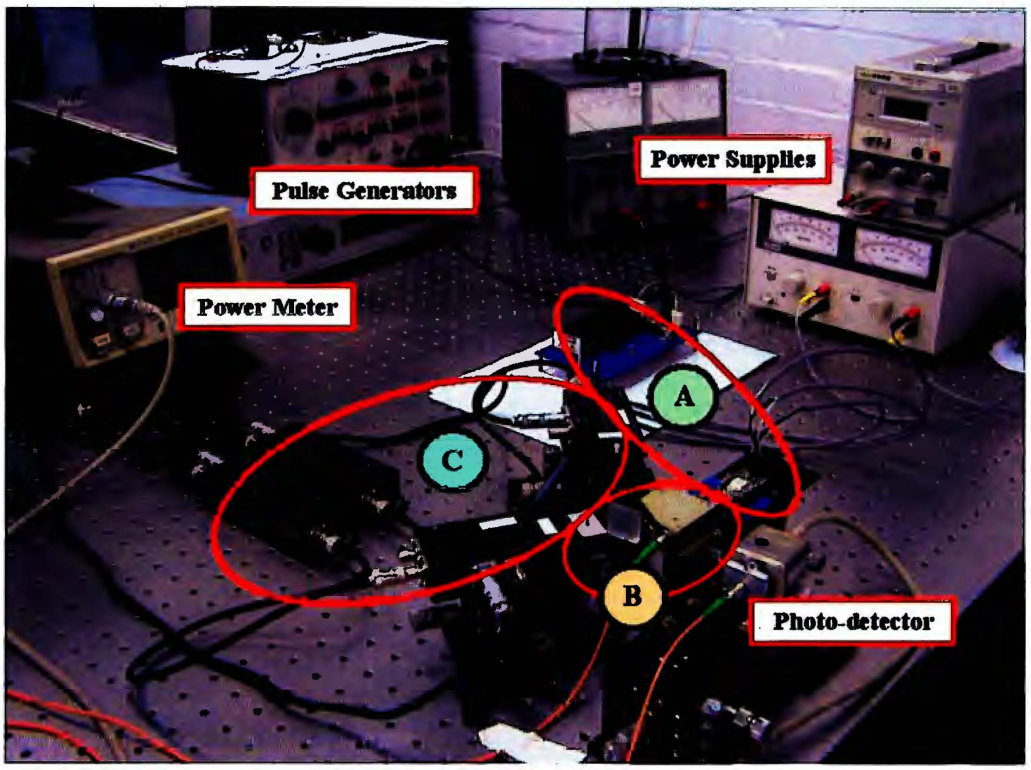

Figure 5.1-1: Nominal temperature profile for performance analysis
A: DC-DC converter, and laser diode driver. B: optical demultiplexer. C: pre-amplification and amplification stages. The computer integrating the analog-to-digital converters and the signal processing capabilities is not shown here.

The following block diagram indicates the flow of data converging from the amplification stage or the pulse generator (to trigger the acquisition) to the computer.

Metrological Requirements and Signal Processing

5.1 Description of the detection system modules 112
5.1.1 The pulsed laser diode 115
5.1.2 The laser diode driver 116
5.1.3 The optical demultiplexer 129
5.1.4 The detector and amplification chain 141
5.1.5 The digitalisation 145

5.2 Architecture of the tested system 146
5.2.1 The stakes of the new design 146
5.2.2 System temperature control 146
5.2.3 Vibration/shock-proof design 150

5.3 Detection performances analysis 151
5.3.1 Noise characteristics 152
5.3.2 Temperature resolution 155
5.3.3 Spatial resolution 156
5.3.4 Measurement time 157
5.3.5 Hot spot detection 159
5.3.6 Optical fibre length 160
5.3.7 Hardware control and monitoring 161

5.4 Digital signal processing opportunities 165
5.4.1 Averaging of the acquired signal data sets 165
5.4.2 Fourier transform and band-pass filter 167
5.4.3 Wiener filter 170
5.4.4 Soft thresholding using wavelet decomposition 175
5.4.5 Conclusion on post-signal processing 184

5.5 Compatibility to on-board system requirements 187

5.6 Conclusion 188

Compliance to the aeronautic qualification and certification tests, compactness and low weight, high F/O detection performances, low cost and system safety and reliability are the development axis described as priorities when analysing the technological status of the Raman backscattering OTDR detection systems used today for ground applications.

The list of necessary improvements is applied on each module to satisfy at system and in future at aircraft level the appropriate technology readiness level. The description of the development strategies per module and the verification of the system performance level are presented here. Signal processing alternatives to the traditional average of Stokes and anti-Stokes data sets are proposed with an evaluation of the associated benefits.

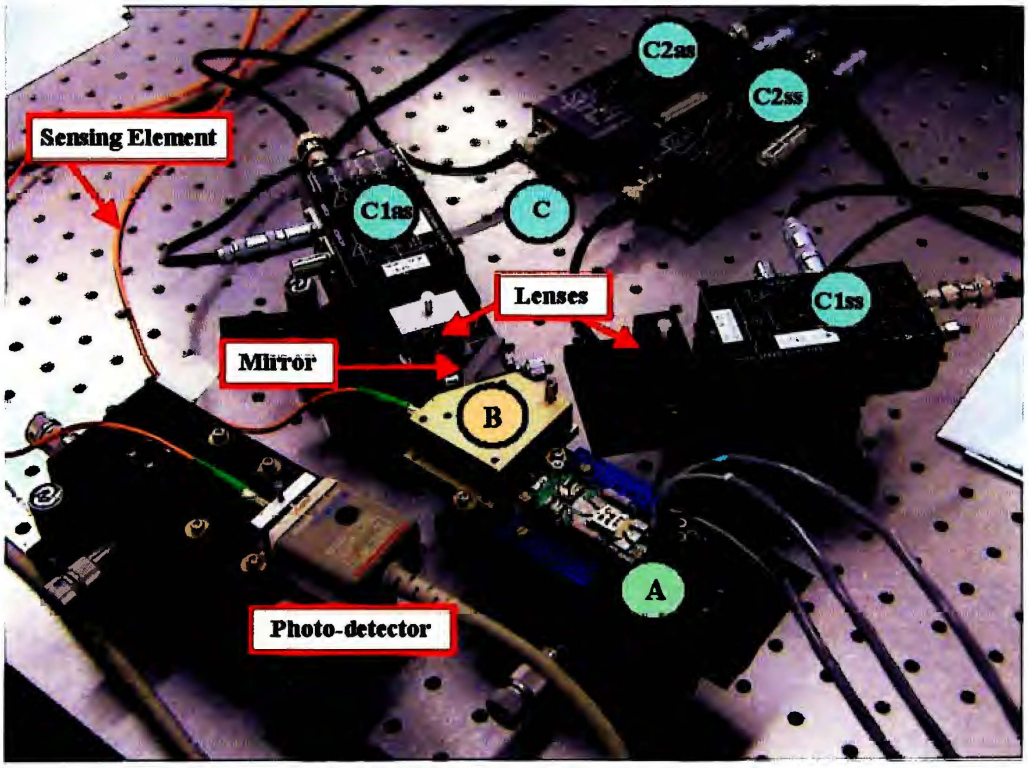

Figure 5.1-2: Optical demultiplexer interfaces

The main challenge associated with the optical demultiplexer is the coupling of sufficial excitation power into an optical fibre and the collection of the largest possible amount of backscattered signals onto two avalanche photo-detectors. The alignment of the optical components is here managed through an intermediate package, which will be described later.

The elements C1ss and C1as are 1GHz high-speed amplifiers, which amplify the signals from avalanche photo-diodes separately for the Stokes and the anti-Stokes signals. Variable gain 100MHz wideband voltage amplifiers are following, C2ss and C2as. Two PCI acquisition boards for the amplified Stokes and anti-Stokes signals are ending the two segregated loops with a digitisation and a transfer of the data sets to the computer memories.

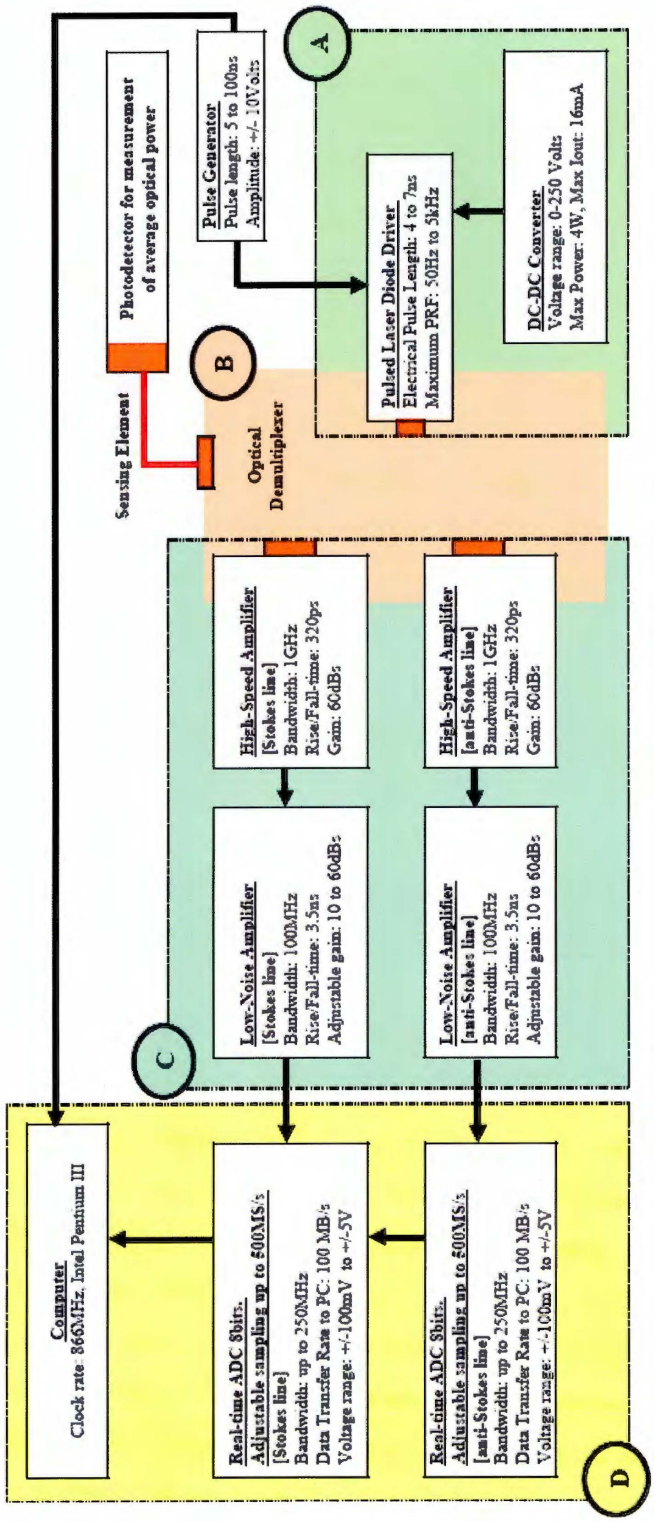

Figure 5.12 Laboratory test bench for distributed fire/overheat detection system

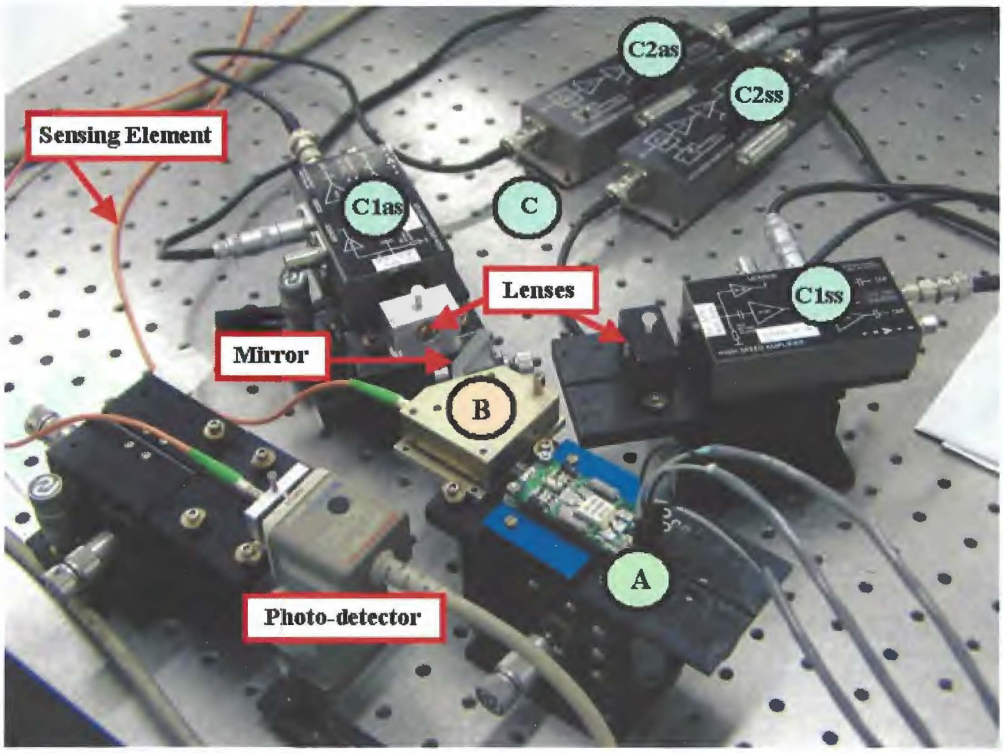

Figure 5.1-2: Optical demultiplexer interfaces

The main challenge associated with the optical demultiplexer is the coupling of sufficial excitation power into an optical fibre and the collection of the largest possible amount of backscattered signals onto two avalanche photo-detectors. The alignment of the optical components is here managed through an intermediate package, which will be described later.

The elements C1ss and C1as are 1GHz high-speed amplifiers, which amplify the signals from avalanche photo-diodes separately for the Stokes and the anti-Stokes signals. Variable gain 100MHz wideband voltage amplifiers are following, C2ss and C2as. Two PCI acquisition boards for the amplified Stokes and anti-Stokes signals are ending the two segregated loops with a digitisation and a transfer of the data sets to the computer memories.

5.1.1 THE PULSED LASER DIODE

The overall system performance depends on the specification of the pulsed laser diode. The diode should emit at wavelengths where the fibre has low losses and where the avalanche photo-detectors are efficient. Its peak power should be such as to obtain a strong spontaneous scattered Raman signal but not exceed the threshold level for stimulated Brillouin and Raman scattering (explained in more details in section 5.1.3). The spectral line width should be small enough to avoid the overlap of the Rayleigh and the Raman scattered signal. To achieve a 1-meter spatial resolution the pulse width should be less than 10ns. The repetition rate should be compliant with the diode duty cycle with a safety factor for reliability reasons, but to reduce the measurement time the pulse repetition rate should be as high as possible. The emitting chip window of the laser diode should be small and compatible with optics for coupling light into an optical fibre.

The price, size, ease of operation, availability and lifetime consideration favour the use of the semiconductor lasers and in optical fibre systems the laser sources employed almost exclusively are semi-conductor laser diodes.

It is well known that intrinsic Raman scattering is greatest at shorter wavelengths (the spontaneous Raman scattering intensity returned from an excitation is dominated by the λ^{-4} dependence term), however, using short wavelengths results in limited "distributed anti/Stokes ratio thermometry" range due to the large fibre losses. Samson has investigated the optimum pump wavelength that maximizes the trade-off between fibre losses and Raman scattering [Samson, 1990]. This analysis shows that for a 100m fibre, the maximum Raman signal for direct detection will occur at an excitation wavelength of 600nm, the maximum for a 1km fibre is around 1000nm using in both cases the peak Raman shift ($\Delta\nu = 440cm^{-1}$) for vitreous SiO_2 and for a fibre with a loss of 5 $dB.km^{-1}$.

Therefore, semiconductor laser diodes working at near IR wavelengths are the most

suitable excitation source for the system when targeting a distributed F/O detection range around 1km.

The pulsed laser driver identified, taking into account the previous considerations, is the SPL_PL90 from OSRAM [OSRAM, 2000]. This laser diode is housed in a plastic package, has a peak emission wavelength at 905nm with a 4nm spectral width (FWHM), a maximum peak output power of 16 W for a maximum operating current of 18 A. The maximum duty cycle of 0.1% is leading for a pulse width of 5ns to a pulse repetition rate for the laser diode driver of 200kHz or 67kHz for a pulse width of 15ns. The injected electric current intensity, at which the laser oscillation begins, threshold current, is 0.8A at the characteristic temperature of 25°C.

The aperture size of the laser is 200μm wide and 2μm high. The beam divergence (which corresponds to the full angle at the point, which is half of peak intensity) is 6° by 34° ($\theta_{||} \times \theta_{\perp}$). The size of the aperture will have to be compared to the diameter of the core of the fibre that we intend to use as sensing element. It will be also noticed that the operating temperature range [-40°C to +85°C], the storage temperature range [-40°C to +100°C], the lifetime at 85°C [MTTF > 29000 hours] and the lifetime at 25°C [MTTF > 290000 hours] seem in conformity with on-board system integration needs. Today, the component is available at 44 Euros per part when ordering at least 500 parts.

5.1.2 THE LASER DIODE DRIVER

A special effort was carried out on the adaptation of a laser diode driver to the necessity of shaping a less than 10ns pulse width and to be able to use the low cost, high reliability OSRAM laser diode. The spatial resolution of the system is indeed strongly dependent on the capability of the driver to generate short pulse widths. The driver has also to be able to feed the laser diode with a high enough current pulse.

Three layouts of mechanical positioning between the Pulsed Laser Diode (PLD) and the driver board were tested. The first involves a diode where the pins are directly soldered on the board as opposed to two other configurations where a 6cm flexible track (Micro Stripline Transmission Line, MSTL) was used to evaluate the influence of a separation of the optical device from the power MOSFET of the driver stage.

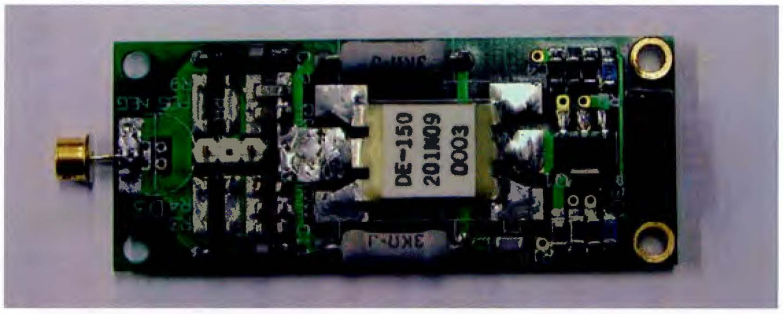

Figure 5.1-3: Driver stage with direct soldering of a PLD on the board
First configuration: analysis of the laser diode response to a driver command

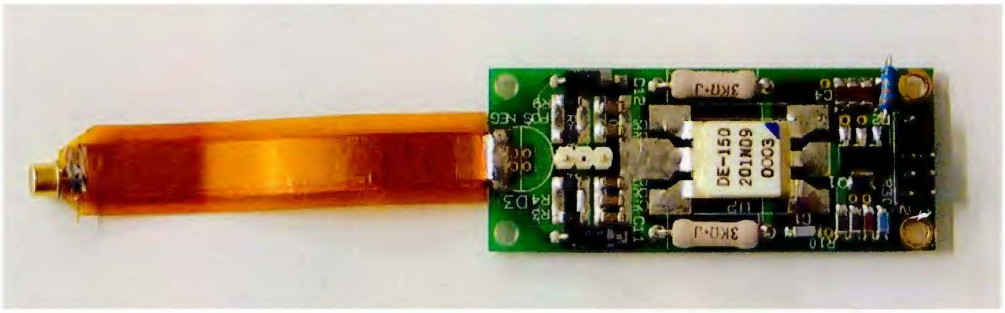

Figure 5.1-4: Driver stage with a PLD deported using a flexible track
Second configuration: verification of the influence of a MSTL on the optical pulse shape.

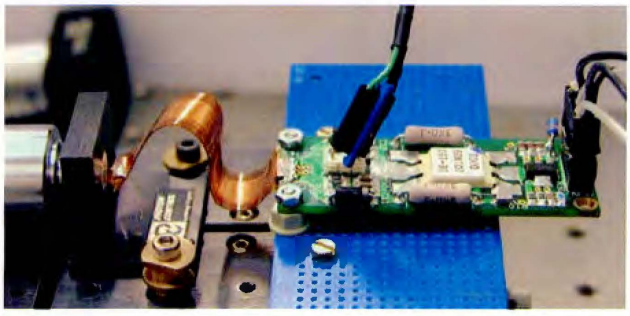

Figure 5.1-5: Driver stage with a PLD separated using a flexible and shaped track
Third configuration: verification of the influence of a curved MSTL on the optical pulse shape.

A DC-DC converter is used to supply the driver and adjust the maximum amplitude of the current pulse. Powered-up with a nominal 12V input voltage (with a current requirement on the order of 7mA), the output voltage range lays between 0 and 250V [16mA output current at 250V]. A small electronic circuit as a command for the DC-DC converter allows regulation of the output voltage using a potentiometer.

The primary function of a laser driver is to provide appropriate currents for bias and modulation of the laser diode. The bias is a constant current that pushes the laser diode operating range beyond its threshold value and into the linear region. Modulation is an alternating current that is switched on and off in synchronisation with the input voltage waveform. The three major pieces of the laser interface puzzle include the output circuit of the laser driver, the electrical characteristics of the laser diode, and the interface between them (which is usually implemented using a printed circuit board).

The power supply of the DEI PCO 7110-40-4 [Directed Energy Incorporated, 2000] uses a +15V voltage for a low current, on the order of 1mA. The DC high voltage supplies the total input capacitance of the driver. The maximum average current that the high voltage supply must provide is determined by the pulse repetition frequency required for the user's application. An approximation (±20%) for the current requirement from the high voltage power supply can be given using the equation 5.1-1. This current is a function of the total input capacitance: the pulse forming network C_{PFN}, the FET capacitance C_{FET} and the stray C_{STRAY}, the high voltage input V_{IN}, and the pulse repetition frequency f.

$$I_{PS} = [C_{PFN} + C_{FET} + C_{STRAY}]V_{IN}.f$$

Equation 5.1-1 Input current definition from the high voltage power supply
For the PCO-7110-40-4: C_{PFN} = 1100pF, C_{FET} = 120pF, C_{STRAY} = 200pF, V_{IN} (max.) = 200V, f (max.) = 50kHz. The current requirement is then I_{PS} = 14mA, which is compatible with the specifications of the DC-DC converter.

The output current depends upon the available charge of C_{PFN}. This charge is directly proportional to the applied voltage. Therefore, varying the applied voltage will cause a concomitant change in the output current.

A successful optical transmitter design demands careful attention to the sources and effects of parasitic inductance. Figure 5.1-6 is a simplified block diagram of the output stage of a laser driver connected to a laser diode. In the actual system there are many distributed parasitic inductances due to bond wires, die pads, etc. For simplicity, in the model of Figure 5.1-6, the distributed inductances have been lumped into two locations: L_{OUT} at the output of the driver (cathode of the laser diode), and L_{ANODE} at the anode of the laser diode.

The transient behaviour of the switching current due to the inductors affects the optical output of the laser diode in a number of ways. The driver modulation output transistor requires a minimum specified voltage in order to switch properly. Parasitic inductance can play also a major role in decreasing voltage headroom during switching.

The inductive load caused by the lead- and bond-wire inductance of the laser package may need a compensating RC shunt network, consisting of a resistor R_F, and a capacitor C_F. The purpose of the RC shunt network is to cancel out the parasitic inductance, thereby maintaining a constant load impedance, which results in a reduction of overshoot and ringing.

The series-damping resistor serves the dual purposes of damping reflections that cause output distortion and creating a stable load. Since package inductance varies for different lasers, the component values for the shunt network may need to be adjusted for optimum operation [Redd *et al.*, 2000].

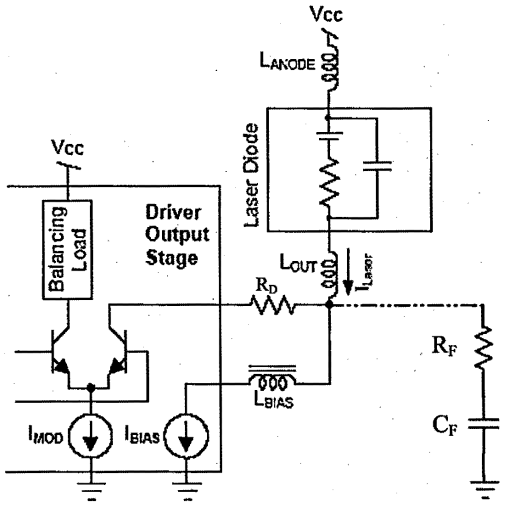

Figure 5.1-6: Simplified model of a laser driver connected to a laser diode

The PCO-7110-40-4 is designed to eliminate storage time effects by using power MOSFETS [IXYS, 2003]. An analysis of the series driver pulse inductance problem revealed that it is nearly impossible to eliminate the ensuing ringing following a 10 to 15 ampere, 4 ns wide pulse into the laser diode. The inductance of the leads [Zuleeg, R. *et al.*, 1985] of the laser diode is calculated using:

$$L_b = \frac{\mu . X_b}{2.\pi} . \left[\ln\left(\frac{2.X_b}{r_c} \right) - 1 \right]$$

Equation 5.1-2 Inductance of the laser diode bonding leads
$\mu = \mu_0 = 4.\pi \times 10^{-7}$ H/m for air. X_b = conductor length, m. r_c = conductor radius, m.

The 2.6 mm-long bonding lead results in about L_b = 2.5nH. The 4 mm-long connecting diode leads can have an inductance evaluated by:

$$L_L = \frac{\mu . X_L}{2.\pi} . \ln\left[\frac{h_L}{r_L} \right]$$

Equation 5.1-3 Inductance of the laser diode leads
$\mu = \mu_0 = 4.\pi \times 10^{-7}$ H/m for air. X_L = leads length, in meter m. h_L = distance between the two conductor leads, in meter m. r_L = conductor lead radius, in meter.

which gives an inductance of 3.5 nH and of 6 nH for the laser diode component.

Figure 5.1-3 is a Micro Stripline constructed of copper and Kapton tape. This type of mechanical construction produces a transmission line that is easily fabricated at very low impedance levels. It is strong, light, extremely flexible and low cost.

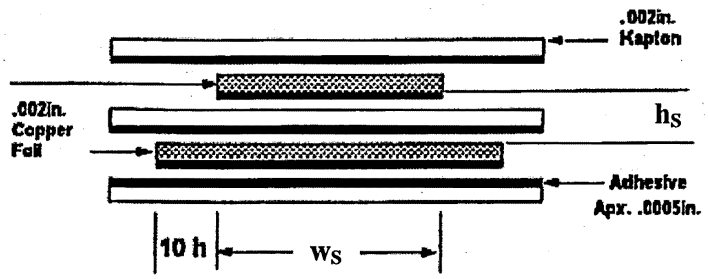

Figure 5.1-7: Micro Stripline Transmission Line architecture [MSTL]

A simplified circuit model for the Laser Driver Module [LDM] is shown in Figure 5.1-8 [Burman *et al.*, 1996]. R_1 is the recharge resistor, C_1 is the energy storage capacitor, L_1 is the lumped total of the system loop inductance, S_1 is the switching device, R_2 is the load resistor and D_1 is the laser diode. This forms a simple RLC network.

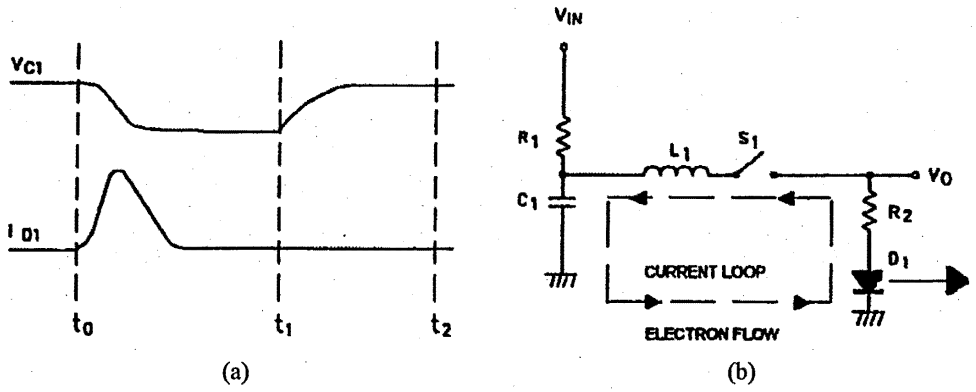

Figure 5.1-8: Simplified circuit model for the Laser Diode Module
(a) Voltage at the energy storage capacitor terminals. (b) Simplified laser driver circuit model.

The components C_1 and L_1 are Pulse Forming Network (PFN) with impedance Z_D. At t_0, C_1 has been charged to V_{IN}, the high voltage and S_1 closes. The discharge path is down through C_1 and up through D_1, R_2, and S_1 producing a current pulse I_{D1} and

One could show that there is no shape difference between an optical pulse generated from a laser driver assembled with or without a straight / bent micro stripline transmission line connected to the PLD. Besides, an optical pulse keeps the same shape when it is coupled into a 3m multi-mode fibre. The fibre portion acts as a delay line, here is measured a delay of 15ns which gives, as expected, an optical pulse velocity within the fibre of about $2.10^8 m.s^{-1}$.

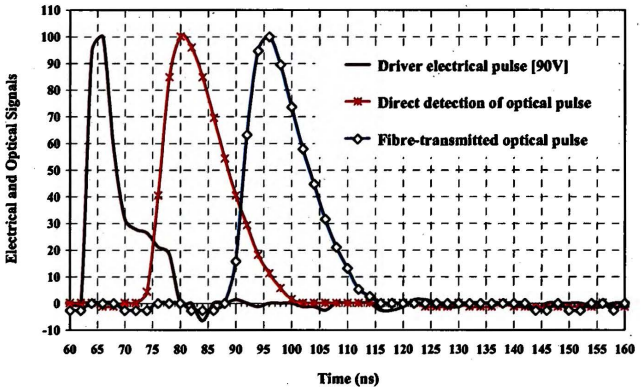

Figure 5.1-9: Normalised shapes of optical pulses air or fibre-transmitted

The three configurations analysed gave a small dispersion in the optical pulse width as a function of the high voltage supplied to the driving stage.

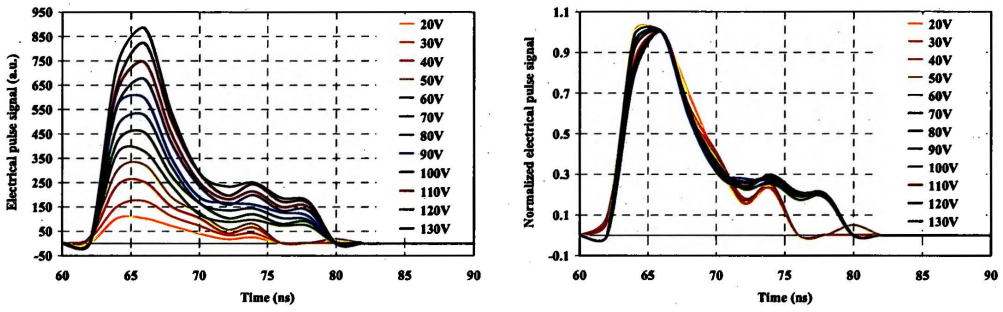

(a) (b)

Figure 5.1-10: Driver configuration with straight MSTL – Electrical Pulse Signal
Electrical pulse shape as a function of the high voltage supplied to the laser driver. For each signal, 100 data sets were required and averaged. (a) Peak amplitude variation as a function of the supplied high voltage variation. (b) Normalized signal to peak amplitude for pulse shape analysis.

Taking into account the loop inductance and the resistive losses in the circuit we can calculate the high voltage required to generate an 18A current pulse in 4ns, which is the approximated rise-time of the laser diode.

$$V_{supply} = R_{DS(on)} I_{PEAK} + R_2 I_{PEAK} + V_{LASER-DIODE} + L_{TOTAL} \frac{di}{dt}$$

$$V_{supply} \cong 0.2\Omega.(18A) + 5\Omega.(18A) + 5V + 10nH.\frac{18A}{4ns} = 144V$$

Equation 5.1-6 Voltage supply to drive the selected laser diode to 18A in 4ns

The total loop capacitor includes only the value of the energy storage capacitor C_1 and can be simply calculated using the following equation:

$$C_1 = \frac{1}{V_{IN}} . I_{Peak} . PW_{\pm 3\sigma}^{Gaussian}$$

$$PW_{\pm 3\sigma}^{Gaussian} = 2.55\ PW_{FWHM}^{Gaussian}$$

Equation 5.1-7 Energy storage capacitor definition

The current pulse is being considered as Gaussian. For a pulse width defined by the width of a Gaussian pulse at half maximum [$PW_{FWHM} = 2\ \sigma\ (2\ \ln(2))^{0.5}$], the capacitor would be discharged at 76%. The capacitor would be discharged at 99.7% for a pulse width of 6 σ. We consider therefore a pulse width $PW_{\pm 3\sigma} = 2.55\ PW_{FWHM}$, which is equal to 10.2ns when specifying a FWHM pulse of 4ns.

The energy storage capacitor is evaluated to be 1.28nF for a discharge taking into account the calculated supplied voltage required to generate a 4ns FWHM pulse width with an operating current of 18A for a pulse peak optical power of 16W [OSRAM, 2000].

This value approaches significantly the manufacturer's value of $C_{PFN} + C_{STRAY} =$ 1.3nF provided in the PCO-7110-40-4 datasheet.

calculated 20% of inductance excess could indeed be responsible for all or part of the extension in time of the electrical pulse width. A second analysis consists in using basic theory to predict overshoot and ringing that result from an over-damped or under-damped LRC circuit. To eliminate overshot and ringing, the circuit must be critically damped, where $R_{critical} = 2\ (L/C)^{0.5}$. From this equation, we can see that as the parasitic inductance increases, the critical resistance will also increase. Assuming that the actual resistance stays constant, increasing the inductance will result in an increasingly under-damped system and increase the overshoot and ringing. The parasitic inductance must be minimized. The fact that these parasitic inductances have not been evaluated, their presence might be the second reason of the long electrical pulse duration. The third investigation would have to check whether the experiment is truly done in a matched impedance configuration.

So as to perform a proper spatial reading of the distributed temperatures along the optical fibre, it is advisable to investigate the jitter level associated with the leading edge of the pulse.

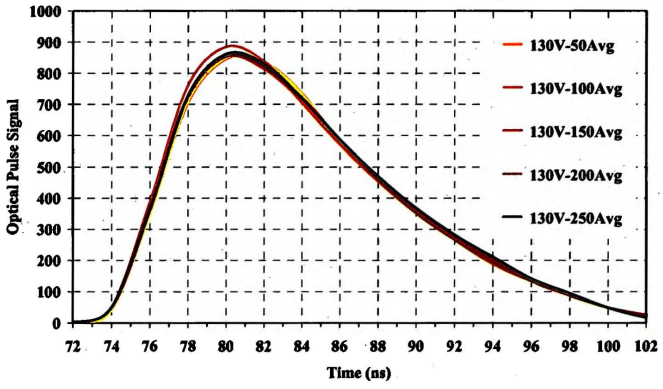

Figure 5.1-12: Driver configuration with straight MSTL – Optical Pulse Signal
Optical pulse shape as a function of the number of averages.

The short-term instability of one reference pulse edge to another was noticed as being less than 1ns.

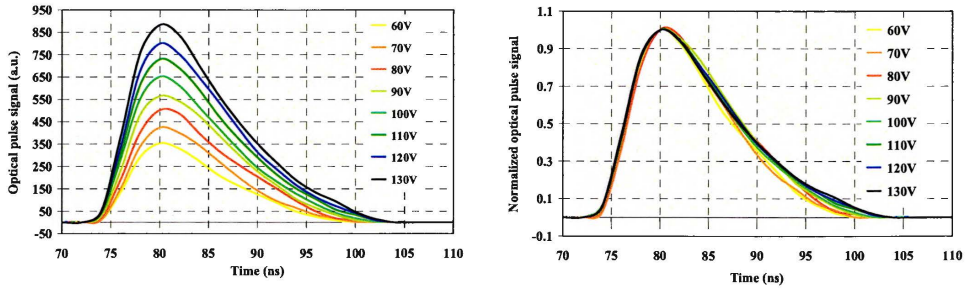

(a) **(b)**

Figure 5.1-11: Driver configuration with straight MSTL – Optical Pulse Signal
Optical pulse shape as a function of the high voltage supplied to laser driver. Each signal type was 100 times acquired and the data sets were then averaged. (a) Peak amplitude variation as a function of the supplied high voltage variation. (b) Normalized signal to peak amplitude for pulse shape analysis.

One may notice, on figures (a) [Figure 5.1-10 and Figure 5.1-11] that the electrical and optical peak amplitudes vary linearly with the high voltage supply. On figures (b) the pulse shape changes when the high voltage exceeds 50V. There is a slight increase of the optical pulse width between 50V and 130V (not more than 1ns).

As a nominal setting, the experiment will be launching a 10W peak optical power pulse, which requires a peak current pulse of 11.25A from 90V high voltage.

The main conclusion of these measurements is of course to notice the important discrepancy between the FWHM of the electrical pulse, about 5ns for the main peak, and the one of the optical pulse, 12ns. Analysing the rise/fall times a possible explanation can be provided [MAXIM High-Frequency/Fiber Communications Group, 2002]. If we neglect the effects of parasitic capacitance and assume a greatly simplified single time constant model, then the rise and fall times can be calculated using the L/R time constant. For a 20%-80% rise time we can use the relationship: $2.\pi.\tau \approx t_{rise}/0.22$ (where $\tau = L/R$ represents the time constant) to calculate a value for L. If we let $R = R_S = 5.6\ \Omega$, t_{rise} about 2ns, $L \approx 8nH$ to be compared to the module inductance of 10nH. While this result is far from exact (it is based on a greatly simplified model) it gives a good idea of the approximate level of inductance that can be tolerated without significantly affecting the rise/fall times. In our case the

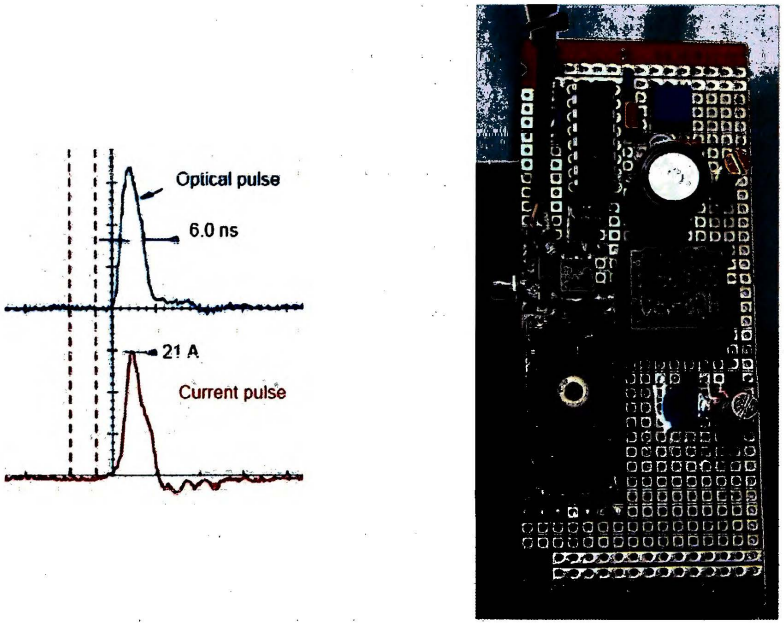

Figure 5.1-14: Improved laser driver module performing 6ns optical pulse width FWHM

The pulse width obtained is about 6ns with a peak current pulse of 21A, which is providing a compliant optical power to the aim of the study. The reliability of the driver stage is however unknown especially when studied with a change of the pulse repetition frequency.

The experiments were nevertheless conducted with the PCO-7110-40-4, which had demonstrated flexibility to the measurement investigations, while a ruggedisation of the improved driver was running concurrently.

As a conclusion, it is possible to say that it was noticed no influence on the global laser driver performances from the pulse period / delay accuracy, and from the trigger delay controlled by the pulse generator. The pulse width was identified as stable within 0.5ns accuracy, while the transition time defined as the interval between the 10% and 90%-amplitude points on the leading/trailing edge was constant. The optical pulse leading edge shown good linearity with applied current and a maximum jitter of 1ns has been observed. The long-term stability over more

An attempt to reduce the optical pulse width through a reduction of the current pulse width was carried out using a different laser diode driver type.

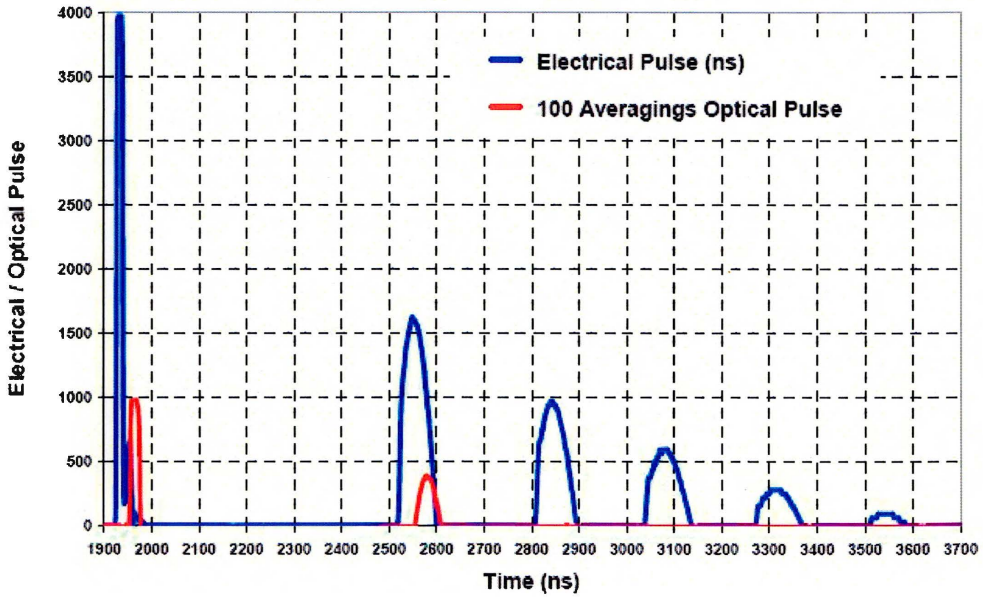

Figure 5.1-13: Multi-electrical / optical pulses

Although the main optical pulse has an 8ns FWHM, the driver design was generating secondary electrical pulses (cf. Figure 5.1-13). At least the first secondary current pulse was of enough amplitude to see a secondary optical pulse generated. This secondary current pulse is therefore above the specified threshold current of the diode at 0.8A. These conditions are indeed not the expected conditions for the pulse emission. The system aims to acquire a full optical fibre length profile for the Stokes and anti-Stokes signal per optical pulse leading to a simple relationship between the spatial resolution and the pulse shape definition.

A second attempt to both cancel the secondary electrical and optical pulses and to reduce even further the optical pulse width has lead to the design shown in Figure 5.1-14.

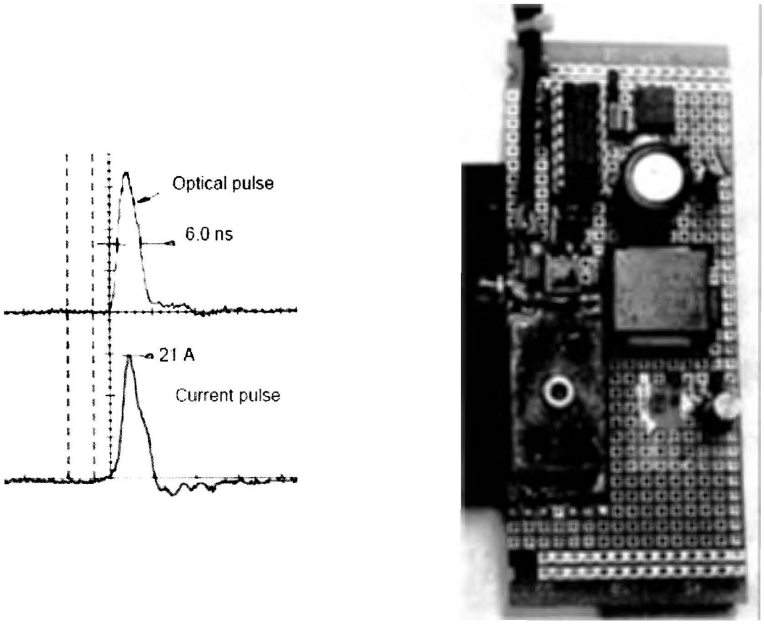

Figure 5.1-14: Improved laser driver module performing 6ns optical pulse width FWHM

The pulse width obtained is about 6ns with a peak current pulse of 21A, which is providing a compliant optical power to the aim of the study. The reliability of the driver stage is however unknown especially when studied with a change of the pulse repetition frequency.

The experiments were nevertheless conducted with the PCO-7110-40-4, which had demonstrated flexibility to the measurement investigations, while a ruggedisation of the improved driver was running concurrently.

As a conclusion, it is possible to say that it was noticed no influence on the global laser driver performances from the pulse period / delay accuracy, and from the trigger delay controlled by the pulse generator. The pulse width was identified as stable within 0.5ns accuracy, while the transition time defined as the interval between the 10% and 90%-amplitude points on the leading/trailing edge was constant. The optical pulse leading edge shown good linearity with applied current and a maximum jitter of 1ns has been observed. The long-term stability over more

than five hours has been checked, and enters the envelope defined by the jitter analysis. The optical pulse peak amplitude levels have been investigated and are found to change with the time within ±5% from a pre-set nominal value. The time taken for pulse levels to settle within level specifications, measured from 90% point on leading edge was short and was not considered to affect the pulse shape. When the system was used under the same environmental conditions and with the same settings, the value was lying within an accuracy window of about 2ns, providing a good repeatability of the experiment. All, these requests were carried out using 50 times averaged data sets for analysis (giving a 25ms acquisition time for a PRF of 2kHz).

Distortions preceding/following an edge have been considered as overshoot or ringing or as a total inductance value problem, which would deteriorate the rise/fall time(s) of the pulse. The phenomena are currently under investigation to reduce the 12ns optical pulse width when using the PCO-7110 laser driver.

5.1.3 THE OPTICAL DEMULTIPLEXER

The optical wavelength demultiplexer is used between a pulsed laser diode, an optical fibre, optical filters and avalanche photo-detectors. The architecture of the demultiplexer has been shown to determine the overall performance of the distributed temperature detection system [Ozawa, Y. *et al.*, 1992]. The PLD light is collimated and focused into the optical fibre and the back-scattered light from the optical fibre filtered through filter F1, which is transmitting the Rayleigh scattering and reflecting the complementary spectrum towards filter F2. Filter F2 transmits the anti-Stokes light, which reaches the APD 1. Filter F3, identical to F1, reflects the Stokes band, which hits APD 2 while passing through filter F4. The coupling efficiency from the pulsed laser diode to the 62.5/125μm gradient-index multimode optical fibre is measured to be about 30% (-5.25dB). The filters are specified to achieve a minimum 90% transmission and 95% reflection ratios (Stokes line: 3x-0.25-0.5dB = -1.25dB; anti-Stokes line: -0.25 -0.5 = -0.75dB).

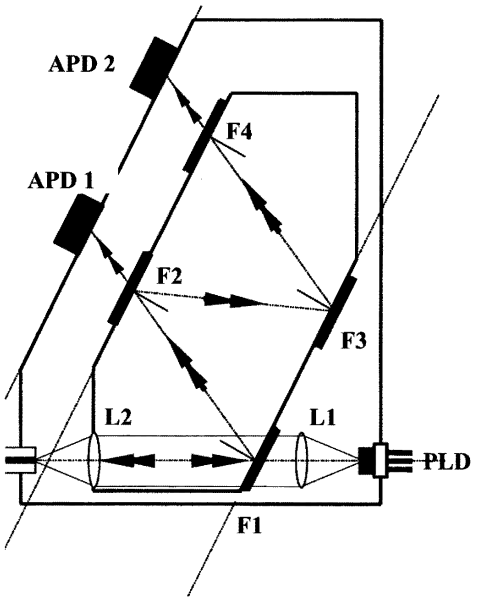

Figure 5.1-15: DTS preferred optical wavelength demultiplexer

The optical wavelength demultiplexer presented here offers flexibility for the integration of the optical elements and for the space allocation management of the associated surrounding electronic modules. Considering the limited space authorized for the fully integrated control unit, one of the constraints is to optimise the filter angles, but still keeping the overall filtering process compatibility.

A description of the backscattering process in the optical fibre and of the OTDR requirements is pointing out the necessity of an optical fibre with large Numerical Aperture, low losses per kilometre, low spatial dispersion at the considered wavelengths and large core diameter. The optical fibre selected was a 62,5/125μm step-index fibre with a 0.22 numerical aperture.

The fibre link carrying a single wavelength ($\Delta\lambda$ = 4nm from the PLD), the presence of the signal will offer the chance for Raman amplification, using the signal as the pump. The amplification will begin from a spontaneous Raman scattered light wave that is propagating along the fibre at the proper wavelength. The stimulated process

will begin and will rob power from the signal and divert it into other wavelengths (cf. Figure 5.1-16). The power lost to the Stokes signals depends on the fibre loss, the Raman gain, and the number of modes carried by the fibre, the numerical aperture of the optical fibre.

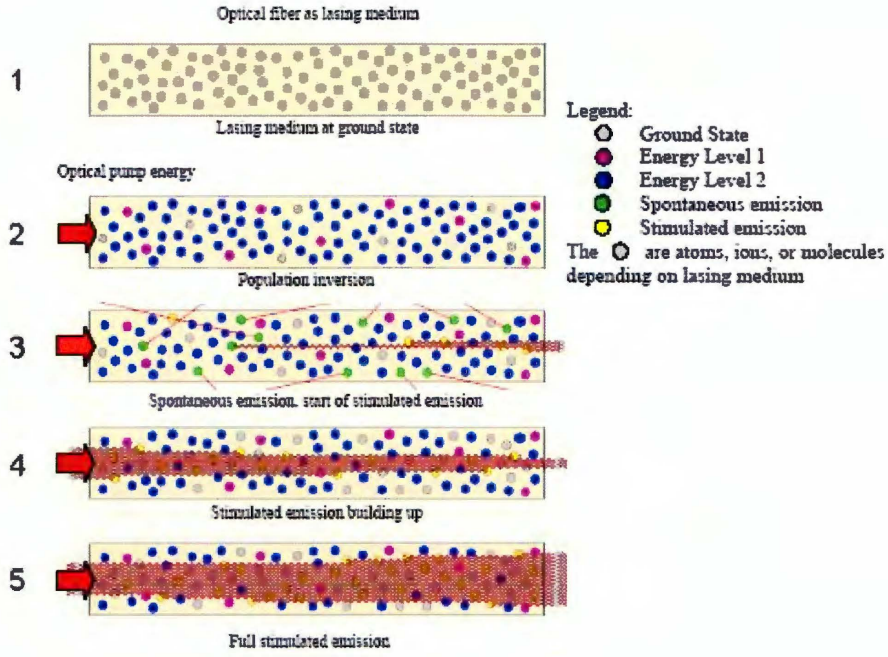

Figure 5.1-16: Spontaneous to stimulated Raman scattering in optical fibres. Pump pulse threshold.

The upper limit on the power that can be injected into the fibre is determined by the power that causes the Stokes power to equal the signal power. This power is [Powers, 1993]:

$$P^{th} \cong \frac{16.A_{eff}}{G_r.L_{eff}}$$

Equation 5.1-8 Pump pulse threshold optical power for stimulated Raman scattering

where G_r is the Raman gain coefficient (1.6×10^{-14} m/W), A_{eff} [Mortensen, 2002]. The numerical aperture (NA) relates to the effective area of the optical fibre, it can be expressed as:

$$NA \cong \left[1 + \pi . \frac{A_{eff}}{\lambda^2}\right]^{-1/2}$$

Equation 5.1-9 Numerical aperture of the step-index multimode fibre [Mortensen, 2002].

where λ is the wavelength of the emitted pulse (905nm) and NA the numerical aperture (0.22). The mode field diameter is defined in the near-field band and leads to a value of $5\mu m^2$ and L_{eff} (597m) is the effective length given by:

$$L_{eff} = \frac{1}{\alpha}.[1 - \exp(-\alpha.L)]$$

Equation 5.1-10 Effective interaction length. [Scheerer, 1996]

where α is the attenuation constant (6.91×10^{-4} m^{-1}, -3dB/km) and L is the considered length of the fibre, 500m [Scheerer, 1996]. The pump pulse threshold optical power is calculated to be 8.6W. For example, the threshold becomes 1.2W as the fibre length goes to 2000m. It is clear that the threshold will decrease with longer fibre lengths. The first order Stokes light is amplified by increasing distance, but it is depleted at sufficiently long distance because of the accompanying generation of the second order Stokes light [Morita *et al.*, 1995]. To take into account this phenomenon, the critical power at the entry of the fibre was calculated to be:

$$P^{th} = \frac{\alpha.\ln[q_c/c_1]}{G_{0,1}.[1 - \exp(-\alpha.L)]} \cong \frac{K}{[1 - \exp(-\alpha.L)]}$$

$$q_c = \frac{1 + c_2}{1 - c_2}$$

Equation 5.1-11 Critical input power of the input pulse in which spontaneous Raman scattering starts to be seriously disturbed. K is a constant.

For commonly used silica fibres c_1 is of the order of 10^{-4} and c_2 is in the range of: $0.1 \leq c_2 \leq 0.6$. The stimulated Raman gain coefficient due to stimulated transition to 1st order Stokes light is $G_{0,1}$ (experimentally estimated value: 2.5×10^{-3} $m/(m^2/W)$). If the temperature distribution along the fibre does not have remarkably large

fluctuation, the coefficients $G_{0,1}$ may be considered to be constant. The constant value K of Equation 5.1-11 was deduced as 2.6W, which is the critical power of the input pulse for an infinitely long silica fibre. The pump pulse threshold optical power is 8.9W and 3.5W for a 500m and 2000m fibre length, respectively.

The collimating and focusing system employed is simple, compact, with an optimised mass and uses low-cost components. Considering first order optical theory [Yang, 1995] one may demonstrate that it is possible to limit confusion at focus from the beam divergence, diffraction and lens spherical aberration. The choice of a lens with a short focal length will help to decrease the effects of the laser beam divergence and of the diffraction, while using aspheric glass condenser lenses will reduce the spherical aberration.

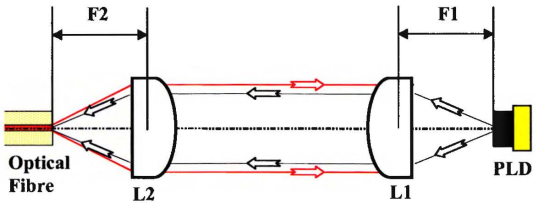

Figure 5.1-17: Collimating and focusing optics

The pulsed laser diode has a beam divergence cone with half-angle Θ of 16° at the half-power points in the direction perpendicular to the diode junction. The irradiance distribution of the Gaussian TEM_{00} beam, namely:

$$I(r) = I_0 . \exp\left[-\frac{2.r^2}{w^2} \right]$$

Equation 5.1-12 Irradiance distribution of the laser diode Gaussian TEM_{00} beam
w(z) is the radius of the $1/e^2$ contour at the plane where the wave front is flat
I_0 is the maximum irradiance

means that $1/e^2$ power points for the Gaussian output beam will be defined by:

$$\theta_{\frac{1}{e^2}} = \left[\frac{2}{\ln(2)}\right]^{0.5} . \theta_{\frac{1}{2}}$$

Equation 5.1-13 Definition of the half-angle relative to the laser diode numerical aperture

To collect all the light power emitted by the diode, the NA of the lens should be larger that the NA of the laser diode, which is 0.46, but the lens used here whose NA is 0.45 and focal length F_1 is 3.6mm was chosen to collimate the light. Despite the losses due to the smaller lens numerical aperture, the system launches enough optical power and keeps a size compatible to the objectives of integration. The diameter of the collimated beam is then $\Phi_L = 2 \times F_1 \times \sin\Theta = 2 \times 3.6 \times 0.46 = 3.3$mm. The focusing length will have therefore the following numerical aperture:

$$NA_F = \frac{\Phi_L}{2.F_2}$$

Equation 5.1-14 Definition of the numerical aperture of the focusing lens
F_2 is the focal length of the focusing lens.

The requirement for the numerical aperture of the optical fibre to be around 0.22, requires a 7.1mm focal length radial gradient plano-convex lens to focus the beam onto the face of the optical fibre. This gave a NA_F of 0.23.

The elliptical cross section of the laser beam and the diode's intrinsic astigmatism contribut in limiting the coupling efficiency of the system. The elliptical cross section of the beam is a result of the rectangular shape of the beam emission facet of the laser diode. Wave optics theory tells us that a beam output from a small aperture has in one certain direction a full divergent angle θ given by:

$$\theta_{[\perp \text{ or } \parallel]} = \frac{4.\lambda}{\pi.W_{[\perp \text{ or } \parallel]}}$$

Equation 5.1-15 Laser diode beam divergence definition
λ is the central emitted wavelength, $W_{\perp \text{ or } \parallel}$ is the size of the aperture perpendicularly or parallely to the diode junction respectively.

The aperture size of the laser diode presents a difference between the fast and slow

axis is about 100 to one (200 × 2 μm^2). The astigmatism is another result of the rectangular facet of the laser diode. The beam emitted from a small facet is equivalent to the beam emitted by an imaginary point source $P_{\perp \text{ or } \parallel}$, whose position can be located by tracing the beam backwards. It can be shown that $P_{\parallel}$ is located behind $P_{\perp}$ because $\theta_{\parallel}$ is smaller than $\theta_{\perp}$. This phenomenon is called astigmatism, and the distance between $P_{\parallel}$ and $P_{\perp}$ is the numerical description of the astigmatism. The existence of astigmatism means that when using a single, standard aspheric lens the beam can be collimated and focused only in one direction, because $P_{\parallel}$ and $P_{\perp}$ cannot simultaneously converge at the focal point of the focusing lens.

One way to improve the coupling efficiency of the collimating and focusing system is therefore to circularise the beam and to use astigmatism correction methods. We can therefore use anamorphic correcting prisms as shown in Figure 5.1-18:

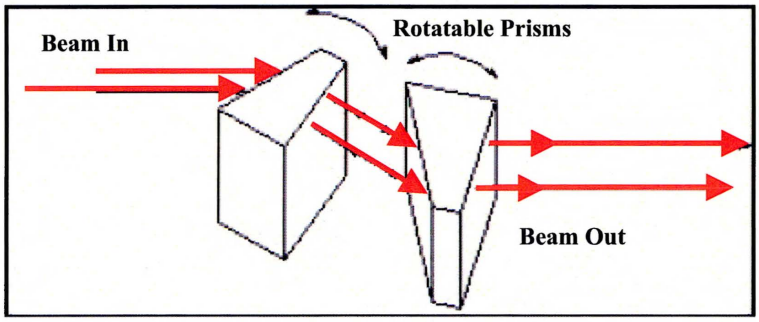

Figure 5.1-18: Beam Circularising for Semiconductor Laser Diodes

The prisms can enlarge or reduce the beam size in one direction while keeping the beam size in another direction unchanged. The enlargement or reduction rate can be adjusted by adjusting the angles of the two prisms, it is therefore not difficult to circularise the elliptical beam. An alternative method, that will both circularise the elliptical beam and correct the astigmatism, is to use a piece of single mode fibre. The laser beam is coupled by two collimating lens into the single mode fibre and the output beam from the fibre is collimated by the third collimating lens. This arrangement sufficiently "mixes up" the beam as it passes through the fibre so that

wavelength and a bandwidth of 12nm for the Stokes and anti-Stokes filters and 15nm for the Rayleigh filter.

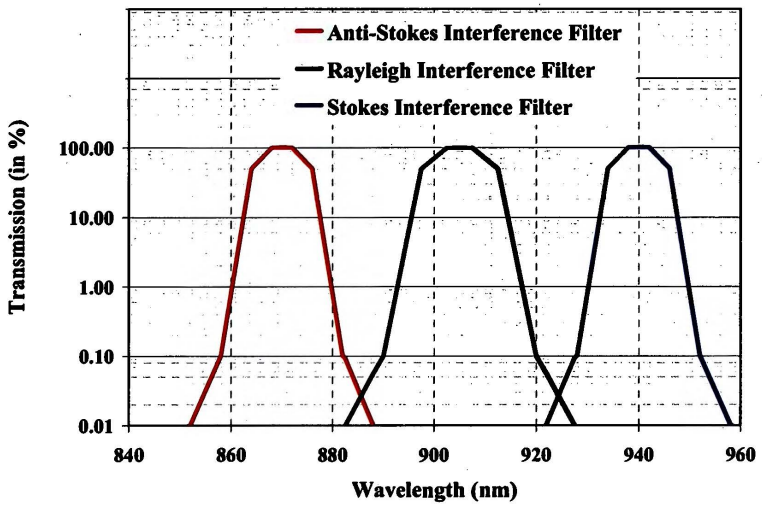

Figure 5.1-19: Transmission windows of the DTS interference filters

The bandwidth (FWHM) of the filters are chosen carefully to let as much Stokes and anti-Stokes optical power as possible enter the detection module but to reject enough Rayleigh signal. The spectral width of the laser diode ($\Delta\lambda_{SW} = \pm 2$nm) and its central wavelength variations ($\Delta\lambda_{CWL_L} = \pm 2$nm) have obviously influences on the overall performances of the system because they are shifting the back-scattered response spectrum within the filter transmission windows, which are fixed by definition. The accuracy of the filter centre wavelength ($\Delta\lambda_{CWL_F} = \pm 3$nm) as well as the thermal behaviour of both the laser diode ($\Delta\lambda_{CWL_L/TP} = \pm 0.3$nm/°C; i.e. ±4.5nm for ±15°C of temperature shift) and of the filters (typically $\Delta\lambda_{CWL_F/TP} = \pm 0.025$nm/°C; i.e. ±0.4nm for ±15°C of temperature shift) are also important to optimise the optical intensity collected through the filtering process. This has the following consequence of necessitating a thermal regulation for an on-board optical demultiplexer.

The thickness of the filters has also to be considered, as the light is not at normal incidence, it will be shifted from the propagation axis, the avalanche photodiodes

selection component with high blocking is required. Units used are Optical Density, OD or 10 to the negative power of transmittance. For example, OD 4 blocking or 10^{-4} transmittance means that there is no transmittance peak(s) in out-of-pass band exceeding 0.01% transmittance.

The transmission curve of the basic all-dielectric Fabry-Perot filter is not of ideal shape. A more nearly rectangular shape would be a great improvement. Further, the maximum rejection of the Fabry-Perot is completely determined by the half-width and the order. The broader filters, therefore, tend to have poor rejection as well as a somewhat unsatisfactory shape. When tuned electric circuits are coupled together, the resultant response curve is rather more rectangular and the rejection outside the pass band rather greater than a single tuned circuit, and a similar result is found for the Fabry-Perot filter [Macleod, 2001]. The filters maybe either metal-dielectric or all-dielectric and the basic form is:

$$|\text{reflector}|\,\text{half-wave}|\,\ldots|\,\text{reflector}|\,\ldots|\,\text{half-wave}|\,\text{reflector}|$$

A filter with N number of half-waves is called a N-cavity filter. The shape of the pass band is a function of number of cavities employed, centre wavelength and the bandwidth. Cavities result in more rectangular shape while less cavities cause a triangular-like shape. The central wavelength of a band pass filter can be changed by tilting it from normal to the direction of the incident light. The dependence of the centre wavelength on incident angle Φ is given by:

$$\lambda_{\Phi} = \lambda_0 \cdot \left[\frac{\sqrt{n^{*2} - \sin^2 \Phi}}{n^*} \right]$$

Equation 5.1-17 Dependency of filter central wavelength on incident angle
λ_{Φ} is the central wavelength at the Φ angle of incidence, λ_0 is the central wavelength at normal incidence, n^* is the effective index of refraction of the total filter ($\cong 2.05$).

To separate the Raman anti-Stokes back-scattering from the Rayleigh signal, a 4-cavity filter is used with a minimum transmission requirement of 85% at central

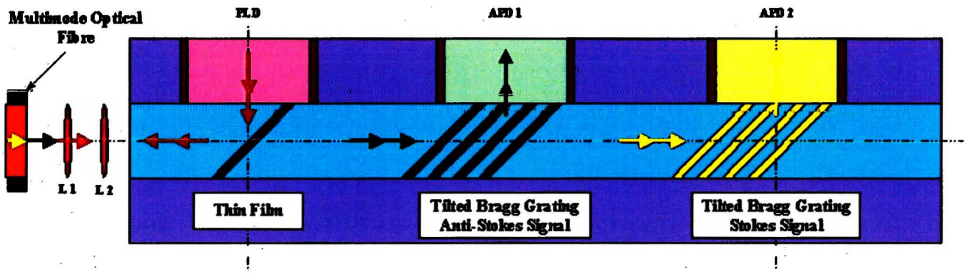

Figure 5.1-21: Demultiplexer based on tilted Bragg grating technology

Tilted fibre Bragg gratings have been demonstrated for applications in wavelength demultiplexing and channel monitoring [Byeong, 2002]. In optical fibres, the tilted structure enables light coupling between the core mode and the cladding. To date, most demonstrated tilted grating devices have been fabricated in single mode fibre, however the necessity of a good optical coupling efficiency between the sensing element and the demultiplexer is calling for a multimode fibre body to embed the tilted filtering Bragg gratings. The length of the gratings would have to be long enough to guarantee a strong enough reflectivity coefficient and the tilt angle would have to be studied to optimise the coupling to the slit brought along the central wave-guide. A grating in a fibre [Zhou *et al.*, 2003] can diffract the core-mode beam into the cladding part. It remains also to achieve a blocking level of "–40dB" between the reflected and transmitted signals per grating, while it was identified today in multimode fibres a maximum of "–25dB" as rejection factor.

will then have to be realigned accordingly.

As an alternative to the interference filters, one may suggest using diffraction gratings, which can have high efficiency and blocking. The major features of a micro-spectrometer would be the excellent mechanical, optical and thermal stability [STEAG microParts GmbH, 2003]. This attractive design would also allow integration of the APDs very easily on an electronic board and would therefore participate ideally to the reduction of the system volume.

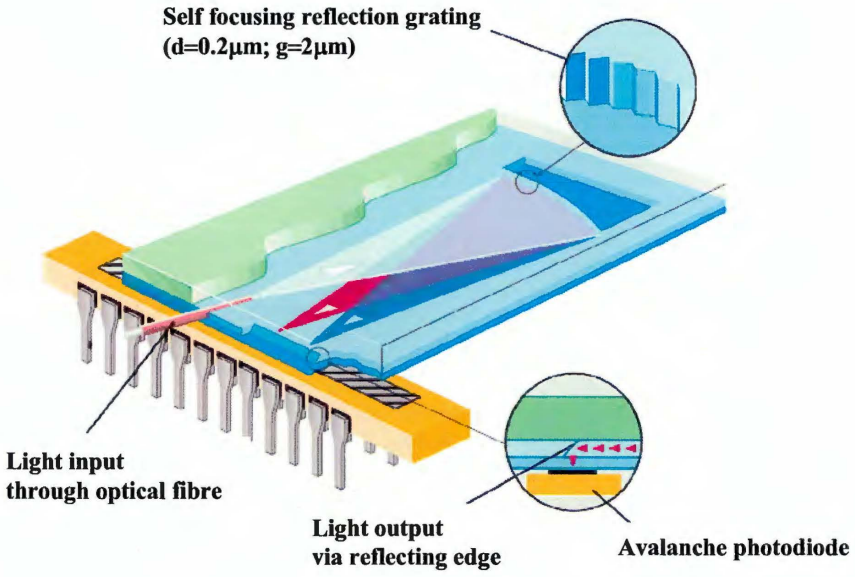

Figure 5.1-20: NIR spectrometer component [STEAG microParts GmbH, 2003]

However, current performances achieved are not compatible with the blocking specification (4 cavity-filter), and the cost of a development too high.

Another alternative to design a compact demultiplexer is proposed to be a module where filtering tilted optical fibre Bragg gratings would select the appropriate Stokes and anti-Stokes bands and redirect the signals perpendicularly towards an electronic board where the APDs would be connected.

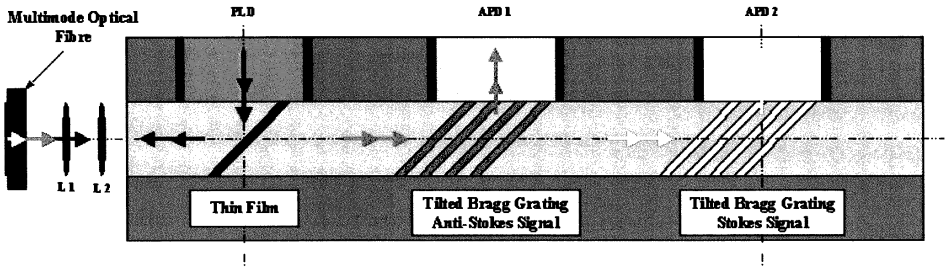

Figure 5.1-21: Demultiplexer based on tilted Bragg grating technology

Tilted fibre Bragg gratings have been demonstrated for applications in wavelength demultiplexing and channel monitoring [Byeong, 2002]. In optical fibres, the tilted structure enables light coupling between the core mode and the cladding. To date, most demonstrated tilted grating devices have been fabricated in single mode fibre, however the necessity of a good optical coupling efficiency between the sensing element and the demultiplexer is calling for a multimode fibre body to embed the tilted filtering Bragg gratings. The length of the gratings would have to be long enough to guarantee a strong enough reflectivity coefficient and the tilt angle would have to be studied to optimise the coupling to the slit brought along the central wave-guide. A grating in a fibre [Zhou *et al.*, 2003] can diffract the core-mode beam into the cladding part. It remains also to achieve a blocking level of "–40dB" between the reflected and transmitted signals per grating, while it was identified today in multimode fibres a maximum of "–25dB" as rejection factor.

5.1.4 THE DETECTOR AND AMPLIFICATION CHAIN

The amplification chain comprises an avalanche photodiode, a high-speed current to voltage amplifier, and a wideband voltage amplifier. The three amplification stages are considered as non-interacting.

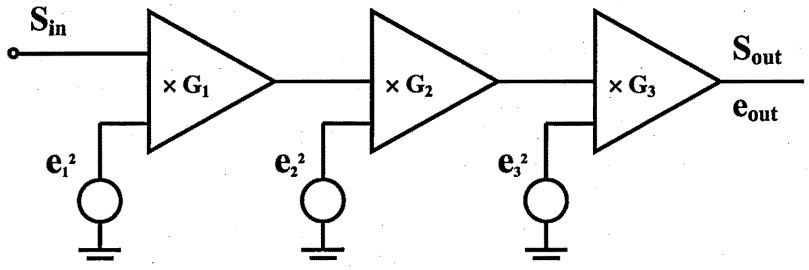

Figure 5.1-22: Nominal temperature profile for performance analysis

The signals and noise at the output are defined by:

$$[S_{out}]^2 = [G_1.G_2.G_3.S_{in}]^2$$
$$[e_{out}]^2 = [G_1.G_2.G_3.e_1]^2 + [G_2.G_3.e_2]^2 + [G_3.e_3]^2$$

Equation 5.1-18 Output signal and noise from the amplification chain

The Signal to Noise Ratio is therefore:

$$SNR = \left[\frac{S_{out}}{e_{out}}\right]^2 = \frac{[G_1.G_2.G_3.S_{in}]^2}{[G_1.G_2.G_3.e_1]^2 + [G_2.G_3.e_2]^2 + [G_3.e_3]^2}$$

Equation 5.1-19 Output signal and noise from the amplification chain

The first amplification stage is the APD itself. An APD includes an absorption region "A", which serves to separate the photo-generated holes and electrons and sweeps one carrier towards the multiplication region "G", designed to exhibit a high electric field so as to provide internal photo-current gain by impact ionisation. The net effect of the avalanche process is a multiplication of the current at the output terminals. The gain factor G is given by $G=I_G/I$ where I_G is the output current with multiplication

and I is the output current without multiplication.

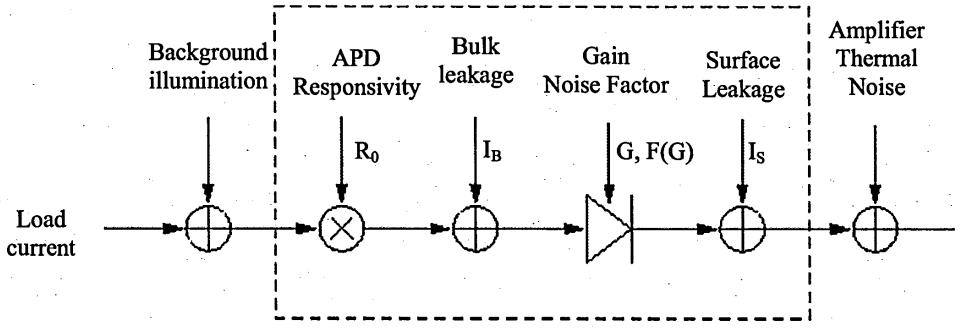

Figure 5.1-23: Nominal temperature profile for performance analysis

The DC current out of an avalanche photodiode is made up of three components, namely the load current I_L, $I_{Background}$ the current due to background illumination sources (here assumed to be zero), and I_D is the dark current of the device. The dark current is the output of the device with no input illumination and is primarily due to thermal generation of charge carriers in the depletion region and surface leakage currents due to surface defects near the edges of the semiconductor [Powers, 1993]. It has to be noted that the APD surface leakage current, I_S, is not multiplied by the APD gain and is modelled here as a constant DC current. The bulk dark current, I_B, on the other hand, is multiplied by the APD gain and is modelled as part of the background radiation. An EG&G Silicon APD C30902E was embedded to the first stage of amplification. The amplified noise source e_1 can therefore be given by the following relation:

$$G_1^2.e_1^2 = \left\langle i_N^2 \right\rangle + \left\langle i_{N\,shot\ surface}^2 \right\rangle$$

Equation 5.1-20 Amplified mean-square noise current from first amplification stage

Where $\langle i_N^2 \rangle$ is the mean-square noise current due to shot noise:

$$\left\langle i_N^2 \right\rangle = 2.q.[I_L + I_B]G_1^2.B.F(G_1)$$

Equation 5.1-21 Mean-square noise current due to shot noise
G_1 is the average current gain and $F(G_1)$ is the excess noise factor that is the measure of the extra noise added by the avalanche process. B is the bandwidth of the electronics accepting the noise. $I_L = R_0.P_i$, R_0 is the unamplified responsivity ($R=G_1.R_0$ = 65 A/W at 150V), P_i is the incident power, calculated to be around 6nW in chapter 4, for the anti-Stokes line before interaction with the APD. I_B is the bulk dark current given here to be equal to 15nA (at 150V).

$$F(G_1) = k.G_1 + \left[2 - \frac{1}{G_1}\right].[1-k]$$

Equation 5.1-22 APD excess noise factor
G_1 is the average APD gain (150 at 150V), k is the ionisation ratio (0.02 for EG&G Silicon APDs). $F(G_1) = 4.95$

The shot noise due to the surface leakage current is:

$$\left\langle i_{N\,\text{shot surface}}^2 \right\rangle = 2.q.I_S.B$$

Equation 5.1-23 Shot noise due to the surface leakage current
I_S is the surface leakage current (2nA), B is the system bandwidth

The system bandwidth is found assuming that the system response is Gaussian. Measuring short optical pulses is done using the technique of autocorrelation. The original pulse is Gaussian, the ratio of the original pulse's HWHM, Δt_{HWHM}, to the auto-correlated pulse's HWHM, ΔT_{HWHM}, is $1/\sqrt{2}$. The time-bandwidth product is $\Delta t_p.\Delta\nu = 0.4413$ for a Gaussian system response. Taking the optical pulse velocity in the fibre, V_p, being $2.10^8 m.s^{-1}$ and a targeted spatial resolution, Δz, of 1m, the required system bandwidth is:

$$B = \frac{0.44}{\Delta t_{HWFM}} = \frac{0.44}{\Delta T_{HWFM}.\sqrt{2}} = \frac{0.44}{\sqrt{2}}.\frac{V_p}{\Delta z}$$

Equation 5.1-24 System bandwidth required from the spatial resolution required
For 1m spatial resolution, the needed bandwidth is found to be 63MHz

However, the overall system bandwidth is given by the smallest bandwidth of the different amplification stages, which is 100MHz allowing a system spatial resolution of 0.6m.

The second amplification stage, the high-speed current to voltage amplifier has a gain of 60dB (50 kV/A), a bandwidth of 1GHz and an equivalent input current noise of 6.6pA/√Hz.

The third stage, the wideband voltage amplifier has a possible variable gain 10 to 60dB, switchable in 10dB steps, a bandwidth of 100MHz and an equivalent input voltage noise of 2.6nV/√Hz.

The third stage is used with a gain of 30dB for both the Stokes and anti-Stokes signals. The anti-Stokes signal is evaluated at 500m from the front end of the fibre at a 470mV level with SNR at 1.34 (1.26dB) and the Stokes signal at 670mV with SNR at 2.67 (4.27dB) [see chapter 4].

The system designed from bought-in component as an output-signal rise time, which results from the rise time of the isolated individual cascaded stages. The input waveform rise time is t_{Pulse}. The successive stages are namely the fibre, the APD, the amplification stages, the jitter from the emitting system and the optical pulse width.

$$\tau_{\Sigma} = \sqrt{t_{Fiber}^2 + t_{Pulse}^2 + t_{Jitter}^2 + t_{APD}^2 + t_{Stage\,2}^2 + t_{Stage\,3}^2} = \frac{2.R_s}{V_g}$$

Equation 5.1-25 System response time and spatial resolution

τ_{Σ} is the system response time, V_g is the group velocity in the optical fibre and R_s is the system spatial resolution. The optical fibre response time is calculated using its optical bandwidth BW_{opt} (200 MHz/km) $t_{Fibre} = 0.316 / (200 \times 0.5) = 3.16 \times 10^{-9}$s for a Gaussian response. The optical pulse width is 12ns. The Jitter is measured to be less than 1ns. The APD response time is 0.5ns. The second and third amplification stage response times are 0.32ns and 3.5ns respectively.

The system response time is found to be 12.95ns, which gives a system spatial resolution of 1.3m.

5.1.5 THE DIGITALISATION

To digitise the amplified signals, a two channels analog-to-digital converter board was interfaced to a PC on a 32 bit PCI bus. Each channel could record an analog input at speeds up to 500 Mega-Sample per second with 8 bit resolution, store the data in a deep on-board memory (2Mbs) and transfer them at a 100MB/s data transfer rate via the PCI bus to PC memory for signal processing. The bandwidth of the ADC being 250MHz, the calculated spatial resolution remained 1.3m. Each recorded sequence was triggered by the pulse generator, which was simultaneously used also to trigger the laser diode driver.

The ADC preferred sampling rate was 200MS/s (one sample every 5ns, which corresponds to a 0.5m sampling length on the fibre) and the voltage input range was ±1V on both 50Ω input channels. An LSB is therefore 7.81mV, the Stokes signal is then at 500m from the front end of the fibre laying over 86 LSB and the anti-Stokes signal over 60 LSB. It is important to note that the specific voltage range was chosen to see the full amplitude of the noisy signals, so as to keep the noise nature preserved for an adequate post-filtering process. For 500 data sets on each board with a PRF of 2kHz, the acquisition time is between 0.25s and 1s (1s if 1 dataset is captured after every 4 pulses). Switch times and data transfer lead to an overall time cycle before processing the data, between 0.5 and 1.2s.

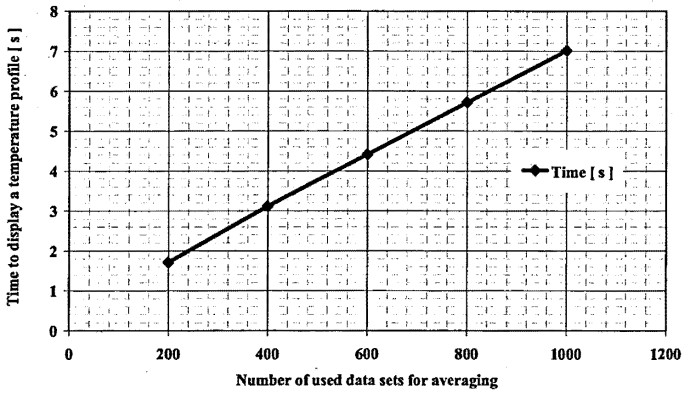

Figure 5.1-24: Time to display a temperature profile as a function of averages on data sets

5.2 ARCHITECTURE OF THE TESTED SYSTEM

The overall system architecture based on a modular design allows to technically progressing on individual parts. The objective of the design tested is to approach, as much as possible, the size, the weight, the reliability and the low cost (here addressed are the recurrent costs) of a qualified onboard detection system. The reduction in size and weight help the electrical power consumption to be lower for a given operating temperature range, while separating the laser diode pins from the PCB may help to reduce the vibration level between the demultiplexer body and the driver board.

5.2.1 THE STAKES OF THE NEW DESIGN

The requirements to be addressed by Airbus to the suppliers of equipment from the ABD0100 [Airbus S.A.S., 1998] will be joined together in the "Purchaser Technical Specification" with the requirements from various directives like the DO-160, DO-178. Both to bring solutions to the operational difficulties linked with the temperature variations of the electronic bays and to increase further the system lifetime figures, the following section focuses on the thermal regulation of the optical demultiplexer and on the qualification tests applicable as vibration-proof checking.

5.2.2 SYSTEM TEMPERATURE CONTROL

Thermal management is a key factor in optimising the optoelectronic DTS part performance. The system will be tested under the tests allocated to category A1, which is an equipment category for installation in a controlled temperature and pressurized location, on an aircraft within which pressures are normally no lower than the altitude equivalent of 15000ft Mean Sea Level (Section 4 and 5 [EUROCAE, 1997]). We will test therefore the system in an operating low temperature of –15°C. This is the lowest temperature at which equipment will normally be exposed and be required to operate. The operating high temperature range is +55°C. The maximum temperature conditions (Short-Time Operating High

Temperature) to which the equipment can be exposed are given as +70°C. It is expected that these temperature conditions will occur infrequently and be of short duration. The Ground Survival Temperatures are the lowest and the highest ground temperatures that the equipment is normally expected to be exposed to during aircraft storage or exposures to climatic extremes are -55°C to +85°C. The equipment is not expected to operate within specification limits at these temperatures but is expected to survive without damage. It will be also important to define tests representing the failure of the internal system that normally provides dedicated cooling for the WDM. The laser diode and the avalanche photodiodes must survive for a limited time in the absence of cooling. Test requirements for this type of equipment shall be specified in the equipment performance specification. Decompression and overpressure tests will also have to be conducted. The Temperature Variation Test will see a temperature variation of 2°C minimum per minute between the low/high and the high/low operational temperatures.

A Peltier element offers effective practical options for heat management in compact optoelectronic devices. A thermoelectric (TE) cooler is a semiconductor-based electronic component that functions as a small heat pump.

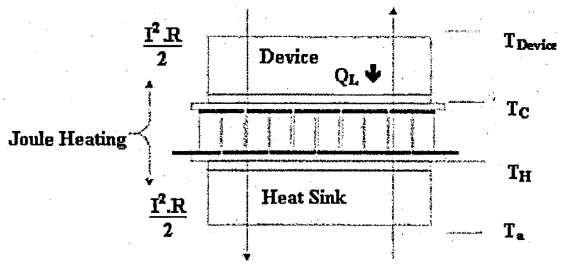

Figure 5.2-1: Peltier component and device under temperature regulation

When low-voltage dc power is applied to a TE module, heat moves through the module from one side to the other in proportion to the applied voltage. One module

face, therefore, will be cooled while the other is simultaneously heated. The phenomenon is fully reversible: with a switch in the polarity of the applied voltage, heat moves in the opposite direction. Thus the same module can function as both heater and cooler with very precise temperature stabilization [Otey *et al.*, 2001].

A thermal load (Q_L) combines the heat generated from the device (Q_f) and that which sneaks from ambient (Q_a) [Huang *et al.*, 1991]. Under steady state conditions, the heat entering is equal to that leaving at the first and second interfaces [cold (of Temperature T_c) and hot side (of Temperature T_h) of the Peltier component]. Writing the thermal equilibrium equation from the first and second interface, a simultaneous system equation is formed and can be solved to find T_h and T_c:

$$T_h = \frac{A_1 - (A_2 + b.K).T_c}{1 - A_2}$$

$$A_1 = T_a.(1 + b.K) + b.I^2.(R_{ex} + 2.N_C.\frac{\rho}{G}) + b.Q_f$$

$$A_2 = 2.N_C.b.S.I$$

$$T_c = \frac{B_2}{B_1}$$

$$B_1 = K + 2.N_C.\left[S.I + \Gamma.G.\left(\frac{1 + b.K}{1 - A_2}\right)\right]$$

$$B_2 = Q_f + K.T_a + 2.N_C.\left[\frac{\rho}{2.G}.I^2 + \Gamma.G.\left(\frac{A_1}{1 - A_2}\right)\right]$$

Equation 5.2-1 Peltier component heat transfers

K is the conduction coefficient from the ambient to the cold side, b is the thermal impedance from the hot side of the Peltier component to the heat sink. T_c is the TEC cold-side temperature, T_h is the hot-side temperature, T_a is the ambient temperature (heat sink temperature and air temperature), R_{ex} is the electrical excess resistance. S is the Seebeck coefficient, I is the current flowing through the Peltier component, ρ is the electrical resistivity of an element, G is the ratio of a Peltier element cross-section area A to its length L, N_C is the number of pairs, or "couples" in the TEC. Γ is the thermal conductivity of an element within the Peltier component. Q_f is the heat generated from the device, evaluated here to be about 12mW when considering an emitted optical pulse of 10W, of duration 12ns, with a PRF of 2kHz and when supported by an electrical pulse of 11.25A with a 90 V support voltage, the electrical pulse width being 6ns.

Using the software "Mathematica" to symbolically solve Equation 5.2-1, one may obtain a cubic equation for the Peltier component current. Finding the three solutions of this equation as a function of the ambient temperature, for a constant cold-side temperature of 25°C in the operational temperature range [-15°C to 70°C] we can derive the current needed over the operational temperature range for the system.

$$R = 2.N_C.\frac{\rho}{G}$$
$$V = (R + R_{ex}).I + 2.Nc.S.(T_a - T_c)$$
$$P = V.I$$

Equation 5.2-2 Peltier component electrical resistance, voltage and electrical power
R is the electrical resistance of the component, R_{ex} is the electrical excess resistance. V is the TEC voltage and P is its electrical power consumption.

The current needed range is –1 to 2A and the voltage drop ± 6V.

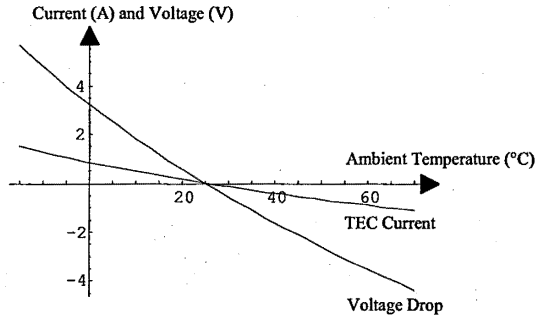

Figure 5.2-2: TEC voltage and current under the operational ambient temperature range for a set constant cold-side temperature (25°C)

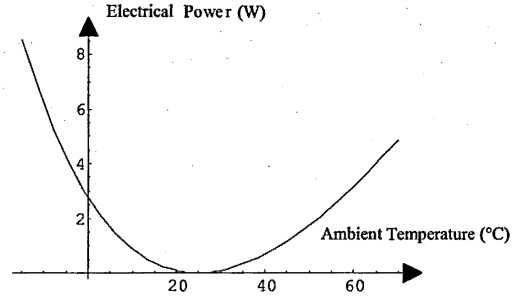

Figure 5.2-3: TEC electrical power range needed to cover the temperature range for qualification

5.3.1 NOISE CHARACTERISTICS

The optical Stokes and anti-Stokes back-scattered optical signal are amplified via the APDs and the amplification stages. They are then digitised and processed, combined to get the temperature profile at each location of the sensing optical fibre. This process sees a large amount of noise entering the acquisition chain. One solution to optimise the detection performances of the system is therefore to post-process the detected signals and to reject the noise influence.

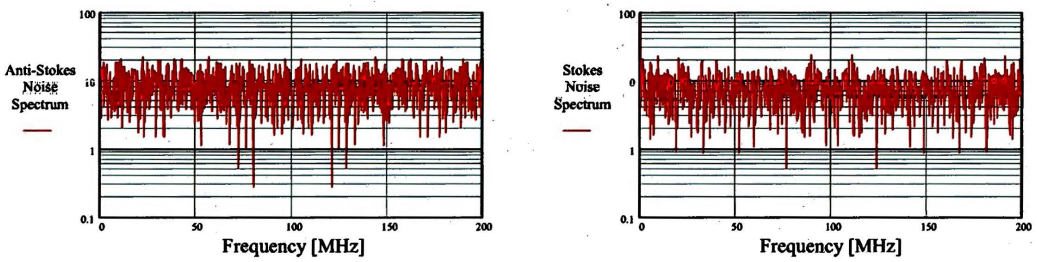

(a) **(b)**

Figure 5.3-2: Frequency spectrum of the detected anti-Stokes and Stokes signals

However, one of the difficulties is to determine the most suitable filter to put in place. Figure 5.3-2 shows that classical filters like band-pass, low/high-pass digital filters will bring only little benefit in the extraction of the noise. After amplification and digitisation, the noise spectrum spread over 200MHz, shown here as a near constant level on both graphs [**(a)**: FFT anti-Stokes signal; **(b)**: FFT Stokes signal].

For the system standard signal processing, the Stokes and anti-Stokes data sets are recorded and N times averaged point by point. The standard deviation of the temperature profile of an optical fibre tested at ambient temperature is inversely proportional to the square root of the number of averages, which indicates that the measurement is corrupted by a random noise with zero mean.

$$\sigma_N = \frac{K}{\sqrt{N}}$$

Equation 5.3-1 Standard deviation as a function of the number of averages on data sets

5.3 DETECTION PERFORMANCES ANALYSIS

The temperature detection is achieved over more than 500m of a multimode optical fibre (fibre cross-section dimensions: 62.5/125µm; numerical aperture: 0.22). The system aims to target the following performances: a spatial resolution of about 1.3m, a sampling resolution of 0.5m, a temperature accuracy of +/-3°C with a temperature profile refreshment time of 3s. Further descriptions of the expected performances can be found in chapter 3.

A reference experimental set-up is chosen to analyse the performance progresses throughout the development. It involves the test bench as presented in paragraph 5.1, and look at the temperature variations of a portion of an optical fibre located at ambient temperature and of a second further portion located into an oven.

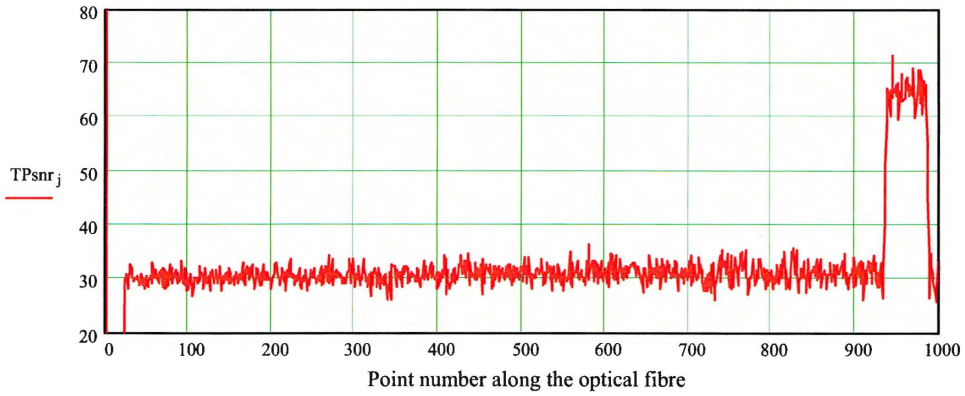

Figure 5.3-1: Nominal temperature profile for performance analysis

A 500m optical fibre is placed in two different temperature environmental conditions. The first portion is located at an ambient temperature of 30°C and at 467m from the control unit, the fibre goes into an oven with an internal air temperature of 64°C. The Stokes and anti-Stokes data sets are each averaged 2500 times before calculating the temperature profile.

The reference signal processing is a standard averaging process on the Stokes and anti-Stokes data sets and can be found for more details in paragraph 5.4.1. With this specific set-up, 2500 averages leads to a mean ambient temperature reading of 30.7°C, and a standard deviation of 1.7°C (cf. Figure 5.3-1).

shot noise. Hence, it is possible to draw the evolution of the SNR for the Stokes and anti-Stokes signals as a function of the distance to the control unit. It can be noticed that both signals are losing about 5dB over 500m.

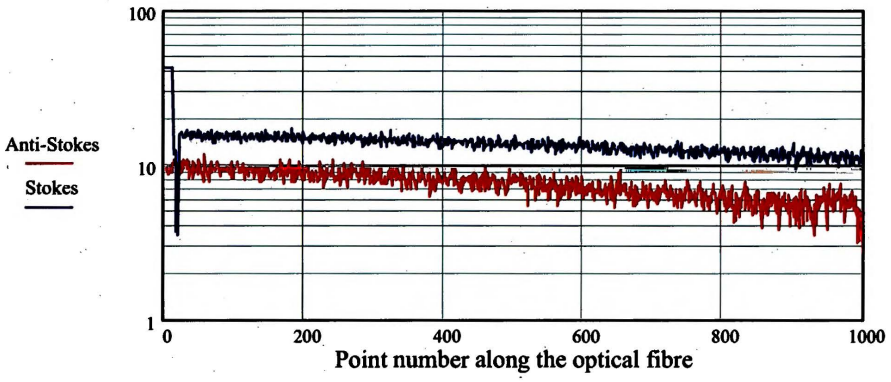

Figure 5.3-4 Signal-to-Noise ratio along the optical fibre

The anti-Stokes signal is the most temperature-dependant signal: SNR for the anti-Stokes signal. The Stokes signal is the least temperature-dependant signal: SNR for the Stokes signal.

Where:

$$SNR = 10.\log_{10}\left[\frac{m}{\sigma^2}\right]$$

Equation 5.3-2 Signal-to-Noise ratio

is the SNR and is calculated using m, which is the signal mean value of the received signal. σ^2 is the noise standard deviation described here as:

$$\sigma_N = \sqrt{\frac{1}{N}\cdot\sum_{i=1}^{N}(X_i - \hat{X})^2}$$

Equation 5.3-3 Standard deviation

where N is the number of data sets used to calculate point by point both the mean value $\hat{x}$ and the standard deviation from a set of value x_i.

The noise at the amplifier chain output will be assumed to be Gaussian, with variance σ^2 and zero-mean.

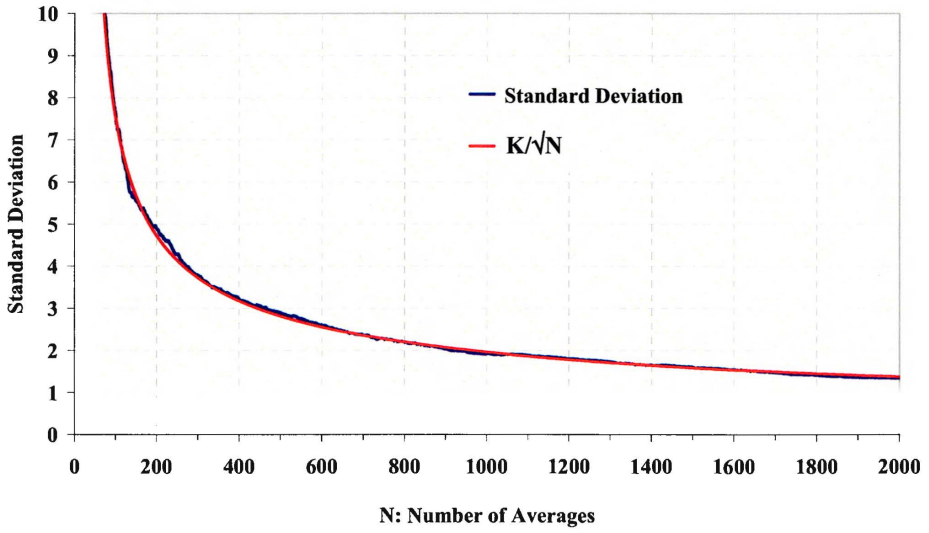

Figure 5.3-3: Standard deviation of a temperature profile as a function of the number of averages
N: number of averages, σ_N: temperature profile standard deviation at ambient temperature, K: constant.

The high level of noise on an individual data set leads to the consideration of methods to sufficiently reduce the noise level to isolate the temperature-related information from the Stokes / anti-Stokes signals.

In incoherent optical imaging systems, the image of an ideal point source is captured as a spatially extended pattern known as the point-spread function. When two closely-located point sources are measured through this kind of optical imaging system, the measured signal is the incoherent sum of the respective shifted point spread functions. A similar phenomenon occurs in signal processing when adding only a few data sets point by point. Up to a certain number of averaged data sets, the resulting distribution of signal levels provides little information on the noise nature and the associated standard deviation is highly fluctuating. This would indicate then that the noise is incoherent.

As described by the Equation 5.3-2, the signal is stochastic and the signal and noise are inter-dependent. Increasing the load current would increase for example the APD

shot noise. Hence, it is possible to draw the evolution of the SNR for the Stokes and anti-Stokes signals as a function of the distance to the control unit. It can be noticed that both signals are losing about 5dB over 500m.

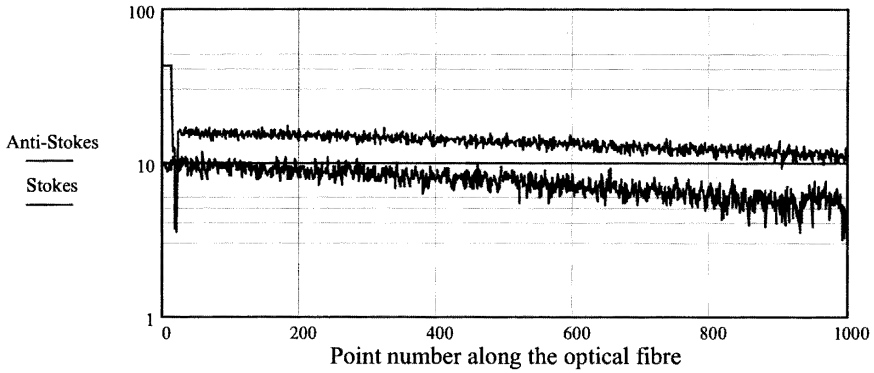

Figure 5.3-4 Signal-to-Noise ratio along the optical fibre

The anti-Stokes signal is the most temperature-dependant signal: SNR for the anti-Stokes signal. The Stokes signal is the least temperature-dependant signal: SNR for the Stokes signal.

Where:

$$SNR = 10.\log_{10}\left[\frac{m}{\sigma^2}\right]$$

Equation 5.3-2 Signal-to-Noise ratio

is the SNR and is calculated using m, which is the signal mean value of the received signal. σ^2 is the noise standard deviation described here as:

$$\sigma_N = \sqrt{\frac{1}{N}.\sum_{i=1}^{N}(X_i - \hat{X})^2}$$

Equation 5.3-3 Standard deviation

where N is the number of data sets used to calculate point by point both the mean value $\hat{x}$ and the standard deviation from a set of value x_i.

The noise at the amplifier chain output will be assumed to be Gaussian, with variance σ^2 and zero-mean.

5.3.2 TEMPERATURE RESOLUTION

The temperature-dependent ratio R(T) of anti-Stokes/Stokes scattered intensities is:

$$R(T) = \left[\frac{\lambda_{SS}}{\lambda_{AS}}\right]^4 . \exp\left[-\frac{h.c.\Delta\nu}{k.T}\right]$$

Equation 5.3-4 Temperature-dependent ratio

where h is Planck's constant, c is the velocity of light, k is Boltzmann's constant and T is the absolute temperature. Equation 5.3-4 holds for any transparent and non-dispersive material, conditions well satisfied by an optical fibre [Dakin *et al.*, 1985]. The temperature sensitivity can be found by differentiating the previous equation:

$$dT = \left[\frac{k.T^2}{h.c.\Delta\nu}\right] . \left[\frac{dR}{R}\right]$$

Equation 5.3-5 Temperature Sensitivity

The peak intensity of the Stokes Raman spectrum of silicate glasses is at about $\Delta\nu = 4.10^4$ m^{-1}. At room temperature the anti-Stokes / Stokes intensity ratio at this wave-number shift is about 0.15. The ratio must be measured to about 3% accuracy for a temperature uncertainty of 3K, when using 100 data set averages.

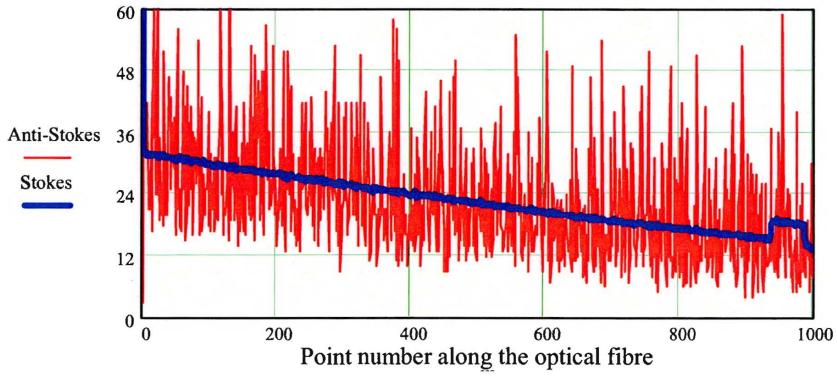

Figure 5.3-5 Averaging for signal denoising
Raw signal (anti-Stokes) and averaged anti-Stokes (Stokes) signal at room temperature for a 500m fibre long fibre. At 467m from the control unit, the fibre in the oven sees an air temperature at 64°C.

The 8 bits digitisation allows a measurement with an accuracy of about ±3%. This is leading to a standard deviation limit for temperature resolution of about ±0.5°C.

The thermal response time of a sensor loop depends strongly on the fibre cladding and cabling structure and on the quality of the thermal contact between the sensor loop and the object whose temperature is to be measured. In general, the heat capacity of fibre with its secondary coating is very low and the response time is below 0.5s. Even with conventional cabling structures the response time is typically of the order of a few seconds.

A section of the tested bare fibre was immersed in hot water (68°C). The length of the section was about 25m. The measurement time was set to 3s (around 500 averages) and the obtained OTDR profile is shown in Figure 5.3-8.

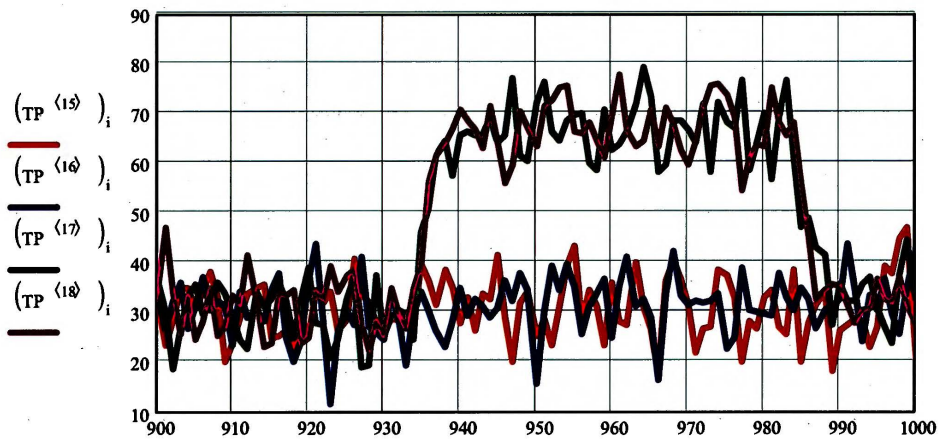

Figure 5.3-8 Measurement time

$TP^{<15>}$, $TP^{<16>}$, $TP^{<17>}$ and $TP^{<18>}$ are successive profiles separated in time by 3s from each other. The naked fibre (commercial multimode graded-index optical fibre: cross-section dimensions 62.5/125/250μm core, cladding and coating) is plunged into the hot water between the temperature profiles $TP^{<16>}$ and $TP^{<17>}$.

From Figure 5.3-8, it can be seen that a quick increase of temperature (increase duration is less than 3s) is detected correctly by the system. It would remain to show which lower duration limit for a temperature increase would affect the system detection accuracy.

5.3.4 MEASUREMENT TIME

The measurement time is quoted as the time interval to acquire and present a complete temperature profile of one fibre sensor loop to a certain temperature resolution. This time includes acquisition of the backscatter signal, averaging processing and display [York Sensors Ltd., 1991].

The measurement time has also to be correlated to the temperature resolution, which relates to the consistency of measured values and is expressed at one standard deviation (1 sigma) of the measurement. The number of data analysed contributes to increasing the temperature resolution but also impacts on the DTS measurement time.

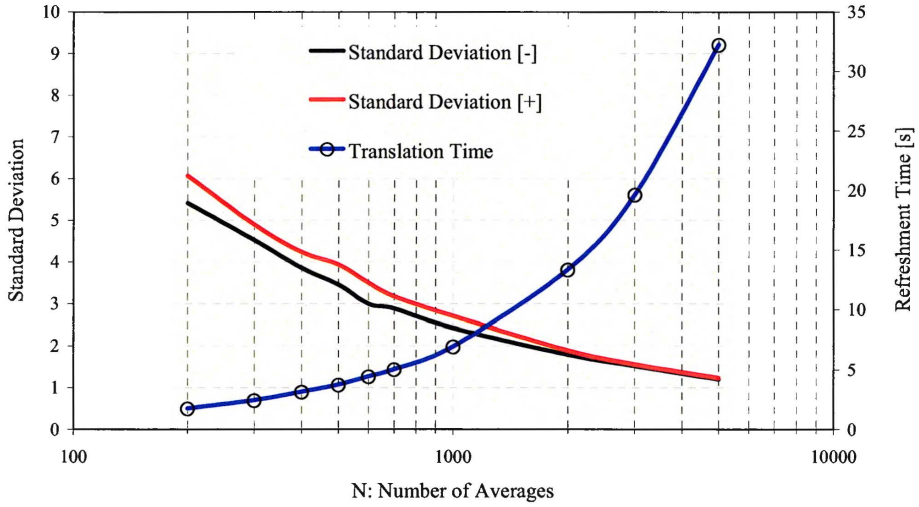

Figure 5.3-7 Temperature standard deviation and measurement time performances

The standard deviation associated with a profile is correlated to its necessary measurement time. This shows that the signal processing based on an averaging principle can reach the objective of less than 3°C temperature resolution but is making impossible (with the current test bench design) the objective of displaying an up-dated temperature profile within 3s.

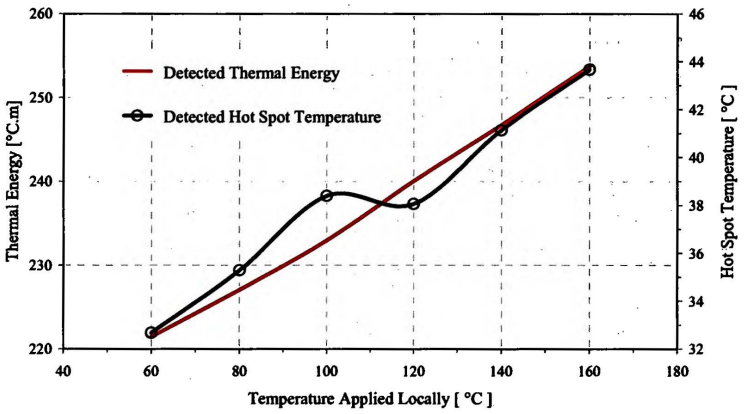

Figure 5.3-10 Hot spot energy detection

The integration of the temperature curve over the length of the impacted zone is a parameter, which can be considered as energy-related, an optical energy spread along the impacted zone.

5.3.6 OPTICAL FIBRE LENGTH

The maximum length of the fibre sensor for which the stated performance specification is maintained is defined as the spatial range. This is determined by the total two-way loss in the fibre and must include the fibre, splices and connectors. The two-way loss for each must be used since the signal of interest travels the length of the fibre out and back. The ultimate limitation is the dynamic range of the DTS itself, which is reached when the return signal is so weak as to be indistinguishable from system noise or is limited by the bandwidth of the fibre.

Figure 5.3-11 shows the response of two fibres with different attenuations. The first optical fibre gives Stokes and anti-Stokes signals attenuated each of about 1dB.km^{-1}, which allows providing a temperature profile over few kilometres.

The second fibre presents a high attenuation, around 9.5dB, and is limiting therefore the spatial range of the system. One may notice especially that at position 700, the reflection from the reference fibre ending (at connector position) is particularly

5.3.5 HOT SPOT DETECTION

The measurement of the DTS response to a local temperature increase (heated zone limited to 0.15m) shows a significant difference between the oven temperature and the value of the detected maximum temperature. When the temperature "hot-spot" occupies a zone that is less than the spatial resolution of the DTS then the measured temperature is lower by approximately the ratio R = [hot-spot width]/[spatial resolution]. In applications where the width is known a correction factor can be estimated.

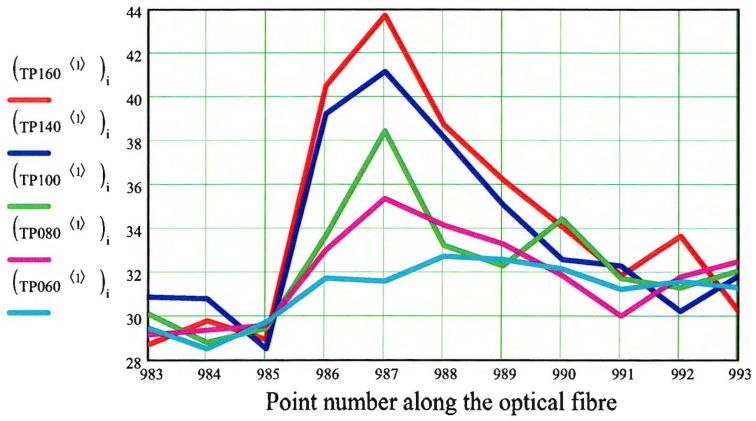

Figure 5.3-9 Hot spot detection

The oven is set successively to the temperatures 60°C, 80°C, 100°C, 140°C and 160°C (respectively $TP060^{\langle 1\rangle}$, $TP080^{\langle 1\rangle}$, $TP100^{\langle 1\rangle}$, $TP140^{\langle 1\rangle}$, $TP160^{\langle 1\rangle}$. It can be seen that the DTS system records lower maximum temperatures and that the zone impacted by a local heating is more than twice the spatial resolution.

Figure 5.3-10 shows that the energy detected from the impacted section is progressing linearly with an increase of the "hot-spot" temperature. A progress of one degree on detection side is noticed for every 8 degrees from the "hot spot".

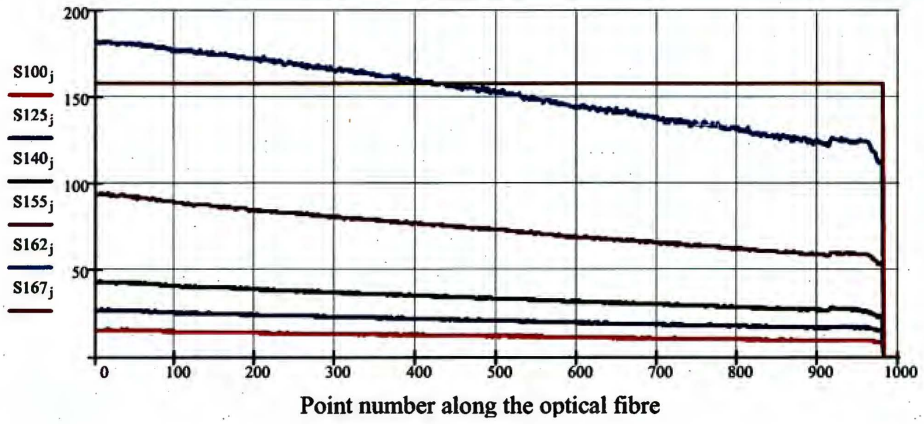

Figure 5.3-12 Levels of detected Stokes signals as a function of the APD input voltage
The Stokes signal S100, S125, S140, S155, S162, S167 corresponds to the APD input voltage=100, 125, 140, 155, 162, 167 V respectively.

to a reverse voltage variation for a constant optical signal as input. One may notice that the APD saturates above the saturation voltage (here about 163V). However, below the saturation voltage, the Stokes profile sees its level rising continuously with the reverse voltage as the APD gain rises.

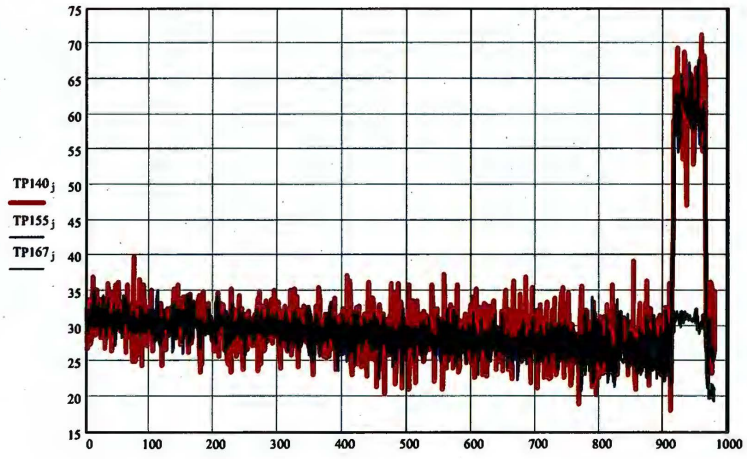

Figure 5.3-13 Temperature profile shape as a function of the APD input voltage

Near the saturation voltage of the Stokes and anti-Stokes APDs, the temperature profile integrity is affected by the differential progression of the APD gains. One

important, which explains also in part the performance of this sensing element. It was found after analysis that the fibre was indeed too firmly winded up on its roll.

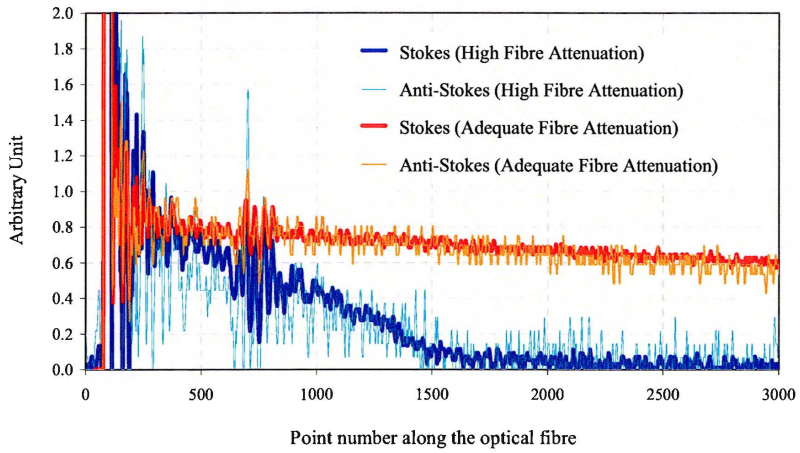

Figure 5.3-11 Influence of the optical fibre attenuation on spatial range

5.3.7 HARDWARE CONTROL AND MONITORING

One of the key parameters with the detector's spectral noise to consider when selecting an APD is the gain-voltage curve. Figure 5.3-12 shows the APD response

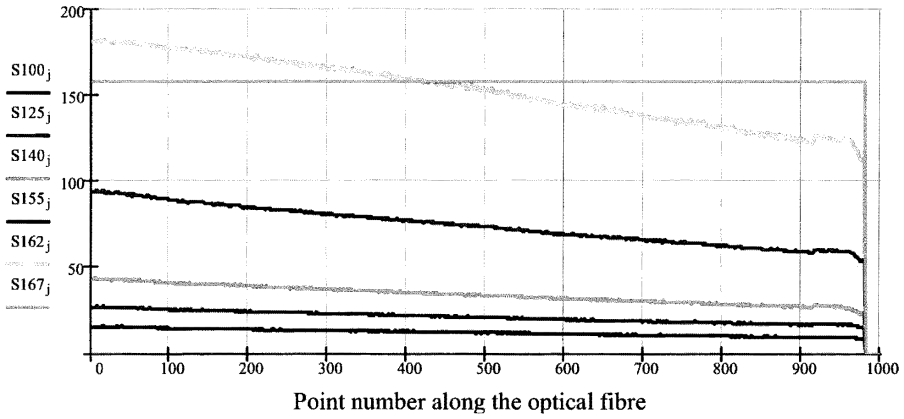

Figure 5.3-12 Levels of detected Stokes signals as a function of the APD input voltage
The Stokes signal S100, S125, S140, S155, S162, S167 corresponds to the APD input voltage=100, 125, 140, 155, 162, 167 V respectively.

to a reverse voltage variation for a constant optical signal as input. One may notice that the APD saturates above the saturation voltage (here about 163V). However, below the saturation voltage, the Stokes profile sees its level rising continuously with the reverse voltage as the APD gain rises.

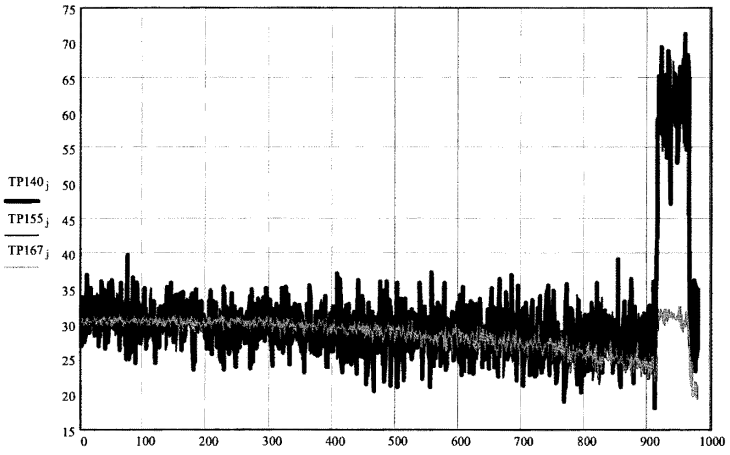

Figure 5.3-13 Temperature profile shape as a function of the APD input voltage

Near the saturation voltage of the Stokes and anti-Stokes APDs, the temperature profile integrity is affected by the differential progression of the APD gains. One

may notice that a direct consequence is to detect a significantly lower temperature range between the ambient temperature and the oven, as well as a distorted profile towards the smallest signals.

So as to determine the optimum APD voltage to apply, the standard deviation of the temperature profile was examined as a function of the reverse voltage. Figure 5.3-14 highlights an APD voltage for which the photodiode is not saturated and the standard deviation is minimum. Nevertheless, to avoid any detection misinterpretation caused by small voltage drift from the APD power supply stage, a lower voltage is chosen within a voltage range where the gain variation is quasi-linear. The test bench was using an APD input voltage of 145V.

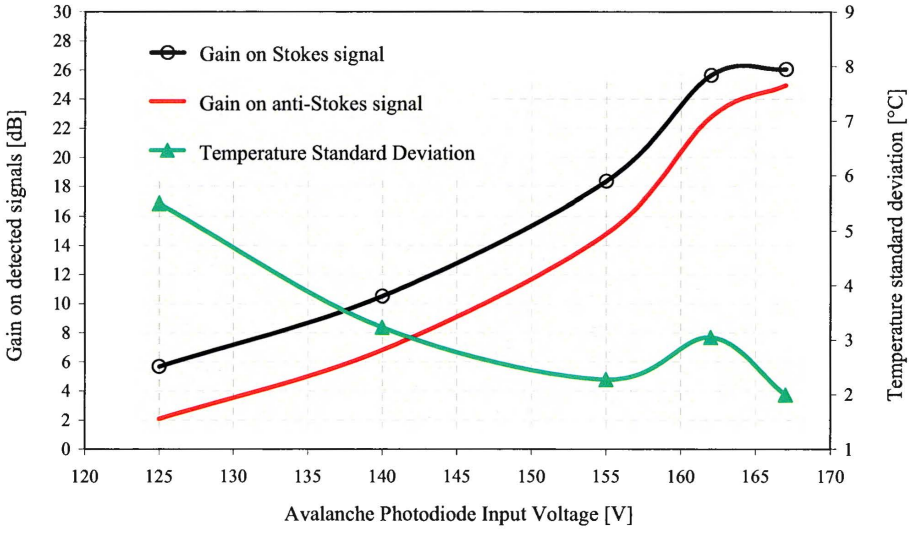

Figure 5.3-14 Levels of detected optical signals levels as a function of the APDs input voltage

More generally, the development of an on-board DTS system will have to focus on

three essential controls, which are namely:

- the thermal control of the wavelength demultiplexer, so as to compensate the thermal external influences and to ensure the respect of the emission and reception specifications which are temperature dependent.
- the control of the input APD voltages to regulate their associated gains.
- the control of the emission power of the laser diode as criteria to evaluate its remaining lifetime.

Some additional controls like the noise level monitoring per channel, the detection of one or several breaks along the fibre and the verification of a correct temperature for the reference coil appear as a minimum required, in order to guarantee the safety and reliability levels of the system.

5.4 DIGITAL SIGNAL PROCESSING OPPORTUNITIES

To reject the noise generated and amplified by the APD and by the cascaded amplification modules, the numerical signals are averaged per point up to a stage where the standard deviation on the point temperature reaches the target of less than +/- 3°C. One solution using the Wiener filter and another using a wavelet denoising filter are evaluated in terms of the temperature standard deviation they can offer as a function of the number of pre-processed averages.

One direct effect of this strategy is also to ease the need of performances of the mass memories and of the high-speed electronic components.

5.4.1 AVERAGING OF THE ACQUIRED SIGNAL DATA SETS

Two acquisition channels are running and storing simultaneously the raw data, which will contribute to determine the temperature profile. The Stokes and anti-Stokes signals are recorded following each laser diode pulse. The data sets are summed point-by-point to a pre-set number (called "number of averages", N_{av}) and a denoising filter based on a simple averaging process allows an increase in the temperature resolution.

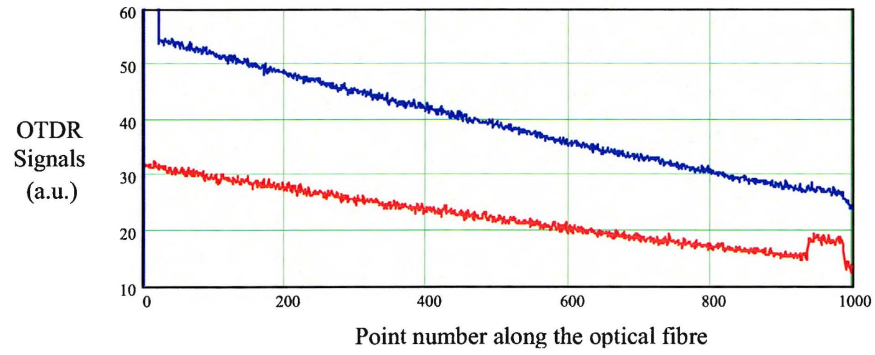

Figure 5.4-1 Stokes and anti-Stokes signals, each averaged 500 times

The Stokes signal is attenuated (over 800 points = 400m) of $10.\log_{10}(31/56)$=-2.57dB i.e. 6.42dB.km^{-1} and the anti-Stokes signal (over 600 points = 300m) of $10.\log_{10}(21/32)$=-1.83dB i.e. 6.09dB.km^{-1}.

One may therefore use a band-pass filter to reject the most contributing frequencies to the noise amplitude. The bandwidth of this desired band-pass filter is relatively wide, we can simply cascade a low-pass filter and a high-pass filter to obtain a band-pass response. Third order Butterworth low/high-pass filters are implemented. The corresponding transfer functions are following.

$$HP(k_n) \equiv \begin{cases} 0 & \text{if } (k_n < k_c^{HP}) \\ \dfrac{1}{s^3 + 2.s^2 + 2.s + 1} & \text{else} \end{cases}$$

$$LP(k_n) = \begin{cases} 0 & \text{if } (k_n > k_c^{LP}) \\ \dfrac{1}{s^3 + 2.s^2 + 2.s + 1} & \text{else} \end{cases}$$

Equation 5.4-4 Low/High-pass filter Butterworth 3rd order transfer functions

The value of s and k_n are given by:

$$s_* = \frac{1}{j.(k_n - k_c^*)}$$

$$k_n = n.\frac{200}{N}$$

Equation 5.4-5 Low and high-pass filter variables

where N is the number of points of each data set and * indicates the consideration of the low or high-pass cut-off frequency, k_c^{LP} and k_c^{HP} respectively.

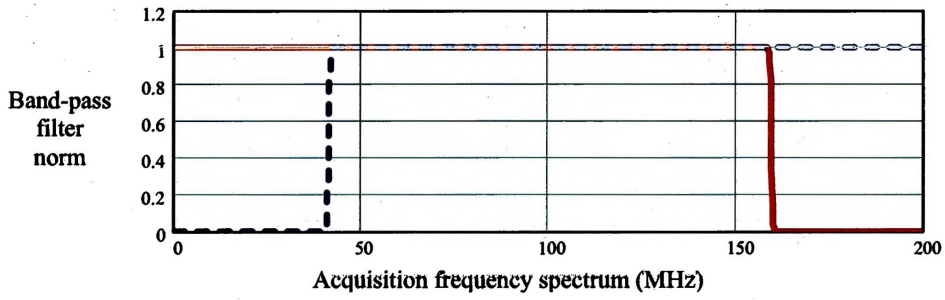

Figure 5.4-3 Band-pass filter resulting of the combination of a low and a high-pass filter
The choice of high or low frequency in the figure are just for illustration.

Stokes and Stokes signals respectively. DL is calculated to be 0.33dB as described in Figure 5.4-1. N_1 is the fibre core index and gives a value for δ_n of 1.026. $R(T_0)$ is the average of the temperature-dependent ratio over the full length of the reference fibre (100m). SR is the sampling resolution using the approximation for a 10ns ADC clock and a 1m sampling resolution (here 0.5m for a 200MHz sampling frequency).

Beyond the physical significance of the value DL and SLE, these values can be adjusted experimentally. The parameter DL contributes to the adjustment of the profile flatness at ambient temperature, while SLE sets the system sensitivity to temperature change. SLE can therefore be fixed using for example the measurement of three fibre zones placed at different temperatures (ambient temperature +X°C; ambient temperature; ambient temperature -X°C where 2.X°C would be the temperature detection range).

5.4.2 FOURIER TRANSFORM AND BAND-PASS FILTER

A noise spectrum analysis is carried out on the acquired data sets to identify the potential filters to put in place so as to obtain a significant noise reduction.

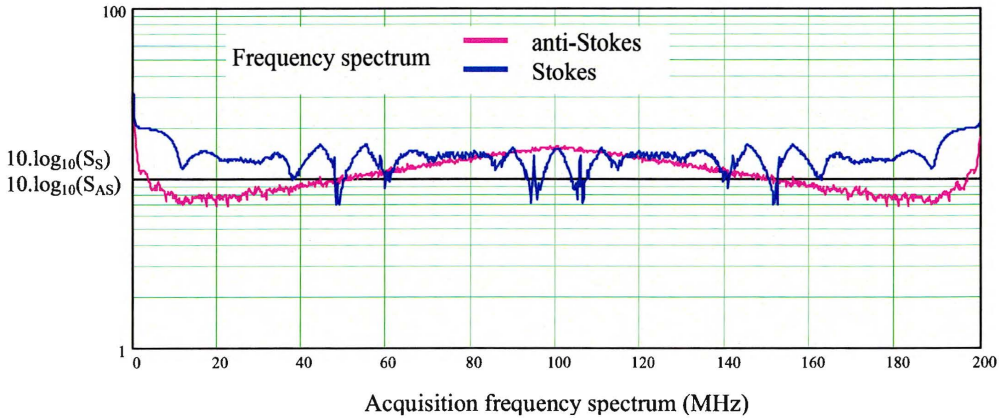

Figure 5.4-2 Noise spectrum of 500 averaged anti-Stokes and Stokes data sets

The analysis reveals that noise levels are close together over the full acquisition frequency range except at low frequencies where the noise amplitudes are increasing.

One may therefore use a band-pass filter to reject the most contributing frequencies to the noise amplitude. The bandwidth of this desired band-pass filter is relatively wide, we can simply cascade a low-pass filter and a high-pass filter to obtain a band-pass response. Third order Butterworth low/high-pass filters are implemented. The corresponding transfer functions are following.

$$HP(k_n) = \begin{cases} 0 & \text{if } (k_n < k_c^{HP}) \\ \dfrac{1}{s^3 + 2.s^2 + 2.s + 1} & \text{else} \end{cases}$$

$$LP(k_n) = \begin{cases} 0 & \text{if } (k_n > k_c^{LP}) \\ \dfrac{1}{s^3 + 2.s^2 + 2.s + 1} & \text{else} \end{cases}$$

Equation 5.4-4 Low/High-pass filter Butterworth 3rd order transfer functions

The value of s and k_n are given by:

$$s_* = \frac{1}{j.(k_n - k_c^*)}$$

$$k_n = n.\frac{200}{N}$$

Equation 5.4-5 Low and high-pass filter variables

where N is the number of points of each data set and * indicates the consideration of the low or high-pass cut-off frequency, k_c^{LP} and k_c^{HP} respectively.

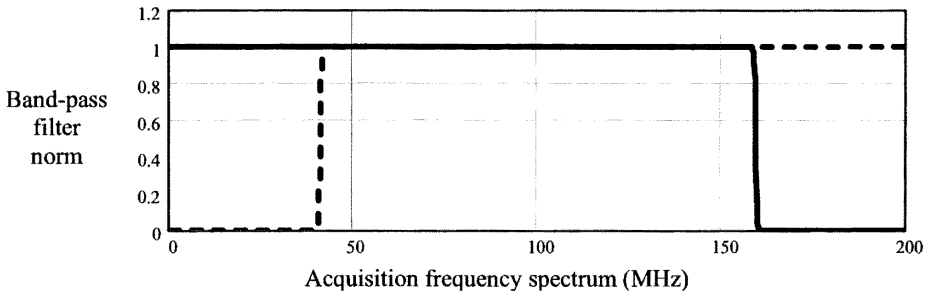

Figure 5.4-3 Band-pass filter resulting of the combination of a low and a high-pass filter
The choice of high or low frequency in the figure are just for illustration.

A band-pass filter is used here for the Stokes and anti-Stokes signals. The band-pass filters are simply obtained by the multiplication of the low/high-pass absolute values of their transfer-functions. The Fourier transforms of the signal data sets are then multiplied with their respective band-pass filter functions. An inverse Fourier transform produces the desired filtered data sets.

Applying the band-pass filter to the experimental data, and adjusting the cut-off frequency values to minimize the temperature standard deviation reveals that a low-pass filter applied to the anti-Stokes data is able to improve the temperature resolution. It is a possibility to reduce the noise without altering the spatial resolution and temperature sensitivity and without bringing additional noise into the final temperature profile. However, this will degrade the spatial resolution and will have therefore to be checked to remain within the performance objectives.

For the anti-Stokes signal, the cut-off frequency used was –2MHz. Using the filtering method on 500 times averaged data sets, at ambient temperature, the temperature standard deviation is reduced from 3.26°C to 3.24°C.

Therefore, a standard low-pass filtering of the data sets is demonstrated as bringing little benefit to temperature signal denoising. In order to improve the SNR for each acquisition channel, another approach can be to assume that the noise is uncorrelated with the signal and is resulting from a convolution between the propagating optical pulse and the impulse response of the fibre.

5.4.3 WIENER FILTER

The initial signals (Stokes and anti-Stokes) have been degraded by the addition of random noise n(z) with known statistical properties (similar to normally distributed), therefore the original signals in question are given by [Jianchao, 1999]:

$$\begin{cases} S_S(z) = p(z) * h_S(z) + n_S(z) \\ S_{AS}(z) = p(z) * h_{AS}(z) + n_{AS}(z) \end{cases}$$

Equation 5.4-6 Decomposed signals including fibre impulse response and added noise components.

Taking the Fourier transform gives:

$$\begin{cases} TFS_S(\omega) = P(\omega).H_S(\omega) + N_S(\omega) \\ TFS_{AS}(\omega) = P(\omega).H_{AS}(\omega) + N_{AS}(\omega) \end{cases}$$

$$\Rightarrow \begin{cases} H_S(\omega) = \dfrac{TFS_S(\omega) - N_S(\omega)}{P(\omega)} \\ H_{AS}(\omega) = \dfrac{TFS_{AS}(\omega) - N_{AS}(\omega)}{P(\omega)} \end{cases}$$

Equation 5.4-7 Impulse response Fourier transforms for the Stokes and anti-Stokes signals.

However, this simple method presents some limitations from the fact that $N_*(\omega)$ are rarely known exactly and that $P(\omega)$ often vanishes or becomes very small for some values of ω (* indicates either the Stokes or anti-Stokes signal).

The objective is therefore to find a filter, which will give the best approximation to $H_*(\omega)$. The Wiener filter gives a least square approximation to $H_*(\omega)$.

$$\begin{cases} H_S(\omega) = W_S(\omega).TFS_S(\omega) \\ H_{AS}(\omega) = W_{AS}(\omega).TFS_{AS}(\omega) \end{cases}$$

$$\Rightarrow \begin{cases} W_S(\omega) = \dfrac{\overline{P_S(\omega)}}{|P_S(\omega)|^2 + S_{n,S}(\omega)/S_{h,S}(\omega)} \\ W_{AS}(\omega) = \dfrac{\overline{P_{AS}(\omega)}}{|P_{AS}(\omega)|^2 + S_{n,AS}(\omega)/S_{h,AS}(\omega)} \end{cases}$$

Equation 5.4-8 Wiener filters based on the optical pulse shape for the Stokes and anti-Stokes signals

$\overline{P_S(\omega)}$ and $\overline{P_{AS}(\omega)}$ are the complex conjugates of $P_S(\omega)$ and $P_{AS}(\omega)$ respectively. $|P_S(\omega)|$ and $|P_{AS}(\omega)|$ are their amplitudes, $S_{n,*}(\omega)$ and $S_{h,*}(\omega)$ are the noise and original signal spectral densities [Haider *et al.*, 1998]. The spectral densities are roughly speaking spectra averaged over all the data sets under consideration. $S_{n,*}(\omega)$ and $S_{h,*}(\omega)$ are here unknown, we define therefore a common procedure to assume a constant ratio λ_* to be then adjusted.

The pulse shape in time is recorded and a normalized polynomial function is associated. This procedure has the advantage of defining a filter, which is independent from the laser peak optical power. The pulse time function is as follows:

$$p(t) = p_{10}.(t-r)^{10} + \ldots + p_2.(t-r)^2 + p_1.(t-r) + p_0$$

$$\Rightarrow \left| \begin{array}{l} p_{10} = -5.2327.10^{-12};\ p_9 = 5.1861.10^{-10};\ p_8 = -1.9290.10^{-8} \\ p_7 = 2.9710.10^{-7};\ p_6 = -2.7499.10^{-7};\ p_5 = -4.5110.10^{-5};\ p_4 = 3.9911.10^{-4} \\ p_3 = 1.2226.10^{-3};\ p_2 = -3.0322.10^{-2};\ p_1 = 5.5267.10^{-2};\ p_0 = 9.9025.10^{-1} \end{array} \right.$$

Equation 5.4-9 Optical pulse time function.

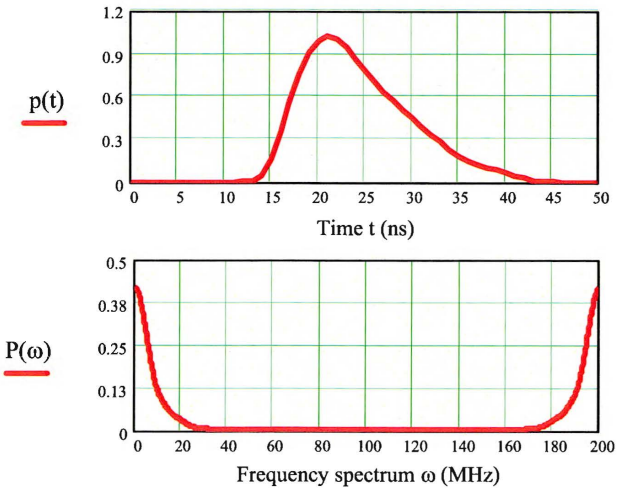

Figure 5.4-4: Optical pulse time function and its associated Fourier transform

signals and the temperature profile is finally determined. To validate the deconvolution method, the temperature information provided by averaged but un-filtered data sets are compared to filtered data sets for the same number of averages. The comparison is built on the temperature results.

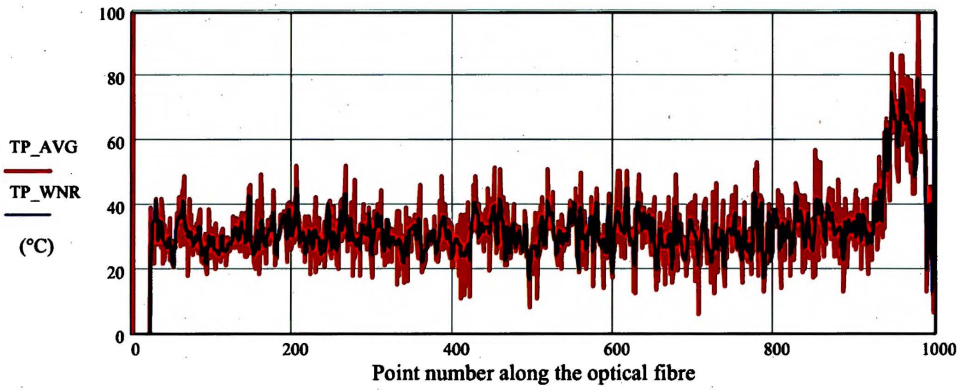

Figure 5.4-6 Anti-Stokes and Stokes data sets 100 times averaged and Wiener filtered
TP_AVG is the temperature profile resulting from averaged data sets, TP_WNR is resulting from Stokes and anti-Stokes data sets averaged then filtered using a Wiener filter adjusted by the calculated and corresponding λ_{*opt} to the number of used averages. The number of averages used here is 100.

It can be noticed that the filter reduces significantly the temperature standard deviation and seems to follow faithfully the temperature changes.

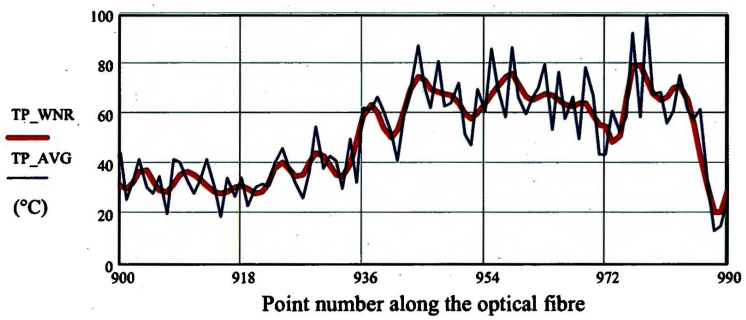

Figure 5.4-7 Temperature Anti-Stokes and Stokes data sets 100 times averaged and Wiener filtered

It is therefore possible, using the Wiener filter, to trigger a certain temperature resolution with a conform selection of the required number of initial averages on the signal data sets.

law of λ_{*opt}. The results for both the Stokes and anti-Stokes signals are shown in the graph below.

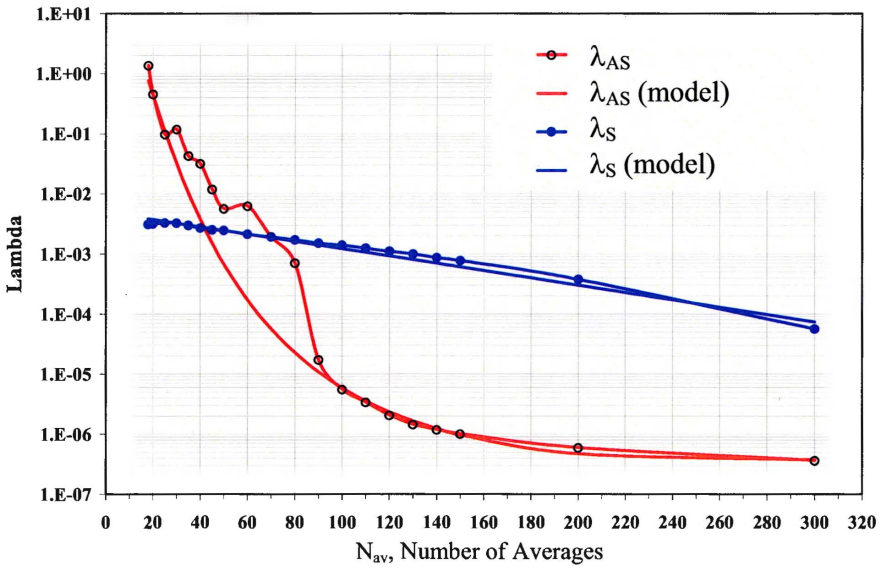

Figure 5.4-5 Spectral density ratio as a function of the number of averaged data sets

The modelled optimum spectral density ratios for the Stokes and anti-Stokes ratio are given by:

$$\lambda_{AS} = \left[a.N_{av}^{b} + c\right]\exp\left[d.\frac{(N_{av}+e)}{(N_{av}+f)}\right] \quad \Rightarrow \quad \begin{vmatrix} a = 4.702.10^{-3} & d = -58.59 \\ b = 7.2539 & e = -1.02 \\ c = -2.8199 & f = 44.585 \end{vmatrix}$$

$$\lambda_{S} = \exp\left[g.\frac{(N_{av}+h)}{(N_{av}+i)}\right] \quad \Rightarrow \quad \begin{vmatrix} g = -1.2618.10^{6} \\ h = 380.55 \\ i = 9.005.10^{7} \end{vmatrix}$$

Equation 5.4-12 Filter optimisation using the spectral density ratio λ_* as variable

The values of the correlation coefficient are close to unity, which results in a good estimation of the impulse response of the optical fibre. After substituting the values of λ_{*opt} in Equation 5.4-10, the inverse Fourier transforms are calculated for both

signals and the temperature profile is finally determined. To validate the deconvolution method, the temperature information provided by averaged but un-filtered data sets are compared to filtered data sets for the same number of averages. The comparison is built on the temperature results.

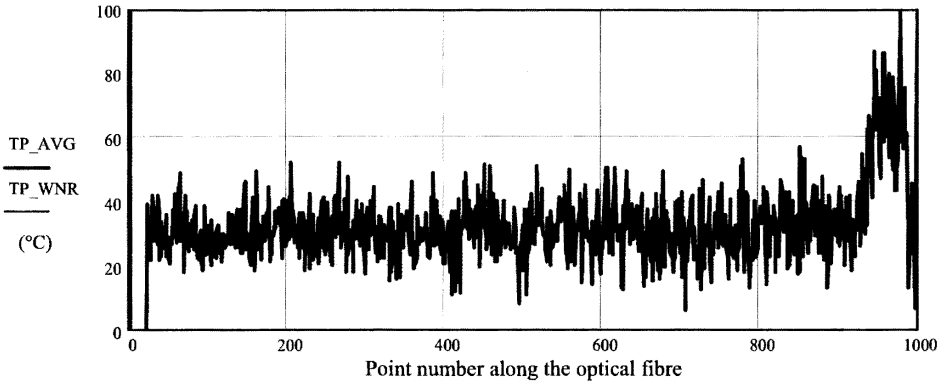

Figure 5.4-6 Anti-Stokes and Stokes data sets 100 times averaged and Wiener filtered
TP_AVG is the temperature profile resulting from averaged data sets, TP_WNR is resulting from Stokes and anti-Stokes data sets averaged then filtered using a Wiener filter adjusted by the calculated and corresponding λ_{opt} to the number of used averages. The number of averages used here is 100.

It can be noticed that the filter reduces significantly the temperature standard deviation and seems to follow faithfully the temperature changes.

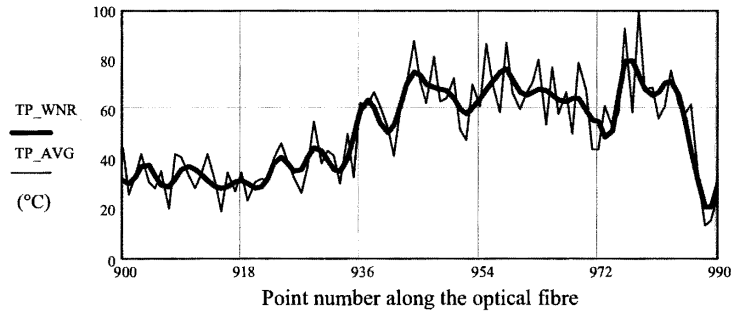

Figure 5.4-7 Temperature Anti-Stokes and Stokes data sets 100 times averaged and Wiener filtered

It is therefore possible, using the Wiener filter, to trigger a certain temperature resolution with a conform selection of the required number of initial averages on the signal data sets.

5.4.4 SOFT THRESHOLDING USING WAVELET DECOMPOSITION

The Fourier transformation is just one of a large class of linear orthogonal transformations which can be used in signal processing. Like the sinusoids in Fourier analysis [Kaiser, 1998], wavelets form bases that can decompose (analyse) and reconstruct (synthesize) signals and images. As a by-product, we obtain the accompanying processing (filtering, compression, denoising, etc.). The simplest wavelet algorithm possible is called the Fast Haar Transform (FHT). Like the Fast Fourier Transform (FFT), the FHT assumes that the given data consists of $N = 2^L$ numbers, but involves only addition, subtraction and division by 2. The FHT is local. A local change in the data signal (e.g. a spike) results in a local change in the FHT coefficients. The resulting change in the FFT coefficients is global since it takes a wide range of frequencies to form a spike. The FHT is real, so that real data gives real FHT coefficients. The FFT of a real signal, on the other hand is complex, this may lead to complex operations on its transform. This short analysis demonstrates some of the wavelet theory advantages for signal denoising. It can be generalized to other fast wavelet algorithms.

A mother wavelet is a function $\psi(x)$ such that $\{\psi(2^j x-k), i, k \in Z\}$ is an orthonormal basis of $L^2(R)$. The basis functions are usually referred to as wavelets. The term mother implies that the functions with different regions of support that are used in the transformation process are derived by dilation and translation of the mother wavelet [Li *et al.*, 2003]. How to find the wavelet ? The key idea is self-similarity. Start with a function $\phi(x)$ that is made up of smaller version itself:

$$\phi(x) = \sum_{k=-\infty}^{\infty} a_k . \phi(2.x - k)$$

Equation 5.4-13 Father wavelet equation

The function $\phi(x)$ is called the scaling function (or father wavelet), a_ks are called filter coefficients or masks. Under certain conditions Equation 5.4-13 gives a wavelet.

$$\psi(x) = \sum_{k=-\infty}^{\infty} (-1)^k . b_k . \phi(2.x - k) = \sum_{k=-\infty}^{\infty} (-1)^k . \bar{a}_{1-k} . \phi(2.x - k)$$

Equation 5.4-14 Wavelet equation under certain conditions

The conjugate of a is $\bar{a}$. These certain conditions are:

$$\left| \begin{array}{ll} \sum_{k=0}^{N-1} a_k = 2 & \text{stability} \\ \sum_{k=0}^{N-1} (-1)^k . k^m . a_k = 0 & \text{convergence} \\ \sum_{k=0}^{N-1} a_k . a_{k+2m} = 0 & \text{orthogonality of wavelets} \\ \sum_{k=0}^{N-1} a_k^2 = 2 & \text{orthogonality of scaling functions} \end{array} \right.$$

Equation 5.4-15 Wavelet dilation equation

The Daubechies wavelets can be generated out of Equation 5.4-15.

$\psi_{j,k}$, j, k $\in$ Z span and is an orthonormal basis of $L^2(R)$. An arbitrary function f $\in$ $L^2(R)$ then can be expressed as follows:

$$f(x) = \sum_{j,k \in Z} d_{j,k} . \Psi_{j,k}(x)$$

Equation 5.4-16 Arbitrary wavelet function

where: $d_{j,k} = \langle f, \Psi_{j,k} \rangle$ are called wavelet coefficients. Note that j controls the observation resolution and k controls the observation location.

Subband coding into octave band channels can be seen as a Discrete Wavelet Transform (DWT). DWT can be implemented using the pyramid interconnect, where the lower levels of the pyramid contain high resolution data and the upper levels of the pyramid contain low resolution data [Markas, 1993].

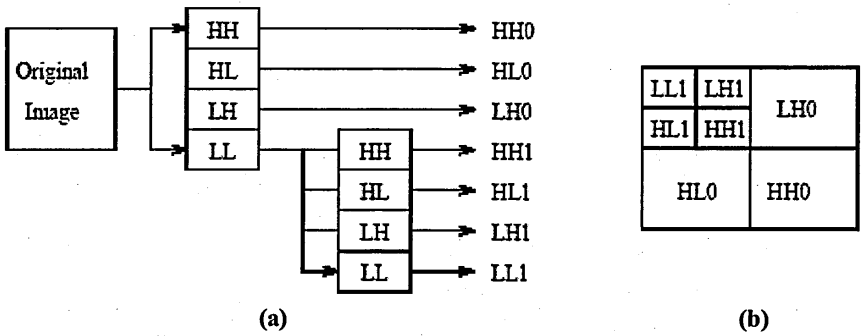

Figure 5.4-8 Image discrete wavelet transform: (a) filtering and decimation, (b) pyramid interconnect

Figure 5.4-8 shows a two-level DWT, as well as the resulting pyramid structure (for the signal processing of an image).

In subband coding, the original temperature profile is split into K frequency bands using an analysis filter [Markas, 1993]. Each subband is then decimated, keeping every k^{th} value. The result of this process is k profiles whose total size is equal to the size of the initial profile. Separable one-dimensional analysis filters are used to achieve a straightforward filter design, to create each subband. The subbands HH_k, HL_k, LH_k, k = 1, 2, …, N_{Level} are called the details, where k is the scale, with N_{Level} being the largest scale in the decomposition. The subband LL_{NLevel} is the low resolution residual. The wavelet-thresholding denoising method filters each coefficient Y_i from the detail subbands with a threshold function to obtain Xe_i (estimated coefficients). The denoised estimate is then:

$$\hat{f} = W^{-1}\hat{X}$$

Equation 5.4-17 Denoised estimate

where W^{-1} is the inverse wavelet transform operator [Chang *et al.*, 2000a].

Noise is a random error or variance of a measured variable. Removing noise from data can be considered as a process of identifying outliers or constructing optimal estimates of unknown data from available noisy data. Wavelet techniques provide an effective way to de-noise and have been successfully applied in various areas

The Stokes and anti-Stokes vectors are lengthened from 1003 elements to $2^{10} = 1024$ elements (N_{elt}) and the fast wavelet Daubechies 4 (wave(S^*)) from Mathcad 2000 Professional (MathSoft, Inc.) is used to calculate the wavelet transform of both signals W*. The number of levels is 9. The 9 levels, the subband coding are given by the vectors W_k, where k is indicating the level concerned. The vectors k are built taking respectively the elements of W* from index "2^k" to "$2^{k+1} - 1$". One may then stretch the different vectors for a representation of the subbands (SB_k^*) on a unique graph (i is the element index of a value from 0 to N_{elt}).

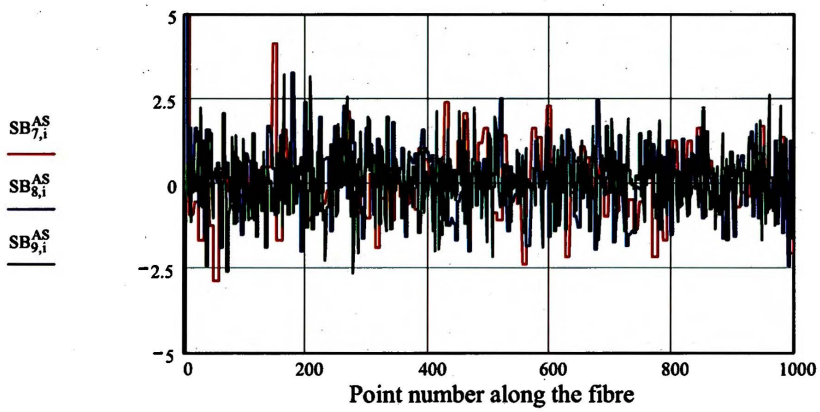

Figure 5.4-9 Wavelet subbands 7, 8 and 9 from the anti-Stokes data set averaged 100 times
Using a wavelet Daubechies 4 decomposition, the 1024 elements of each data set lead to a group of 9 subbands. The highest frequencies are represented here through level 9.
Anti-Stokes wavelet coefficients for sub-bands 7, 8 and 9 (respectively SB_7, SB_8, SB_9) are shown here with arbitrary units.

When there are multiple copies available, it is possible to combine averaging and thresholding. The first operation is linear, the second is not. The calculation ordering could make a difference, but it is shown that the advantage of one method over the other is small and because averaging before thresholding requires less calculation, this is the preferred method. The method uses variable threshold values, adaptive to different subband characteristics.

$$T_{k,N_{av}} = \left[\frac{1}{N_{av}}\right]^{P_*(N_{av})} \cdot \left[\frac{\sigma^2}{\sigma_k}\right]$$

Equation 5.4-20 Adaptive subband threshold

where σ^2 is the noise variance, which is estimated from the subband HH_1:

Since wavelet thresholding has worked well for one copy of corrupted image (here the back-scattered data sets), we consider its extension to multiple copies. The wavelet coefficients are often grouped into subbands of different scales. The small coefficients are more likely due to noise and the large coefficients due to important signal features. These small coefficients can be thresholded without affecting the significant features of the image. The wavelet coefficients are given by:

$$N_{Level} = \frac{\ln(N_{elt})}{\ln(2)} - 1$$

$$W^* = \text{wave}(S^*) \quad \Rightarrow \quad \left| W_k^* = \text{submatrix}[\, W^*_{(2^k,\ 2^{k+1}-1)}] \right.$$

$$SB^*_{k,i} = W^*_{k,\text{floor}\left[\frac{i}{Nelt/2^k}\right]}$$

Equation 5.4-19 Wavelet coefficients and expand function.

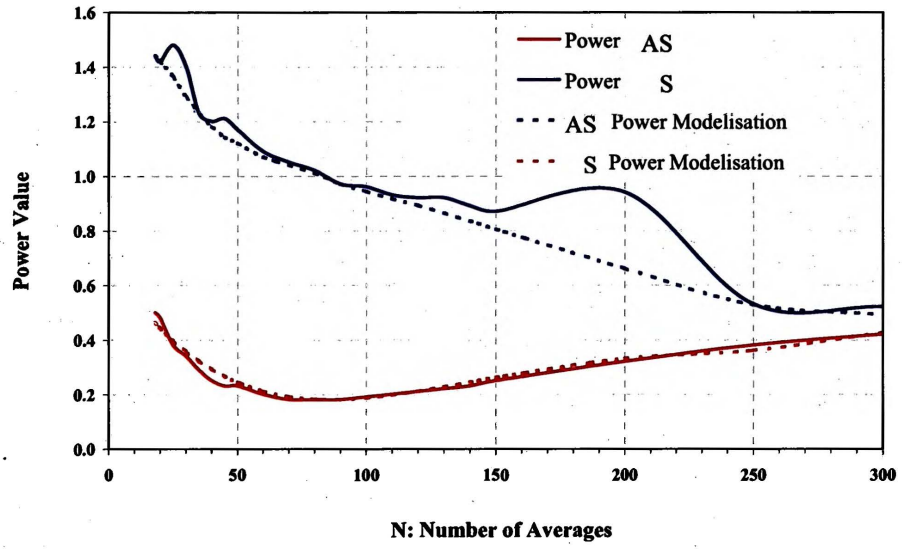

Figure 5.4-10 Subband threshold power values

The polynomials have the following expression:

$$P_{AS}(N_{av}) = p_4.N_{av}^4 + p_3.N_{av}^3 + p_2.N_{av}^2 + p_1.N_{av} + p_0$$
$$P_S(N_{av}) = q_4.N_{av}^4 + q_3.N_{av}^3 + q_2.N_{av}^2 + q_1.N_{av} + q_0$$

$$\Rightarrow \left| \begin{array}{l} p_4 = 7.185.10^{-10};\ p_3 = -5.469.10^{-7};\ p_2 = 1.460.10^{-4};\ p_1 = -1.484.10^{-2};\ p_0 = 6.850.10^{-1} \\ q_4 = 9.555.10^{-10};\ q_3 = -6.447.10^{-7};\ q_2 = 1.519.10^{-4};\ q_1 = -1.735.10^{-2};\ q_0 = 1.695 \end{array} \right.$$

Equation 5.4-22 Power value polynomials for subband thresholding according to the number of pre-processed averages.

A qualitative observation of the resulting signals has shown that to preserve the overall objectives of the study (namely to keep or improve the detection performances while decreasing the needs in terms of hardware memory), it is necessary to not stick on the correlation coefficient results but to increase the value of the powers. Increasing these values of a unit allows not degrading the shape of the temperature profile, which stays similar to the outcome of the traditional purely averaging signal processing.

$$\sigma^2 = \left[\frac{\text{median}(|Y_i|)}{0.6745}\right]^2, \quad Y_i \in \text{subband } HH_1$$

Equation 5.4-21 Noise variance of subband HH_1

and σ_k is the standard deviation of the subband under consideration [Kaur *et al.*, 1999].

The definition of the function $P_*(N_{av})$ is conducted using the same methodology as in the Wiener filter construction, except that its value is increased by a safety factor to keep the spatial resolution in line with the application performance requirements.

The optimal value is indeed not so straightforward and is in fact a function of the number of the available copies and of the relative energy between noise and signal. Its value is approximated by a linear function by portions and fluctuates from about 1.6 to 1, as the number of used copies increases.

The optimum correlation coefficient values as a function of the number of initial averages are used to calculate the powers $P_*(N_{av})$. The power values obtained build a polynomial to predict the threshold values per subband, as a function of the number of averages and for each OTDR signal. These results are following the indications made by Chang, S.G., Yu, B. and Vetterli, M. [Chang *et al.*, 2000b], which give a power value of 1 when the signals are transformed then averaged and a value of 0.75 when averaged then transformed.

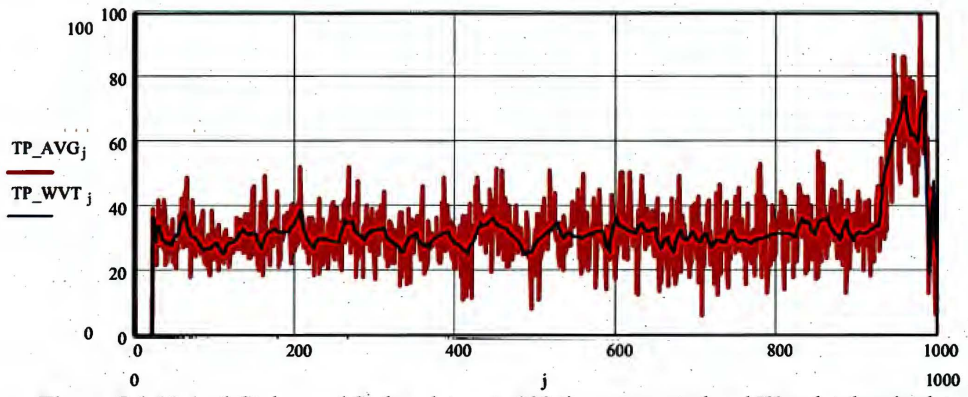

Figure 5.4-11 Anti-Stokes and Stokes data sets 100 times averaged and Wavelet denoised
TP_AVG is the temperature profile resulting from averaged data sets, TP_WVT is resulting from Stokes and anti-Stokes data sets averaged then filtered using the soft-thresholding Wavelet decomposition. The filter is adjusted by the calculated and corresponding λ_{*opt} to the number of used averages. The number of averages used here is 100.

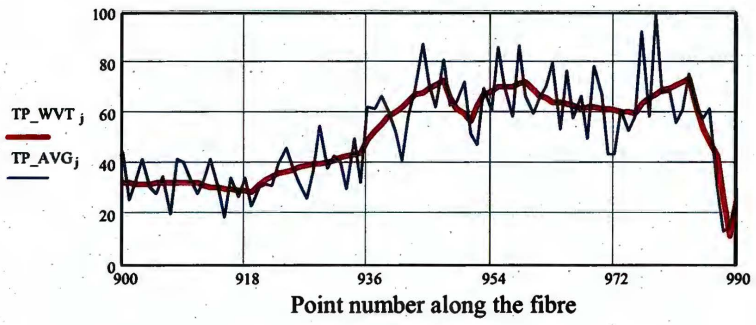

Figure 5.4-12 Wavelet denoised temperature profile
Temperature profile using 100 times averaged data sets, TP_AVG, and with the application of a Wavelet Denoising Filter, TP_WVT.

5.4.5 CONCLUSION ON POST-SIGNAL PROCESSING

The signal processing using a standard averaging principle, the combination of pre-processed averages and Wiener filtering, pre-processed averages and the wavelet thresholding technique were proposed as alternatives to the lack of performances of a traditional digital low/high-pass Butterworth filter. The investigation showed that the

$$W^*_{N_{Level}} = \text{submatrix}[\, W^*_{(2^{N_{Level}},\ 2^{N_{Level}+1}-1)}]$$

$$L_k = 2^{k+1} - 2^k$$

$$M^* = \frac{\text{median}(W^*_{N_{Level}-1})}{0.6745}$$

$$M^*_k = \frac{\sum_{j=2^k}^{2^{k+1}-1} W^*_{k,j}}{L_k}$$

$$\sigma^*_k = \left[\frac{1}{L_k} \cdot \sum_{j=2^k}^{2^{k+1}-1} (W^*_{k,j} - M^*_k)^2 \right]^{0.5}$$

$$TH^*_k = \left[\frac{1}{N_{av}} \right]^{(P_*(N_{av})+1)} \cdot \left[\frac{M^{*2}}{\sigma^*_k} \right]$$

Equation 5.4-23 Subband thresholds for wavelet denoising

The function "$P_*(N_{av})$" initially introduced in Equation 5.4-20 is therefore here converted into "$P_*(N_{av})+1$" and the threshold principle is operated on each coefficient.

$$\text{if } \left| W^*_k \right| < \left| TH^*_k \right| \Rightarrow \begin{cases} \text{then } W^*_k = 0 \\ \text{else } W^*_k = W^*_k \end{cases}$$

Equation 5.4-24 Filtering process for wavelet denoising

Hence, it is possible to compare graphically the temperature profiles resulting from a simple averaging with a soft-thresholding using wavelet decomposition. It is noticeable that for the same number of pre-processed averages, the temperature resolution is significantly improved. The first observations show no degradation of the spatial resolution and is confirmed on Figure 5.4-13, where the temperature edge is spatially correctly restituted.

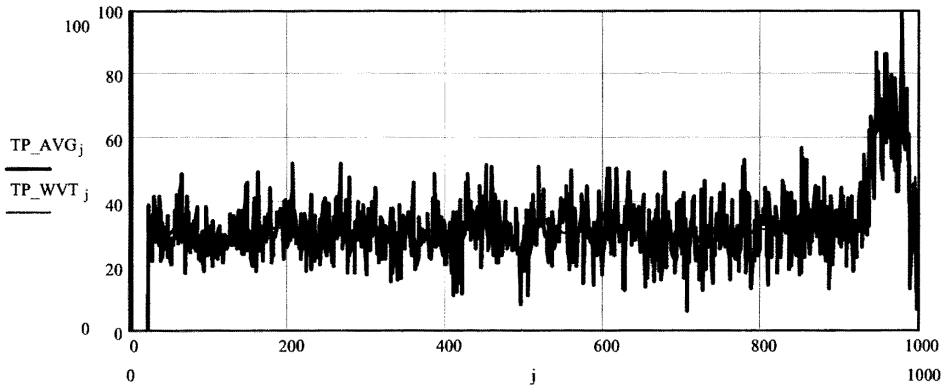

Figure 5.4-11 Anti-Stokes and Stokes data sets 100 times averaged and Wavelet denoised
TP_AVG is the temperature profile resulting from averaged data sets, TP_WVT is resulting from Stokes and anti-Stokes data sets averaged then filtered using the soft-thresholding Wavelet decomposition. The filter is adjusted by the calculated and corresponding $\lambda_{\bullet opt}$ to the number of used averages. The number of averages used here is 100.

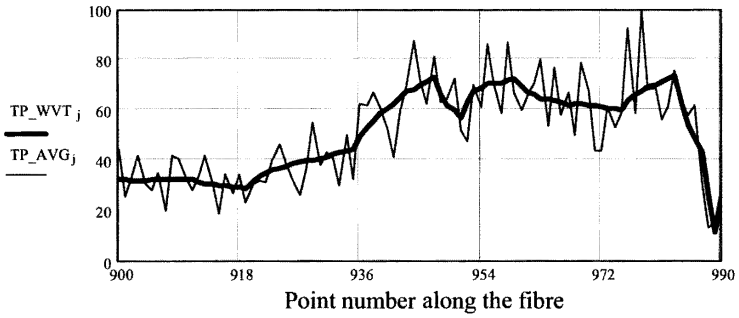

Figure 5.4-12 Wavelet denoised temperature profile
Temperature profile using 100 times averaged data sets, TP_AVG, and with the application of a Wavelet Denoising Filter, TP_WVT.

5.4.5 CONCLUSION ON POST-SIGNAL PROCESSING

The signal processing using a standard averaging principle, the combination of pre-processed averages and Wiener filtering, pre-processed averages and the wavelet thresholding technique were proposed as alternatives to the lack of performances of a traditional digital low/high-pass Butterworth filter. The investigation showed that the

optimal results are in fact a function of the number of available data sets. A near-optimal threshold, based on the optimum value of the correlation coefficient, was therefore proposed for both the Wiener and Wavelet filtering techniques. Besides, the wavelet decomposition thresholding method show substantial improvement on the temperature resolution (measured by the temperature standard deviation) over the typical averaging method and moderate improvement over the Wiener filtering.

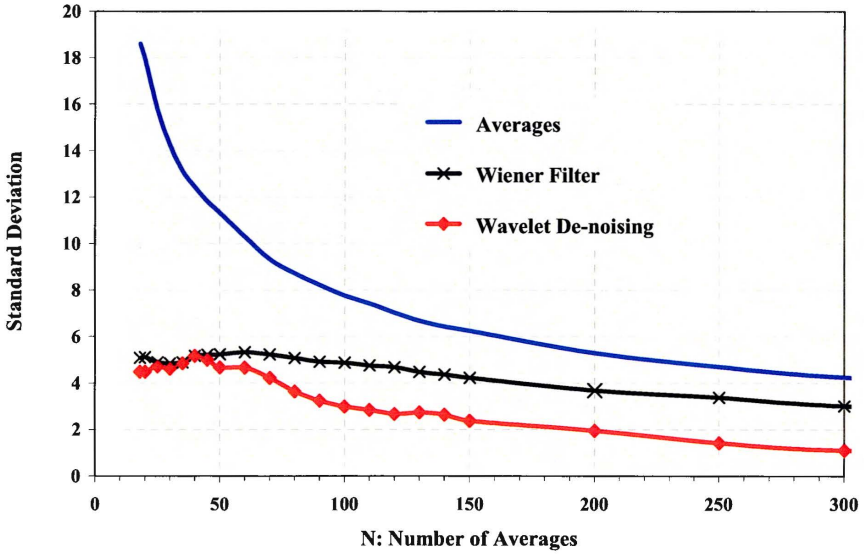

Figure 5.4-13 Standard deviation on temperature profile for three different denoising techniques Averaging, Wiener filtering and Wavelet denoising. On x axis: number of averaged data sets used before calculation of the distributed temperature profile; on y axis: the corresponding standard deviation.

The wavelet denoising filter is bringing a real benefit in increasing with a few data sets, the targeted temperature accuracy as opposed to the Wiener filter, which requires to identify the optical pulse shape first.

The wavelet denoising algorithm provides smoothness and better edge preservation at the same time and does not require any knowledge of the detection system hardware performances. The needed temperature accuracy of ±3°C is reached with

the Wiener filter with 300 copies of both the Stokes and anti-Stokes when 100 are only necessary with the wavelet denoising method.

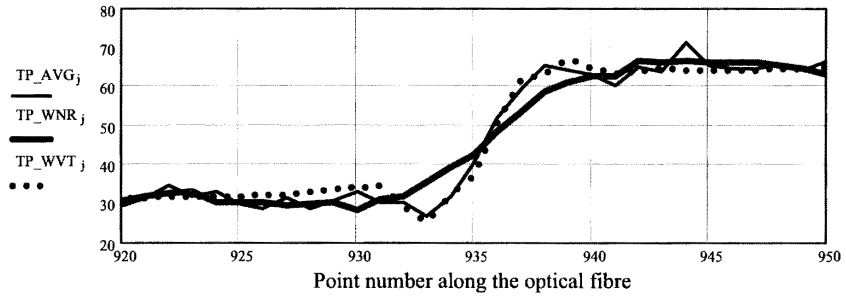

Figure 5.4-14 Filtering method impact on spatial resolution
Spatial resolution after averaging, Wiener filtering, Wavelet denoising. Temperature profile using 2500 times averaged data sets, TP_AVG; combined with the Wiener filter, TP_WNR; combined with the application of a Wavelet denoising filter, TP_WVT.

The spatial resolution of the system is about 1.3m. The temperature rise from the ambient temperature to the oven hot air is detected over a distance strongly related to the system spatial resolution. Post-processing the data using the Wiener filter results in approximately doubling the DTS spatial resolution, while the wavelet filter post-processing brings the same level of performance as a standard averaging process.

5.5 COMPATIBILITY TO ON-BOARD SYSTEM REQUIREMENTS

The environmental tests, described in the EUROCAE DO-160D standards, highlight the importance of a performing design principle for the optical module and its surrounding electronic boards [EUROCAE, 1997]. It is indeed believed that the electronic amplification and the control unit can meet without major non-conformities, the specifications of an on-board aeronautic system. Most of the integration work would have therefore to be conducted to guarantee a reliable withstanding to the environmental constraints, especially to vibration and shocks.

Nature of the test	Standard	Category - CU	Category - SE
Temperature and Altitude	DO160-D / Section 4	A1	
Temperature Variation	DO160-D / Section 5	C	
Humidity	DO160-D / Section 6	A	TBD
Shocks	DO160-D / Section 7	B	TBD
Vibration	DO160-D / Section 8	R	TBD
Magnetic Effect	DO160-D / Section 15	A	
Induced Signal Susceptibility	DO160-D / Section 19	Z	
Frequency Radio Susceptibility	DO160-D / Section 20	V	
Radio Frequency Emissions	DO160-D / Section 21	L	
Effects induced by Lightening	DO160-D / Section 22	A2-C2	
Explosion Proofness	DO160-D / Section 9		TBD
Water Proofness	DO160-D / Section 10		TBD
Proofness to various Liquids	DO160-D / Section 11		TBD
Sand and Dust	DO160-D / Section 12		TBD
Fungus Proofness	DO160-D / Section 13		F / TBD
Salt Mist	DO160-D / Section 14		S / TBD

Table 5.5-1 Compliance table for DTS main aeronautic qualification tests
CU: Control Unit. SE: Sensing Element. TBD: To Be Defined.

Table 5.5-1 lists the different tests to be performed on the control unit or on the optical cable for an application of fire protection in the cargo compartment. One may therefore clearly identify the benefit of having to design a cable to be able to resist water, sand and dust… as opposed to the current systems, which present electronics to these environmental constraints. However, it remains to define further what have to be the tests for this new monitoring application (see Chapter 3), and possibly also to isolate the control unit to prevent the laser diode transmission line from radiating interfering magnetic fields with the surrounding avionics.

5.6 CONCLUSION

In this chapter the methodology and the construction details to build and optimize a modular OTDR DTS have been explained. The description of the system modules has highlighted the improvement potentials while demonstrating the system capability to reach the detection performances requested from Chapter 3.

Axes of development were preferred so as to guarantee the conformity to on-board environmental constraints. The demultiplexer design is proven to be temperature controllable using a Peltier element of maximum electric power 9W for an operating avionic bay temperature range of [-15°C;+70°C]. The laser diode was decoupled in vibration from the driver board via a flexible transmission line.

The detection performances were analyzed also through the measurement results, which have made clear the importance of an APD voltage regulation and the insufficiencies of the standard signal processing for a reduced number of averages as far as the temperature resolution is concerned. The standard averaging method is achieving ±8°C for 100 averages of the Stokes and anti-Stokes data sets. From these results, an enhancement of the measurement and data processing capabilities is proposed using two different signal-processing schemes. Considering the noise level and image spectral densities, the first possibility was studied using the optical pulse shape and a Wiener filter [±5°C for 100 averages]. The second technique uses a wavelet denoising algorithm [±3°C for 100 averages]. The soft-thresholding technique using wavelet decomposition improves significantly the temperature resolution without degrading the spatial resolution.

The conformity analysis to aeronautic qualification tests did not reveal any showstopper. A rapid improvement of the spatial resolution was identified as possible with the development of the laser diode driver, which would need to generate an 8ns optical pulse width to achieve a sub-meter system spatial resolution.

REFERENCES

Agante, P. M. and Marques de Sa, J. P. "ECG Noise Filtering Using Wavelets with Soft-thresholding Methods". Proceedings Computers in Cardiology'99. (1999) pp.535-542.

Airbus S.A.S. ABD0100. Equipment - Design - General Requirements for Suppliers. X.ABD, issue D. (1998).

Alfrey, A. J. "Cooling System Design for Scientific Applications Using Thermoelectric Coolers: A Case Study in Cooling Large Laser Diodes". Technical Note #1, v. 1.03. (2002) pp.0-39.

Burman, R. and Krausse, G. J. "A High Current, Fixed Narrow Pulse Width Laser Diode Driver". Directed Energy Inc. Application Note. (1996) pp.1-15.

Byeong, H. L. "Multislit Interpretation of Cascaded Fiber Gratings". Journal of Lightwave Technology. (2002) Vol. 20. Iss. 9. pp.1750-1761.

Chang, S. G., Yu, B., and Vetterli, M. "Adaptive Wavelet Thresholding for Image Denoising and Compression". IEEE Transactions on Image Processing. (2000a) Vol. 9. Iss. 9. pp.1532-1546.

Chang, S. G., Yu, B., and Vetterli, M. "Wavelet Thresholding for Multiple Noisy Image Copies". IEEE Transactions on Image Processing. (2000b) Vol. 9. Iss. 9. pp.1631-1635.

Dai-fei, G., Wei-hong, Z, Zhen-ming, G, and Jian-qiang, Z. "A Study of Wavelet Thresholding Denoising". IEEE Proceedings of ICSP2000. (2000) pp.329-332.

Dakin, J. P., Pratt, D. J., Bibby, G. W., and Ross, J. N. "Temperature Distribution Measurement using Raman Ratio Thermometry". SPIE Fiber Optic and Laser Sensors III. (1985) Vol. 566. pp.249-256.

Directed Energy Incorporated. "Datasheet: PCO-7110 Laser Diode Driver Module. Installation and Operation Notes". http://www.directedenergy.com/Products/laser.htm. (2000) Vol. #9100-0214. Iss. 3. pp.1-11.

Donoho, D. L. "De-Noising by Soft-Thresholding". IEEE Transactions on Information Theory. (1994)

EUROCAE. EUROCAE ED-14D / RTCA DO-160D. Environmental Conditions and Test Procedures for Airborne Equipment. (1997).

Galeener, F. L., Mikkelsen, J. C., Geils, R. H., and Mosby, W. J. "The relative Raman cross sections of vitreous SiO2, GeO2, B2O3, and P2O5". Applied Physics Letters. (1978) Vol. 32. Iss. 1. pp.34-36.

Haider, B., Lewin, P. A., and Thomenius, K. E. "Pulse Elongation and Deconvolution Filter for Medical Ultrasonic Imaging". IEEE Transactions on ultrasonics, ferroelectrics, and frequency control. (1998) Vol. 45. Iss. 1. pp.98-113.

Herrera, R. E., Sun, M., Charles, P. J., Dahl, R. E., Ryan, N. D., and Sclabassi, R. J. "Removal of Non-White Noise from Single Trial Event-Related EEG Signals Using Soft-Thresholding". Proceedings of the 22nd Annual EMBS International Conference. (2000) pp.793-795.

Huang, S. Y. and Yanushefski, K. A. "Performance and Reliability of Redundant Thermoelectric Coolers". IEEE. (1991)

IXYS. "Datasheet: DE150-201N09A RF Power MOSFET". http://www.directedenergy.com. (2003) Vol. #9200-0241. Iss. 3.

Jianchao, Y. "Motion Blur Identification Based on Phase Change Experienced After Trial Restorations". Proceeding of International Conference on Image Processing. (1999) Vol. 3.

Kaaresen, K. F. and Bolviken, E. "Blind Deconvolution of Ultrasonic Traces Accounting for Pulse Variance". IEEE Transactions on Ultrasonics, Ferroelectrics, and Frequency Control. (1999) Vol. 46. Iss. 3. pp.564-573.

Kaiser, G. "The Fast Haar Transform". IEEE Potentials. (1998) Vol. 17. Iss. 2. pp.34-37.

Kaur, L., Gupta, S., and Chauhan, R. C. "Image Denoising using Wavelet Thresholding". Department of CSE, SLIET, Longowal Punjab, India. (1999)

Li, T., Li, Q., and Zhu, S. Ogihara M. "A Survey on Wavelet Applications in Data Mining". SIGKDD Explorations. (2003) Vol. 4. Iss. 2. pp.49-68.

Macleod A. H. "Thin-Film Optical Filters". Chapter: "Band-pass filters". Edited by "Institute of Physics Publishing". *J. W. Arrowsmith Ltd., Bristol.* pp.257-347. (2001).

Markas, T. "Hardware Implementations of Data Compression Algorithms for Aerospace Type Applications". AIAA Paper 93-4563. Computing in aerospace Conference, 9th, San Diego, CA. (1993)

MAXIM High-Frequency/Fiber Communications Group. "Parasitic Inductance Effects in the Design of 10Gbps Optical Transmitters". Application Note. (2002) Vol. HFAN-2.0.1. Iss. Rev 0. pp.1-3.

Morita, Jiro, Yoshimura, Takeaki, and Minemoto, Takumi. "Input Power Conditions for Distributed Fiber Optic Temperature Sensors in Raman Optical Time-Domain Reflectometry". Optical Review. (1995) Vol. 2. Iss. 1. pp.62-64.

Mortensen, N. A. "Effective area of photonic crystal fibers". Optics Express. (2002) Vol. 10. Iss. 7.

pp.341-348.

OSRAM. "Datasheet: Pulsed Laser Diode in Plastic Package 10..16 W Peak Power. SPL_PLxx". http://www.osram-os.com. (2000)

Otey, R. and Moskowitz, B. "Keeping Cool. Thermoelectric coolers offer efficient solid-state heat-management options.". OE magazine. (2001)

Ozawa Y. and others [Inventors], "Fiber Optic Distributed Temperature Sensor System", Nb: US005113277A (1992).

Powers J. P. "An introduction to Fiber Optic Systems". Edited by "2nd". *Richard D. Irwin.* (1993).

Redd, J. and Tan, Q. "Interfacing laser-driver circuits with laser diodes". Lightwave. Special Reports. (2000) pp.164-168.

Salazar, J., Turo, A., Chavez, A., Ortega, J. A., and Garcia, M. J. "Deconvolution problem to produce ultrasonic short pulses". IEE Proceedings - Science, Measurement and Technology. (1998) Vol. 145. Iss. 6. pp.317-320.

Samson, P. J. "Analysis of the wavelength dependence of Raman backscatter in optical fibre thermometry". Electronics Letters. (1990) Vol. 26. Iss. 3. pp.163-165.

Scheerer, C. "OTDR pulse power limit in on-line monitoring of optical fibres owing to stimulated Raman scattering". Electronics Letters. (1996) Vol. 32. Iss. 7. pp.679-680.

STEAG microParts GmbH. "The microspectrometer". Microoptics presentation. http://www.steag-microparts.de/.

Taxt, T. and Strand, J. "Noise Robust Two-dimensional Blind Deconvolution of Ultrasound Images". IEEE Ultrasonics Symposium . (1997) pp.1465-1470.

Yang, S., "Design and construction of a Raman OTDR system for distributed optical fibre sensing". UMIST. Manchester. (1995).

York Sensors Ltd. "Technical aspects of optical fibre distributed temperature sensing". Company article. (1991)

Zhong, S. and Cherkassky, V. "Image Denoising using Wavelet Thresholding and Model Selection". Proceedings of the IEEE International Conference on Image Processing. (2000)

Zhou, K., Simpson, G., Chen, X., Zhang, L., and Bennion, I. "Two-dimensional optical power distribution of side-out-coupled radiation from tilted FBGs in multimode fibre". Electronics Letters. (2003) Vol. 39. Iss. 8.

Zuleeg R. and Notthoff J. K. [Inventors], "Self-Detecting Optical Sensors", Nb: US004505582 (1985).

DTS Applied to Aircraft Cargo / Baggage Compartment

6.1 Early and multicriteria detection 192

6.2 Description of the water mist detection – activation concept 193
6.2.1 Total flood or zoning protection 193
6.2.2 The objectives of the MPS test procedures 193
6.2.3 The DTS as a tool for the evaluation of extinguishing agents 194

6.3 Installation of an optical fibre-based sensing element in aircraft 195
6.3.1 A specific cable design 195
6.3.2 The fibre blowing technique 195

6.4 Test programs 197

6.5 Detection-activation algorithms 198
6.5.1 Algorithms for initial fire detection 199
6.5.2 Algorithms for fire monitoring 204
6.5.3 Algorithms for fire suppression 205
6.5.4 Fire signature identification 207

6.6 Conclusion 210

Current detection technology used in aircraft cargo compartment relies mostly on particulate sensing by light beam scattering or ionisation type detectors. The detection system must provide a visual indication to the flight crew within one minute after the start of a fire and the effectiveness of the detection system must be shown for all approved configurations and conditions. Complementary to smoke detectors the DTS has the potential to detect and monitor a fire and to trigger the activation of a suppression system.

The DTS was developed to fulfil the requirements associated to the most stringent fire phases and in compliance with the detection and installation specificities of the cargo hold environment. The definition of the appropriate detection logic and the related alarm thresholds are the main research directions. Continuity between the dedicated algorithms for an early detection, the identification of high heat release rates and the monitoring of a fire controlled by the Water Mist extinguishing agent is investigated through the analysis of particular detection criteria.

6.1 EARLY AND MULTICRITERIA DETECTION

The harsh environment of an aircraft cargo compartment makes accurate fire detection and short time response a difficult task [Alankar Gupta, 2000]. Class A and B cargo areas are accessible in flight, so that a fire can be suppressed by the actions of a crewmember with a hand-held extinguisher. A class C cargo area is inaccessible in flight. Remote fire detection and suppression capabilities are required for class C spaces, as well as fire resistant wall panels. On freighter, cargo spaces specified as class E are required to be equipped with fire detectors and independent ventilation control, but not fixed fire suppression systems.

The study is focusing primarily on class C compartments. In this environment, when the smoke and / or temperature exceed a threshold level, an alarm is triggered in the cockpit and the crew responds according to established procedures written in the Aircraft Flight Manual. In the event of a detector alarm, the usual crew procedure is to discharge fire suppression agent. As seen in chapter 2, the nuisance alarm rate in cargo compartment is significant and calls for more reliability of the alarm process.

The improvement of the detection accuracy and reliability is provided by a multi-criteria detection logic [Foo, 1996]. This logic increases the system immunity to false alarm using cross-analyses of the different detector information (i.e. for instance, combination of smoke, temperature and spatial temperature gradient signals). In most of the case, the sensitivity of each individual detector is also increased by a decrease of the individual warning thresholds per type of sensor.

By installation, the possibility for the DTS to access to the danger location makes it very attractive as a detection system to complement smoke detectors for an early and multi-criteria detection.

6.2 DESCRIPTION OF THE WATER MIST DETECTION – ACTIVATION CONCEPT

A cargo compartment fire suppression system must prevent, either by fire control or inerting, the propagation – development of a fire [Yao *et al.*, 1999]. The agent/system for cargo compartments must also meet the requirements of FAR 25.851, Part B and FAR 25.1309. The agent/system must be suitable for fires likely to occur. The agent/system must be able to provide fire suppression over a period of up to the maximum diversion time, which could be in excess of 200 minutes, depending on the aircraft type and route structure. Last conversations with aircraft manufacturer specialists indicate a needed duration of 540 minutes.

6.2.1 TOTAL FLOOD OR ZONING PROTECTION

As opposed to a "total flood" protection of the cargo, like systems using Halon gas, a zoning protection system, based on Water Mist extinguishing agent needs to selectively activate the appropriate nozzle(s) [Ndubizu *et al.*, 1998]. As soon as a fire detection has been confirmed, an alternative solution to the exclusive use of Water Mist (WM), is to inert the cargo compartment with an inerting gas like Nitrogen. In that case, the Water Mist is then used as a cooling, suppressing agent. The European FIREDETEX project [FIREDETEX, 2001] evaluates the couple WM-Nitrogen and uses the DTS to monitor and activate locally the suppression system [Back III *et al.*, 2000]. Dedicated detection and control algorithms are linked also to that application.

6.2.2 THE OBJECTIVES OF THE MPS TEST PROCEDURES

The proposed testing procedures aim to contribute to the establishment of a "minimum performance standard" for testing the replacement of agents for equivalent performance to Halon 1301 in aircraft cargo compartment fire suppression systems [Prasad *et al.*, 1999]. The Federal Aviation Administration in conjunction with the International Halon Replacement Working Group sponsored this developmental work [Reinhardt *et al.*, 2000].

into, using water. The stainless steel tube is due to be installed for the full aircraft lifetime, the fibre would be connected to the control unit only on two points, doing fusion splicing or simple connector connection and could monitor the danger situation over two or more cargo compartments within an aircraft.

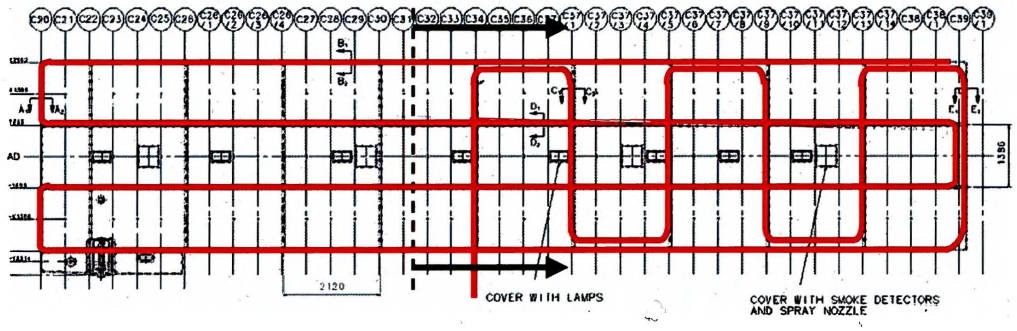

Figure 6.3-2: Cargo Hold ceiling representation with DTS sensing element

The length of the Cargo Hold is reaching 20m, its width is 4m and its height 1.8m. The full compartment was used for calibration tests and the 56m^3 compartment delimited here by the dotted line between the frames 31 and 32 was used to evaluate the performance of the combined detection-activation system for the "Minimum Standard Specification" test campaign.

The deployment of the fibre for the test campaign was realized at a 36.6m.min^{-1} deployment rate, for a total length deployed of 140m using a pump pressure of 76 to 97bars. The flow out was comprised between 700 and 800 cl/min. The weight of the tubing installed was 44g.m^{-1}.

6.3 INSTALLATION OF AN OPTICAL FIBRE-BASED SENSING ELEMENT IN AIRCRAFT

The Sensing Element (the optical fibre) has to be installed for a long-term usage in the cargo compartment. The system lifetime, which is in part defined by the Sensing Element installation, has to be regarded as a key parameter to the acceptance of an optical fibre system in an aircraft environment.

6.3.1 A SPECIFIC CABLE DESIGN

The design of a specific cable seems to be necessary. This cable should have integrated mechanical protections and a limited bending radius so as for the person in charge of system installation, never to be in a position to damage the fibre.

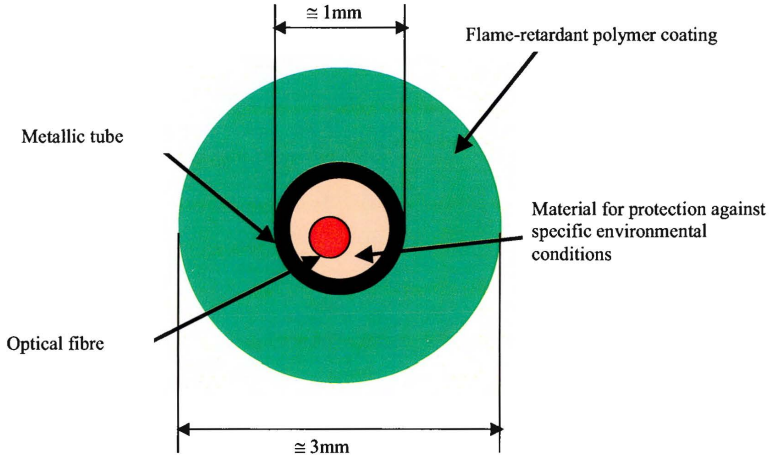

Figure 6.3-1: Cable definition for on-board F/O detection applications

Unfortunately first consultations with cable manufacturers return signals of non-manufacturability.

6.3.2 THE FIBRE BLOWING TECHNIQUE

The selected installation principle was to integrate a stainless steel tube sensor along the structure to be controlled (this hollow tube has a 3mm outer diameter), the tube wall thickness is about 0.5mm, its length can be 600m. It is then easy to blow a fibre

6.5 DETECTION-ACTIVATION ALGORITHMS

Detection algorithms shall allow to detect rapidly and reliably a F/O situation. It is expected also that the DTS shall monitor the evolution of the danger and shall appropriately command/activate an extinguishing system to suppress the fire or to realize a temperature decrease. Focusing on a "fire situation", it is therefore important to understand the characteristics of a fire development at an early stage, of a fire when in conflict with a suppression means and of a fire about to die.

The complexity of the cargo hold environment is stressing the importance of the multi-criteria detection. However, the benefits of a multi-criteria detection for a fire suppression are either unknown or neglected. This paragraph is therefore addressing the performance of a few of selected detection criteria and proposing ways forward to enhance the DTS efficiency to trigger a water-mist based suppression system.

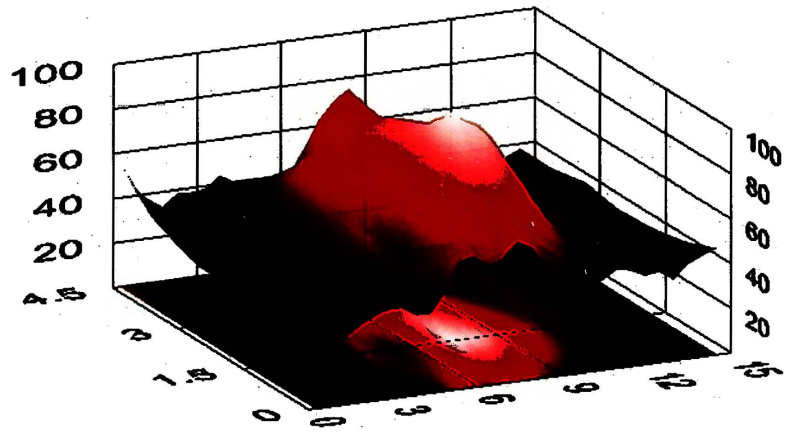

Figure 6.5-1: 3D temperature representation of the raw DTS data

The repetitively acquired 3D temperature profiles (matrix TP) give the detection system the opportunity to better analyze the situation using temporal and spatial informations.

6.4 TEST PROGRAMS

The test conducted used the different types of fire sources and of fire configurations described in the "Minimum Performance Standard" [November 2002, DOT/FAA/AR-TN02/XX]. Before this test campaign, the system was evaluated also according to the EN54 building standard for fire detection system evaluation or certification. These test result databases allow to refine the alarm thresholds for first detection, fire monitoring, fire suppression, or to identify the fire signatures.

Figure 6.4-1: Test chamber furnished with original cargo lining material
Cargo compartment based on an AIRBUS A340-200 forward compartment.

The EN54 in this special context has dealt as a guideline for setting up the fires [Gottuk *et al.*, 2002]. The fibre optical cable was installed for the test campaign of nuisance alarm [Grosshandler, 1998], although the unfavourable test conditions for the smoke detectors were not representative for the DTS. The DTS was used at this occasion as an environmental temperature controller.

criteria.

The covariance matrix is calculated from the temperature signal as follows:

$$TPavg_{i,j} = TP_{i,j} - \frac{1}{N.M}.\sum TP_{i,j}$$

$$COV(TP,TP) = \frac{1}{N^2}.TPavg^T.TPavg$$

Equation 6.5-2 Covariance Matrix of the temperature signal TP
The temperature signal is modified using the temperature average detected at each time t. The indexes i and j are the indexes along the directions x and y respectively.

As primary detection criteria, both the maximum value of the covariance matrix and the sum of all elements of this matrix are selected.

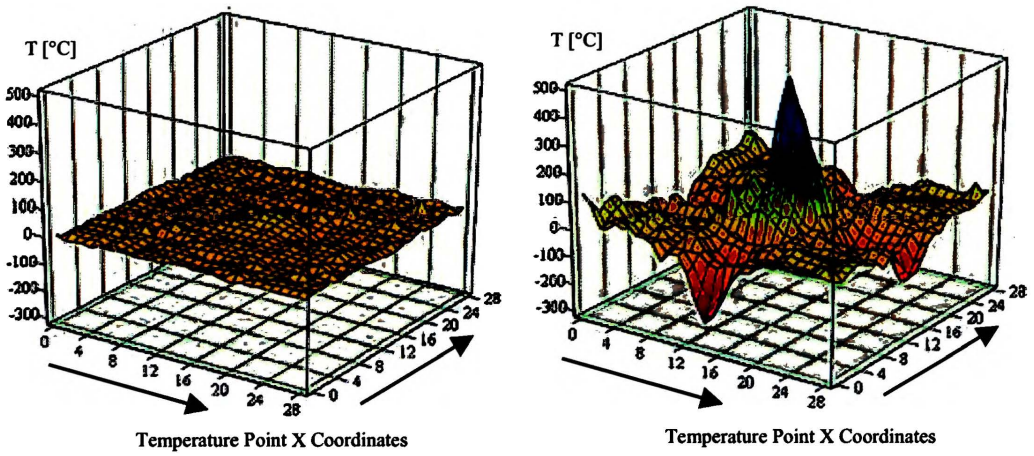

(a) (b)

Figure 6.5-2: Covariance of the cargo hold ceiling temperature
(a) is the early temperature covariance of a smouldering fire. (b) is the covariance 5 minutes later.

A Temperature Time Derivative operator is also built to detect with more efficiency a temperature increase, while reducing the noise level. The operator is using the temperature information of the last 10 samples. The sampling interval being 4.5s, the oldest event was recorded 40s ahead of the current acquisition. The operator can be described by the following equations:

6.5.1 ALGORITHMS FOR INITIAL FIRE DETECTION

The detection system has to early detect the fire even in situations when fire-like events occur simultaneously. This capability of the system is important, so as to fulfill the system validation tests, which specify a detection within a minute when fire. The detection of a temperature increase is a spatial analysis that can be dealt with specific algorithms like the temperature time derivative, the power spectrum density, the maximum of the temperature covariance, the covariance integration and the analysis of the spatial frequency of the fire modes.

The maximum temperature detection provides an instantaneous way to appreciate the situation criticality. Material performance to long-term exposure to fire (for a material like cargo lining for example) can also be appreciated knowing the maximum temperature applied.

The temperature matrix TP is Fourier transformed and the associated Power Spectrum Density (PSD) is calculated. The PSD represents the magnitude of the various frequency components of the temperature signal. Evaluating the power spectrum is a way to isolate periodic features or noise. By looking at the power spectrum, it is possible to see how much energy (power) is contained in the different frequency components of the signal. The power in each frequency component can be obtained by squaring the magnitude of that frequency component.

$$TFtp(u,v) = TF\{TP(x,y)\}$$

$$PSD(u,v) = \frac{1}{N^2} TFtp(u,v).\overline{TFtp(u,v)}^{T}$$

Equation 6.5-1 Power Spectrum Density

TP is the matrix of temperature points located in {x; y}. TF{} indicates a Fourier Transform. PSD is the Power Spectrum Density matrix; u and v are the spatial frequencies corresponding to directions x and y respectively. N is the number of recorded temperature points along the main axis of the cargo hold.

The sum of all the PSD matrix elements, at each time t, is retained as F/O detection

3) Rebuild the pre-transformed matrix using the Wavelet transformed columns.

4) Transpose the pre-transformed matrix.

5) Wavelet transform on the columns of the transposed matrix.

6) Noise filtering using a global threshold.

7) Inverse Wavelet transform of the filtered matrix (from point 4 to 2).

Where point 6 is detailed with the following equation:

$$Th = \delta^2.\sigma.\sqrt{2.\log(N)}$$

Equation 6.5-4 Wavelet denoising technique: threshold definition.
δ is a constant. σ is the standard deviation of the Wavelet transformed picture. N is the number of elements of the picture (32^2).

The filtering process is putting to 0 the Wavelet coefficients having a value lower than the defined threshold [Han *et al.*, 2002].

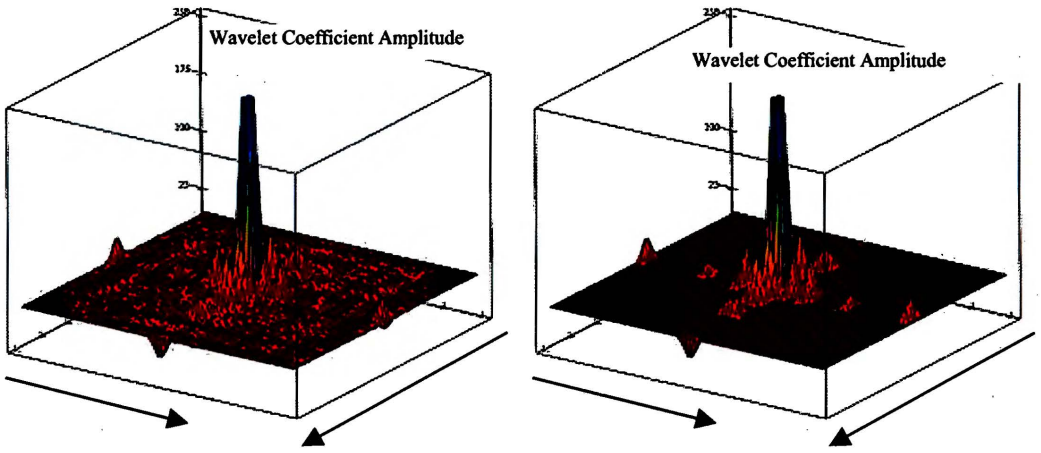

Wavelet Transform Coordinates

(a)

Wavelet Transform Coordinates

(b)

Figure 6.5-3: Wavelet Transform of the cargo hold ceiling temperature
(a) Non-filtered Wavelet Transform. (b) Filtered Wavelet Transform.

$$C_k = \frac{(1-\kappa)}{[\kappa.(RK-1)]}.k+1$$

$$\begin{cases} S^{n}_{k,\{i,j\}} = C_k.TP^{n-k}_{i,j} \\ S^{n-1}_{k,\{i,j\}} = C_k.TP^{n-k-1}_{i,j} \end{cases}$$

$$\Rightarrow \quad DTP_{\{i,j\}} = \frac{Sr^{n}_{\{i,j\}} - Sr^{n-1}_{\{i,j\}}}{\Delta t}$$

$$\begin{cases} Sr^{n}_{\{i,j\}} = \sum_{k=0}^{RK-1} S^{n}_{k,\{i,j\}} \\ Sr^{n-1}_{\{i,j\}} = \sum_{k=0}^{RK-1} S^{n-1}_{k,\{i,j\}} \end{cases}$$

Equation 6.5-3 Temperature Time Derivative

The coefficients C(j) allow providing more importance to the latest temperature records. κ is an integer ($\kappa = 10$), RK is the number of samples integrated into the calculations (RK = 10). DTP is the temperature time derivative, where Δt is the time interval between 2 samples (4.5s).

The equivalent detection surface per temperature point is about $0.34m^2$ (0.508m × 0.667m). The surface associated to the number of points exceeding $1.75°C.s^{-1}$ can be calculated. The maximum temperature time derivative multiplied by this surface gives a value, which is directly proportional to the heat flux per second (assuming a constant thermal conductivity of the air in the initial environmental and operating conditions [-40°C; +70°C]).

Wavelet denoising techniques can be used to remove noise by thresholding the wavelet coefficients. The methodology used to filter out the noisy picture is summarized.

1) The initial temperature picture is increased in size so as to present a 2^n number of points to a Daubechies 4 wavelet transform (4 matrices of 7×29 points are stacked to build a 28×29 matrix. This matrix is then completed on the edges with value 0 so as to build up the final matrix of 32×32 points).
2) Wavelet transform on the columns of the constructed matrix.

3) Rebuild the pre-transformed matrix using the Wavelet transformed columns.

4) Transpose the pre-transformed matrix.

5) Wavelet transform on the columns of the transposed matrix.

6) Noise filtering using a global threshold.

7) Inverse Wavelet transform of the filtered matrix (from point 4 to 2).

Where point 6 is detailed with the following equation:

$$Th = \delta^2 . \sigma . \sqrt{2 . \log(N)}$$

Equation 6.5-4 Wavelet denoising technique: threshold definition.
δ is a constant. σ is the standard deviation of the Wavelet transformed picture. N is the number of elements of the picture (32^2).

The filtering process is putting to 0 the Wavelet coefficients having a value lower than the defined threshold [Han *et al.*, 2002].

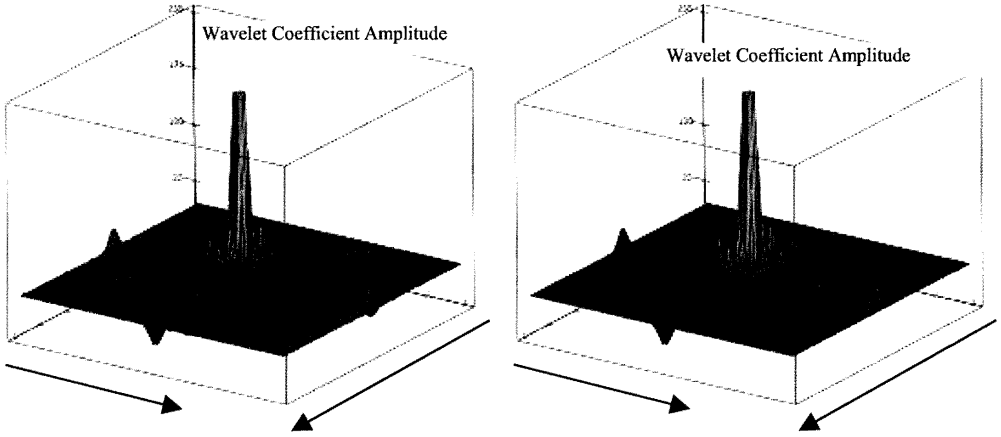

Figure 6.5-3: Wavelet Transform of the cargo hold ceiling temperature
(a) Non-filtered Wavelet Transform. (b) Filtered Wavelet Transform.

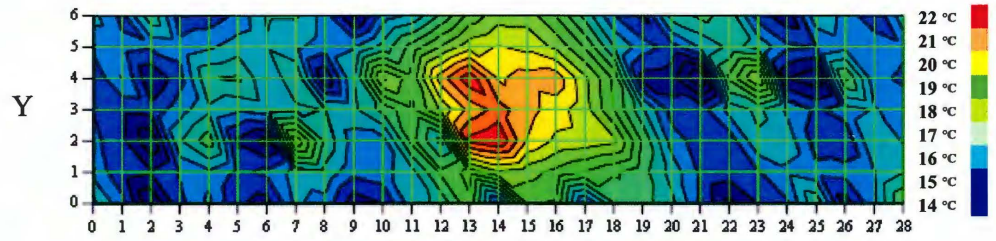

(a)

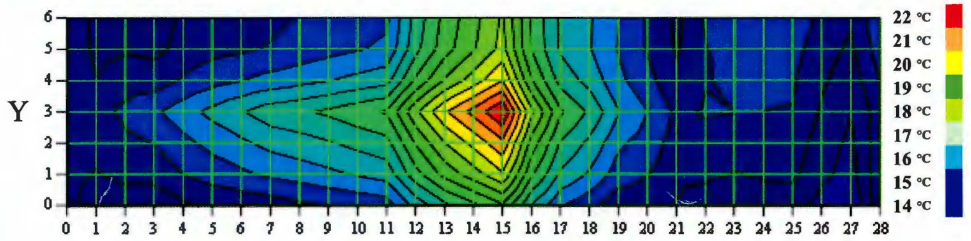

(b)

Figure 6.5-4: Temperature at cargo hold ceiling with and without Wavelet denoising (a) Non-filtered temperature. (b) Denoised temperature profile. The maximum temperature reached on (a) is 24.6°C for a standard deviation of ±3°C. On (b), the maximum temperature reached is also 24.6°C but for a standard deviation of ±2.5°C.

Though a degradation of the maximum temperature value is noticeable after filtering, the fire event is in that case better extracted from temperature background. It is possible to adjust the "strength" of the filter by modifying the value of δ. The effect can be controlled by the value of the correlation coefficient between the two pictures.

All criteria described in this paragraph can be safely implemented in a detection algorithm so as to contribute to an early detection, within a multi-criteria detection algorithm. It remains that like every detection criteria they will have to be submitted to test, to evaluate what might be the influences of operational environmental conditions. These standard fluctuations may impact on their respective future utilizations.

6.5.2 ALGORITHMS FOR FIRE MONITORING

Cargo hold fires may generate smoke and heat in considerable amount and are therefore particularly life-threatening as described in chapter 2. One may choose to isolate three distinctive periods within a fire (see Figure 6.5-5):

- Initially the smoke is the first activation criteria; temperatures and temperature time derivatives are indeed small or not significant with regard to their standard operational fluctuations.

- The second one is the most dangerous phase when temperatures and temperature time derivatives may respectively reach from DTS readings $[\delta T/\delta t;\ T] = [17°C/s;\ 490°C]$.

- The third one is when the fire is under control and the activation requirements become infrequent.

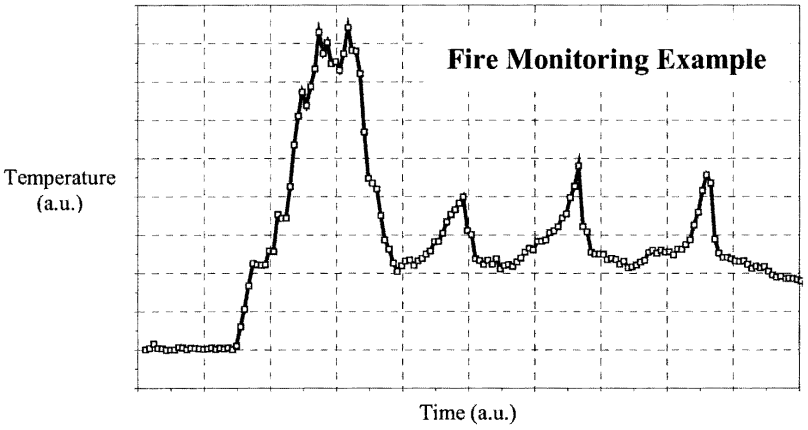

Figure 6.5-5: Fire control and monitoring
A detection-activation algorithm is defined to activate appropriately the system using Water Mist as fire suppression agent. The diagram shows DTS temperatures as a function of the acquisition time.

These three periods are clearly visible for fires like cardboard box fires, but can be identified easily for all fires developing enough to be threatening for the integrity of

the cargo. The first period can be managed using for example a low temperature time derivative or a low "maximum-temperature" threshold. However these thresholds must be above a false alarm threshold that has to be determined through complementary tests. The fine adjustment of these low thresholds is also securing the fact that the maximum temperature will not reach a value exceeding the cargo lining specifications.

Period 3 is offering a significant potential for water consumption savings. The fire being controlled, it means the temperature dropped down to around 100°C, a subsequent activation has to occur only when fire growth is again identified as a threat. This means that for water saving reasons, and taking advantage of the saturated water vapour in the cargo compartment (fire suppression principle), the subsequent activation could occur only when the temperature reaches about 130°C. Further investigation shall be conducted and should be part of a "water saving program".

6.5.3 ALGORITHMS FOR FIRE SUPPRESSION

During the project FIREDASS [Brite Euram Project, 1995], the detection/activation systems were acting as a closed loop, e.g. the number of activated nozzles followed directly the variations in temperature of the detection criteria (raw temperature, temperature time derivative, spatial temperature gradient). It was identified that the system response time was depending on the sum of several delay effects as follows:

- confirmation duration (9s for a smoke detector; between 3.7s and 7.4s for the DTS). The confirmation time was required to reduce false alarm rate.
- communication of activation queries to the activation system (a non-optimised system is showing: 1 to 2s delay).
- nozzle activation (air and water flow in piping: 1 to 3s).
- time needed by sprayed water to reach the fire zone (≅ 1s to 2s).

This gives a minimum delay of 6s (3.7 + 1 + 1 + 1 → 6s) and a maximum delay of 15s (7.4 + 2 + 3 + 2 → 15s). This effectively meant that the logic module possibly sometimes generated too many activations because not enough time was allocated to look at the efficiency of the mist on the fire.

Three detection parameters were also identified as being able to improve the performance of the water mist system, namely: a reduction of the confirmation time, an increase of the sampling frequency and a selection of additional criteria taking into account the threat area and activating more selectively the appropriate nozzles.

As opposed to FIREDASS, the study was aiming to reduce the complexity of the overall system.

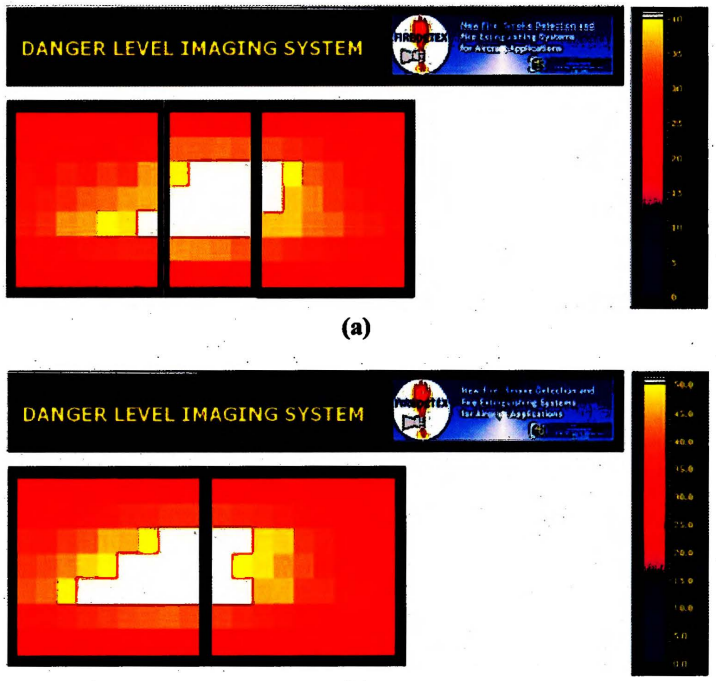

Figure 6.5-6: Test chamber furnished with original cargo lining material
(a): is the test rig divided into 3 distinct WM activation zones. **(b)**: test rig divided into 2 separate WM activation zones. The fire can evolve within the test compartment and the objective to save water along the suppression process can be analyzed for a 2 or 3 activation zone system configuration.

The detection system was therefore only triggering the activation of the

extinguishing system but not its de-activation. The activation duration of the nozzle of a certain zone was indeed pre-set from 15s to 60s. Besides, the activation logic was addressing a cargo hold zone and not any more separate nozzle(s). As represented in Figure 6.5-6, the algorithm is able to generate a cargo hold area with two or three zones to be able to be triggered by the detection system, for activation. No evidence of water saving was found; neither were found lower "maximum temperatures" at the cargo ceiling when comparing the results of similar tests conducted under the Minimum Performance Standard procedures.

6.5.4 FIRE SIGNATURE IDENTIFICATION

The 2-dimensional Fourier transform is widely used, for instance to specify the resolving power of an image device, to design and to analyze (2-dimensional) image filters, to model the noise characteristics, and to model the image of textured surfaces [Van der Heijden, 1994]. We can introduce 2-dimensional, complex, harmonic functions.

$$g(x, y) = G \exp(2.\pi.j.(x.u + y.v))$$

$$G = A.\exp(j\phi) \quad \text{and} \quad j = \sqrt{-1}$$

Equation 6.5-5 2D, complex, harmonic functions

A, u, v and ϕ are real scalars. A is called the amplitude, ϕ is the phase, u and v are the spatial frequencies in the x and y direction, respectively. These quantities can also be transferred to polar coordinates.

$$g(x, y) = G.\exp(2.\pi.j.\rho.(x.\cos\theta + y\sin\theta)) \quad \text{with} \quad \left| \begin{array}{l} u = \rho.\cos\theta \\ v = \rho.\sin\theta \\ \rho^2 = u^2 + v^2 \end{array} \right. \Leftrightarrow \lambda = \frac{1}{\rho} \Leftrightarrow \left| \begin{array}{l} x = \lambda.\cos\theta \\ y = \lambda.\sin\theta \\ \lambda^2 = x^2 + y^2 \end{array} \right.$$

Equation 6.5-6 2D, complex, harmonic functions with polar coordinates

ρ is the spatial frequency of the harmonic function. The orientation of the function equals $1/\rho$. The orientation of the function is given by λ.

Calculating the Power Spectral Density (PSD), it is possible to calculate the spatial frequency resulting from the two spatial frequency contributions along x and y. This frequency is supposed to be able to track better the propagation of a thermal wave, which theoretically in case of a fire propagates concentrically. So, one may obtain:

$$\begin{cases} u_m = \dfrac{2.\pi}{\Delta x}.m \\ v_n = \dfrac{2.\pi}{\Delta y}.n \end{cases} \quad \Leftrightarrow \quad s_k = \sqrt{u_m^2 + v_n^2}$$

Equation 6.5-7 Spatial frequency for concentric thermal wave analysis
k, m, n are zero or positive integers. The integer s value ranges between 0 and 350.

The couple {u; v} is found for each value of the radius s and the spectrogram in Figure 6.5-7 is built from the 2D Power Spectrum Density matrix.

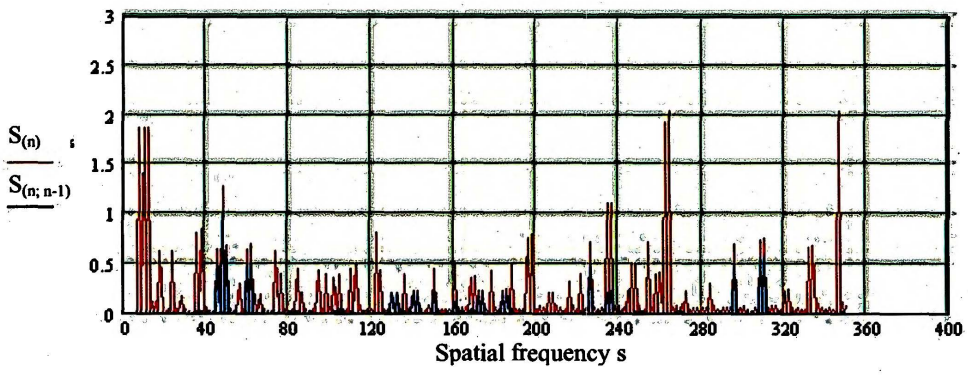

Figure 6.5-7: Spatial frequency analysis for fire mode tracking

$S_{(n)}$ is the histogram obtained at the current time. $S_{(n;\ n-1)}$ is the histogram difference between the current time and the previous sampling. $S_{(n;\ n-1)}$ allows to see, in which mode the energy is appearing or in which mode the energy is transferred.

It is therefore possible to analyze the spectrogram as a function of time for different fires and to note the changes when a fire is present and is evolving.

Filtering the mode with a magnitude higher than 2 and selecting the common modes from the different fires, one may obtain the mode illumination as a function of time of Figure 6.5-8.

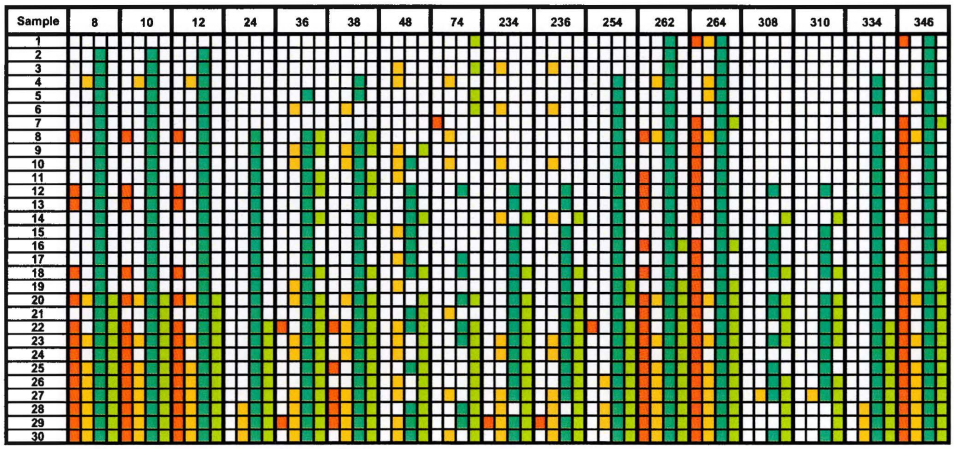

Figure 6.5-8: Fire mode analysis for fire signature identification
The detected fire temperatures are considered as "significant" at sample 1. The fire is progressing and is considered as having reached a "reasonable" maturity 30 samples later.

Energetic Fire – Position at the middle of the Cargo – Maximum Temperature seen ≥ 70°C
Small Fire – Position at the middle of the Cargo – Maximum Temperature seen ≤ 40°C
Energetic Fire – Position at a corner of the Cargo – Maximum Temperature seen ≥ 70°C
Small Fire – Position at a corner of the Cargo -- Maximum Temperature seen ≤ 40°C

The samples are separated in time of 4.5s. It can be seen that energetic fires have preferably a mode contribution at low (mode 8 to 12) and high spatial frequencies (modes 264 to 284, 334 and 346 as well) and that small fires tend to begin with middle spatial frequencies and to distribute largely among the modes when fire is growing. It remains also, as described in 6.5.1, to evaluate the influence of A/C operational conditions on these performances and to consolidate these results in front of a larger fire database.

6.6 CONCLUSION

The performance objective of fire detection in cargo compartments is to sense a starting fire at a small size. Therefore designed mitigation strategies including discharging suppressant, shutting off compartment ventilation, diversion to the nearest acceptable airport, and evacuation can effectively limit the fire damage and the life safety hazard. With the adoption of FAR 25.858 in 1980, the detection time acceptable was reduced to one minute. It is therefore absolutely necessary to identify detection criteria with an important sensitivity to fire and immunity to nuisance environmental conditions. In this chapter were proposed several candidates as criteria for an early detection and fire control/monitoring using the Water Mist as an extinguishing agent.

The Water Mist has been selected, as suppression agent, along the European project FIREDASS and associated to Nitrogen inerting along FIREDETEX. The analysis of the associated detection–activation concept shows that a zoning protection and also activation on-demand per nozzle is preferable to minimize the water consumption. The implication on the cost, weight and reliability for the full system shall be investigated further in cooperation with the aircraft manufacturers so as to find the optimum compromises on the system architecture. The DTS has shown along these projects its full capabilities and further development are focusing on the sensing element integration so as to guarantee a short response time and appropriate mechanical protection.

Test campaigns have also allowed tuning the alarm thresholds for the different fire phases. The suppression performance can be further optimized with an accurate definition of the activation timings.

The DTS installation configuration at the ceiling of the cargo compartment allows also exploring the suitability of new detection criteria like the spreading of the spatial frequencies, which may lead to a precise identification of the fire signature.

REFERENCES

Alankar Gupta, P. E. "Options for Aircraft Cargo Compartment Fire Protection.". (2000)

Back III, G. G., Beyler, C. L., and Hansen, R. "A Quasi-Steady-State Model for Predicting Fire Suppression in Spaces Protected by Water Mist Systems.". Fire Safety Journal. (2000) Vol. 35. pp.327-362.

Brite Euram Project. "Fire Detection and Suppression Simulation Project". Project Nb. BE95-1977. (1995)

FIREDETEX. "New Fire/Smoke Detection and Fire Extinguishing Systems for Aircraft Applications.". (2001) Iss. G4RD-CT-1999-00057 / GRD1-1999-10342.

Foo, S. Y. "A Rule-Based Machine Vision System for Fire Detection in Aircraft Dry Bays and Engine Compartments.". Knowledge-Based Systems. (1996) Vol. 9. pp.531-540.

Gottuk, D. T., Peatross, M. J., and Roby, R. J. Beyler C. L. "Advanced Fire Detection Uing Multi-Signature Alarm Algorithms.". FIRE Safety Journal. (2002) Vol. 37. pp.381-394.

Grosshandler, W. L. "Nuisance Alarms in Aircraft Cargo Areas and Critical Telecommunications Systems: Proceedings of the Third Detector Workshop.". NIST. (1998) Iss. NISTIR 6146.

Han, K. J. and Tewfik, A. H. "Hybrid Wavelet Transform Filter for Image Recovery". (2002)

Ishii, H., Kawamura, K., Ono, T., and Megumi, H. and Kikkawa A. "A Fire Detection System using Optical Fibres for Utility Tunnels.". Fire Safety Journal. (1997) Vol. 29. pp.87-98.

Ndubizu, C. C., Ananth, R., Tatem, P. A., and Motevalli, V. "On Water Mist Fire Suppression Mechanisms in a Gaseous Diffusion Flame.". Fire Safety Journal. (1998) Vol. 31. pp.253-276.

Prasad, K., Li, C., and Kailasanath, K. "Simulation of Water Mist Suppression of Small Scale Methanol Liquid Pool Fires.". Fire Safety Journal. (1999) Vol. 33. pp.185-212.

Reinhardt, J. W. and Blake D. and Marker T. "Development of a Minimum Performance Standard for Aircraft Cargo Compartment Gaseous Fire Suppression Systems.". U.S. Department of Transportation, Federal Aviation Administration. (2000) Iss. DOT/FAA/AR-00/28.

US Department of Transportation. "Options to the Use of Halons for Aircraft Fire Suppression Systems-2002 Update.". (2002) Iss. DOT/FAA/AR-99/63.

Van der Heijden Ferdinand. "Image Based Measurement Systems. Object Recognition and Parameter Estimation ". *John Wiley & Sons Ltd.* pp.21-32. (1994).

Yao, B., Fan, W., and Liao, G. "Interaction of Water Mists with a Diffusion Flame in a Confined Space". Fire Safety Journal. (1999) Vol. 22. pp.129-139.

Conclusions and Future Work

Understanding the detection requirements linked to the operational constraints and to cascade these constraints so as to derive the metrological requirements were two priorities in this work. The hardware simplification of different system modules is offering the perspective of successful system integration into a volume of a Smoke Detection Control Unit (SDCU). Independently from the system architecture, a specific digital signal processing can reduce the temperature profile standard deviation of about a factor 3. The DTS system confronted to real fire situations during extensive ground test campaigns and conducted in a A340 cargo compartment has shown its full capability to early detect fires as well as to control the activity of an extinguishing system while continuously monitoring the evolution of the temperature.

7.1 OVERALL CONCLUSIONS

The analysis of the aircraft accident scenarios and the status on the unwanted alarms generated by on-board detection systems call for an improvement of the definition of the detection objectives and of the associated chain of alert.

A status of the probability of accidents/incidents as a function of the detection area is taken to guide the technology selection assuming that the stringency of the environment defines in part the technology to consider.

A rate of about 200 false alarms for every alarm due to verified smoke source show how it is important to find solutions either to improve the reliability of current detectors in A/C cargo compartment or to think about introducing more of multi-criteria detection in the decision logic of the warning system. To introduce a new

technology as part of the fire detection decision process is beginning therefore through an investigation of the degree of maturity of the potential candidate.

Technology Selection. The technological selection process is rather simple in terms of measurement performances, since the technologies available have specificities, which are or are not compliant with aeronautic application constraints. Raman Optical Reflectometry systems came out dedicated to a group of four possible aeronautic applications: The Thermal Cargo Monitoring, Wire F/O Detection System (electrical cables protection), Cabin Temperature Control (cabin temperature regulation for passenger comfort and possibly cabin fire detection system) and Hidden Area Fire Detection (protection of areas not easy to access and then where maintenance operation are not frequent). The Raman Reflectometry system can be playing the role of a complementary fire detection system to the smoke detectors and/or the role of a detection system for "zoning extinguishing".

The signal processing type to be used to collect Raman back-scattered signals has been the object of several investigations: the time domain, the frequency domain analysis, the photon counting and the correlation OTDR options. The analog Raman OTDR has been selected.

Raman OTDR Analysis. The Rayleigh and Raman scattering processes were explained and the spectral broadening of the Raman spectral lines estimated to about 12nm is taken as sizing criteria for the demultiplexer filters. The radar equations associated to the anti-Stokes and Stokes signals are highlighting the influencing parameters, like for example the coupled optical energy into the fibre. The fibre attenuation and the optical pulse width are said to play a major role in the system detection range and the spatial resolution respectively. Besides, the material dispersion, the wave-guide dispersion and the modal delay are widening the propagating pulse in time domain. The cumulative effect of these dispersions is limiting the achievable spatial resolution. Although the backscatter factor for a multimode step-index fibre is 50% higher than the one of a graded-index, one shall

select the later to be in a position to reach a 1m spatial resolution for a 500m long sensing element. The choice of the operating wavelength is driven by the fibre spectral attenuation, the desired range of the system, but also by the low-cost, reliability, and the power figures of the laser diode and the spectral responsivity of the corresponding photodetectors. A NIR wavelength is selected. The relationships were established between the spatial, the temperature resolutions, the detection range, the refreshment time and the system configuration.

Finally, resulting from an optical signal at a distance z and considering a total budget of 12dB of total optical losses, the APD photocurrents before multiplication are evaluated to be about 1nA for the anti-Stokes signal and 5nA for the Stokes signal.

DTS Optimisation. In this chapter the methodology and the construction details to build and optimise a modular OTDR DTS have been explained. The description of the system modules has highlighted the improvement potentials while demonstrating the system capability to reach the detection performances requested from Chapter 3.

The demultiplexer design is proven to be temperature controllable using a Peltier element of maximum electric power 9W for an operating avionic bay temperature range of [-15°C;+70°C]. The laser diode was decoupled in vibration from the driver board via a flexible transmission line.

The detection performances were analysed also through the measurement results, which have made clear the importance of an APD voltage regulation and the insufficiencies of the standard signal processing for a reduced number of averages as far as the temperature resolution is concerned. The standard averaging method is achieving ±8°C for 100 averages of the Stokes and anti-Stokes data sets. From these results, an enhancement of the measurement and data processing capabilities is proposed using two different signal-processing schemes. Considering the noise level and image spectral densities, the first possibility was studied using the optical pulse shape and a Wiener filter [±5°C for 100 averages]. The second technique uses a

wavelet denoising algorithm [±3°C for 100 averages]. The soft-thresholding technique using wavelet decomposition improves significantly the temperature resolution without degrading the spatial resolution.

The conformity analysis to aeronautic qualification tests did not reveal any showstopper. A rapid improvement of the spatial resolution was identified as possible with the development of the laser diode driver, which would need to generate an 8ns optical pulse width to achieve a sub-meter system spatial resolution.

DTS Cargo Compartment Detection. With the adoption of FAR 25.858 in 1980, the acceptable detection time of a fire was reduced to one minute. It is therefore absolutely necessary to identify detection criteria with an important sensitivity to fire and immunity to nuisance environmental conditions. In this chapter were proposed several candidates as criteria for an early detection and fire control/monitoring using the Water Mist as an extinguishing agent.

The Water Mist has been selected, as suppression agent, along the European project FIREDASS and associated to Nitrogen inerting along FIREDETEX. The analysis of the associated detection–activation concept shows that a zoning protection and also activation on-demand per nozzle is preferable to minimize the water consumption. Test campaigns have also allowed tuning the alarm thresholds for the different fire phases. The suppression performance can be further optimized with an accurate definition of the activation timings.

The DTS installation configuration at the ceiling of the cargo compartment allows also exploring the suitability of new detection criteria like the spreading of the spatial frequencies, which may lead to a precise identification of the fire signature.

The DTS was used in the frame of a MPS fire test campaign to explore some potential ways to better exploit the outputted detectors signals, to better follow the danger evolution and to provide earlier an alarm with more confidence.

7.2 Recommendations and Future Research

The investigation of the repercussion of a reduction of the pulse width of the laser diode has not been carried out but needs to be evaluated so as to identify the maximum DTS range achievable when decreasing the energy launched into the fibre and increasing the spatial resolution.

The voltage regulation of the APDs has a direct influence on the level and noise of the amplified electrical signals from the respective optical Stokes and anti-Stokes inputs. Adjustable and automatic voltage regulation could bring substantial benefit for the systems so as to be re-configured for optimal detection performances.

The thermal regulation of the optical module is one of the key features to guarantee that the system will sustain its performance objectives within the aeronautic operational temperature range. The laser diode, the APDs and the wavelength filters are included in this design directive.

The redundancy requirements for the sensing element and for the optical module will have to be clarified by the aircraft manufacturer safety and reliability specialists as well as with the designated certification specialists. This could lead to put into the system two optical modules as described in this research with their associated electronic interfaces. This might be optimised by having a single DTS controlling two cargo compartments. Independently from redundancy questions, it will have to be demonstrated that it is possible to monitor the rear and forward cargo hold with one sensing element and one control unit only.

The Water Mist protection system will have to be optimized to be cost, weight and reliability competitive vis-à-vis other system needing purely the use of inerting agents for example.

The DTS has shown along these projects its full capabilities and further development are focusing on the sensing element integration so as to guarantee a short response time and appropriate mechanical protection.

For the specific application, cargo fire detection and water mist activation, suitable algorithms have been developed to target low water consumption and an efficient structure integrity control. Some further efforts, especially in the activation logic and the adjustment of the associated activation thresholds could bring additional weight savings for the A/C, when limiting the water consumption.

The analysis of the spatial frequency distributions, generated by the temperature grid at the cargo ceiling level, should be continued so as to identify the particular modes impacted by a fire. The on-going work shall aim to design the system such that it knows enough about fire itself to make a decision on signal patterns that it has not encountered before.

Glossary

μm	micro-meter
*	In place of either the anti-Stokes or Stokes signal
A	Ampere
A/C	Aircraft
ADC	Analog to Digital Converter
AI	Avionics Integrity
AM	Amplitude Modulation
AMPS	Ampère
APD	Avalanche Photodiode
APSD	Acceleration Power Spectral Density
APU	Auxiliary Power Unit
AS	Anti-Stokes
ASE	Amplified Spontaneous Emission
AVLAN	Avionics Local Area Network
BLD	Bleed Leak Detection
BTL	Bell Telephone Laboratories
CCD	Charge Coupled Device
CFD	Computational Fluid Dynamic
cm	centimetre
CMC	Central Maintenance Computer
CMOS	Complementary Metal Oxide Semi-conductor
C-OFDR	Coherent Optical Frequency Domain Reflectometry
CPC	Conductive Polymeric Composition
CTC	Cabin Temperature Control
CU	Control Unit
CW	Continuous Wave
DAC	Digital to Analog Converter
DART	Distributed Anti-Stokes Raman Thermometry
DC-DC	Direct Current – Direct Current, voltage amplifier
DS	Detection System
DSC	De-icing System Control
DTS	Distributed Temperature Sensor
DWT	Discrete Wavelet Transform
EFD	Engine Fire Detection
EMI	Electromagnetic Interference
ES	Extinguishing System

ETDR	Electrical Time Domain Reflectometry
EV	Enhanced Value
F/O	Fire / Overheat
FAA	Federal Aviation Administration
FBG	Fibre Bragg Grating
FET	Field Effect Transistor
FFT	Fast Fourier Transform
FHT	Fast Haar Transform
FIREDASS	Fire Detection And Suppression Simulation
FM	Frequency Modulation
FMCW	Frequency Modulated Continuous Wave
FWC	Flight Warning Computer
FWHM	Full Width Half Maximum
GHz	Giga Hertz
GRESS	General Requirements for Equipment and System Suppliers
HAD	Hidden Area Fire Detection
HSCT	High Speed Civil Transport
HWHM	Half Width Half Maximum
IHRWG	International Halon Replacement Working Group
km	kilometre
LDM	Laser Driver Module
LGD	Landing Gear overheat Detection
LRU	Line Replaceable Unit
LSB	Least Significant Bit
Mb	Mega bits = 10^6bits
MCU	Modular Concept Unit
MHz	Mega-Herz
MOSFET	Metal Oxide Semiconductor Field Effect Transistor
MP	Measurement Parameter
MSC	Measurement Selection Criteria
MSTL	Micro Stripline Transmission Line
MTTF	Meantime To Failure
MW	Mega Watt = 10^6 Watts
N	Number of pre-processed averages
NA	Numerical Aperture
nA	nano-Amper
nm	nanometer
NRC	Non Recurrent Costs
OBIGGS	On-Board Inert Gas Generating System
OBOGS	On-Board Oxygen Generating System
OD	Optical Density
OFDR	Optical Frequency Domain Reflectometry

OLAN	On-board Local Area Network
OTDR	Optical Time Domain Reflectometry
PCB	Printed Circuit Board
PCI	Peripheral Component Interconnect, a 32-bit local computer bus
PFN	Pulse Forming Network
PLD	Pulsed Laser Diode
PM	Phase Modulation
POTDR	Polarisation Optical Time Domain Reflectometry
PSD	Power Spectrum Density
PTS	Purchaser Technical Specification
QF	Quality Factor
R&D	Research and Development
RC	Recurrent Cost
RF	Ranking Factor
RFI	Request For Information
RFP	Request for Proposal
RFTI	Request For Technical Information
RMS	Root Mean Squared
R-OFDR	Raman Optical Frequency Domain Reflectometry
ROM	Rough Order of Magnitude
S	Stokes
S_{AS}	anti-Stokes signal
SE	Sensing Element
SNR	Signal-to-Noise Ratio
S_S	Stokes signal
TCM	Thermal Cargo Monitoring
TC-SPC	Time Correlated Single Photon Counting
TDR	Time Domain Reflectometry
TE	Thermoelectric
TEC	Thermoelectric Cooler
TF	Fourier Transforme
VCSEL	Vertical Cavity Surface Emitting Laser
VLCT	Very Large Commercial Transport
WDM	Wavelength De-Multiplexer
WFD	Wire Fire/Overheat Detection System
WM	Water Mist
YAG	Yttrium Aluminium Garnet